

Suitability of *Typha* Fibre in Composite Applications
at Different Stages of Plant Development

by

Mohammed Shahadat Hossain

A Thesis submitted to the Faculty of Graduate Studies of

The University of Manitoba

in partial fulfilment of the requirements of the degree of

MASTER OF SCIENCE

Department of Biosystems Engineering

University of Manitoba

Winnipeg

Copyright © 2022 by Mohammed Shahadat Hossain

Abstract

Typha latifolia L., commonly known as cattail, has already been established as a natural source of fibre for textiles and composite applications when using fully mature plants. An investigation was conducted to determine cattail fibre properties for composite applications from five different growth stages ranging from vegetative to mature plants. The reliability of cattail fibres of three different lengths was characterized by a two-parameter Weibull distribution model using both linear regression (LR) and Maximum Likelihood Estimation (MLE) methods. It was found that cattail fibres from all growth stages were reliable for composite applications, as the Weibull modulus was found to be greater than unity. However, it was impossible to calculate a reliability-rank of fibres due to irregular defects profile in the fibre and inherent limitations of the Weakest Link Theory of the Weibull distribution model. To overcome these limitations, a method to check the suitability of cattail fibres was developed in Python by creating high, average, and low threshold limits values based on the mechanical properties of flax. Failure to rank fibres from the growth stages using the Weibull distribution model was investigated by examining the sources of variations. It was found that fibres from the central part of leaf were finer and weaker than those from the dorsal and ventral sections. The chemical makeup of fibres at various growth stages was found to have no significant differences. This research suggests that cattail plants may be used from all development stages to extract fibre for composite applications. Multiple harvesting could be possible in one growth cycle.

Acknowledgement

I would like to praise almighty Allah (SWT) for his blessings to me and let me keep patience throughout the journey to my M.Sc. degree and protects me from all kinds of sickness.

I want to express my gratitude to my supervisor, Dr. Nazim Cicek, and my co-supervisor, Dr. Mashiur Rahman, for allowing me to work on waste biomass fibre. Without their guidance and intellectual advice, I might not be able to complete this thesis successfully. I would like to express special thanks to Dr. Rahman for his continuous support, guidance, and suggestions that helped me tremendously to complete my thesis. I am blessed to have the opportunity to study and conduct research under his supervision. I sincerely thank Dr. Cicek for his valuable comments and ideas throughout the study. I extend my gratitude to NSERC and Dr. Cicek for helping me with their financial grant support.

I want to thank all my lab mates for their assistance during my research experiments. Special thanks go to Md Shadhin, who helped me, trained me to use experimental instruments, and guided me. I would also like to thank my friends, Md Imran and Mostafizur Rahman, who supported me immensely while studying.

Last but not least, my most profound appreciation goes to my wife and mother for their support.

Dedication

I want to dedicate my work to my beloved wife, who gave me immense mental support from the beginning of my study. Without her help, it was not possible to complete my study.

Table of Content

Abstract	ii
Acknowledgement	iii
Dedication	iv
Table of Content	v
List of Tables	x
List of Figures	xii
Abbreviations	xix
Chapter 1 Introduction	1
1.1 Natural Fibres	1
1.2 Cattail Fibres	2
1.2.1 Scope of Cattail Fibre	3
1.2.2 Industrial Use of Cattail Fibre	3
1.3 Impact of Maturity on Fibre Properties	4
1.4 Impact of Length on Fibre Properties	5
1.5 Impact of Extraction method on Fibre Properties	6
1.6 Variation on Properties of Natural Fibre	7
1.7 Scope of Weibull Distribution	7
1.7.1 Effect of Weak-Link Theory on Weibull Distribution	8
1.8 Scope of the Thesis	9
Chapter 2 Materials and Methods	11

2.1 Cattail Fibre extraction	11
2.1.1 Plant Collection and Phenological Growth Stage Identification	11
2.1.2 Alkali Retting in Water Bath	13
2.1.3 Washing, Neutralizing and Drying	14
2.2 Measurement of Fibre Properties	15
2.2.1 Yield (%) Measurement	16
2.2.2 Mechanical Properties Measurement	16
2.2.2.1 Sample Preparation	16
2.2.2.2 Diameter Measurement	17
2.2.2.3 Humidity Conditioning of Fibre	18
2.2.2.4 Tensile Test of Cattail Fibre	19
2.3 Statistical Analysis: ANOVA	20
2.4 Statistical Analysis: Weibull Distribution	20
2.4.1 Weibull Analysis with Linear Regression Method	20
2.4.2 Weibull Analysis with Maximum Likelihood Estimation (MLE)	22
2.4.2.1 Weibull Distribution Using Python Code	24
2.4.3 Sample Calculation of Weibull distribution – Linear Regression Method	25
2.4.4 Sample Calculation of Weibull distribution – MLE Method	28
2.5 Suitability Analysis and Ranking	32
2.5.1 Selection of Limit Value	32
2.5.2 Decision for Suitability and Ranking: Process Flow	33

2.5.3 Use of Python Code for Suitability (%)	33
2.5.4 Use of Python Code for Ranking (Combination of Growth Stage and Length)	33
2.6 Image analysis	35
2.6.1 ESEM and EDS Analysis	35
Chapter 3 Statistical Analysis: ANOVA and Weibull Distribution – Results and Discussion	36
3.1 Statistical Analysis Using ANOVA	36
3.2 Statistical Analysis Using Weibull Distribution	36
3.2.1 Weibull Analysis of Tensile Stress – Linear Regression (LR) Method	37
3.2.2 Weibull Analysis of Tensile Stress Using Python	53
3.2.3 Weibull Analysis of Modulus – Linear Regression (LR) Method	55
3.2.4 Weibull Analysis of Modulus Using Python	71
Chapter 4 Suitability Analysis – Results and Discussion	78
4.1 Suitability (%)	78
4.1.1 Single Parameter – Tensile Stress	79
4.1.2 Single Parameter – Tensile Strain	80
4.1.3 Single Parameter – Modulus	80
4.1.4 Two Parameters – S/R	80
4.1.5 Two Parameters – Y/R	81
4.1.6 Two Parameters – S/Y	81
4.1.7 Three Parameters - S/R/Y	81
4.2 Ranking	82

4.2.1 Ranking along the fibre length (L1, L2 and L3)	83
4.2.2 Ranking along the five growth stages	86
4.2.2.1 Ranking for individual parameter, parameter combinations and limit values (fixed length)	86
4.2.2.1.1 Rank for average of lengths and limit values (fixed parameter and parameter combination)	87
4.2.2.1.2 Ranking for average length and parameter combinations (fixed limit value)	88
4.2.2.1.3 Ranking for average of lengths and limit values (fixed parameters and parameter combinations)	89
4.2.3 Ranking (5x3) for the combination of five growth stages and three lengths	92
4.2.4 Ranking within parameters and parameter combination	95
Chapter 5 Image Analysis and Chemical Composition – Results and Discussion	99
5.1 ESEM Analysis of Fibres from Different Growth Stages	99
5.2 Effect of fibre diameter on the formation of calcium oxalate plates	108
5.2.1 Relation between the number of plates and the fibre diameter	114
Chapter 6 Sources of Variation on Mechanical Properties – Results and Discussion	118
6.1 Yield (%) of growth stages	118
6.2 Moisture regain (%)	119
6.3 Diameter variations and their effect on mechanical properties	120
6.4 Fibre breakage point and causes of mechanical properties variations	122
6.4.1 Types of breakage	122

6.4.2 Effect of breakage type on mechanical properties	124
6.5 Fibre Location Effect	125
6.6 Effect of Outliers	129
6.6.1 Effect of outliers on Tensile Stress	130
6.6.2 Effect of outliers on Modulus	131
6.6.3 Effect of outliers on Weibull Parameters	132
Chapter 7 Conclusions	134
7.1 Limitations and Future Work	137
References	138
Appendix	147

List of Tables

Table 2.1 Optimum parameters used for cattail fibre extraction	13
Table 2.2: Summary of testing fibre properties	16
Table 2.3: Sample ID	17
Table 2.4: Limit values of mechanical properties of flax fibre	32
Table 3.1: Weibull parameter of tensile stress obtained from linear regression method	37
Table 3.2: Example data set of 5 sample fibres	26
Table 3.3: Example calculation of reliability for 5 data set	28
Table 3.4: Weibull parameters of tensile stress using Python	53
Table 3.5: Weibull Parameters of modulus (Linear Regression – Excel)	56
Table 3.6: Weibull parameters for modulus using Python	71
Table 4.1: Suitability (%) of cattail fibre	79
Table 4.2: Average suitability (%) of different growth stages	82
Table 4.3: Ranking along the length	84
Table 4.4: Average Ranking of lengths	85
Table 4.5: Ranking of 5 growth stages	86
Table 4.6: Ranking along combination of growth stage and length	93
Table 4.7 Ranking of different parameters	95
Table 4.8: Summary table of ranking	97
Table 5.1: Dimensions and frequency of Calcium Oxalate plates at various growth stages	105
Table 5.2: Atomic % of cattail fibre at different growth stages	107
Table 5.3: Dimensions and frequency of Calcium Oxalate plates from different extraction methods	113
Table 5.4: Average atomic % of elements from different extraction method	116

Table 6.1: Fibre yield (%) of different growth stages	118
Table 6.2: Moisture Regain (%) of different growth stages at 75.5% RH	120
Table 6.3: Fibre breaking point and types of breakage for different growth stage	124
Table 6.4: Mechanical properties of fibre at different breaking point	125
Table 6.5: Mechanical properties of fibres from different locations	128
Table 7.1: Summary table	136

List of Figures

Figure 2.1: Cattail plant of (a) non-flower (NF) stage; (b) flower (F) stage; (c) late flower (LF) stage; (d) flower without male inflorescence (FM) stage; (e) mature (M) stage	13
Figure 2.2: Water bath for cattail fibre extraction with control panel	13
Figure 2.3: Extracted fibre of (a) NF stage; (b) F stage; (c) LF stage; (d) FM stage; (e) M stage	15
Figure 2.4: Flow chart of cattail fibre extraction	15
Figure 2.5: Sample fibre with frames of (a) 1-inch; (b) 2-inches; (c) 3-inches	17
Figure 2.6: Microscope connected with monitor for diameter measurement	18
Figure 2.7: Fibre kept in a desiccator for humidity conditioning	19
Figure 2.8: Flow chart of Weibull distribution using Python	25
Figure 2.9: (a) Process flow of suitability analysis; (b) flowchart of suitability (%) using Python; (c) flowchart of ranking (combination of growth stage and length) using Python	34
Figure 2.10: Environmental Scanning Electron Microscope (Manitoba Institute for Materials, University of Manitoba)	35
Figure 3.1: Relationship between the difference between experimental and predicted Weibull values with the coefficient of variation (CV%) of tensile stress	38
Figure 3.2: Relationship between shape parameter and coefficient of variation of tensile stress	40
Figure 3.3: $\ln(\ln(1/1-F))$ vs $\ln(\text{Tensile Stress})$ curve for 5 growth stages with L1 length and the DR estimator	42
Figure 3.4: $\ln(\ln(1/1-F))$ vs $\ln(\text{Tensile Stress})$ curve for 5 growth stages with L2 length and the DR estimator	43

Figure 3.5: $\ln(\ln(1/1-F))$ vs $\ln(\text{Tensile Stress})$ curve for 5 growth stages with L3 length and the DR estimator	43
Figure 3.6: $\ln(\ln(1/1-F))$ vs $\ln(\text{Tensile Stress})$ curve for 5 growth stages with L1 length and the MR estimator	44
Figure 3.7: $\ln(\ln(1/1-F))$ vs $\ln(\text{Tensile Stress})$ curve for 5 growth stages with L2 length and the MR estimator	44
Figure 3.8: $\ln(\ln(1/1-F))$ vs $\ln(\text{Tensile Stress})$ curve for 5 growth stages with L3 length and the MR estimator	45
Figure 3.9: $\ln(\ln(1/1-F))$ vs $\ln(\text{Tensile Stress})$ curve for 5 growth stages with L1 length and the HE estimator	45
Figure 3.10: $\ln(\ln(1/1-F))$ vs $\ln(\text{Tensile Stress})$ curve for 5 growth stages with L2 length and the HE estimator	46
Figure 3.11: $\ln(\ln(1/1-F))$ vs $\ln(\text{Tensile Stress})$ curve for 5 growth stages with L3 length and the HE estimator	46
Figure 3.12: Tensile stress vs Probability of survival curve of 5 growth stages with L1 length and the DR estimator	48
Figure 3.13: Tensile stress vs Probability of survival curve of 5 growth stages with L2 length and the DR estimator	49
Figure 3.14: Tensile stress vs Probability of survival curve of 5 growth stages with L3 length and the DR estimator	49
Figure 3.15: Tensile stress vs Probability of survival curve of 5 growth stages with L1 length and the MR estimator	50
Figure 3.16: Tensile stress vs Probability of survival curve of 5 growth stages with L2 length and the MR estimator	50

Figure 3.17: Tensile stress vs Probability of survival curve of 5 growth stages with L3 length and the MR estimator	51
Figure 3.18: Tensile stress vs Probability of survival curve of 5 growth stages with L1 length and the HE estimator	51
Figure 3.19: Tensile stress vs Probability of survival curve of 5 growth stages with L2 length and the HE estimator	52
Figure 3.20: Tensile stress vs Probability of survival curve of 5 growth stages with L3 length and the HE estimator	52
Figure 3.21: Weibull graph for the Table 3.2 data set	27
Figure 3.22: Relationship between tensile stress and probability of survival- example calculation	28
Figure 3.23: Relation between shape and scale parameter obtain from Excel and Python	54
Figure 3.24: Relationship between the difference between experimental and predicted Weibull average values with the coefficient of variation (CV%) of modulus	57
Figure 3.25: Relationship between shape parameter and coefficient of variation (%) of modulus	57
Figure 3.26: Relationship between CV% and the percentage difference between scale parameter and average experimental modulus	58
Figure 3.27: Relationship between CV% and the percentage difference between scale parameter and average Weibull modulus	59
Figure 3.28: Relationship between CV% and the percentage difference between scale parameter and standard deviation of modulus	60
Figure 3.29: $\ln(\ln(1/1-F))$ vs $\ln(\text{modulus})$ curve of 5 growth stages with L1 length and the DR estimator	60

Figure 3.30: $\ln(\ln(1/1-F))$ vs $\ln(\text{modulus})$ curve of 5 growth stages with L2 length and the DR estimator	61
Figure 3.31: $\ln(\ln(1/1-F))$ vs $\ln(\text{modulus})$ curve of 5 growth stages with L3 length and the DR estimator	61
Figure 3.32: $\ln(\ln(1/1-F))$ vs $\ln(\text{modulus})$ curve of 5 growth stages with L1 length and the MR estimator	62
Figure 3.33: $\ln(\ln(1/1-F))$ vs $\ln(\text{modulus})$ curve of 5 growth stages with L2 length and the MR estimator	62
Figure 3.34: $\ln(\ln(1/1-F))$ vs $\ln(\text{modulus})$ curve of 5 growth stages with L3 length and the MR estimator	63
Figure 3.35: $\ln(\ln(1/1-F))$ vs $\ln(\text{modulus})$ curve of 5 growth stages with L1 length and the HE estimator	63
Figure 3.36: $\ln(\ln(1/1-F))$ vs $\ln(\text{modulus})$ curve of 5 growth stages with L2 length and the HE estimator	64
Figure 3.37: $\ln(\ln(1/1-F))$ vs $\ln(\text{modulus})$ curve of 5 growth stages with L3 length and the HE estimator	64
Figure 3.38: Modulus vs Probability of survival curve of 5 growth stages with L1 length and the DR estimator	66
Figure 3.39: Modulus vs Probability of survival curve of 5 growth stages with L2 length and the DR estimator	67
Figure 3.40: Modulus vs Probability of survival curve of 5 growth stages with L3 length and the DR estimator	67
Figure 3.41: Modulus vs Probability of survival curve of 5 growth stages with L1 length and the MR estimator	68

Figure 3.42: Modulus vs Probability of survival curve of 5 growth stages with L2 length and the MR estimator	68
Figure 3.43: Modulus vs Probability of survival curve of 5 growth stages with L3 length and the MR estimator	69
Figure 3.44: Modulus vs Probability of survival curve of 5 growth stages with L1 length and the HE estimator	69
Figure 3.45: Modulus vs Probability of survival curve of 5 growth stages with L2 length and the HE estimator	70
Figure 3.46: Modulus vs Probability of survival curve of 5 growth stages with L3 length and the HE estimator	70
Figure 3.47: Relationship between shape parameter of modulus and CV% - Python (LR method with DR estimator) and Excel (LR method with DR estimator)	72
Figure 3.48: Relationship between the shape parameters of modulus by Python programming (LR and MLE) and standard deviation	73
Figure 3.49: Relationship between shape parameter of modulus by Python programming (LR and MLE) and CV%	73
Figure 3.50: Relationship between the (%) difference of scale parameters from MLE and LR of modulus with the CV%.	74
Figure 3.51: Relationship between scale parameters of modulus obtained from Python and standard deviation	75
Figure 3.52: Relationship between the difference percentage of scale parameters of modulus from MLE and LR with the standard deviation.	75
Figure 3.53: Relationship between the shape parameters and fibre lengths	76
Figure 4.1: Average ranking of different growth stages considering different parameters (average of length and average limit value data)	88

Figure 4.2: Ranking of growth stages considering all conditions with different limit value for average length (average of lengths and parameter combinations)	89
Figure 4.3: Ranking of growth stage considering (a) 1 parameter-S; (b) 1 parameter-R; (c) 1 parameter-Y; (d) 2 parameters-S/R; (e) 1 parameter-S; (f) 2 parameters-Y/R; (g) 3 parameters-S/R/Y	91
Figure 4.4: No. of the highest ranking of growth stages from the ranking along both length and growth stages	94
Figure 4.5: Average combined ranking of growth stage and length	94
Figure 4.6: Average ranking of parameters with different limit value	96
Figure 5.1: ESEM image of fibres from NF stage - (a) Fibre 1 (b) Fibre 2 (c) Fibre 3 (d) Fibre 4	100
Figure 5.2: ESEM image of fibre from F stage - (a) Fibre 1 (b) Fibre 2 (c) Fibre 3 (d) Fibre 4	101
Figure 5.3: ESEM image of fibre from LF stage - (a) Fibre 1 (b) Fibre 2 (c) Fibre 3 (d) Fibre 4	102
Figure 5.4: ESEM image of fibre from FM stage - (a) Fibre 1 (b) Fibre 2 (c) Fibre 3 (d) Fibre 4	103
Figure 5.5: ESEM image of fibre from M stage - (a) Fibre 1 (b) Fibre 2 (c) Fibre 3 (d) Fibre 4	104
Figure 5.6: Different parts of cattail leaf and locations of fibre	109
Figure 5.7: ESEM image of mechanically extracted mature fine fibre from the center of leaf (a) Fibre 1; (b) Fibre 2; (c) Fibre 3; (d) Fibre 4	110
Figure 5.8: ESEM image of chemically extracted mature fine fibre (a) Fibre 1; (b) Fibre 2; (c) Fibre 3; (d) Fibre 4	111

Figure 5.9: ESEM image of chemically extracted mature coarse fibre (a) Fibre 1; (b) Fibre 2; (c) Fibre 3; (d) Fibre 4	112
Figure 6.1: Water content (%) of cattail plant from 5 different growth stages	119
Figure 6.2: Relation between diameter and tensile stress	121
Figure 6.3: Relation between diameter and modulus	122
Figure 6.4: (a) Schematic diagram of granular failure; (b) Schematic diagram of brittle fracture; (c) Schematic diagram of ductile fracture; (d) Schematic diagram of fibrillar failure; (e) Schematic diagram of tensile fatigue (f) ESEM image of Node point (Adapted from Yu, 2021)	123
Figure 6.5: (a) Three-dimensional (3D) X-Ray image of cattail leaf; (b) X-Ray image of longitudinal section of cattail leaf; (c) X-Ray image of cross-section of cattail leaf	126
Figure 6.6: X-Ray image of (a) Dorsal fibre (b) Ventral fibre (c) Central fibre	127
Figure 6.7: Variation of (a) Diameter; (b) Tensile stress; (c) Modulus of fibres from different locations	129
Figure 6.8: Average tensile stress (a) before removing outliers; (b) after removing outliers	130
Figure 6.9: Average modulus (a) before removing outliers; (b) after removing outliers	131

Abbreviations

ASTM	American Association of Textile Chemists and Colorists
ANOVA	Analysis of Variance
ESEM	Environmental Scanning Electron Microscopy
EDS	Energy-Dispersive X-ray Spectroscopy

Chapter 1 Introduction

For decades, cotton and polyester fibres have been used widely in apparel and non-apparel textile applications like composites, implants (medical textiles), wound dressings, and so forth. Automobile and aviation industries also use polyester, nylon, glass, carbon, aramid, and polypropylene fibres (Wambua et al., 2003). However, these synthetic fibres are not environmentally friendly to produce, are expensive, and generate greenhouse gases (Khan, 2016). For example, the Japanese Carbon Fibre Manufacturers Association reported in a life-cycle assessment (LCA) that 20 tons of carbon dioxide gas is emitted into the environment to produce 1 ton of carbon fibre used for composites (Shioya & Kikutani, 2015). Similarly, Joshi et al. (2004) found that 1 ton of glass fibre production emits 2.04 tons of carbon dioxide. In addition, both these fibres require a high amount of energy for production and are not biodegradable (Barber & Pellow, 2006). A sustainable, renewable waste biomass fibre needs to be found.

1.1 Natural Fibres

Because they are eco-friendly, lightweight, strong, and economical, natural fibres have already begun to replace expensive synthetic fibres like glass fibre in numerous engineering applications, including the automobile and aviation industries. In recent years, the use of natural fibres (flax and hemp) in composite materials has increased because legislation is forcing automobile manufacturers to recycle and reuse materials, resulting in a growing number of bio-based materials with biodegradable and eco-friendly resources (Ashik & Sharma, 2015; Pickering et al., 2016); fibre-reinforced composites can create lightweight parts with optimum mechanical properties (Yan et al., 2014). Flax is one of the most used fibres for composites in the automobile and aviation industries (Avril et al., 2012).

Flax and hemp are both natural lightweight fibres but are grown as agricultural crops, which increases production costs. In addition, these plants can be harvested only once a year, leading to an inconsistent supply of fibres throughout the year, which is not appropriate for industries.

1.2 Cattail Fibres

Cattail is a waste biomass fibre extracted from the *Typha latifolia* L. plant and may be a suitable replacement for flax fibre. Cattail fibres' mechanical properties are similar; it is lighter than flax (density of flax: 1.5 g/cc; density of cattail: 1.25 g/cc), and production is cheaper since cattail grows naturally and abundantly in bogs and fens, roadside ditches, riverine, prairie pothole and lacustrine marshes; and wet meadows (Mortazavi & Moghadam, 2009; Grace & Harrison, 1986). Several species of *Typha* plant are available all over the world: *Typha latifolia*, the most common and prevalent species, typically known as cattail, spread across the entire northern hemisphere and Australia (McLellan & Moustafa, 2011); *Typha angustifolia* is also widespread and is considered an invasive species in North America (Stuckey & Salamon, 1987); *Typha domingensis* is found in the Southern parts of America and Australia (Akkol et al., 2011). In addition, *Typha orientalis*, is found in Australia, Asia, and New Zealand (Harris, 1999). While *T. laxmannii*, *T. minima*, and *T. shuttleworthii* are limited to Asia and southern Europe (Clegg, 1967). Among these numerous species, *Typha latifolia* is used in this study. Since cattail grows naturally, it does not require any crop inputs (such as fertilizer, fuel, or agrochemicals). In addition, cattail can be harvested multiple times in a calendar year: perhaps a solution for a consistent supply of fibres throughout the year. Cattail, harvested multiple times per year and used for composites in industries, would add tremendous value to the composite industry in consistent supply, low cost, and sustainability. *The current research aims to determine the suitability of cattail fibres from different growth stages.*

1.2.1 Scope of Cattail Fibre

Since cattail species are productive, abundant, and rich in feed value, despite their invasive characteristics, they have long been considered a potential crop (Dubbe et al., 1988). Water filtration and flood protection are vital functions of cattail plants that provide a protective covering for wildlife (Houlahan et al., 2006; Morton, 1975). Many indigenous populations use cattail for many purposes (J. F. Morton, 1975), such as rugs, sandals, room partitions, ropes, and coarse mats, all made from the stems and leaves of cattail (Dalziel, 1937). Cattail pollen and floss have been used as fillers in pillows and mattresses. (Marsh, 1959 as cited in Morton, 1975) confirmed that instead of kapok manufactured in Chicago, numerous cattail flosses were used in life jacket manufacturing in World War II, and the flosses have been used in sleeping bags and baseballs as filling materials (Timmons et al., 1963). Ancient people also believed that the cattail flowers had healing powers for injuries from cuts and burns (Maiden, 1889, as mentioned in Morton, 1975).

Cattail's distinctive attributes include its global distribution, local availability, rapid growth, recycling, hygroscopicity, biodegradability, non-abrasive nature, and availability in several forms (Othman et al., 2012). Recent studies show that all of these characteristics have attracted the attention of researchers hoping to take advantage of the versatility of cattail in various industrial applications.

1.2.2 Industrial Use of Cattail Fibre

A study by Krus et al. (2014) revealed that *Typha angustifolia* L. leaves provide excellent thermal insulation and load-bearing properties. Because of these attributes, it is an excellent contender for the production of sustainable building materials with high load-bearing capacity and thermal insulation. Another study was conducted on the structure of cattail fibre assemblies to determine their performance in removing spilled oil from water (Cao et al., 2018). The study's results revealed that the oleophobic and hydrophobic

properties of the cattail fibre could effectively remove around 70% to 90% of oil contamination. Bajwa et al. (2015) showed that cattail fibres could be used as a component in producing composite panels characterized by their high mechanical properties. A study was conducted by Wuzella et al. (2011) to develop biobased and binder-free composite materials. The study's results revealed that the mechanical properties of these materials are up to 15% higher than the traditional natural fibre-based composites like cotton. Further, the cellulose content from the cattail plant can be used to produce nanofibres that are ideal for various applications such as packaging and electronic display (Thiripura Sundari & Ramesh, 2012). These discoveries have discovered that the cattail fibres can replace traditional fibres in the production of bio-based composite materials. Hasan et al. (2022) optimized an extraction method, and Shadhin et al. (2021) used the fibre to produce a fibre-reinforced composite. However, all the research on cattail fibre has used mature cattail plants; no work has applied the plant fibre's different maturities (growth stages) to composites.

1.3 Impact of Maturity on Fibre Properties

The maturity of the hemp plant negatively impacts fibre quality due to the development of fibre cells in the plant with the plant's maturity. Obtaining the stem section with solely primary fibres or minimal secondary fibre content is desirable for hemp or any other bast fibre, as secondary fibre development reduces the fibre quality for textile application (Hernandez et al., 2007). In addition, the final production and quality of flax fibre crops are affected by each stage of fibre cell growth of the plant. The molecular development of flax fibres has a massive impact on the improvement of fibre characteristics that helps the fibre in using versatile applications (Mokshina et al., 2018). The mechanical and physical properties of the secondary cell wall of the cotton fibre are vital in yarn and fabric quality. That is why completing secondary wall growth before drying is crucial for cotton production.

A fully grown, mature cotton plant contains fibres with a developed secondary cell wall that cannot be found in the young cotton plant (Cotton Incorporated, n.d.).

Vetayasuporn, (2007) identified that the cattail leaf consists of mostly cellulose (63%), hemicellulose (9.6%), moisture content (9.6%), lignin and pectin (9.6%) and others (8.2%). Cattail plants grow in a colony with ramets, including leaf development and their related rhizomes and inflorescences (Grace & Harrison, 1986). Witztum & Wayne (2014) noticed fibres in the dorsal and ventral parts of *the Typha* leaf in such an orientation that creates a tensegrity structure that gives the leaf stability. In addition, they noticed a reduced fibre length in the leaf with plant maturity. During cattail maturation, the plants undergo several developmental phases, such as the vegetative, flower, and mature stages. The cattail fibre extracted from these different growth stages may be similar or suitable for specific applications. Depending on the fibre quality, it might be possible to harvest cattail plants multiple times annually, as a recent study by Koga et al. (2022) found no difference in mechanical and hygroscopic properties of cattail fibres harvested at 90 and 120 days. In this work, the authors regrew cattails from the rhizomes in a controlled environment.

1.4 Impact of Length on Fibre Properties

Fibre length is one of the most significant factors impacting the behaviour of composites because fibre length has a crucial function in forming an interfacial bonding between the matrix and the fibre. Theoretically, longer fibres show improved thermosetting of composite, and abrasive wear resistance, while shorter fibres are compatible with thermoplastic composites (Abdelbary & Mohamed, 2021). However, in wear conditions, the abrasive particles destroy the longer fibres locally, while the remainder contributes to the composite's wear resistance. In contrast, excessively short fibres reduce the load-bearing capacity and are responsible for an excessive wear rate, while excessively long fibres result in simple fibre pull-out (Abdelbary & Mohamed, 2021). *Therefore, in the present study, three*

different fibre lengths were used from five different growth stages to determine their suitability in composites.

1.5 Impact of Extraction method on Fibre Properties

Several previous studies have shown that the reduction in the degree of polymerization of the cellulose chain due to the expanding amount of mechanical processing stages in fibre extraction and processing causes degradation of the mechanical properties of the cattail fibre (Hughes, 2012). Minimally processed fibres may result in good composites and fibres with good mechanical properties (Miao & Finn, 2008). Appropriate parameters of the retting process must be determined to obtain fibre with higher-quality mechanical properties. The retting process involves dissolving the non-cellulosic resources from the fibre bundle via enzyme treatment (Lee et al., 2020). Depending on the retting process and conditions, this complex process can affect fibre quality. For example, over-retted fibre might suffer a loss of strength, whereas under-retted fibres might not separate from one another (Preisner et al., 2014). Retting might be accomplished in several ways: water retting, chemical retting, enzyme retting, and dew retting (Sadrmanesh & Chen, 2019). Enzyme retting is the most popular of these processes due to the soft process conditions, specificity, and excellent selectivity.

In contrast, chemical retting requires the least retting time with well-regulated fibre quality (Lee et al., 2020). However, Lee et al. (2020) declare that water and dew retting are cheaper, give a higher fibre yield (%), and create a smaller amount of pollution, even though these processes are more time-consuming. Besides these retting methods, a few less popular and non-commercial techniques of retting can be seen, for example, microbial retting (Ramaswamy et al., 1994), microwave retting (Nair et al., 2013), and gel retting (Pandey, 2016), to name a few.

Numerous retting procedures were implemented in past studies to extract fibre from the cattail leaf: water retting, enzyme retting, acid retting, alkali retting, and alcohol retting (Chakma, 2018; Sana et al., 2014). Chakma (2018) declared that all retting processes failed to work on cattail fibre extraction except for alkali retting. However, he could not conclude the alkali concentration, temperature, time, and material: liquor (M:L) ratio and their effects on extraction quality. However, Hasan (2019) further discovered the optimum retting conditions (time, temperature, and concentraion) for cattail fibre extraction. They tried to extract on a tiny scale (1 to 3 g) but could not make any conclusions about the large-scale commercial process.

1.6 Variation on Properties of Natural Fibre

Due to the enormous variability of natural textile fibre, the fineness or coarseness varies from fibre to fibre and along the length of the same fibre (Lafranche et al., 2015). As a result, the measured tensile properties (stress and modulus) data using a predetermined diameter value is inaccurate. Natural textile fibre like flax has a tensile strength ranging between 343 and 2000 MPa and Young's modulus between 15 and 103 GPa, respectively (Yan et al., 2014; Yukseloglu & Yoney, 2016). Many researchers have applied statistical analysis, such as analysis of variance (ANOVA), but failed to obtain any significant differences in mechanical properties due to large standard deviations (Zafeiropoulos & Baillie, 2007).

1.7 Scope of Weibull Distribution

Since cattail is a natural fibre, its physical and mechanical properties vary widely (Shadhin et al., 2022). Currently, Weibull distribution, a statistical analysis based on the weak link effects, is commonly applied to predict the tensile properties of fibre-reinforced composites, and decisions can be made on the reliability of biomass fibres (Morton et al., 1996). However, the severity of variations in these fibres makes it difficult to conclude the

reliability and differences among the samples based on the Weibull modulus. In addition, the traditional Weibull probability plot is based on a match between the model's probability plots and the shape of the data. Due to the non-linearity of the Weibull transformations, the shape of the plot of data randomly produced from a distribution model can be drastically different from the shape of the theoretical Weibull probability plot (Jiang, 2014).

Moreover, it is unreliable to choose the distribution model according to the shape of the plot curve (Jiang, 2014), thereby making decisions based on the Weibull distribution is not advisable. Moreover, Naik & Fronk, (2016) mentioned the increase of tensile stress and modulus with an increase in kenaf fibre's gauge length, and the Weibull parameters fluctuated with an increase in fibre length. Therefore, the result did not fit with the weak-link theory.

1.7.1 Effect of Weak-Link Theory on Weibull Distribution

Weibull distribution is based on the weakest link theory, which means testing a fibre material at a shorter gauge length will provide higher strength. While evaluating the fitness of the Weibull model with fibre strength distributions, tensile tests are performed on several fibres having exactly the same radius and length by varying the gauge length. The Weibull parameters are attained from the experimental data by both the maximum likelihood and linear regression methods (Quinn & Quinn, 2010). While the majority of the research found the usefulness of the weakest link theory and Weibull distribution model when using shorter length fibre (up to 10 mm), some suggested that the model does not work for a larger gauge length and strain rate (100 mm^{-1}) (Pan et al., 1997). Further, a single natural fibre like cattail contains multiple flaw populations, such as nodes, oxalate plates, and so forth (Yu, 2021); therefore, their strength distributions cannot be obtained from the standard Weibull distribution. Furthermore, the Weibull model cannot differentiate and rank the same fibre from different growth stages.

Fibre would break at the weakest point while the tensile load is applied to a whole fibre length, whereas it would not have broken at the weakest point if two equal halves of the length were used. Therefore, the weakest point is not independent; rather, it depends on fibre length. This weak-link effect can change the value of the tensile properties of the fibre. For a non-woven mat, Martin et al. (2016) used 50mm fibre lengths, whereas others used various lengths. The outcomes of the Weibull distribution exposed a fundamental weakness in the weak-link modelling. The Weibull plots showed strong linearity for most of the distribution, although spots at the extremities deviated from the line. However, the shallow values have the most significant impact on weak link failure. That might be why Pickering & Murray, (1999) discovered 8-25% errors in estimating tensile stresses at 2-500 mm from results at 1 mm gauge length. The two-parameter Weibull distribution was found to fit polyester strengths (Amaniampong & Burgoyne, 1994), although the three-parameter distribution was preferable for breaking strain. The application of Weibull to evaluate the length effects on the strength of the wool fibre is discussed by Zhang et al. (2002).

1.8 Scope of the Thesis

In this study, to resolve the limitations of the Weibull model, a computational method is used to check the suitability of cattail fibres for composite applications by comparing them with flax fibre properties. In brief, the flax fibre properties of the highest, average, and lowest values will be thresholds which will be compared with the cattail fibre properties for the purpose of ranking. The details analyzing the process are given in Chapter 2.

The primary objective of this research is to check the variability of cattail fibres from five different growth stages using the Weibull distribution model (Chapter 3) and rank the cattail fibre properties from five different growth stages using Python computer programming (Chapter 4). Finally, the work investigates the fibre development in the cattail

plant from five different growth stages (Chapter 5) and checks the sources of variation in the cattail fibres (Chapter 6).

Chapter 2 Materials and Methods

2.1 Cattail Fibre extraction

2.1.1 Plant Collection and Phenological Growth Stage Identification

Cattail plants of five different growth stages were collected from Kings Park, Winnipeg, Manitoba (Latitude: 49° 47' 53.16" N and Longitude: -97° 07' 21.72" W) between July and August 2021.

The phenological growth stages were chosen following the research of Sobrero et al. (1997) on another species of cattail named *Typha subulate* located in Argentina. The authors identified growth stages as corm re-growth, the emergence of new shoots from rhizome buds, vegetative growth, flowering (emergence of pistillate and staminate flowers, spathe leaf, anthesis of male flower, loss of male flower, anthesis of female flower), fruit formation, dispersal, and senescence. Further, we communicated with Dr. Randy Wayne (Professor, Cornell University, email: row1@cornell.edu) through email to find names for the growth stages since he had worked with the growth stages of *Typha* plants. His reply was, “*Typha is such a wonderful plant. I am happy to hear that you are working on it. Allan and I only characterized the plants as Vegetative and Flowering, so you can make up your own classification system that best describes the plants you want to characterize-between immature and mature vegetative plants. You could use a continuous scale and classify them by the number of leaves (and call them, for example, plants with three leaves) or a discontinuous scale, for example, fewer than a certain number of leaves (3-5). You could call [those plants] immature, and plants with a greater number of leaves you can call mature.*”

Following the study of Sobrero et al. (1997), the cattail plants, which are just grown and do not have any shoot or flower, were identified as a non-flower (NF) stage or the

emergence of a new shoot (Figure 2.1a, yellow circled). The plants whose floral heads are covered by the pistillate, and staminate spathe leaf were identified as flower (F) stage (Figure 2.1b). In addition, plants with long, thick shoots with both male and female inflorescence were collected and identified as late flower (LF) stage or anthesis of male flower (Figure 2.1c). Moreover, the plants whose male inflorescence of the shoot had fallen were collected as a flower without the male inflorescence (FM) stage or loss of male flower (Figure 2.1d). The brown-coloured matured plants (M) or seeds dispersed from the previous year's growth are shown in Figure 2.1e.

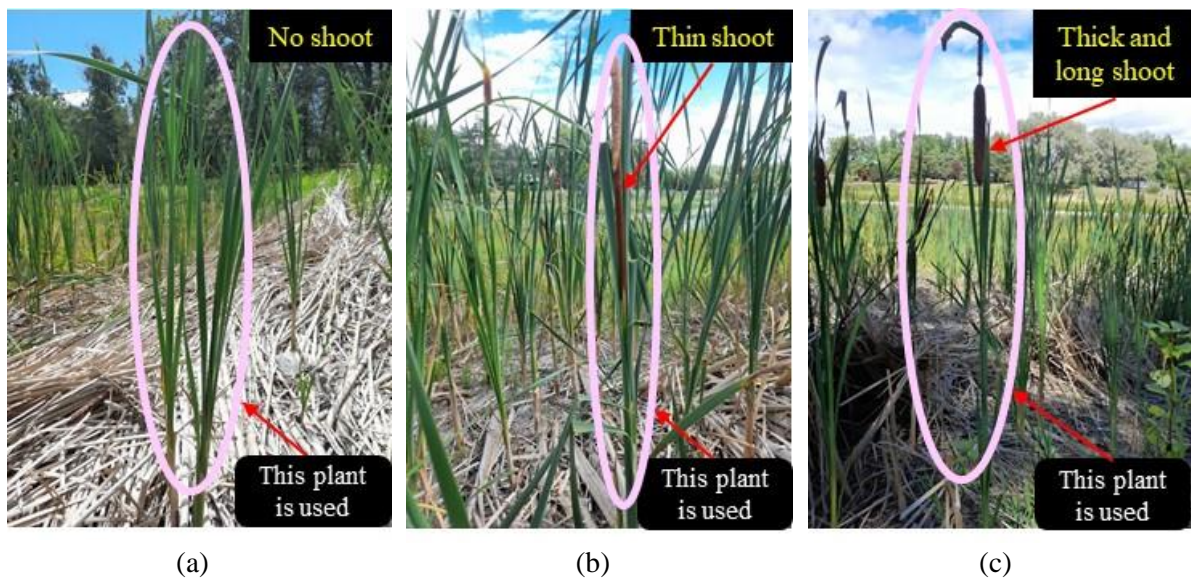


Figure 2.1: Cattail plant of (a) non-flower (NF) stage; (b) flower (F) stage; (c) late flower (LF) stage; (d) flower without male inflorescence (FM) stage; (e) mature (M) stage

2.1.2 Alkali Retting in Water Bath

The collected cattail plants were pre-cut to 6 inches, and each layer of bark and leaf was separated. The weight of these leaves was measured using an electronic balance. The cut leaves and bark were added to a pre-heated alkaline solution in a water bath with a capacity of 12–15 L (Figure 2.2).

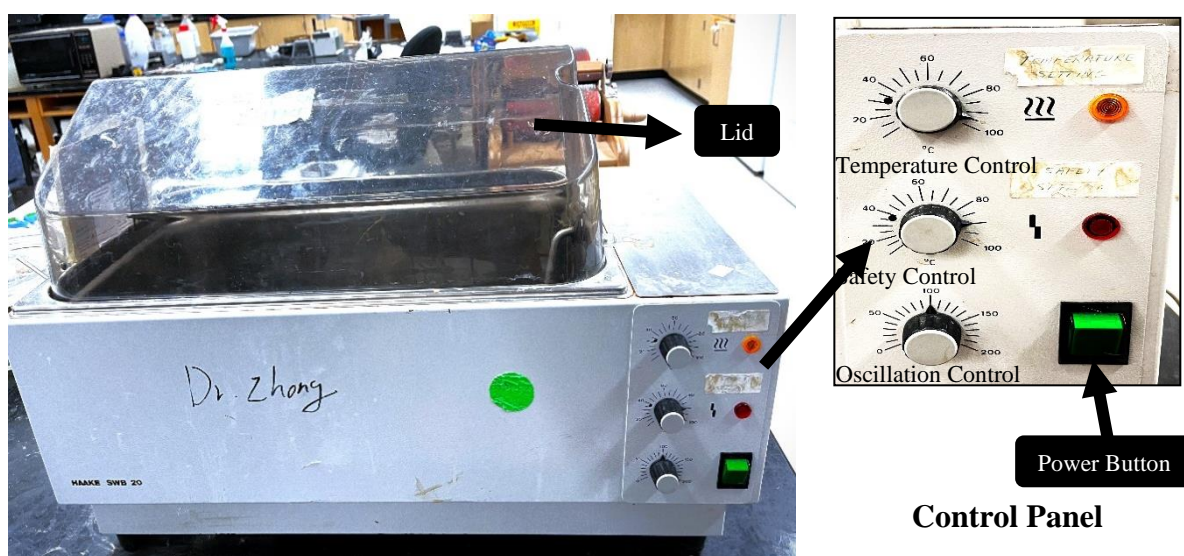


Figure 2.2: Water bath for cattail fibre extraction with control panel

The optimum parameters for alkali retting of cattail fibre, developed by Hasan et al. (2022), are shown in Table 2.1.

Parameters	Optimum Values
Alkali	5% (w/v) KOH solution
Temperature	90°C
Time	4 hours
M:L (Material:Liquor)	1:20

A stock solution of 5% (w/v) KOH (Fisher Scientific, Ontario, Canada) was used in alkali treatment, and 7 litres of the solution was taken from that stock solution and filled up

the water bath. The bath was heated until the temperature reached 90°C. At this point, 200g cattail leaves and bark sample were added to the heated alkali solution and maintained for 4 hours at 90°C. During this process, an oscillation of 100 rpm was implemented. The temperature of the solution was monitored using a thermometer, and the solution was stirred at regular intervals of 20 minutes to ensure the consistent retting of all the samples.

2.1.3 Washing, Neutralizing and Drying

When the fibres were individualized from the melted leaves and bark, they were placed under a continuous flow of hot and then cold water for 5 minutes each. Then the specimen was neutralized using 2% (v/v) acetic acid solution (Fisher Scientific, Ontario, Canada) and again washed with cold water for 5 minutes. Finally, the extracted fibres were dried at room temperature for 24 hours. This procedure was repeated for the plants of all five growth stages. It is worth mentioning that this extraction procedure was based on a previous study by Rahman et al. (2021). The dried extracted fibres of 5 growth stages are displayed in Figure 2.3. A flowchart of the whole extraction process is presented in Figure 2.4.

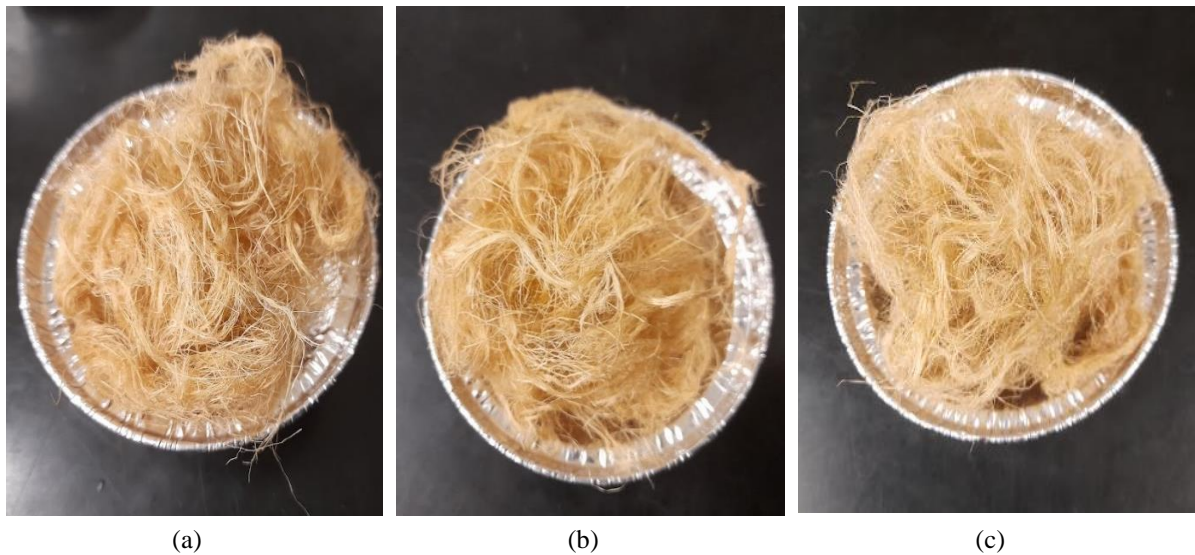




Figure 2.3: Extracted fibre of (a) NF stage; (b) F stage; (c) LF stage; (d) FM stage; (e) M stage

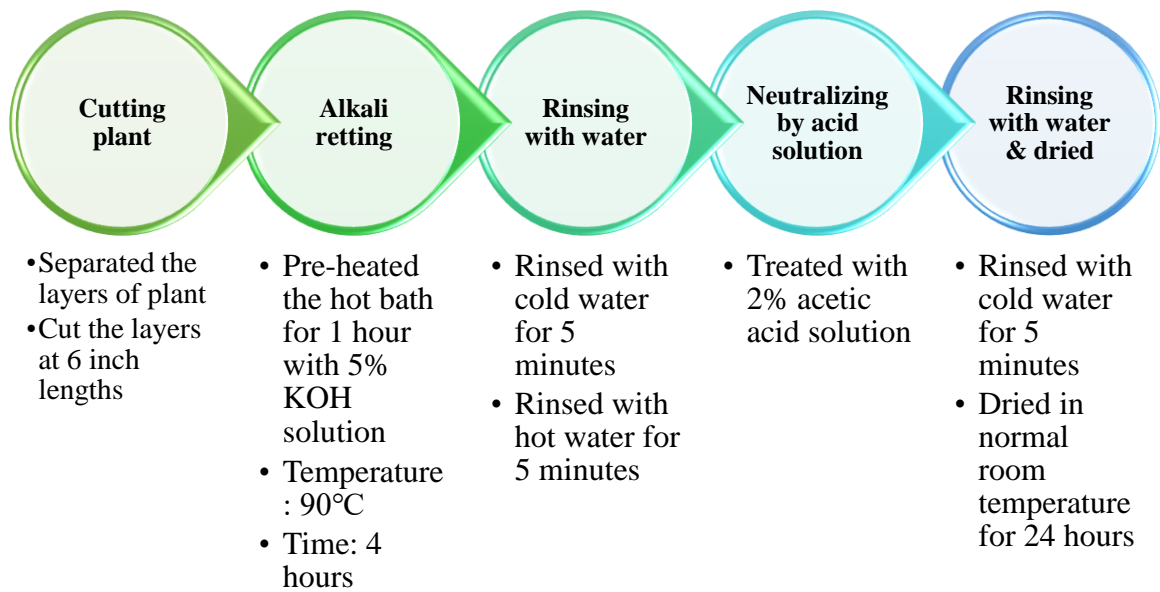


Figure 2.4: Flow chart of cattail fibre extraction

2.2 Measurement of Fibre Properties

The properties of fibre diameter, yield percentage, and tensile properties (tensile stress, tensile strain, Young's modulus, load at break) were measured. A summary of the testing equipment and methods is listed in Table 2.2.

Table 2.2: Summary of testing fibre properties

Properties	Equipment/Methods
Yield (%)	Thermo scientific oven and weight balance
Diameter	Microscope
Mechanical Properties	Instron tensile tester

2.2.1 Yield (%) Measurement

Fibre yield (%) is the ratio of the oven-dried mass of cattail fibre after retting to the mass of cattail plants before retting. The yield (%) of fibre from each of the five growth stages was calculated using Equation 2.1, where M_a is the mass of the extracted fibre and M_b mass of the cattail leaf before extraction.

$$\text{Yield (\%)} = \frac{M_a}{M_b} \times 100\% \quad \text{Equation 2.1}$$

2.2.2 Mechanical Properties Measurement

The mechanical properties of tensile stress, tensile strain, modulus of elasticity (Young's modulus), and load at break were determined. In order to measure the mechanical properties of cattail fibre, a few steps had to be done, such as sample preparation, diameter measurement, conditioning, and tensile testing.

2.2.2.1 Sample Preparation

Fifty single fibres were taken from each batch (5 growth stages \times 3 lengths) to measure the mechanical properties. Each fibre was attached to a paper frame of 1-inch (square hole), 2-inch (circular hole), and 3-inch (circular hole) length (Figure 2.5). Single cattail fibres were selected from each batch and glued to the square or circular hole in the center of the paper frame, as shown in Figure 2.5.

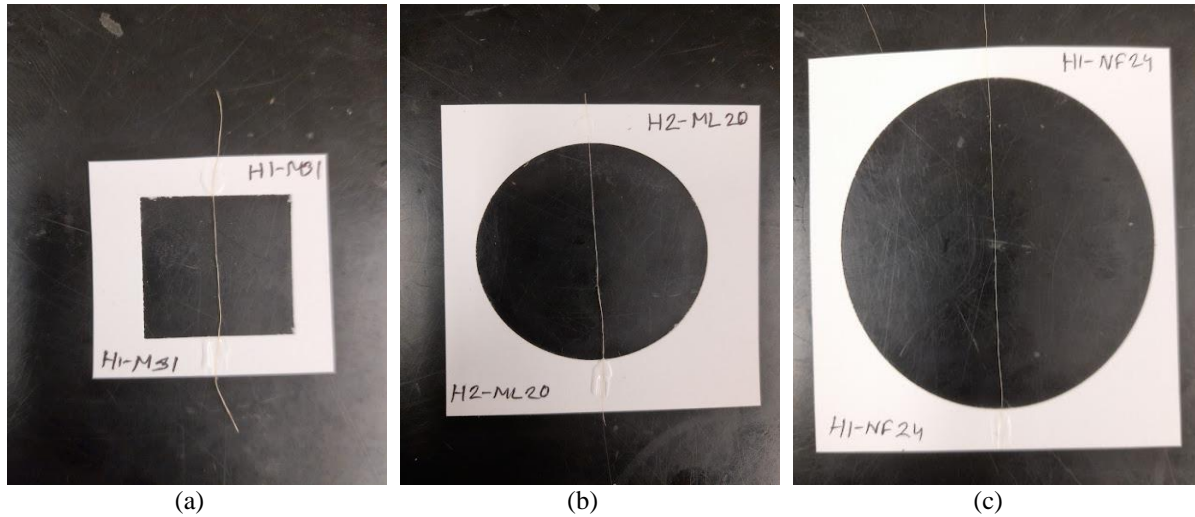


Figure 2.5: Sample fibre with frames of (a) 1-inch; (b) 2-inches; (c) 3-inches

Each fibre from each batch was marked with a unique sample identification (ID) number so that they were traceable. Sample ID was given according to Table 2.3.

Table 2.3: Sample ID

M-L1	FM-L1	LF-L1	F-L1	NF-L1
M-L2	FM-L2	LF-L2	F-L2	NF-L2
M-L3	FM-L3	LF-L3	F-L3	NF-L3

M: Mature stage; F: Flower stage; LF: Late flower stage; FM: Flower without male inflorescence stage; NF: Non-flower stage; L1, L2, L3: fibre length for testing 1-inch, 2-inches, and 3-inches.

2.2.2.2 Diameter Measurement

Using a microscope, the cattail fiber's diameter was measured (Motic, China). The frame was put on a glass slide, and a monitor was used to observe the fibre which is linked to a projection microscope at 90x magnification (Figure 2.6). The diameter of a single fibre mounted on the frame was measured in micrometres (μm). Natural fibres frequently vary in diameter along the length of a single fibre (Morton et al., 1996), hence the diameters were measured at the thinnest visible point., as the breakage region of the fibre would be expected to be at the thinnest place.

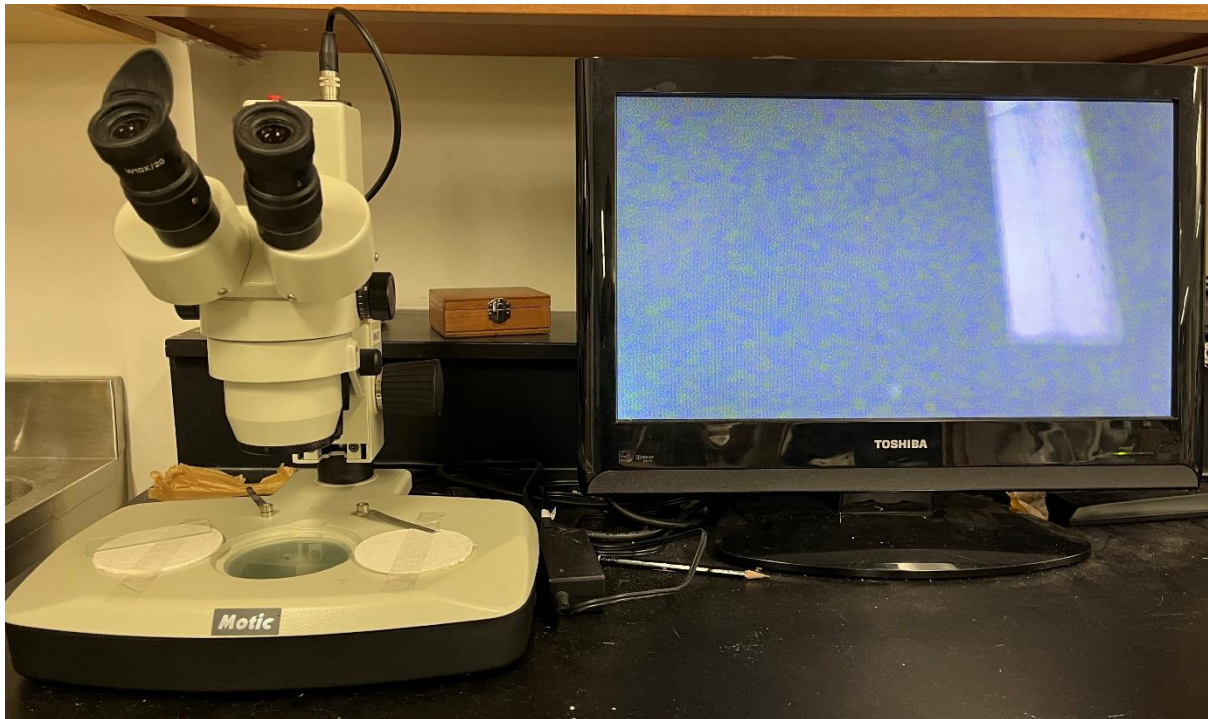


Figure 2.6: Microscope connected with monitor for diameter measurement

2.2.2.3 Humidity Conditioning of Fibre

In order to make the mechanical properties comparable among the five growth stages and three lengths, fibres from all batches were conditioned at a specific relative humidity of 75.5% at room temperature for 24 hours. Conditioning was done using a desiccator (Figure 2.7) containing sodium chloride (NaCl) solution, where a hygrometer was placed in the desiccator to monitor the maintenance of consistent relative humidity. In order for the fibres to absorb moisture, fibre attached with frames were maintained all together on a plate and put in the desiccator.

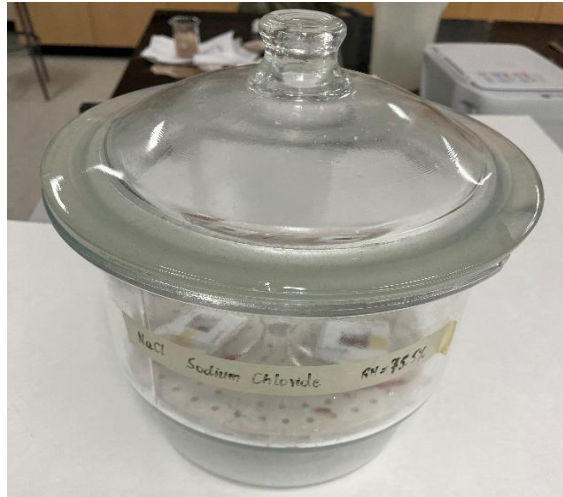


Figure 2.7: Fibre kept in a desiccator for humidity conditioning

2.2.2.4 Tensile Test of Cattail Fibre

The mechanical properties of cattail fibre, such as tensile stress, tensile strain, modulus (Young's), and the load at the break, were measured using an Instron Tensile Tester machine (Model: 5965, SI: VS02075661, Norwood, USA), following the ASTM D3822 standard. To avoid changing the fibre's moisture content, the desiccator containing the fibre frames was brought to the Instron Tensile Tester, where the frames were removed one by one and instantly attached to the testing machine.

The sample fibre frames were set between two jaws of the Instron Tensile Tester in such a manner that the inner length (1 inch, 2 inches, and 3 inches) of the paper frame acted as the gauge length, i.e., the gauge length for measuring the strain was the fibre length inside the hole of the frame. After clamping the frame, the two vertical side edges of the frame were cut with scissors so that the tension was only on the fibre. The upper jaw moved at 20 mm/min in an upward direction, using a 1 kN load cell. "Instron Bluehill 2" software (version 2.26) was used to operate the machine and collect the data. The data was taken at 10ms intervals. All the results of mechanical properties for each fibre from each batch were acquired from the software.

2.3 Statistical Analysis: ANOVA

One-way Analysis of Variance (ANOVA) with the Tukey Post Hoc test was carried out to calculate the statistical significance of the value of tensile stress, tensile strain, and modulus among the batches.

2.4 Statistical Analysis: Weibull Distribution

Weibull distribution was used to characterize the entire distribution of tensile stress and modulus, along with the failure behaviour and reliability analysis of the experimented tensile properties. The two-parameter Weibull distribution has been used in this study to identify the probabilistic tensile stress and modulus, followed by reliability analysis of cattail fibre. The most popular two methods are used to determine the Weibull parameters, i.e., shape parameter and scale parameter.

2.4.1 Weibull Analysis with Linear Regression Method

While using two-parameter Weibull distribution, the cumulative distribution function, stated in Equation 2.2, was used to identify the cumulative probability of failure [F(x)] of cattail fibre for a given set of data (tensile stress or modulus) x, where α and β are the shape and scale parameters, respectively.

$$F(x) = 1 - e^{-\left(\frac{x}{\beta}\right)^\alpha} \quad \text{Equation 2.2}$$

The simplest format of this equation can be generated by applying the natural logarithm twice on Equation 2.2, as shown in Equation 2.3.

$$\ln \left[\ln \frac{1}{1 - F(x)} \right] = \alpha \ln (x) - \alpha \ln (\beta) \quad \text{Equation 2.3}$$

Equation 2.3 can be compared with the equation of straight-line represented in the form of Equation 2.4 and found that $Y = \ln \left[\ln \frac{1}{1 - F(x)} \right]$, $X = \ln (x)$ and $c = -\alpha \ln (\beta)$

$$Y = mX + c \quad \text{Equation 2.4}$$

Various probability estimators are used to determine the probability of failure. These include the median rank estimator (Equation 2.5), Hazen's equation (Equation 2.6), and mean rank estimator (Equation 2.7).

$$F(x) = \frac{i - 0.3}{N + 0.4} \quad \text{Equation 2.5}$$

$$F(x) = \frac{i - 0.5}{N} \quad \text{Equation 2.6}$$

$$F(x) = \frac{i}{N + 1} \quad \text{Equation 2.7}$$

Here, N is the number of experimental measurements, and i is the rank (i^{th} datum) after arranging all the experimental values of tensile properties in ascending order.

$\ln \left[\ln \frac{1}{1 - F(x)} \right]$ and $\ln(x)$ were plotted on a graph, and the value of shape and scale parameters were calculated using the equation of the Weibull line and comparing it with Equation 2.4 after calculating the value of the probability of failure, $F(x)$ using Equation 2.5, Equation 2.6, and Equation 2.7 separately.

The experimental value (x) would be equal to the average Weibull value (σ_{avg}) if the probability of failure, $F(x)$, is 50% (Quinn & Quinn, 2010). Putting these values into Equation 2.3 and after simplification, Equation 2.8 can be formed. Moreover, the average Weibull value (σ_{avg}) can be calculated using the shape and scale parameters in Equation 2.8.

$$\sigma_{\text{avg}} = e^{\frac{\alpha \ln(\beta) - 0.3665}{\alpha}} \quad \text{Equation 2.8}$$

Reliability analysis can also be performed using the Weibull model with the help of Bernard's approximation (Equation 2.9), where probability of survival or reliability of a property, $R(x)$, can be determined.

$$R(x) = 1 - F(x) \quad \text{Equation 2.9}$$

2.4.2 Weibull Analysis with Maximum Likelihood Estimation (MLE)

The maximum likelihood estimation (MLE) method is also used to identify the shape and scale parameters of the two-parameter Weibull distribution. This method calculates the shape and scale factors that maximize the likelihood or give the highest probability of producing the data attained from the tensile testing. In this case, the probability density function (pdf) is used (Equation 2.10) while considering the data are independent and identically distributed.

$$F(x) = \frac{\alpha}{\beta^\alpha} x^{\alpha-1} e^{-\left(\frac{x}{\beta}\right)^\alpha} \quad (x \geq 0; \alpha \geq 0; \beta \geq 0) \quad \text{Equation 2.10}$$

The likelihood function for n number of observations shown in Equation 2.11 is the product (\prod) of the pdf (Equation 2.12).

$$L(x) = \prod_1^n F(x) \quad \text{Equation 2.11}$$

$$\Rightarrow L(x) = \prod_1^n \frac{\alpha}{\beta^\alpha} x^{\alpha-1} e^{-\left(\frac{x}{\beta}\right)^\alpha}$$

$$\Rightarrow L(x) = \frac{\alpha}{\beta^\alpha} \prod_1^n x^{\alpha-1} \times e^{-\left(\frac{\sum x}{\beta}\right)^\alpha} \quad \text{Equation 2.12}$$

Afterwards, to simplify the calculation, the natural logarithm is used.

$$\begin{aligned} \ln[L(x)] &= \ln \left[\frac{\alpha}{\beta^\alpha} \prod_1^n x^{\alpha-1} \times e^{-\left(\frac{\sum x}{\beta}\right)^\alpha} \right] \\ &= \ln \left(\frac{\alpha}{\beta^\alpha} \right)^n + \ln \left[\prod_1^n x^{\alpha-1} \right] + \ln \left[e^{-\left(\frac{\sum_1^n x}{\beta}\right)^\alpha} \right] \\ &= n \ln \left(\frac{\alpha}{\beta^\alpha} \right) + (\alpha - 1) \ln \left[\prod_1^n x \right] - \left(\frac{\sum_1^n x}{\beta} \right)^\alpha \end{aligned}$$

$$= n \ln(\alpha) - \alpha n \ln(\beta) + (\alpha - 1) \sum_1^n \ln(x) - \left(\frac{\sum_1^n x}{\beta} \right)^\alpha$$

Equation 2.13

Partially differentiating Equation 2.13 with respect to α ;

$$\frac{\partial(\ln L)}{\partial \alpha} = n \cdot \frac{1}{\alpha} - n \cdot \ln(\beta) + \sum_1^n \ln(x) - \frac{1}{\beta^\alpha} \sum_1^n [x^\alpha \ln(x)] - [-n \cdot \ln(\beta)]$$

$$= \frac{n}{\alpha} + \sum_1^n \ln(x) - \frac{1}{\beta^\alpha} \sum_1^n [x^\alpha \ln(x)]$$

Equation 2.14

Again, partially differentiating Equation 2.13 with respect to β ;

$$\frac{\partial(\ln L)}{\partial \beta} = -\alpha n \cdot \frac{1}{\beta} - \left[-\alpha \frac{1}{\beta^{\alpha+1}} \sum_1^n x^\alpha \right]$$

$$= -\frac{\alpha n}{\beta} + \frac{\alpha}{\beta^{\alpha+1}} \sum_1^n x^\alpha$$

Equation 2.15

The likelihood is maximized by setting the derivatives to zero. From Equation 2.15,

$$0 = -\frac{\alpha n}{\beta} + \frac{\alpha}{\beta^{\alpha+1}} \sum_1^n x^\alpha$$

$$\Rightarrow \frac{\alpha n}{\beta} = \frac{\alpha}{\beta^{\alpha+1}} \sum_1^n x^\alpha$$

$$\Rightarrow \frac{\alpha n}{\beta} = \frac{\alpha}{\beta^\alpha \beta} \sum_1^n x^\alpha$$

$$\Rightarrow \beta^\alpha = \frac{1}{n} \sum_1^n x^\alpha$$

$$\Rightarrow \beta = \left(\frac{1}{n} \sum_1^n x^\alpha \right)^{\frac{1}{\alpha}} \quad \text{Equation 2.16}$$

Again, in Equation 2.14, putting the derivatives to zero,

$$\begin{aligned} 0 &= \frac{n}{\alpha} + \sum_1^n \ln(x) - \frac{1}{\beta^\alpha} \sum_1^n [x^\alpha \ln(x)] \\ \Rightarrow \frac{n}{\alpha} + \sum_1^n \ln(x) &= \frac{1}{\beta^\alpha} \sum_1^n [x^\alpha \ln(x)] \\ \Rightarrow \frac{n}{\alpha} + \sum_1^n \ln(x) &= \frac{1}{\frac{1}{n} \sum_1^n x^\alpha} \sum_1^n [x^\alpha \ln(x)] ; \text{ (From Equation 2.16)} \\ \Rightarrow \frac{n}{\alpha} + \sum_1^n \ln(x) &= \frac{n}{\sum_1^n x^\alpha} \sum_1^n [x^\alpha \ln(x)] \\ \Rightarrow \frac{1}{\alpha} + \frac{\sum_1^n \ln(x)}{n} &= \frac{\sum_1^n [x^\alpha \ln(x)]}{\sum_1^n x^\alpha} \\ \Rightarrow \alpha &= \left[\frac{\sum_1^n [x^\alpha \ln(x)]}{\sum_1^n x^\alpha} - \frac{\sum_1^n \ln(x)}{n} \right]^{-1} \quad \text{Equation 2.17} \end{aligned}$$

To solve these two equations (Equation 2.16 and Equation 2.17) and find out the value of α and β , iterative computational methods (example: Newton-Raphson method, Gradient method) are popular. In this case, a computer programming language (Python) with a ‘Weibull’ library is used to compute the parameters.

In Python programming language, Weibull statistical modelling can be done in two methods: MLE (Maximum Likelihood Estimation) and LR (Linear Regression) with the ‘Weibull’ library. The coding is the same for both cases except for the name of the method.

2.4.2.1 Weibull Distribution Using Python Code

Weibull distribution was conducted using Python; the source code and pseudocode are shown in Appendix A 40 and A 41. The flow chart provided in Figure 2.8 summarizes the algorithm.

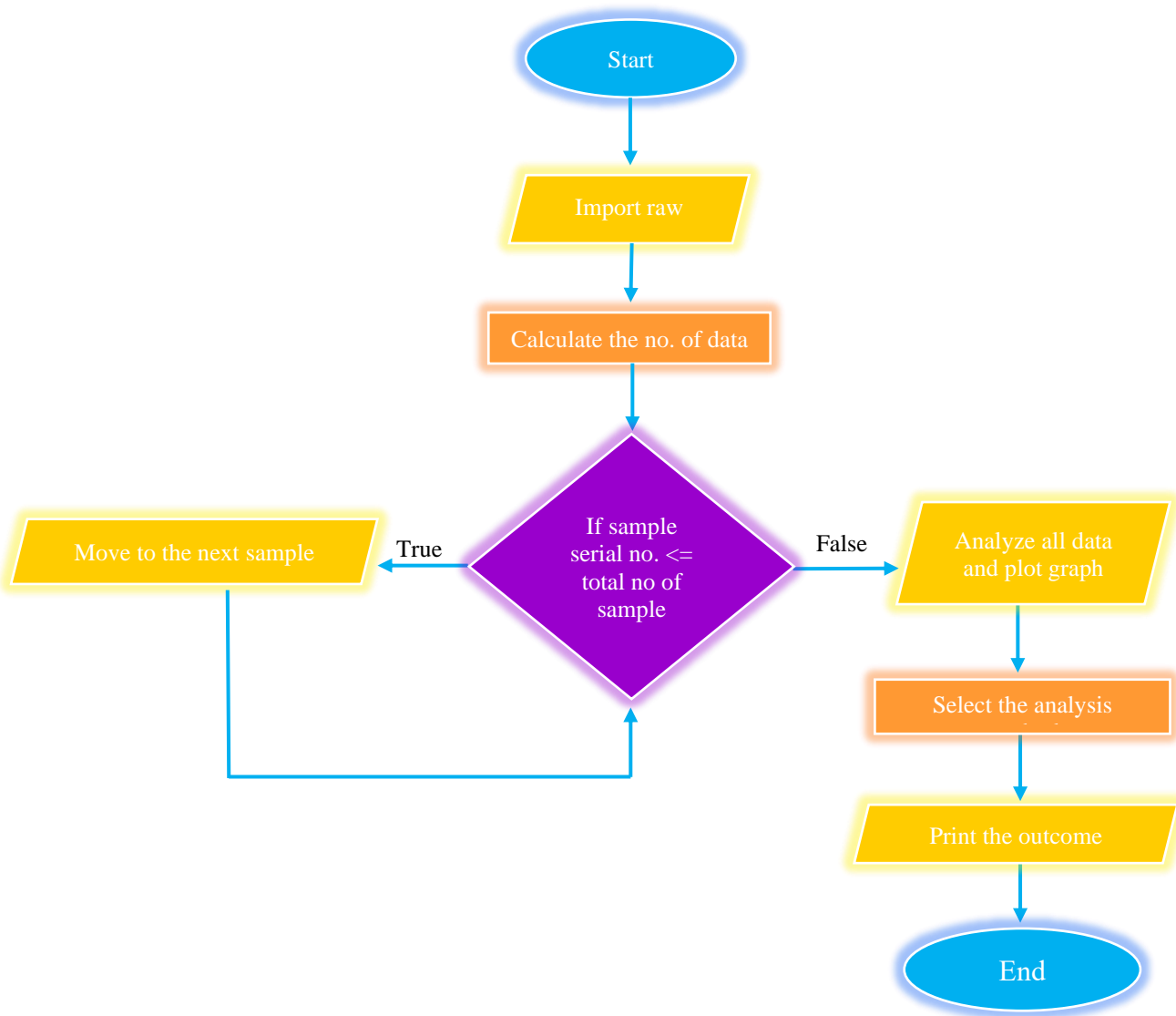


Figure 2.8: Flow chart of Weibull distribution using Python

2.4.3 Sample Calculation of Weibull distribution – Linear Regression Method

The following example uses a set of arbitrary data to demonstrate the process of preparing the Weibull distribution graph. Presume that five fibres gave tensile stress readings of 564, 263, 658, 259, and 487 MPa. This small data set is selected for presenting an illustration of the graph; however, a larger data set is advisable for an appropriate outcome for this distribution. The data set is first arranged in ascending order, as shown in the second column of Table 2.4, and the order number (i) is shown in the first column.

Table 2.4: Example data set of 5 sample fibres

<i>i</i>	Tensile stress (MPa)	$X = \ln(\text{tensile stress})$	$F(x) = (i-0.3)/(n+0.4)$	$Y = \ln[\ln(1/(1-F))]$
1	259	5.556828062	0.12962963	-1.974458694
2	263	5.572154032	0.31481482	-0.972686141
3	487	6.188264123	0.50000000	-0.366512921
4	564	6.335054251	0.68518519	0.144767396
5	658	6.489204931	0.87037037	0.714455486

The natural logarithm of the tensile stress values is calculated (shown in the third column of Table 2.4) to be plotted along the x-axis of the Weibull graph. According to many literature sources (Bergman, 1984; Langlois, 1991; Steen et al., 1992; Sullivan & Lauzon, 1986; Trustrum & Jayatilaka, 1979), the number of samples should be greater than 20 to obtain less biased estimates of the Weibull distribution. The accumulative probability of failure, $F(x)$, is estimated and allocated to an individual datum, as shown in the fourth column in Table 2.4. Three estimators [median rank estimator (Equation 2.5), Hazen's Equation (Equation 2.6), and the Mean rank estimator (Equation 2.7)] were used in the main calculation, and the result was discussed in Chapter 2. However, the median rank estimator (Equation 2.5) is used in this example. Applying the DR estimator, $F(x)$ was estimated to be 0.1296 or 12.96% for the first ($i=1$) datum, as shown in the fourth column in Table 2.4, which signifies that 12.96% of fibres are weaker than the tested specimen that broke at 259 MPa among all tested fibres in a batch, and 87.04% would be stronger. The double logarithm of $[1/(1-F(x))]$ is calculated, shown in the last column of Table 2.4 and plotted along the y-axis of Weibull graph in accordance with Equation 2.3 as shown in Figure 2.9.

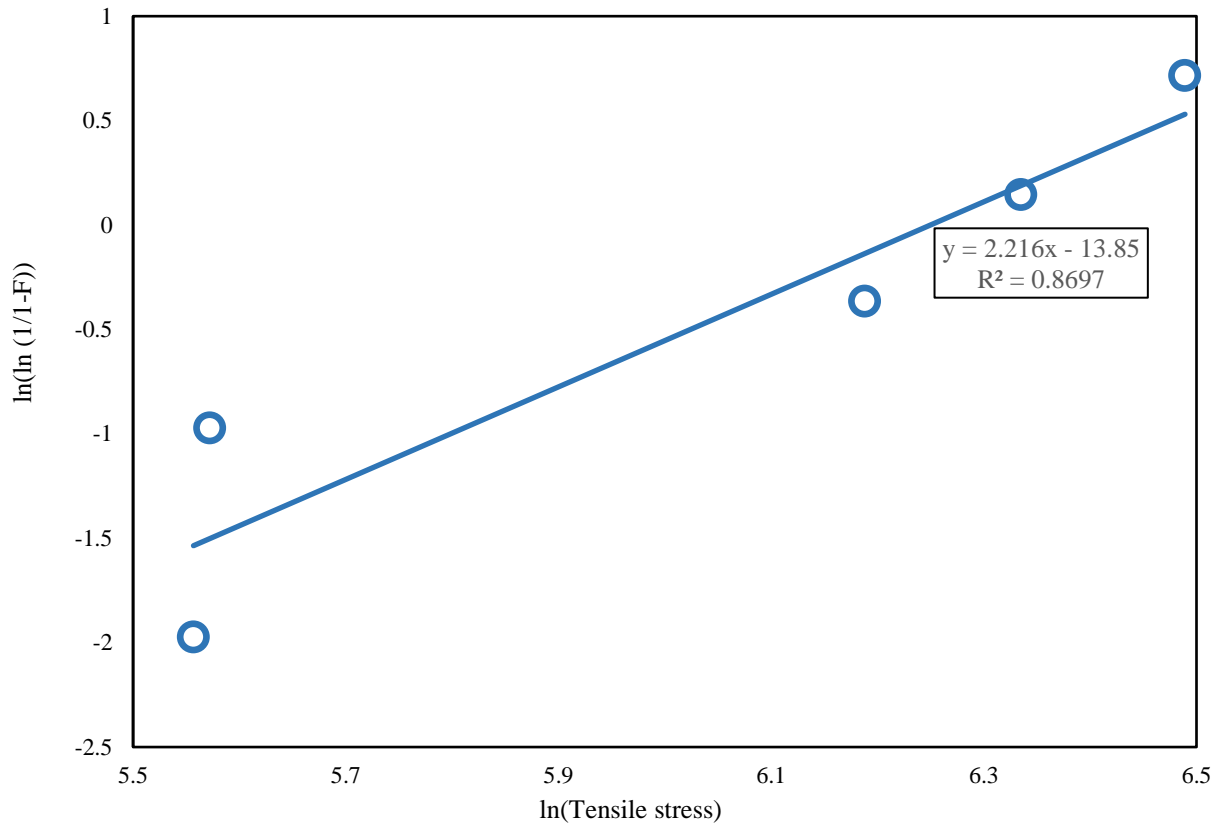


Figure 2.9: Weibull graph for the Table 2.4 data set

Figure 2.9 shows the data is not uniformly distributed along the axes, and a line is fitted through the data set using linear regression. The equation of the regression line is compared with the standard equation of straight line i.e., $y = mx + c$. In this example, the slope of the regression line, $m = 2.216$ and intercept of y-axis (c), -13.85 , are compared to the standard equation of a straight line where 2.216 is the shape parameter (α) or Weibull modulus of tensile stress for this data set. In addition, scale parameter (β) or characteristics strength is computed using equation: $\beta = e^{\left(-\frac{c}{\alpha}\right)}$ and the value is 518.01 MPa. Moreover, the correlation for the regression line is 86.97% for this example.

Probability of survival is calculated using Equation 2.9 and shown in the last column of Table 2.5.

Table 2.5: Example calculation of reliability for 5 data set

i	Tensile stress (MPa)	$F(x) = (i-0.3)/(n+0.4)$	$R = 1-F(x)$
1	259	0.129629630	0.870370370
2	263	0.314814815	0.685185185
3	487	0.500000000	0.500000000
4	564	0.685185185	0.314814815
5	658	0.870370370	0.129629630

The value of tensile stress is plotted on the horizontal axis, and the probability of survival of individual data set is on vertical axis to produce the data shown in Figure 2.10.

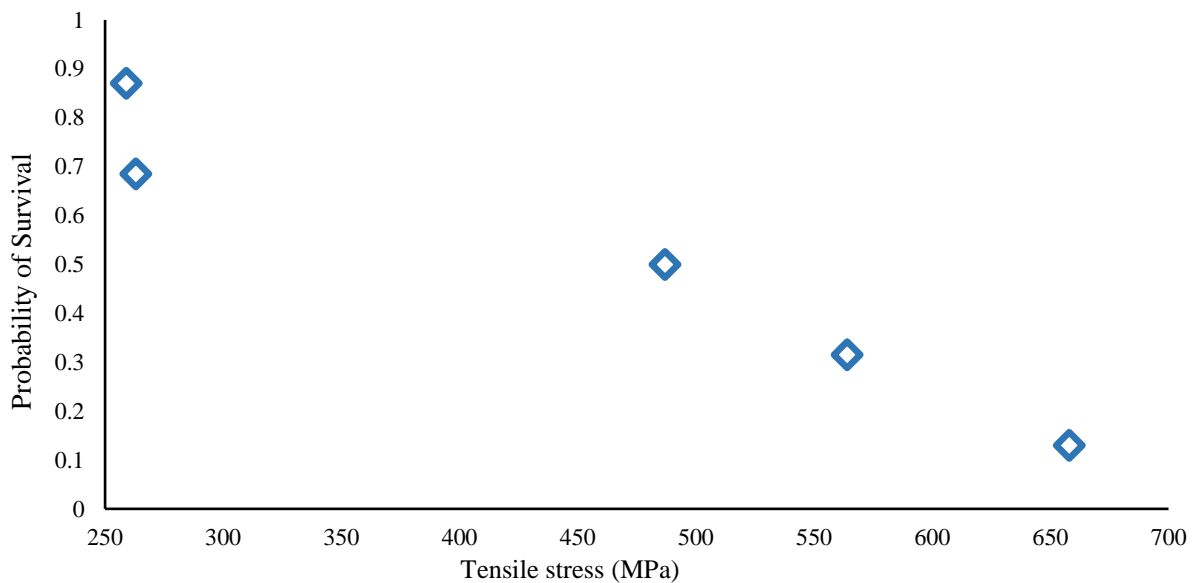


Figure 2.10: Relationship between tensile stress and probability of survival- example calculation

It can be concluded that the probability of survival decreases with an increase in tensile stress.

2.4.4 Sample Calculation of Weibull distribution – MLE Method

Let, five fibres gave tensile stress readings of 2118, 263, 658, 259, and 487 MPa (these values are arbitrary value) which are needed to be analyzed the Weibull distribution using MLE method. Putting these value to Equation 2.17,

$$\alpha = \left[\frac{\sum_1^n [x^\alpha \ln(x)]}{\sum_1^n x^\alpha} - \frac{\sum_1^n \ln(x)}{n} \right]^{-1}$$

$$\Rightarrow \alpha = \left[\frac{[2118^\alpha \ln(2118)] + [1780^\alpha \ln(1780)] + [2521^\alpha \ln(2521)] + [1937^\alpha \ln(1937)] + [1209^\alpha \ln(1209)]}{2118^\alpha + 1780^\alpha + 2521^\alpha + 1937^\alpha + 1209^\alpha} - \frac{\ln(2118) + \ln(1780) + \ln(2521) + \ln(1937) + \ln(1209)}{5} \right]^{-1}$$

$$\Rightarrow \alpha = \left[\frac{[2118^\alpha \ln(2118)] + [1780^\alpha \ln(1780)] + [2521^\alpha \ln(2521)] + [1937^\alpha \ln(1937)] + [1209^\alpha \ln(1209)]}{2118^\alpha + 1780^\alpha + 2521^\alpha + 1937^\alpha + 1209^\alpha} - 7.528 \right]^{-1}$$

Equation 2.18

Numeric iterative method is used to solve Equation 2.18. That is why, different numeric values of α will put to both of the sides [left side (L.S.) and right side (R.S.)] of Equation 2.18 to identify the values of α that fulfills the conditions of Equation 2.18.

If $\alpha=1$, putting the value to Equation 2.18

$$\text{L.S.} = 1$$

$$\text{R.S.} = \left[\frac{[2118^1 \ln(2118)] + [1780^1 \ln(1780)] + [2521^1 \ln(2521)] + [1937^1 \ln(1937)] + [1209^1 \ln(1209)]}{2118^1 + 1780^1 + 2521^1 + 1937^1 + 1209^1} - 7.528 \right]^{-1}$$

$$= 20$$

Therefore, L.S. \neq R.S.

Again if $\alpha=2$, putting the value to Equation 2.18

$$\text{L.S.} = 2$$

$$\text{R.S.} = \left[\frac{[2118^2 \ln(2118)] + [1780^2 \ln(1780)] + [2521^2 \ln(2521)] + [1937^2 \ln(1937)] + [1209^2 \ln(1209)]}{2118^2 + 1780^2 + 2521^2 + 1937^2 + 1209^2} - 7.528 \right]^{-1}$$

$$= 10.09$$

Therefore, L.S. \neq R.S.

Again if, $\alpha=3$, putting the value to Equation 2.18

$$\text{L.S.} = 3$$

$$\text{R.S.} = \left[\frac{[2118^3 \ln(2118)] + [1780^3 \ln(1780)] + [2521^3 \ln(2521)] + [1937^3 \ln(1937)] + [1209^3 \ln(1209)]}{2118^3 + 1780^3 + 2521^3 + 1937^3 + 1209^3} \right]^{-1}$$

$$= 7.46$$

Therefore, L.S. \neq R.S.

Again if, $\alpha=4$, putting the value to Equation 2.18

$$\text{L.S.} = 4$$

$$\text{R.S.} = \left[\frac{[2118^4 \ln(2118)] + [1780^4 \ln(1780)] + [2521^4 \ln(2521)] + [1937^4 \ln(1937)] + [1209^4 \ln(1209)]}{2118^4 + 1780^4 + 2521^4 + 1937^4 + 1209^4} \right]^{-1}$$

$$= 6.13$$

Therefore, L.S. \neq R.S.

Again if $\alpha=5.10$, putting the value to Equation 2.18

$$\text{L.S.} = 5.10$$

$$\text{R.S.} = \left[\frac{[2118^{5.1} \ln(2118)] + [1780^{5.1} \ln(1780)] + [2521^{5.1} \ln(2521)] + [1937^{5.1} \ln(1937)] + [1209^{5.1} \ln(1209)]}{2118^{5.1} + 1780^{5.1} + 2521^{5.1} + 1937^{5.1} + 1209^{5.1}} \right]^{-1}$$

$$= 5.30$$

Therefore, L.S. \neq R.S.

Again if $\alpha=5.20$, putting the value to Equation 2.18

$$\text{L.S.} = 5.20$$

$$\text{R.S.} = \left[\frac{[2118^{5.2} \ln(2118)] + [1780^{5.2} \ln(1780)] + [2521^{5.2} \ln(2521)] + [1937^{5.2} \ln(1937)] + [1209^{5.2} \ln(1209)]}{2118^{5.2} + 1780^{5.2} + 2521^{5.2} + 1937^{5.2} + 1209^{5.2}} \right]^{-1}$$

$$= 5.25$$

Therefore, L.S. \neq R.S.

Again if $\alpha=5.22$, putting the value to Equation 2.18

$$\text{L.S.} = 5.22$$

$$\text{R.S.} = \left[\frac{[2118^{5.22} \ln(2118)] + [1780^{5.22} \ln(1780)] + [2521^{5.22} \ln(2521)] + [1937^{5.22} \ln(1937)] + [1209^{5.22} \ln(1209)]}{2118^{5.22} + 1780^{5.22} + 2521^{5.22} + 1937^{5.22} + 1209^{5.22}} - 7.528 \right]^{-1}$$

$$= 5.24$$

Therefore, L.S. \neq R.S.

Again if $\alpha=5.23$, putting the value to Equation 2.18

$$\text{L.S.} = 5.23$$

$$\text{R.S.} = \left[\frac{[2118^{5.23} \ln(2118)] + [1780^{5.23} \ln(1780)] + [2521^{5.23} \ln(2521)] + [1937^{5.23} \ln(1937)] + [1209^{5.23} \ln(1209)]}{2118^{5.23} + 1780^{5.23} + 2521^{5.23} + 1937^{5.23} + 1209^{5.23}} - 7.528 \right]^{-1}$$

$$= 5.23$$

Therefore, finally, L.S = R.S.

So, the scale parameter (α) is 5.23. Now, putting this value on Equation 2.16

$$\beta = \left[\frac{1}{5} (2118^{5.23} + 1780^{5.23} + 2521^{5.23} + 1937^{5.23} + 1209^{5.23}) \right]^{\frac{1}{5.23}}$$

$$\Rightarrow \beta = 2081.85$$

So, the scale parameter (β) is 2081.85 GPa.

2.5 Suitability Analysis and Ranking

The suitability of cattail fibres in composite applications in composites was analyzed across the five growth stages and three lengths to find out the appropriate batch and rank them afterwards.

2.5.1 Selection of Limit Value

Since flax fibres are widely used in composite applications, the value of the mechanical properties of flax fibres was taken as threshold values to rank the properties of cattail fibres from five different growth stages. However, since flax is a natural fibre, its reported mechanical properties vary widely. Thus, selecting the limit values was challenging. To the best of our accessibility in the literature on flax fibre mechanical properties, the high, average, and low values were taken as limit values.

In the literature, we identified the highest tensile stress (S) value of 2000 MPa and the lowest value of 343 MPa, while the highest modulus (Y) was found to be 103 GPa (Yan et al., 2014), and the lowest modulus was 15 GPa (Yukseloglu & Yoney, 2016). Moreover, the highest tensile strain (R) was noticed at 3.3% and the lowest at 1.2% (Yan et al., 2014). The highest (HLV), lowest (LLV) and average (ALV) limit values were established and shown in Table 2.6. For average threshold values, data from Charlet et al. (2010) was taken as these data appear to be approximately the middle value of the lowest and highest data points. The limit values shown in Table 2.6 were defined using the literature values just mentioned.

Table 2.6: Limit values of mechanical properties of flax fibre

Limit Value	Tensile stress (MPa)	Tensile strain (%)	Modulus (GPa)
LLV	343	3.3	15
ALV	1253	2.5	54
HLV	2000	1.2	103

LLV - Low Limit Value; ALV- Average Limit Value; HLV- High Limit Value

For composites, high tensile stress, high modulus, and low strain are preferable. Using Python programming language, every fibre of each batch (50 samples) was examined to

calculate the percentages of fibre that can fulfill the limit requirements using these limit values as a threshold. In addition, 3 parameters (S/R/Y), 2 parameters (S/R, Y/R, and S/Y), and 1 parameter (S, R, and Y) are considered as a condition for examining the suitability percentage for composites.

2.5.2 Decision for Suitability and Ranking: Process Flow

Figure 2.11a gives a flow chart of the overall four-layer process of the suitability analysis. In the first part of the analysis process, 3 types of parameters (1 parameter, 2 parameters and 3 parameters) and 7 parameter combinations (S/R/Y, S/R, Y/R, S/Y, S, R, Y) were established. In addition, 3 limit values (LLV, ALV, HLV) were introduced, which made the analysis process easier to compare with the flax threshold values. Moreover, the 5 growth stages (NF, F, LF, FM, M) added an extra dimension to this analysis, leading to the suitability (%) of cattail fibre. From this, suitability (%) ranking at various dimensions was done that gave concrete results. The overall analysis was done using Python. Hence, the coding conditions for all batches were not exact; an example of them is presented here.

2.5.3 Use of Python Code for Suitability (%)

The source code (Appendix A 42) and pseudocode (Appendix A 43) of suitability (%) using 3 parameters with high limit value was conducted using Python. A sample flow chart is shown in Figure 2.11b.

2.5.4 Use of Python Code for Ranking (Combination of Growth Stage and Length)

After calculating the suitability (%), a combined ranking along the growth stages and lengths was established. Finally, the 15-sample batch of each group was ranked using Python presented in the flow chart (Figure 2.11c). The source code and pseudocode are presented in Appendix A 44 and A 45, respectively.

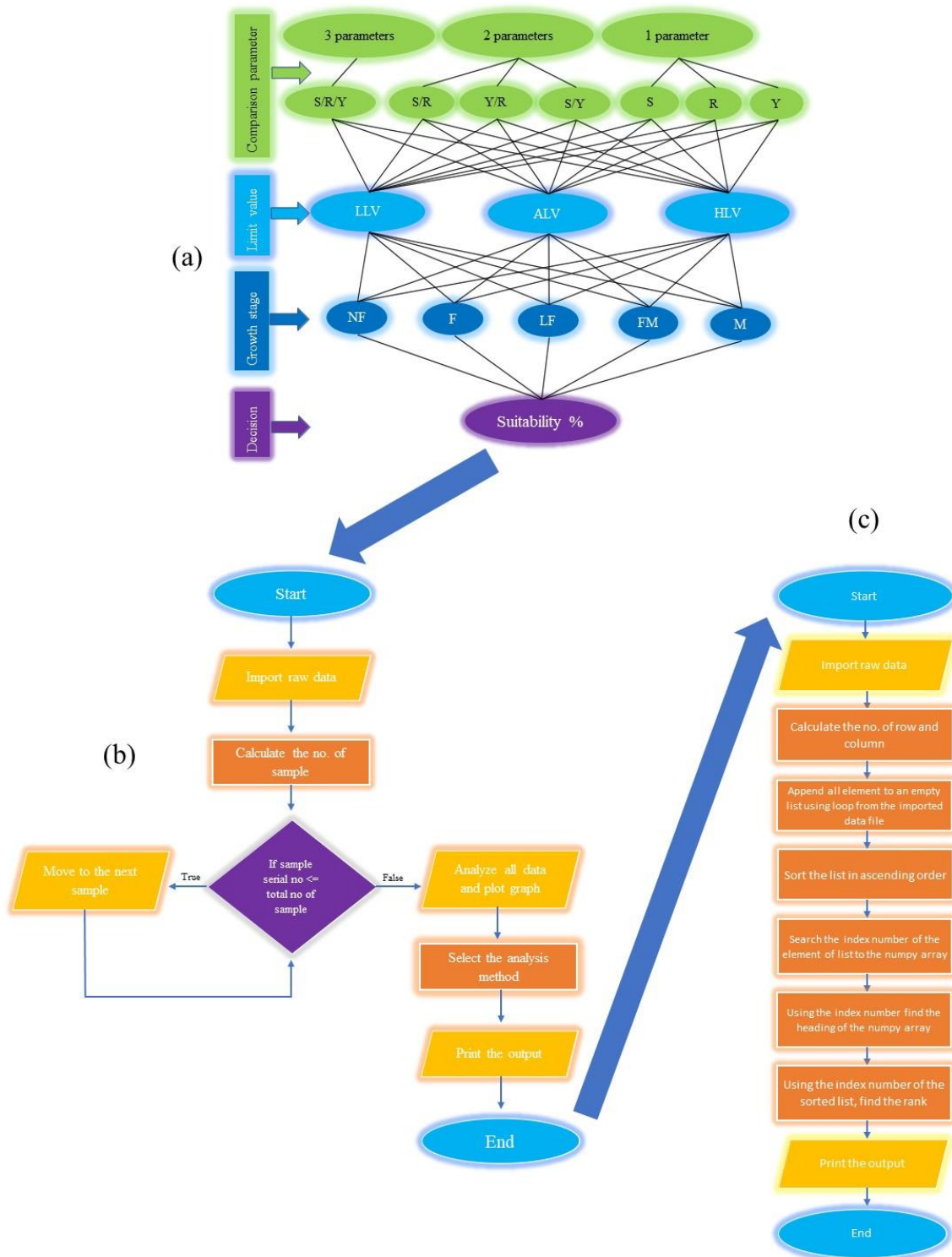


Figure 2.11: (a) Process flow of suitability analysis; (b) flowchart of suitability (%) using Python; (c) flowchart of ranking (combination of growth stage and length) using Python

2.6 Image analysis

2.6.1 ESEM and EDS Analysis

The surfaces of the fibres from different growth stages were examined in an ESEM (Environmental Scanning Electron Microscope: FEI Quanta 650 FEG) in the Manitoba Institute for Materials (MIM) at the University of Manitoba (Figure 2.12) at a voltage of 10.0 kV and a pressure of 120 Pa. In addition, Energy-dispersive X-ray spectroscopy (EDS) analysis was done for each growth stage. Mechanically extracted fine fibre and chemically extracted fine and coarse fibre from the mature stage were also examined using ESEM and EDS.

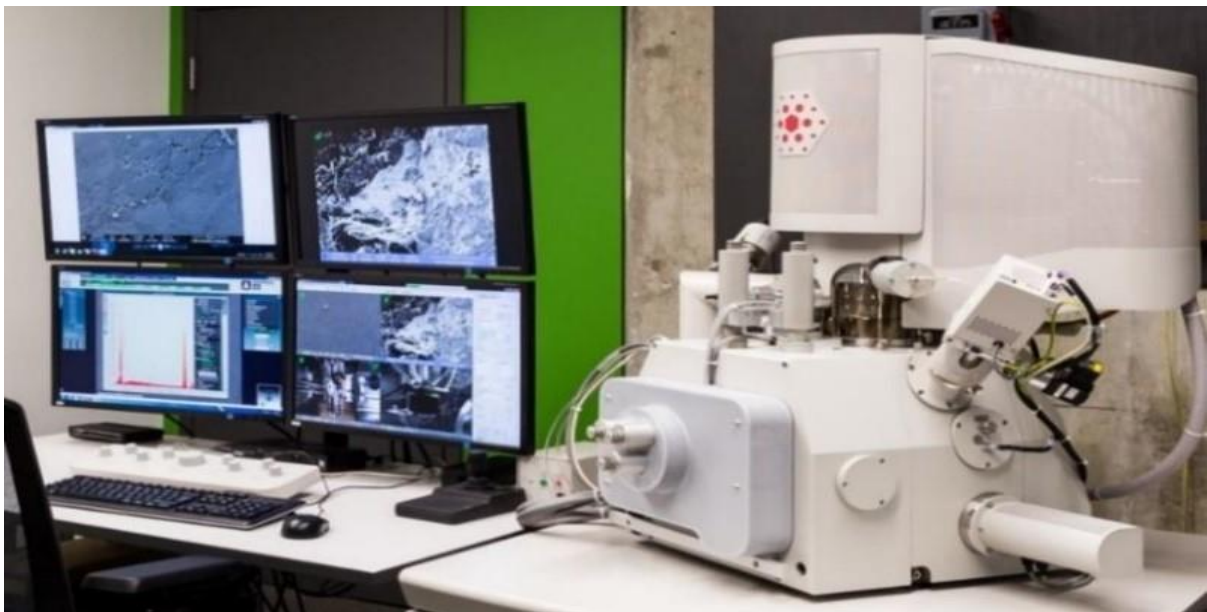


Figure 2.12: Environmental Scanning Electron Microscope (Manitoba Institute for Materials, University of Manitoba)

Chapter 3 Statistical Analysis: ANOVA and Weibull Distribution

– Results and Discussion

3.1 Statistical Analysis Using ANOVA

A large variation in mechanical properties of cattail fibres was observed, as shown in Table 3.1. Other natural fibres also show similar variations (Shadhin, 2021). Before conducting Weibull analysis of the mechanical properties data, ANOVA with Tukey post hock was carried out to find out the difference among the fibres from the different growth stages.

For the 15 batches of fibres (five growth stages \times three lengths), a total of 105 pairs were compared using one-way ANOVA. The tensile stress data and the ANOVA analysis are shown in Appendix A 16, A 17, and A 18, also in the appendix showing the significant differences (p values) of tensile strain and Young's modulus, respectively, among the 15 batches. For tensile stress, a significant difference ($p < 0.05$) was found in only 13 of 105 pairs shown as green marked in Appendix A 16. However, only 40 pairs of strain and seven pairs of Young's modulus are found to be statistically significant.

Therefore, based on the ANOVA analysis, a decision cannot be made regarding the reliability of cattail fibre for the composite applications; therefore, a Weibull analysis of the mechanical properties of cattail fibres was conducted.

3.2 Statistical Analysis Using Weibull Distribution

Weibull distribution was conducted on the experimental data of tensile stress and modulus from five growth stages of cattail fibre with three different lengths (1, 2 and 3 inches).

3.2.1 Weibull Analysis of Tensile Stress – Linear Regression (LR) Method

Table 3.1 depicts the Weibull parameters of tensile stress for 15 batches (five growth stages \times three lengths) of samples computed using three estimators. A sample calculation is given in Section 2.4.3 Sample Calculation of Weibull distribution – Linear Regression Method.

Table 3.1: Weibull parameter of tensile stress obtained from linear regression method

ID	\bar{X}_{stress} (MPa)	σ_{avg} (MPa)			α			β (MPa)			R^2_{σ}		
		DR	HE	MR	DR	HE	MR	DR	HE	MR	DR	HE	MR
NF-L1	1215 [903]	1053	1056	1049	1.52	1.57	1.46	1340	1333	1348	0.97	0.97	0.98
NF-L2	1047 [614]	986.0	987.8	984.2	1.81	1.88	1.73	1207	1200	1217	0.93	0.94	0.92
NF-L3	747 [252]	744.1	745.0	742.8	3.01	3.12	2.89	840.3	837.9	843.4	0.98	0.98	0.98
F-L1	1288 [824]	1138	1142	1135	1.47	1.52	1.41	1460	1452	1473	0.98	0.98	0.98
F-L2	1035 [534]	989.4	990.7	987.1	2.23	2.30	2.14	1166	1162	1172	0.97	0.97	0.97
F-L3	958 [483]	912.9	914.8	911.0	2.18	2.25	2.09	1080	1076	1085	0.98	0.98	0.99
LF-L1	738 [440]	681.7	683.0	680.2	1.66	1.73	1.59	849.8	844.2	857.0	0.95	0.96	0.94
LF-L2	684 [472]	626.7	628.4	625.2	1.92	1.98	1.85	758.3	756.0	762.3	0.94	0.94	0.95
LF-L3	542 [429]	458.5	459.6	456.9	1.41	1.46	1.35	594.5	591.0	598.9	0.98	0.98	0.98
FM-L1	584 [334]	535.4	536.5	533.9	1.64	1.70	1.57	669.5	665.8	674.2	0.97	0.97	0.97
FM-L2	645 [531]	580.8	582.2	579.1	1.86	1.91	1.79	707.7	705.3	710.9	0.87	0.86	0.87
FM-L3	500 [298]	471.1	471.8	470.2	2.04	2.12	1.95	563.7	561.0	567.1	0.95	0.95	0.94
M-L1	1058 [881]	843.5	846.8	839.7	1.14	1.18	1.09	1164	1156	1176	0.97	0.97	0.97
M-L2	1500 [973]	1369	1372	1366	1.81	1.88	1.74	1676	1668	1687	0.98	0.98	0.98
M-L3	834 [367]	817.1	818.4	815.7	2.67	2.76	2.56	937.3	934.7	941.3	0.97	0.96	0.96

Standard deviation is presented in square bracket; \bar{X}_{stress} : Experimental tensile stress; σ_{avg} : Weibull average; α : shape parameter; β : scale parameter; DR: median rank estimator; HE: Hazen estimator; MR: mean rank estimator;

The experimental average tensile stress (\bar{X}_{stress}) was 1500MPa in the M-L2 batch, which is the highest among the 15 batches; however, the standard deviation for this batch was also one of the highest (973MPa). Fibres from F-L1 (1288 \pm 824 MPa), NF-L1 (1215 \pm 903 MPa), NF-L2 (1047 \pm 614 MPa), F-L2 (1035 \pm 534 MPa), and M-L2 (1058 \pm 881 MPa) batches are some of the stronger fibres. In contrast, the FM-L3 batch had the lowest (500 \pm 298 MPa) tensile stress, followed by LF-L3 (542 \pm 429 MPa) and FM-L1 (584 \pm 535 MPa). Overall, no trend is noticed regarding the tensile stress of the fibres from different growth stages. Several authors found higher standard deviation on mechanical properties of

natural fibres without statistically significant differences when comparing variables like cultivars (Charlet et al., 2010) and surface treatment (Zafeiropoulos & Baillie, 2007).

The predicted average of Weibull tensile stress (σ_{avg}) for all three estimators is always lower than the corresponding experimental values (x_{stress}). The σ_{avg} value calculated by Hazen's equation (HE) estimator is the highest, followed by median rank (DR) and mean rank (MR) estimators (Table 3.1). It appears that the closeness of the \bar{x}_{stress} and σ_{avg} values depend on the standard deviation of the experimental data set. In the majority of the cases, the higher the coefficient of variation, the larger the difference between the experimental and the predicted average Weibull tensile stress values for all three estimators (Figure 3.1). The differences between the experimental and predicted values are independent of the growth stage and fibre length.

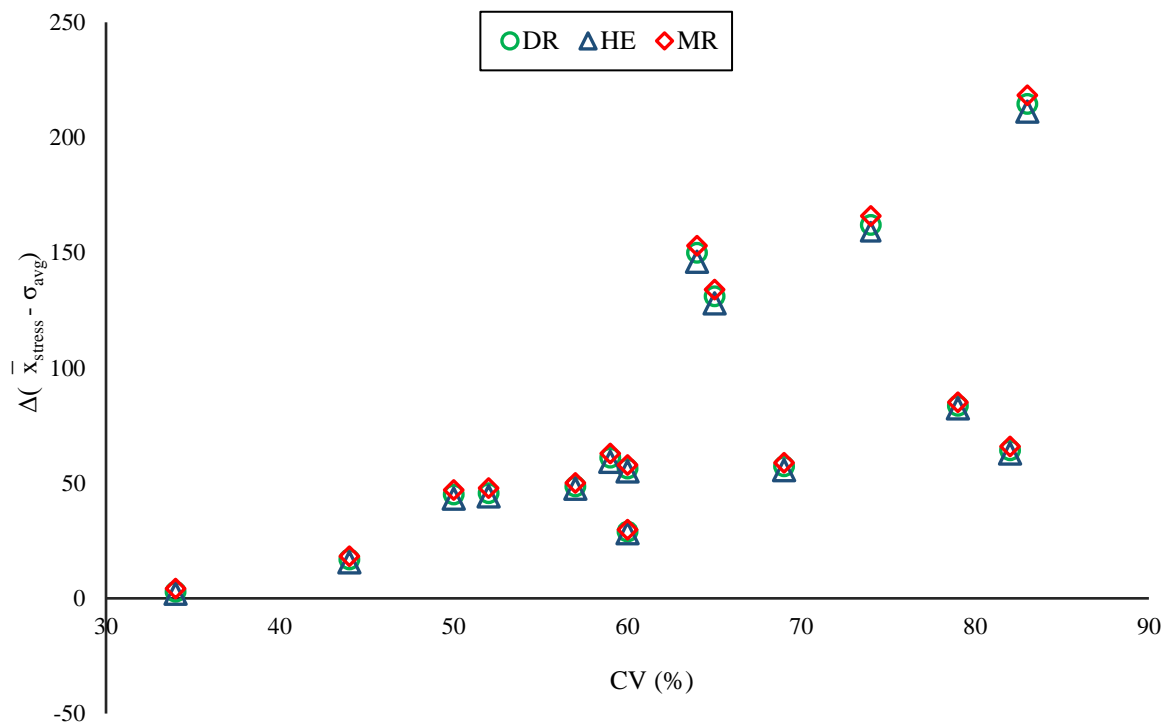


Figure 3.1: Relationship between the difference between experimental and predicted Weibull values with the coefficient of variation (CV%) of tensile stress

Average Weibull tensile stress is calculated using Equation 2.8, where shape and scale parameters are used as input. The scale parameter of tensile stress is always higher than the

average Weibull value for the 15 batches and three estimators. In Equation 2.8, the natural logarithm of scale parameter is used, making the value smaller, impacting the overall average Weibull tensile stress.

The shape parameters lie between 1 and 3 for all 15 batches (five growth stages and three lengths) for all three estimators. There is no trend observed between the shape parameters and the fibre lengths. This relationship will be discussed in detail later in this chapter. The range of shape parameters was between 1.14 (M-L1) and 3.01 (NF-L3); 1.18 (ML-L1) and 3.12 (NF-L3); and 1.09 (M-L1) and 2.89 (NF-L3), for DR, HE and MR estimators, respectively (Table 3.1). By considering the shape parameter values, the cattail fibres for all five growth stages are suitable for composite applications as the minimum value required is 0.5 or above (Monteiro et al., 2013). For a specific growth stage and fibre length, the HE estimator generated the highest shape parameter, followed by DR and MR estimators.

The coefficient of variation of the average experimental data set has a negative impact on the shape parameters, as shown in Figure 3.2. The two largest shape parameters were obtained for the two lowest coefficient variations (CV%), which are 3.01 and 2.67 (estimator: DR), 3.12 and 2.76 (estimator: HE), and 2.89 and 2.56 (estimator: MR).

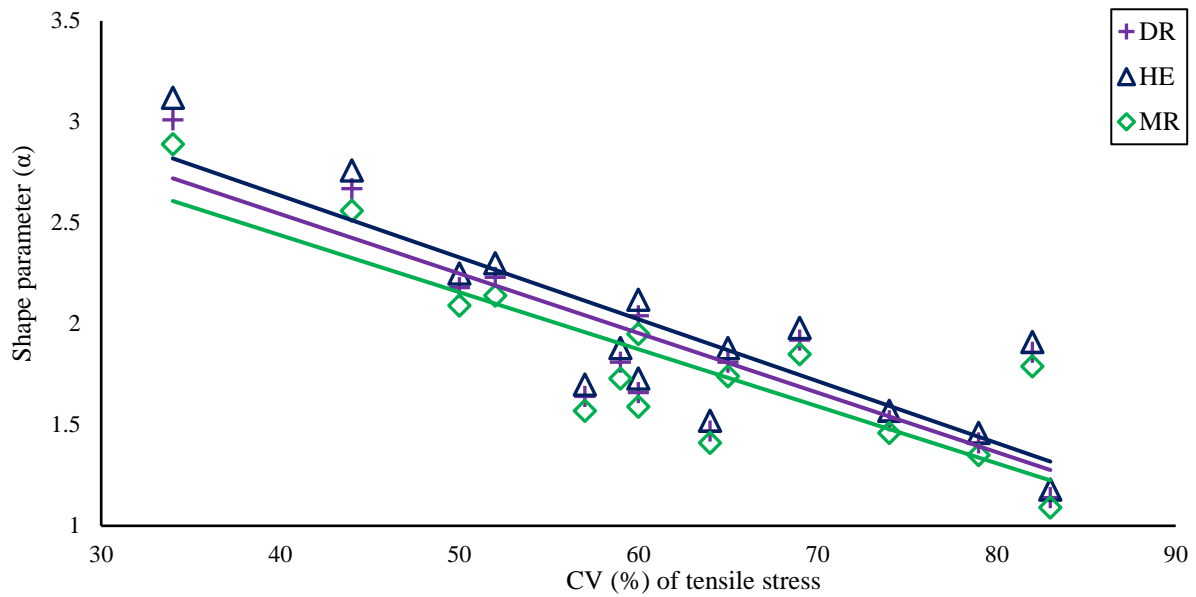


Figure 3.2: Relationship between shape parameter and coefficient of variation of tensile stress

The scale parameters (β) are always higher than the corresponding predicted Weibull average (σ_{avg}) and average experimental values of tensile stress, \bar{x}_{stress} for all three estimators (Table 3.1). The lowest scale parameters are found using the HE estimator followed by DR and MR estimators. This trend is opposite to the shape parameters where the largest shape parameters were obtained by HE estimator followed by DR and MR estimators (Table 3.1).

Since a higher scale parameter indicates widely distributed data with a higher variability, the scattered distribution of data will shift the points away from the origin in the curve of $\ln(x)$ vs $\ln(\ln(1/1-F))$ while plotting the curve. Thus, the trendline will be less stiff (lower slope) due to the expanding value of the x-axis. Therefore, the slope becomes lower, decreasing the shape parameter. The inverse relationship between scale and shape parameters is desirable for composite applications and has been reported by others (Stacey, 2020).

Moreover, the scale parameter (β) depends on the shape parameter (α) value, the number of samples, and individual experimental tensile stress that can be calculated from Equation 2.16. The experimental average of tensile stress is equal to the scale parameter when $\alpha=1$ (Equation 2.16). In addition, the scale parameter is less than the experimental

average tensile stress value if $\alpha < 1$ and vice versa. Since the value of α is always greater than unity for 15 batches, the value of β is always greater than the experimental average values. Also, the scale parameter increases with the increasing number of samples when all other conditions remain the same. However, the scale parameter is higher if the individual experimental value is scattered or if a single datum is much higher than the average value. This phenomenon is described by the two-parameter Weibull equations below.

If the left side of Equation 2.8 is zero, the scale parameter (β) of tensile stress will be equal to the experimental value.

$$\alpha \ln (x) - \alpha \ln (\beta) = 0$$

$$\Rightarrow \alpha \ln (x) = \alpha \ln (\beta)$$

$$\Rightarrow \ln (x) = \ln (\beta)$$

$$\Rightarrow x = \beta$$

So, putting this value into Equation 2.8,

$$\ln \left[\ln \frac{1}{1 - F(x)} \right] = 0$$

$$\Rightarrow \ln \frac{1}{1 - F(x)} = 1$$

$$\Rightarrow \frac{1}{1 - F(x)} = e$$

$$\Rightarrow 1 - F(x) = \frac{1}{e}$$

$$\Rightarrow F(x) = 1 - \frac{1}{e}$$

$$\Rightarrow F(x) = 0.632 \text{ (63.2\%)}$$

Therefore, β of tensile stress would be equal to the experimental value at 63.2% probability of failure. However, the average Weibull tensile stress (σ_{avg}) is equal to the experimental value at 50% probability of failure (Quinn & Quinn, 2010). Where the experimental value (x) is equal to β , the regression line intersects the x-axis; whereas, due to the lower probability of failure (50%), the y-value would be lower than zero when $x=\sigma_{avg}$, which goes underneath the x-axis. For that point, the value of x-axis would be lower than the intersecting point. That is why the value of β is slightly greater than the value of σ_{avg} .

The correlations of tensile stress of 15 batches are between 0.86 and 0.99 (Table 3.1) for all three estimators. In addition, the goodness to fit of all the batches is above 90% except for FM-L2 with the lowest R^2 values of 0.87, 0.86 and 0.87, respectively, for DR, HE, and MR estimators (Table 3.1).

Weibull graph for tensile stress using the linear regression method is shown in Figure 3.3 to Figure 3.11. It is worth mentioning here that the two-parameters of Weibull distribution in these figures were calculated using these Weibull lines.

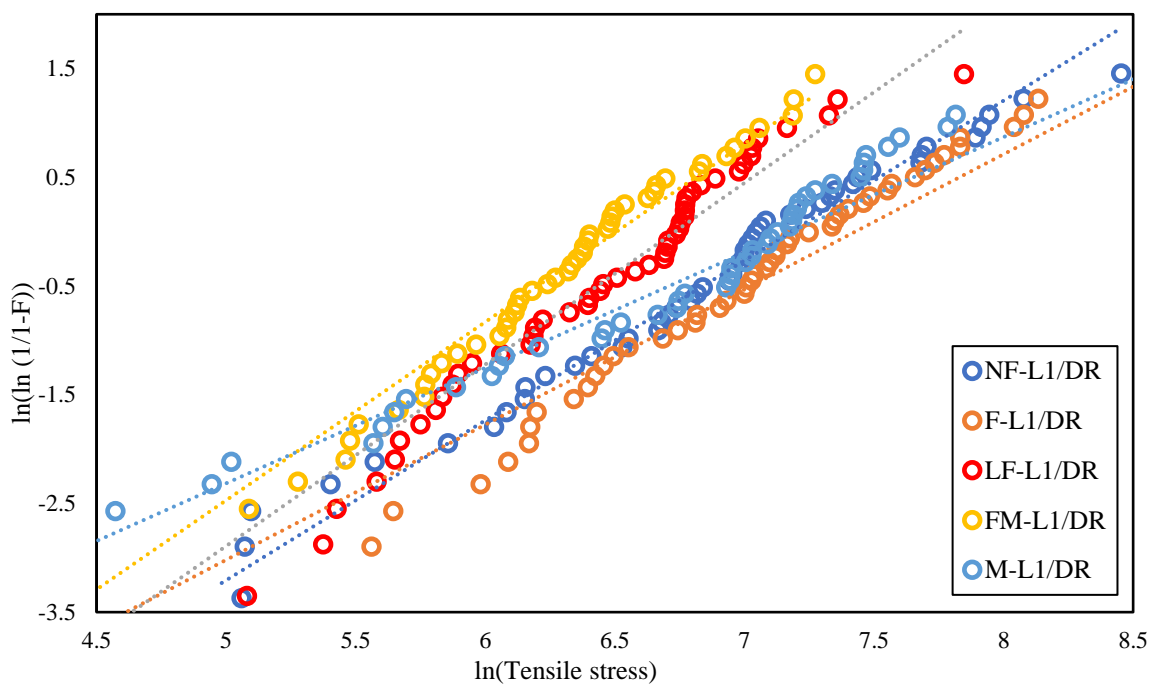


Figure 3.3: $\ln(\ln(1/(1-F)))$ vs $\ln(\text{Tensile Stress})$ curve for 5 growth stages with L1 length and the DR estimator

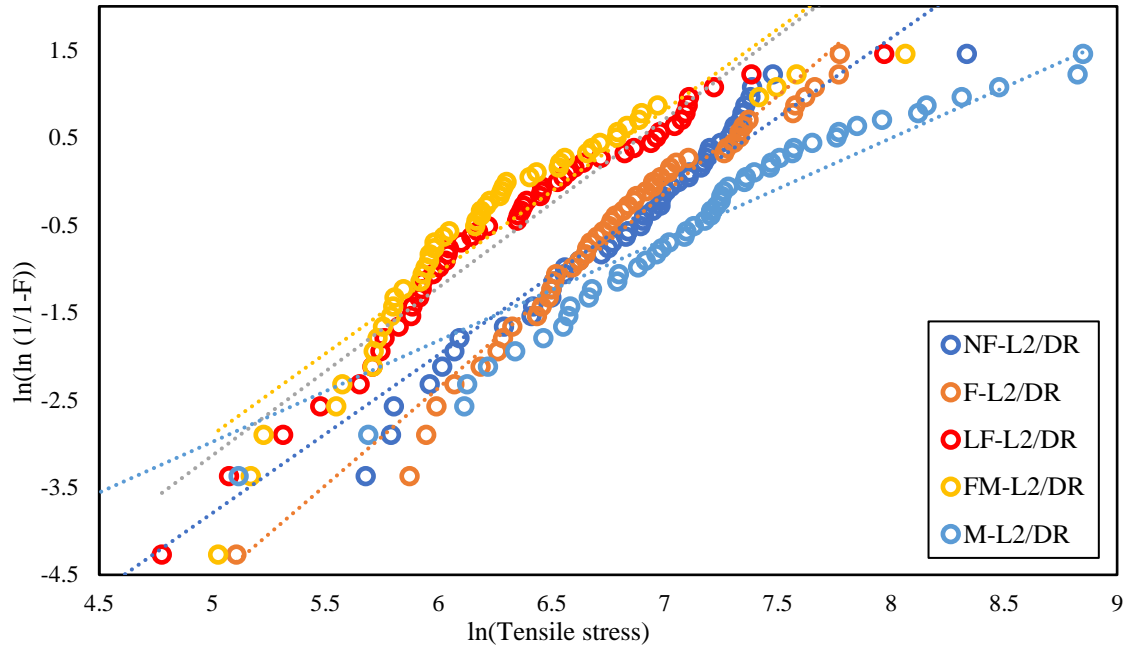


Figure 3.4: $\ln(\ln(1/(1-F)))$ vs $\ln(\text{Tensile Stress})$ curve for 5 growth stages with L2 length and the DR estimator

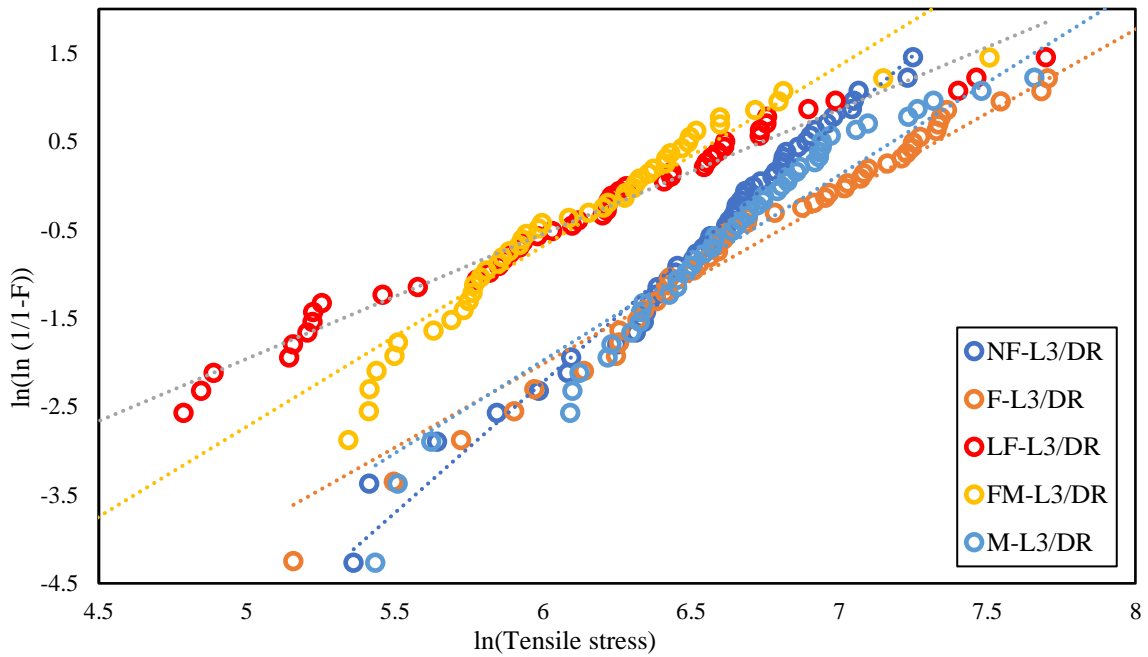


Figure 3.5: $\ln(\ln(1/(1-F)))$ vs $\ln(\text{Tensile Stress})$ curve for 5 growth stages with L3 length and the DR estimator

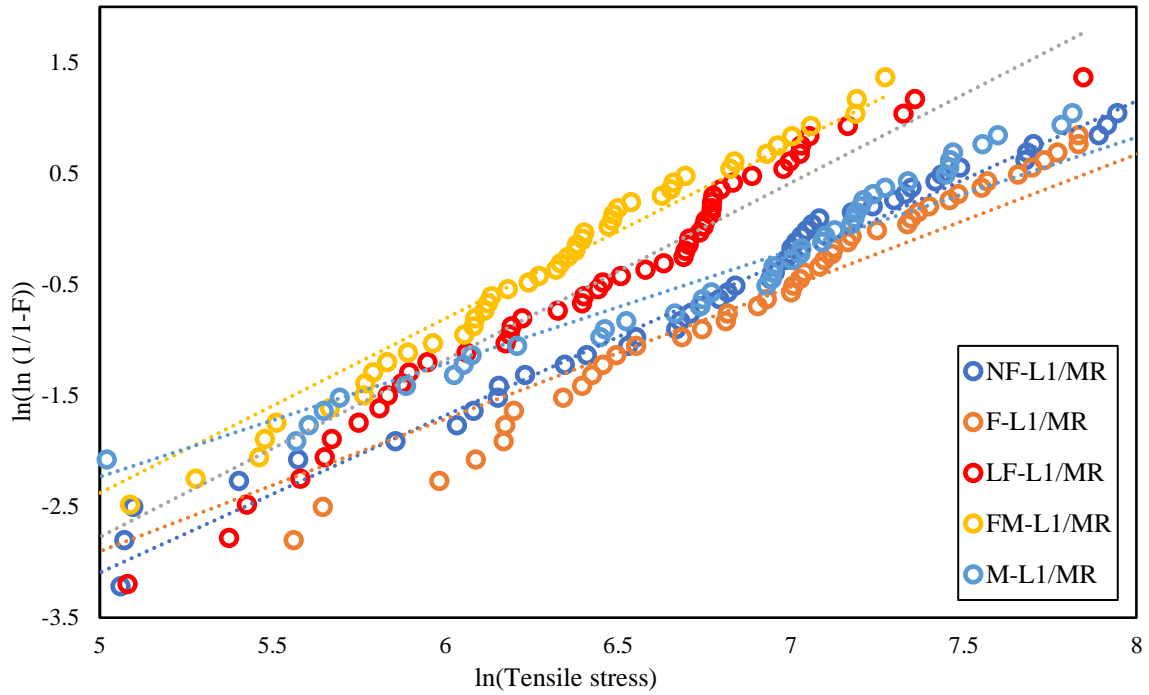


Figure 3.6: $\ln(\ln(1/(1-F)))$ vs $\ln(\text{Tensile Stress})$ curve for 5 growth stages with L1 length and the MR estimator

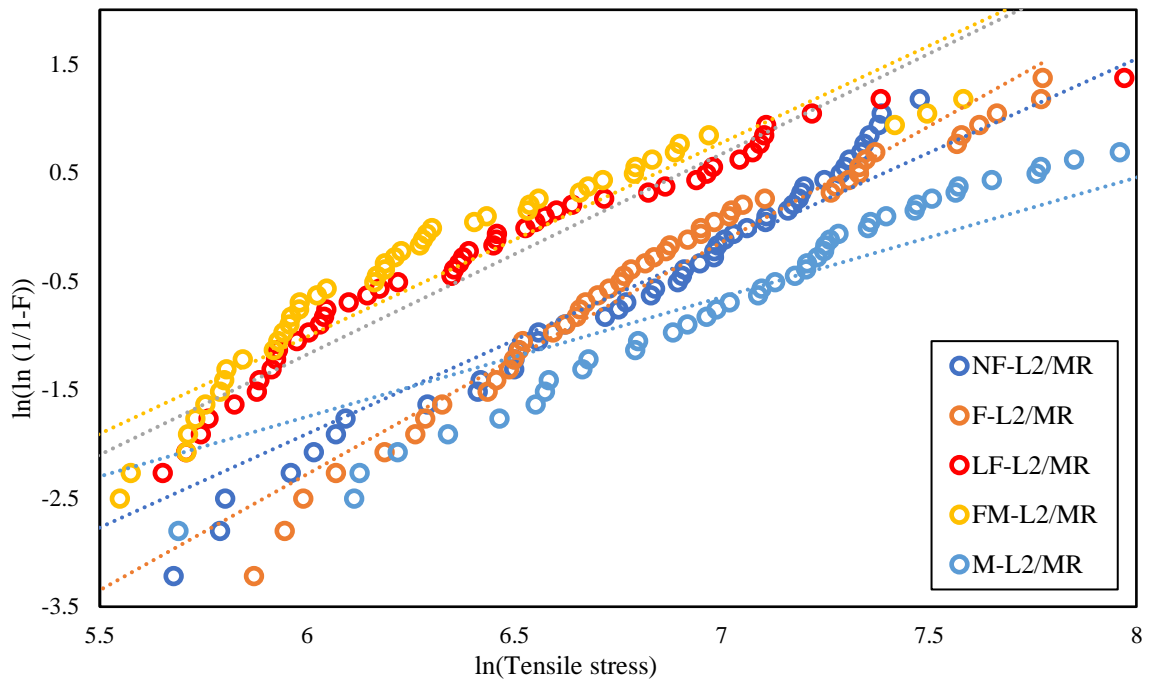


Figure 3.7: $\ln(\ln(1/(1-F)))$ vs $\ln(\text{Tensile Stress})$ curve for 5 growth stages with L2 length and the MR estimator

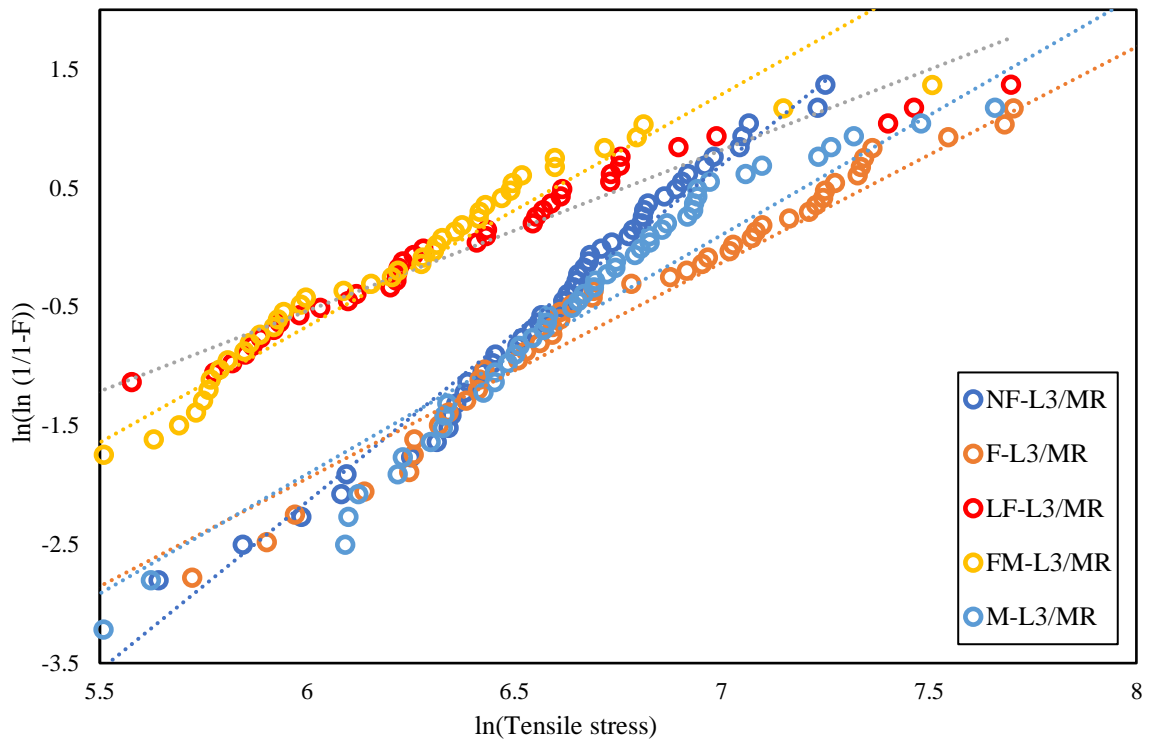


Figure 3.8: $\ln(\ln(1/(1-F)))$ vs $\ln(\text{Tensile Stress})$ curve for 5 growth stages with L3 length and the MR estimator

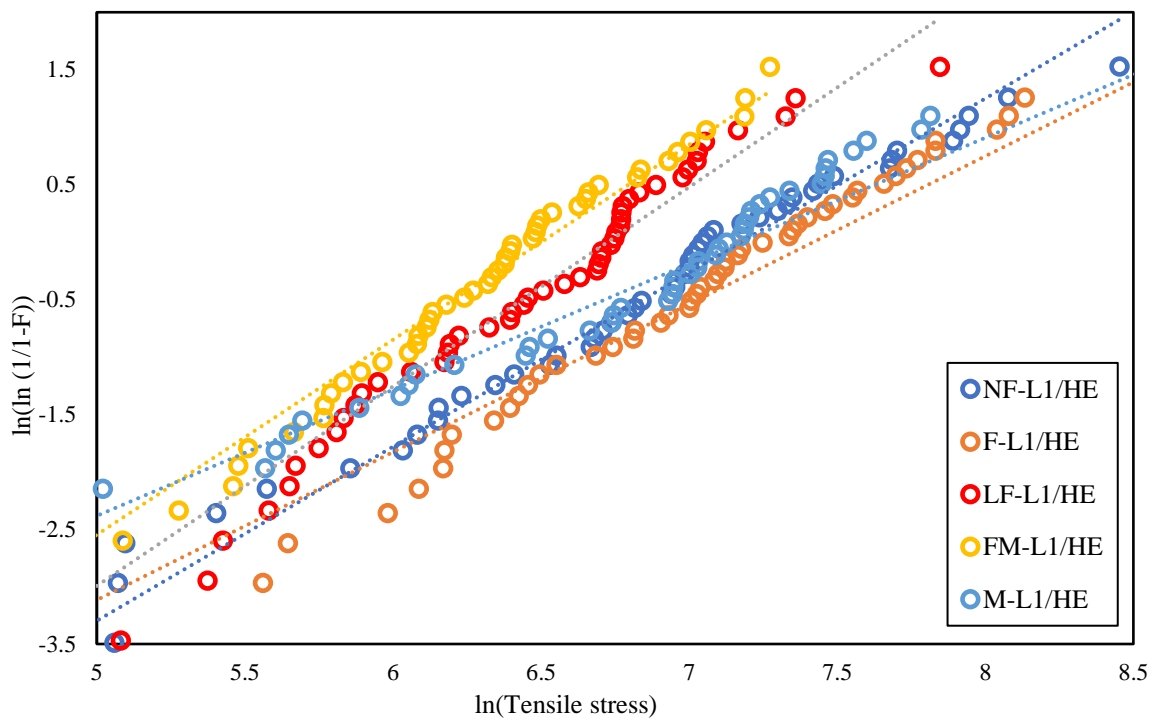


Figure 3.9: $\ln(\ln(1/(1-F)))$ vs $\ln(\text{Tensile Stress})$ curve for 5 growth stages with L1 length and the HE estimator

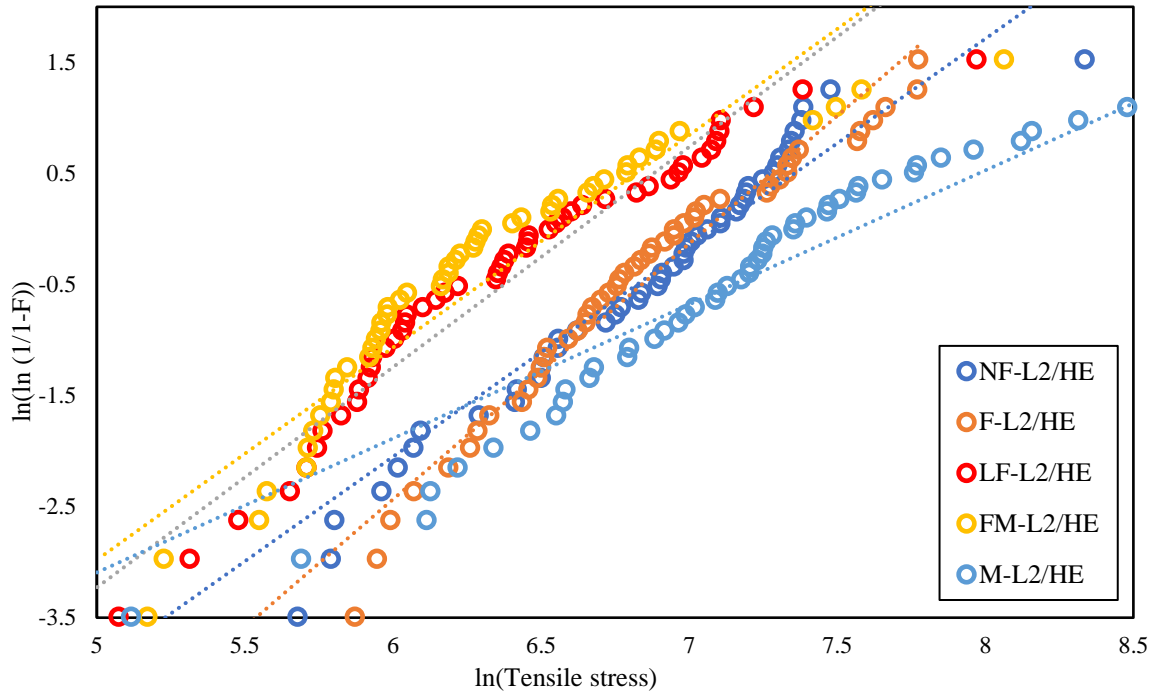


Figure 3.10: $\ln(\ln(1/(1-F)))$ vs $\ln(\text{Tensile Stress})$ curve for 5 growth stages with L2 length and the HE estimator

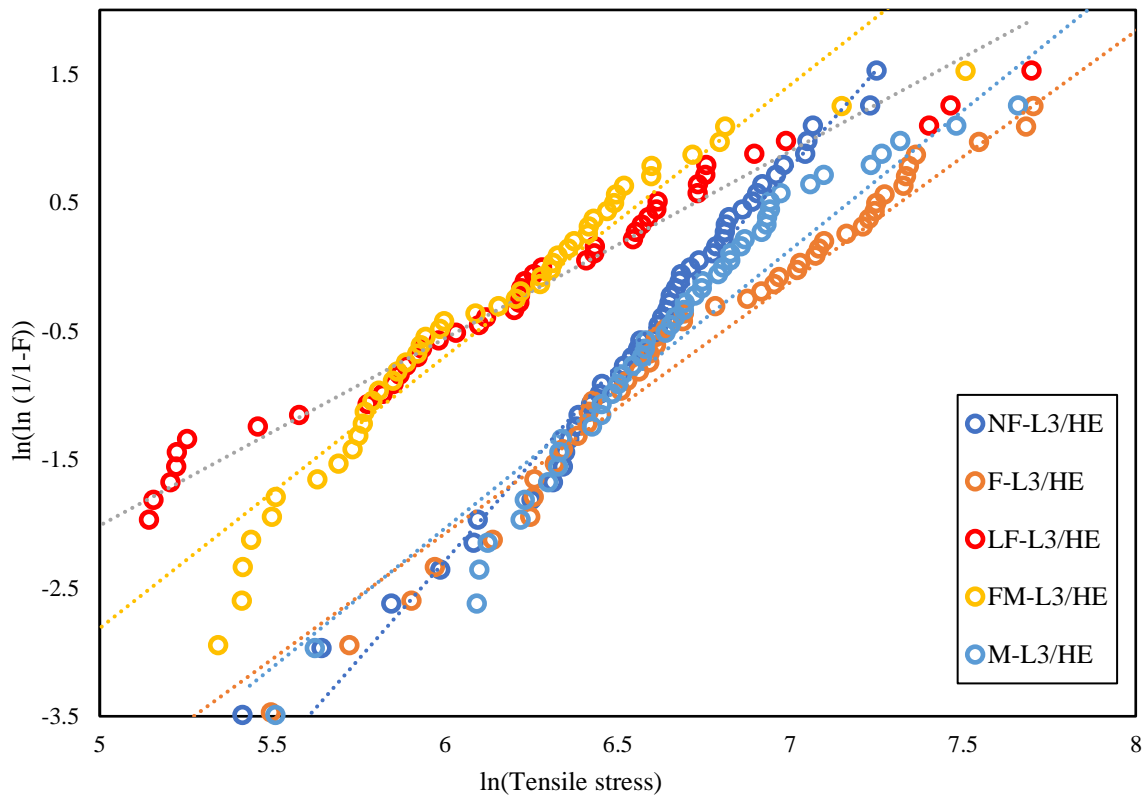


Figure 3.11: $\ln(\ln(1/(1-F)))$ vs $\ln(\text{Tensile Stress})$ curve for 5 growth stages with L3 length and the HE estimator

Figure 3.12 to Figure 3.20 represent the relation between the tensile stress and probability of survival of all five growth stages and three lengths using three different estimators. It can be stated from these curves that the reliability of the datasets becomes lower with an increase in the tensile stress. The rate of decrease in the probability of survival with an increase in tensile stress varies from batch to batch and estimator to estimator also. A sample calculation is given in Section 2.4.3 Sample Calculation of Weibull distribution – Linear Regression Method.

Figure 3.12 to Figure 3.14 show the tensile stress vs probability of survival curve of L1, L2 and L3 of five growth stages using the DR estimator. In Figure 3.12, it can be seen that the F-L1 batch is the most reliable among the five-growth stages of L1 length using the DR estimator, followed by M-L1 and NF-L1. In addition, the probability of survival of M-L2 seems to be the highest (Figure 3.13) among the five growth stages of L2 length, followed by the F-L2 and N-L2 batches, while the DR estimator was used in the Weibull distribution. Moreover, in the case of L3 length and the DR estimator, it was noticed that the reliability of F-L3 batch was highest among the five growth stages, followed by the M-L3 and NF-L3 batches (Figure 3.14).

In Figure 3.15, the probability of survival was highest at the F-L1 batch among the five growth stages of L1 lengths while using the MR estimator, followed by the M-L1 and NF-L1 batches. In addition, the value of the reliability of the M-L2 batch was higher than any other batches (Figure 3.16) of five growth stages, considering only L2 length and using the MR estimator in the Weibull distribution. The second and third highest values were noticed at F-L2 and NF-L2 batches. Moreover, the probability of failure was found to be the lowest at the F-L3 batch among the five growth stages (Figure 3.17), with the L3 length followed by the M-L3 and NF-L3 batches, using the MR estimator.

Figure 3.18 depicts that the highest reliability was found at the F-L1 batch among the growth stages of L1 length using the HE estimator on the Weibull distribution. The following batches are M-L1 and NF-L1, whereas the lowest probability of survival was found in the FM-L1 batch. In addition, the M-L2 batch holds the highest probability of survival (Figure 3.19) among the five growth stages of L2 length if the HE estimator is implemented, followed by the F-L2 and NF-L2 batches. The reliability of the F-L3 batch was found to be the best (Figure 3.20) among the growth stages of L3 length using the HE estimator, followed by the M-L3 and NF-L3 batches.

From Figure 3.12 to Figure 3.20, it can be stated that the data set of the flower (F) stage has the highest reliability for both L1 and L3 lengths; whereas the mature (M) stage has the highest reliability for the L2 length, applicable for each of the DR, MR, HE estimators.

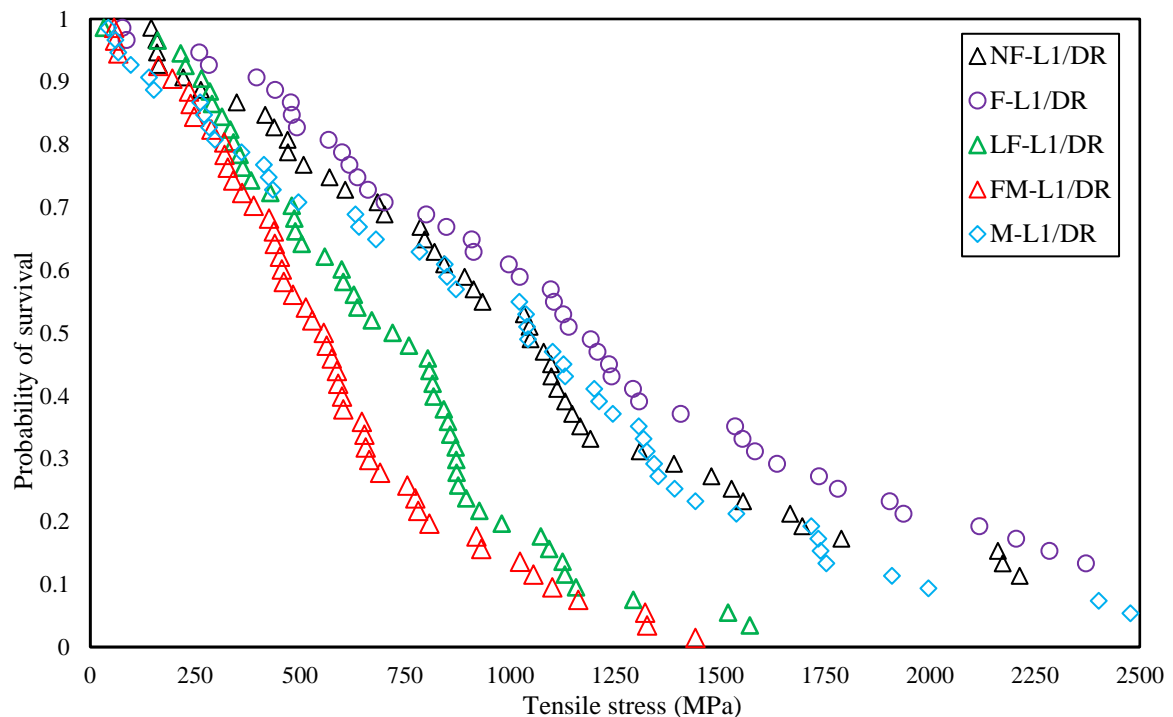


Figure 3.12: Tensile stress vs Probability of survival curve of 5 growth stages with L1 length and the DR estimator

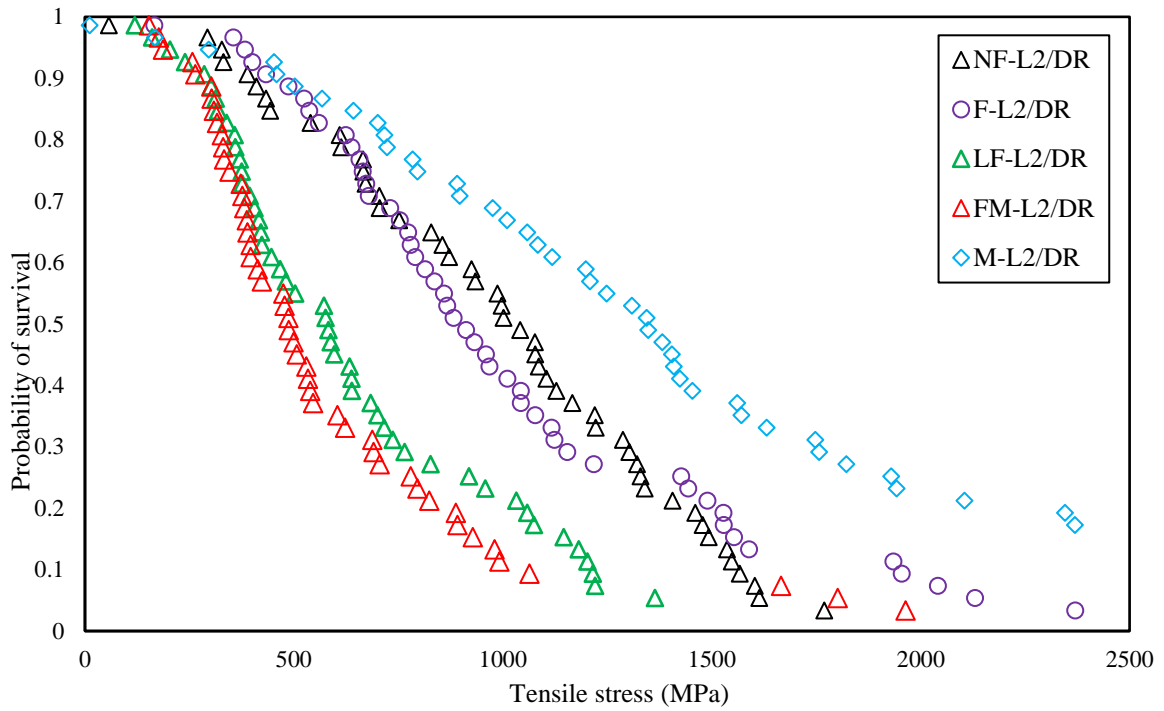


Figure 3.13: Tensile stress vs Probability of survival curve of 5 growth stages with L2 length and the DR estimator

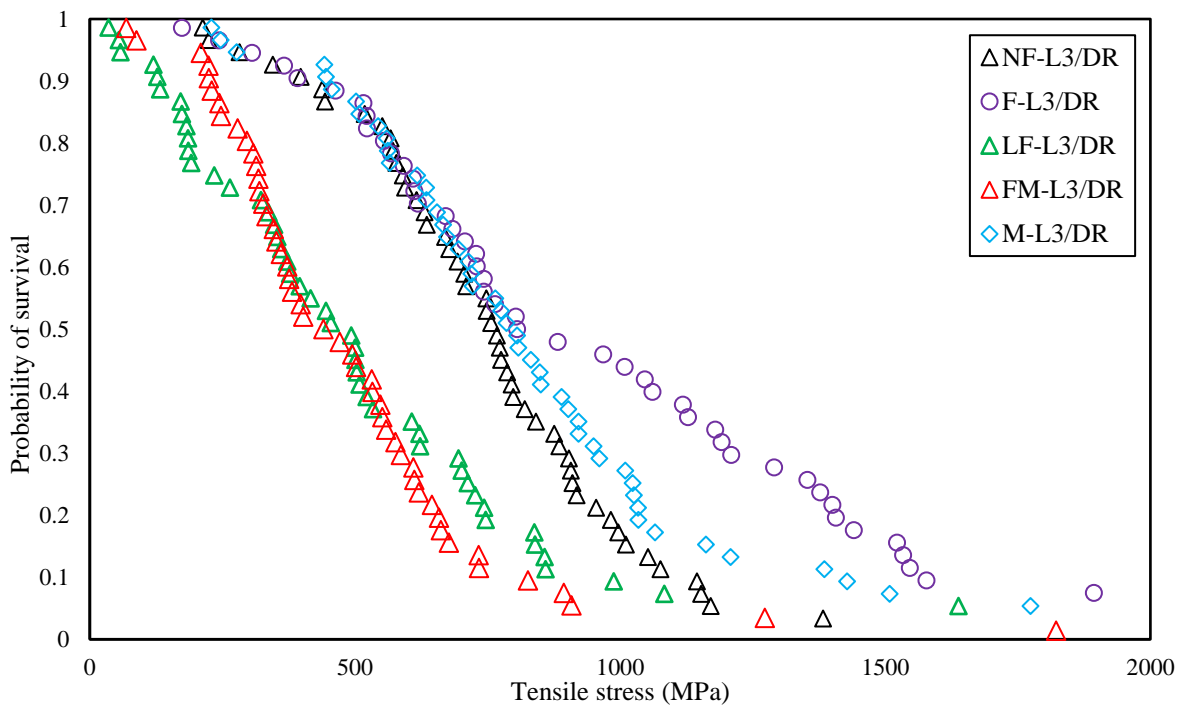


Figure 3.14: Tensile stress vs Probability of survival curve of 5 growth stages with L3 length and the DR estimator

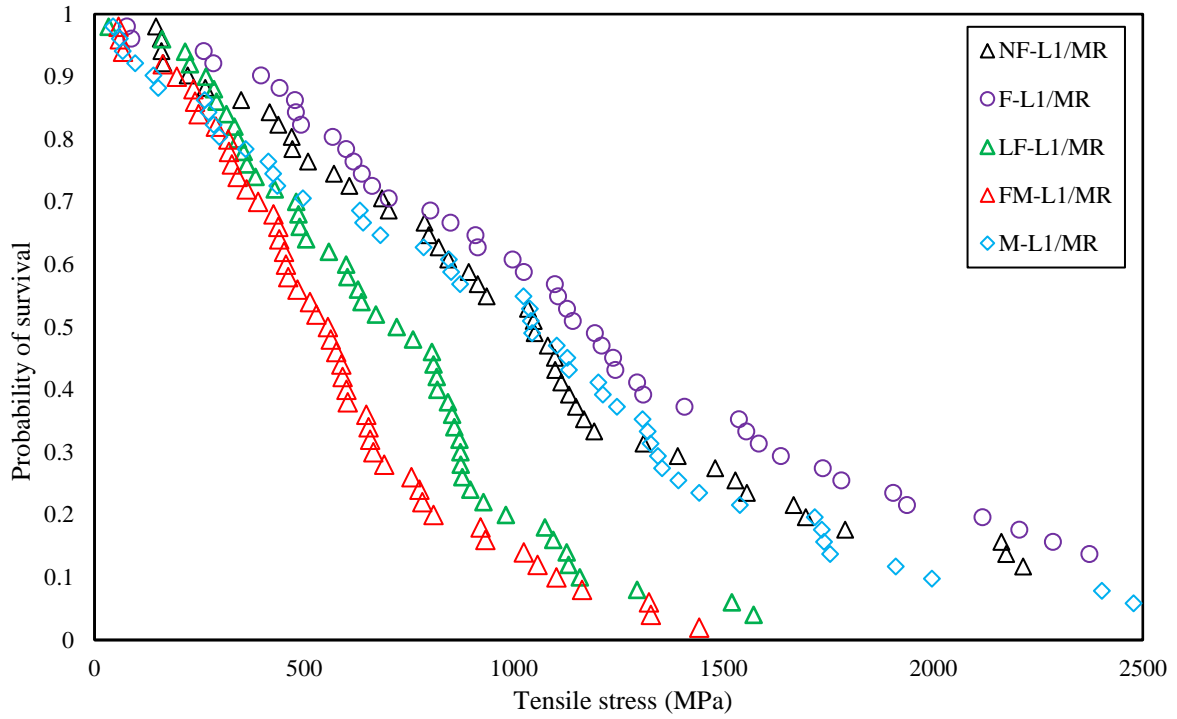


Figure 3.15: Tensile stress vs Probability of survival curve of 5 growth stages with L1 length and the MR estimator

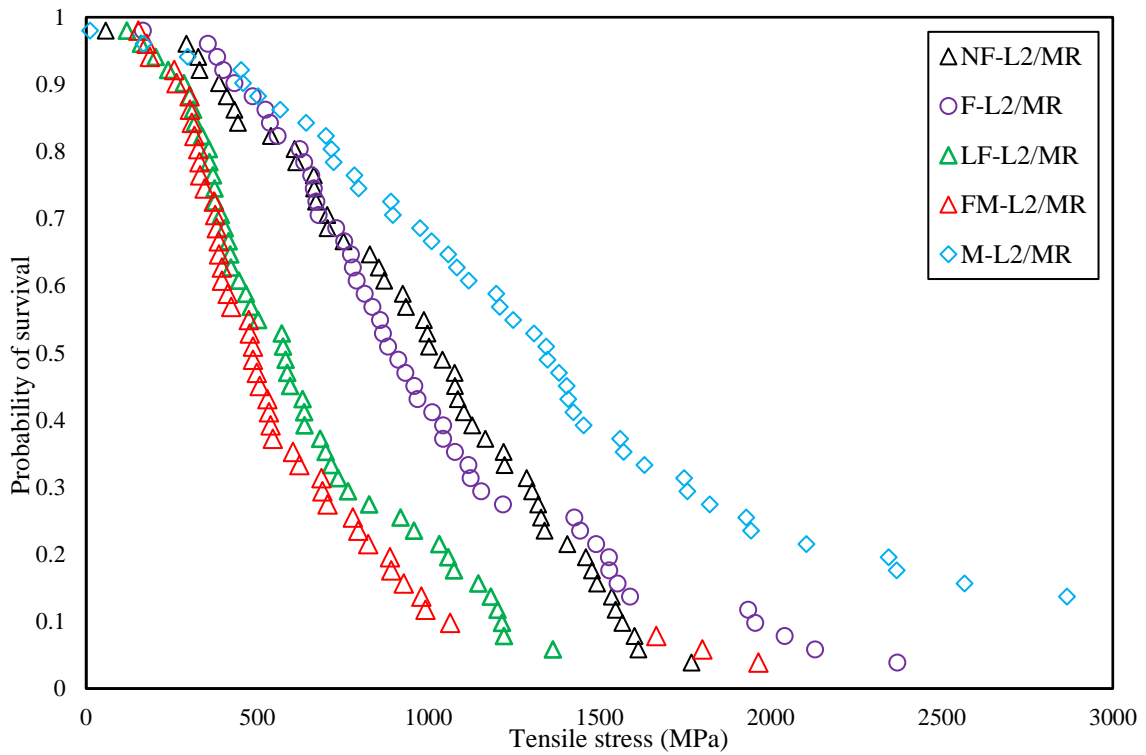


Figure 3.16: Tensile stress vs Probability of survival curve of 5 growth stages with L2 length and the MR estimator

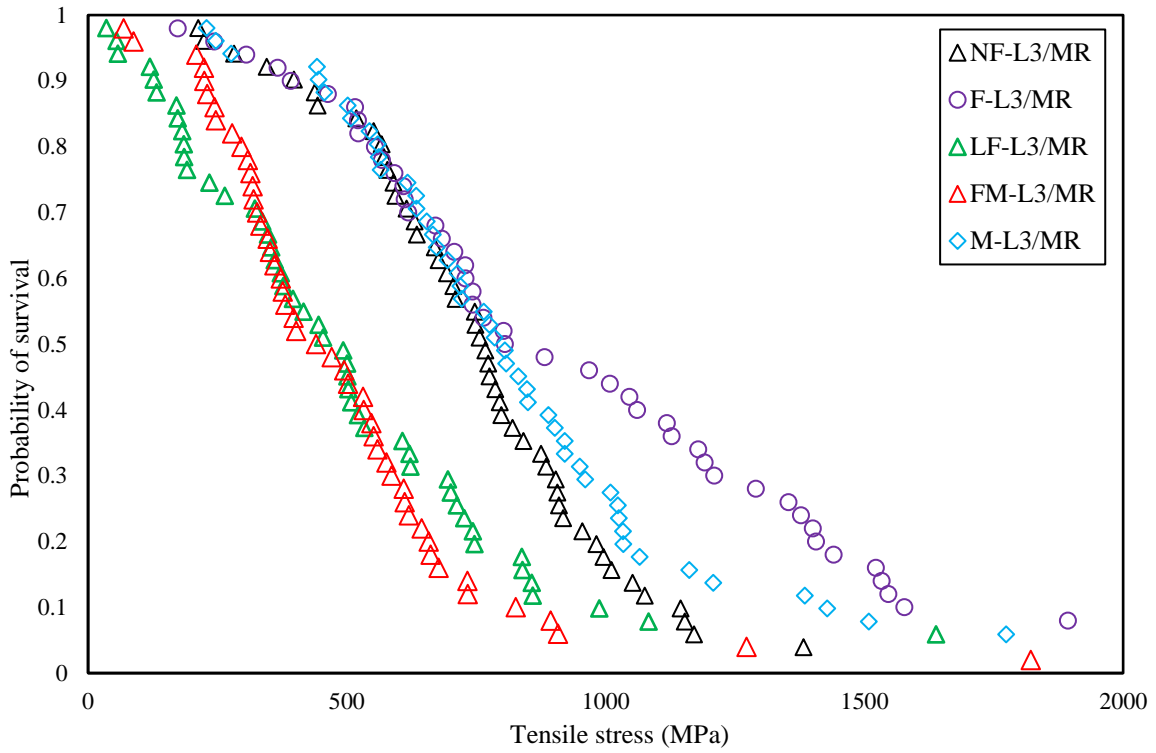


Figure 3.17: Tensile stress vs Probability of survival curve of 5 growth stages with L3 length and the MR estimator

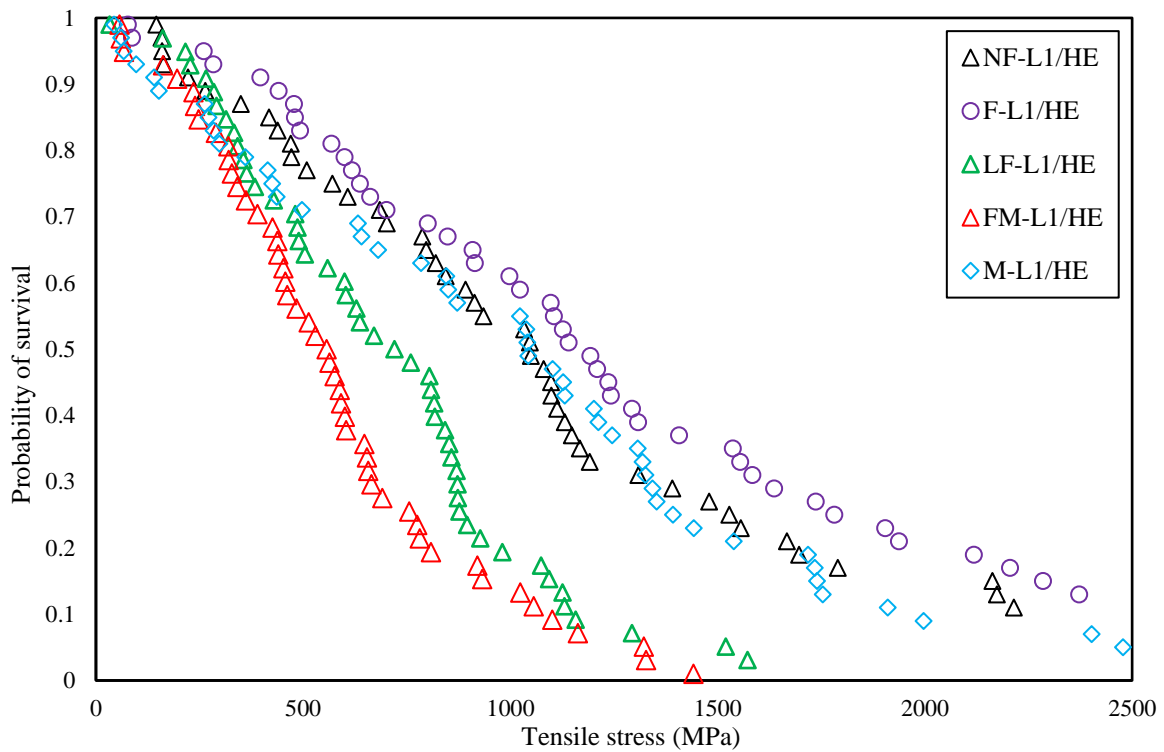


Figure 3.18: Tensile stress vs Probability of survival curve of 5 growth stages with L1 length and the HE estimator

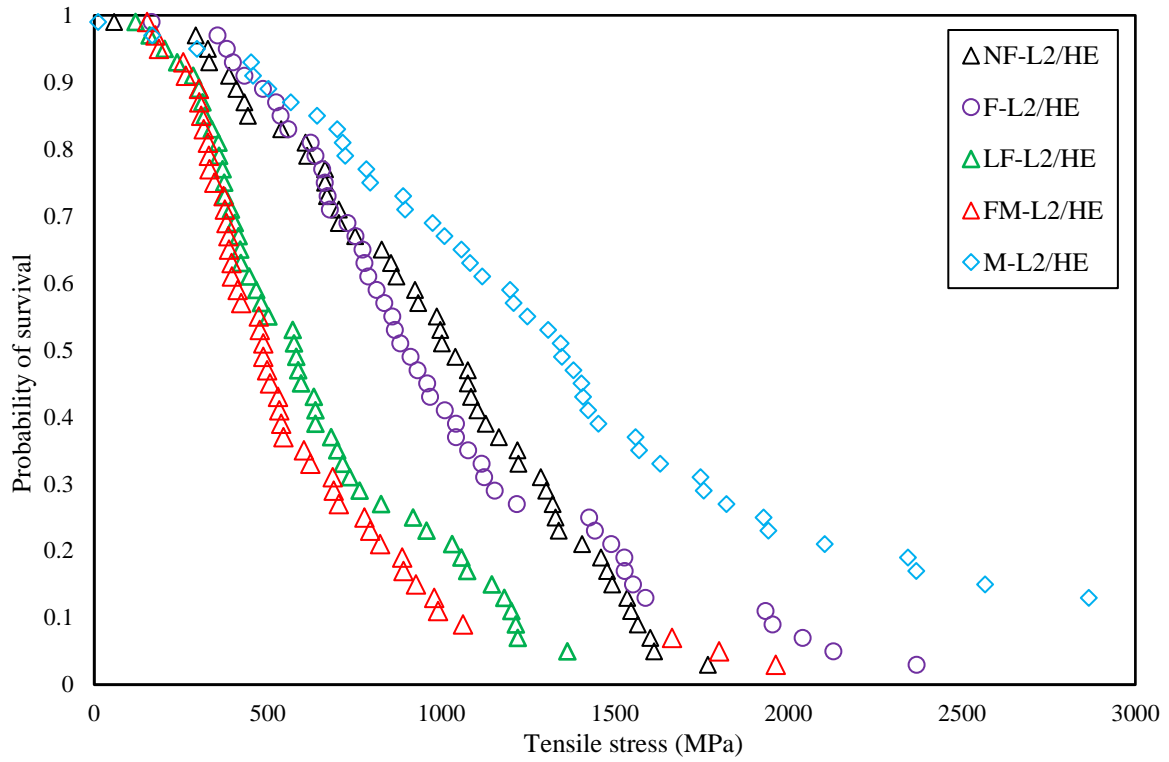


Figure 3.19: Tensile stress vs Probability of survival curve of 5 growth stages with L2 length and the HE estimator

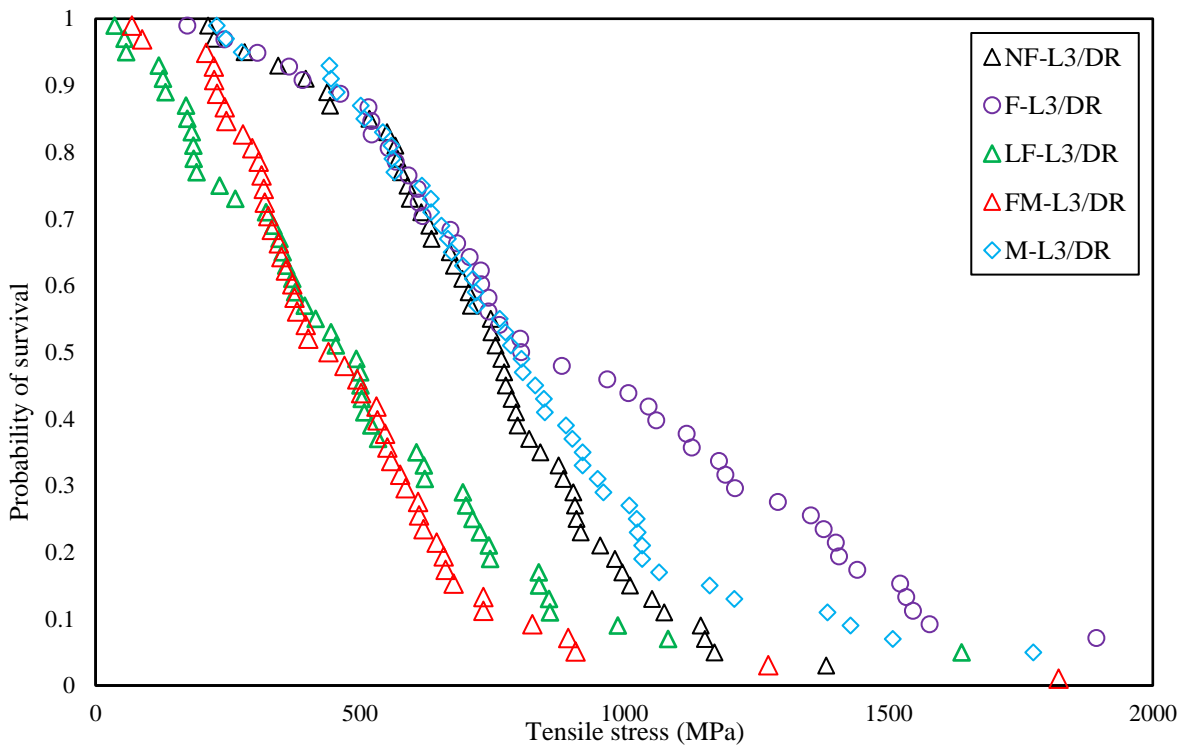


Figure 3.20: Tensile stress vs Probability of survival curve of 5 growth stages with L3 length and the HE estimator

3.2.2 Weibull Analysis of Tensile Stress Using Python

Table 3.2 delineates the Weibull parameters of tensile stress using both Linear Regression (LR) and Maximum Likelihood Estimation (MLE) methods. While MLE does not require any estimator (a sample calculation is provided in Section 2.4.3 Sample Calculation of Weibull distribution – Linear Regression Method), DR estimator was used for LR method.

Table 3.2: Weibull parameters of tensile stress using Python

ID	LR method (estimator: DR)			MLE method		
	α	β (MPa)	R^2_{σ}	α	β (MPa)	σ_{avg} (MPa)
NF-L1	1.56	1326	0.97	1.45	1347	1046
NF-L2	1.95	1182	0.93	1.81	1177	961.3
NF-L3	3.07	837.1	0.98	3.31	832	744.8
F-L1	1.49	1451	0.98	1.61	1436	1144
F-L2	2.29	1157	0.97	2.09	1173	984.3
F-L3	2.22	1076	0.98	2.13	1084	912.6
LF-L1	1.75	835.9	0.95	1.76	828.7	672.9
LF-L2	2.03	746.4	0.94	1.62	769.6	613.8
LF-L3	1.44	590.2	0.98	1.37	594.6	455.0
FM-L1	1.69	662.3	0.97	1.82	655.9	536.3
FM-L2	2.14	679.6	0.87	1.45	720.7	559.7
FM-L3	2.15	556.0	0.95	1.82	564.6	461.6
M-L1	1.17	1148	0.97	1.24	1135	844.6
M-L2	1.85	1666	0.97	1.67	1688	1355
M-L3	2.77	930.5	0.97	2.40	941.2	807.9

It can be seen from Table 3.2 that the α of tensile stress using the LR method that uses DR estimator is higher than 1.0 for all fifteen batches ranging from 1.14 to 3.07. The values of α obtained using linear regression method by Python programming are always higher than the Excel method, while the correlation coefficient (R^2_{σ}) for both methods is the same ranging from 0.87 to 0.98.

The value of β in all fifteen batches is closer to the σ_{avg} than the Excel method for DR estimator. The value of β calculated by Python regression is always lower than the Excel method in all fifteen cases. The inverse relationship between α and β is slightly more pronounced with Python programming than the Excel method (Figure 3.21). For each batch of cattail fibre, the Python Weibull shape parameter is on the right-hand side of the x-axis

while the shape parameter is on the lower side of the y-axis when compared with the Excel value.

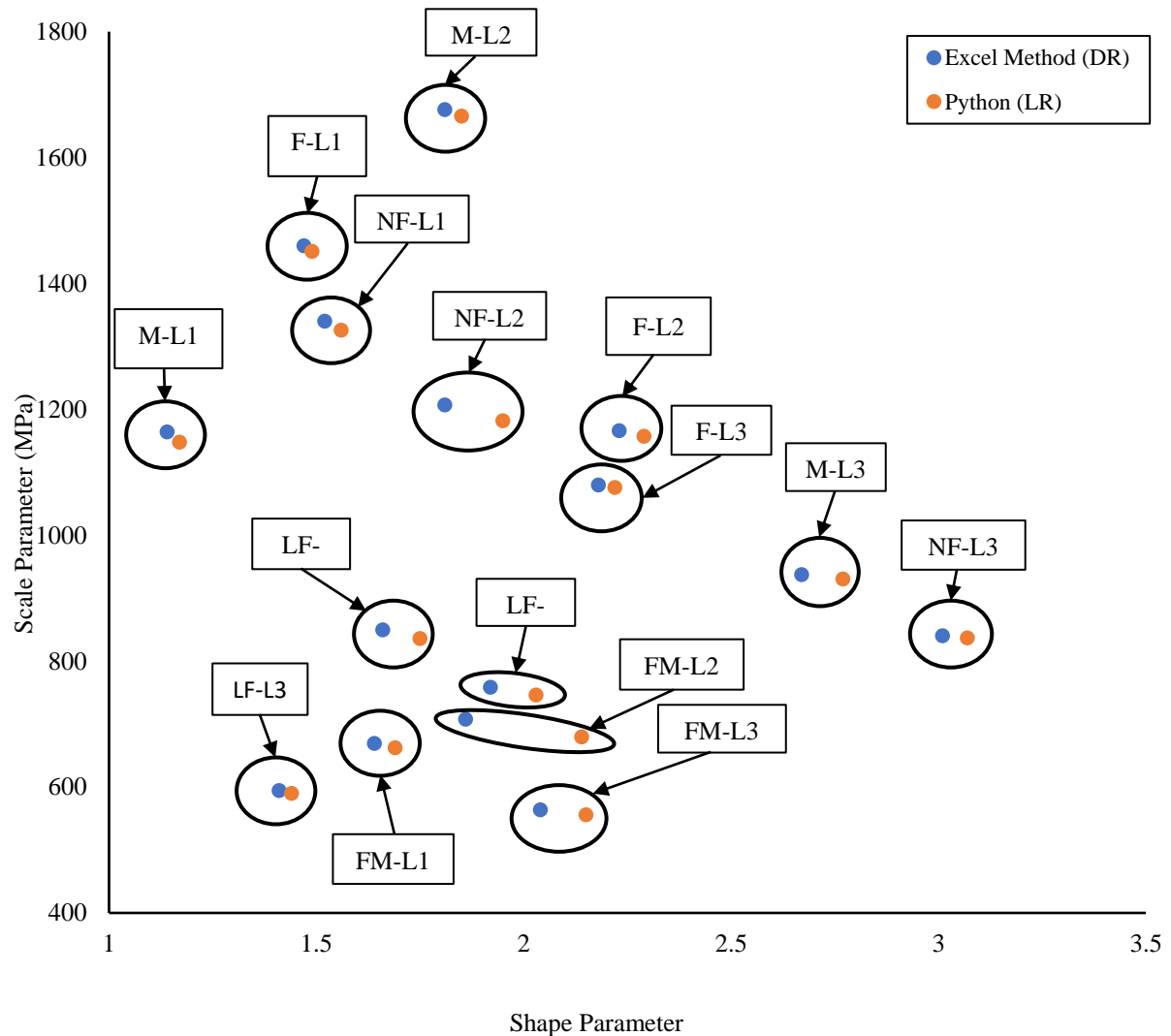


Figure 3.21: Relation between shape and scale parameter obtain from Excel and Python

The differences between Weibull parameters in Python and Excel regression methods could be due to the difference in the method of illustrating the regression line as suggested by Reddit (2018).

In the MLE method, the Weibull shape parameters are always greater than 1.0 and lie between 1.24 (M-L1) and 3.31 (NF-L3). There are differences in shape parameters for DR (linear regression) and MLE estimators. As discussed earlier, the Weibull shape parameter

depends on the data fluctuation (standard deviation) in LR method, while in MLE method the x^α value of each data contributes to the shape parameter shown in Equation 2.17.

Weibull average in MLE is always lower than the experimental tensile stress values (Table 3.2). The difference in \bar{x}_{stress} value and the σ_{avg} is the lowest or almost non-existent if α value is high. For example, the difference is minuscule for the two samples, NF-L3 (difference for DR estimator is 2.9 MPa, for HE estimator is 2 MPa, and for MR estimator is 4.2 MPa) and M-L3 (difference for DR estimator is 16.9 MPa, for HE estimator is 15.6 MPa, and for MR estimator is 18.3 MPa) with the shape parameters of 3.31 and 2.40, respectively, while the largest difference (for DR estimator: 214.5 MPa, for HE estimator: 211.2 MPa, and for MR estimator: 218.3 MPa) was found for the lowest shape parameter which is 1.24 for M-L1 (Table 3.1).

Similar to LR method, the scale parameter in MLE is always higher than both experimental and average Weibull tensile stresses.

3.2.3 Weibull Analysis of Modulus – Linear Regression (LR) Method

Weibull analysis was conducted with the data of modulus (Young's) from 15 batches using three estimators, and the results are shown in Table 3.3.

Table 3.3: Weibull Parameters of modulus (Linear Regression – Excel)

ID	\bar{x}_{modulus} (GPa)	E_{avg} (GPa)			α			β (GPa)			R^2_{σ}		
		DR	HE	MR	DR	HE	MR	DR	HE	MR	DR	HE	MR
NF-L1	45.19 [28.78]	41.65	41.76	41.51	1.91	1.97	1.83	50.47	50.31	50.69	0.94	0.93	0.95
NF-L2	55.29 [26.38]	53.42	53.52	53.30	2.40	2.48	2.30	62.23	62.04	62.49	0.98	0.98	0.98
NF-L3	47.32 [19.77]	46.23	46.30	46.14	2.45	2.53	2.35	53.68	53.51	53.92	0.98	0.98	0.98
F-L1	65.44 [41.72]	59.01	59.17	58.82	1.73	1.78	1.66	72.94	72.66	73.33	0.97	0.96	0.97
F-L2	29.51 [14.76]	28.34	28.41	28.27	2.32	2.38	2.24	33.20	33.13	33.30	0.94	0.93	0.95
F-L3	65.59 [27.96]	64.68	64.80	64.56	2.90	2.99	2.78	73.41	73.25	73.65	0.91	0.90	0.92
LF-L1	37.22 [22.53]	34.67	34.75	34.57	1.99	2.05	1.92	41.67	41.54	41.85	0.95	0.94	0.96
LF-L2	43.37 [29.97]	39.80	39.89	39.68	1.93	1.99	1.86	48.11	47.95	48.31	0.91	0.90	0.91
LF-L3	44.06 [31.03]	39.96	40.06	39.84	1.83	1.89	1.76	48.81	48.65	49.03	0.93	0.92	0.93
FM-L1	32.79 [15.29]	31.83	31.90	31.75	2.49	2.56	2.39	36.88	36.80	37.00	0.94	0.93	0.95
FM-L2	40.77 [23.29]	39.07	39.14	38.99	2.37	2.45	2.28	45.60	45.46	45.78	0.92	0.91	0.92
FM-L3	33.35 [21.19]	31.72	31.77	31.65	2.31	2.39	2.23	37.16	37.05	37.31	0.88	0.87	0.88
M-L1	55.71 [30.22]	53.39	53.53	53.24	2.31	2.39	2.22	62.56	62.39	62.82	0.91	0.90	0.92
M-L2	47.87 [26.92]	45.22	45.32	45.10	2.14	2.21	2.06	53.66	53.51	53.88	0.95	0.94	0.96
M-L3	60.72 [28.10]	59.48	59.56	59.36	2.77	2.86	2.66	67.89	67.72	68.12	0.93	0.93	0.94

Standard deviation is presented in square bracket; \bar{x}_{modulus} : Experimental modulus; E_{avg} : Weibull average; α : shape parameter; β : scale parameter; DR: median rank estimator; HE: Hazen estimator; MR: mean rank estimator

The average Weibull modulus (E_{avg}) is lower than the experimental values with the correlations, which were higher than 0.88 for all 15 batches using the three estimators (Table 3.3). However, the E_{avg} obtained by three estimators is slightly different for all five growth stages and three lengths, which follows the order: HE>DR>MR in terms of the closeness to E_{avg} . The difference between experimental and E_{avg} calculated using DR, HE and MR estimators are directly proportional to the coefficient of variation of the experimental modulus values, as shown in Figure 3.22.

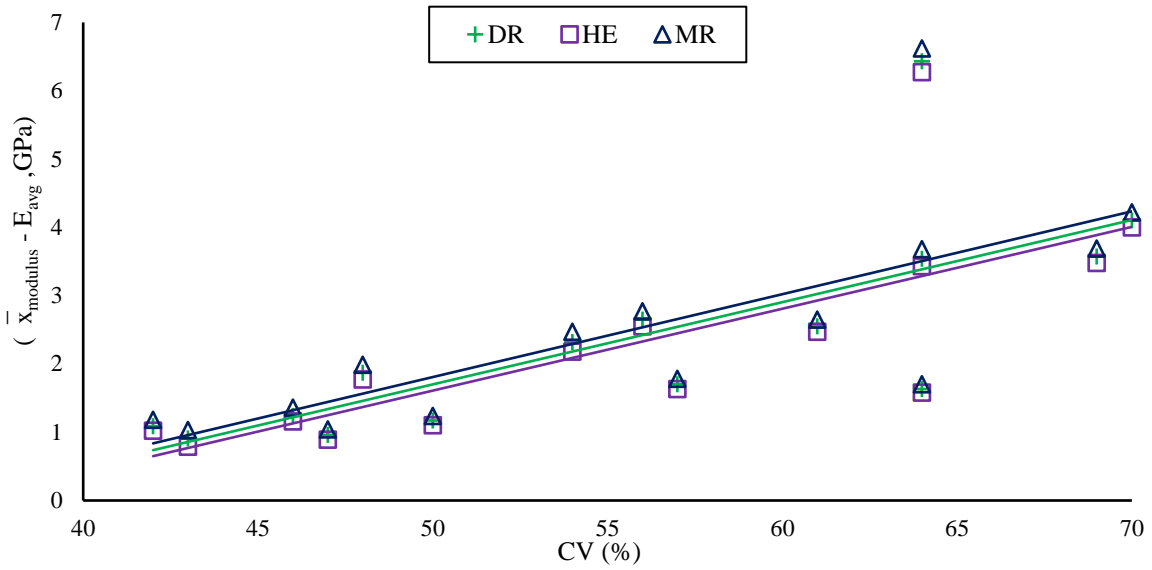


Figure 3.22: Relationship between the difference between experimental and predicted Weibull average values with the coefficient of variation (CV%) of modulus

The α values are above 1.0 for all 15 batches, with the lowest being 1.66 (F-L1, estimator: MR) and the highest being 2.99 (F-L3, estimator: HE). Similar to the shape parameter for tensile stress, there is no clear trend obtained for either growth stages or fibre lengths. For a specific batch of samples, the shape parameter in descending order is: HE>DR>MR and is inversely proportional to the coefficient of variation of the experimental average modulus (Figure 3.23).

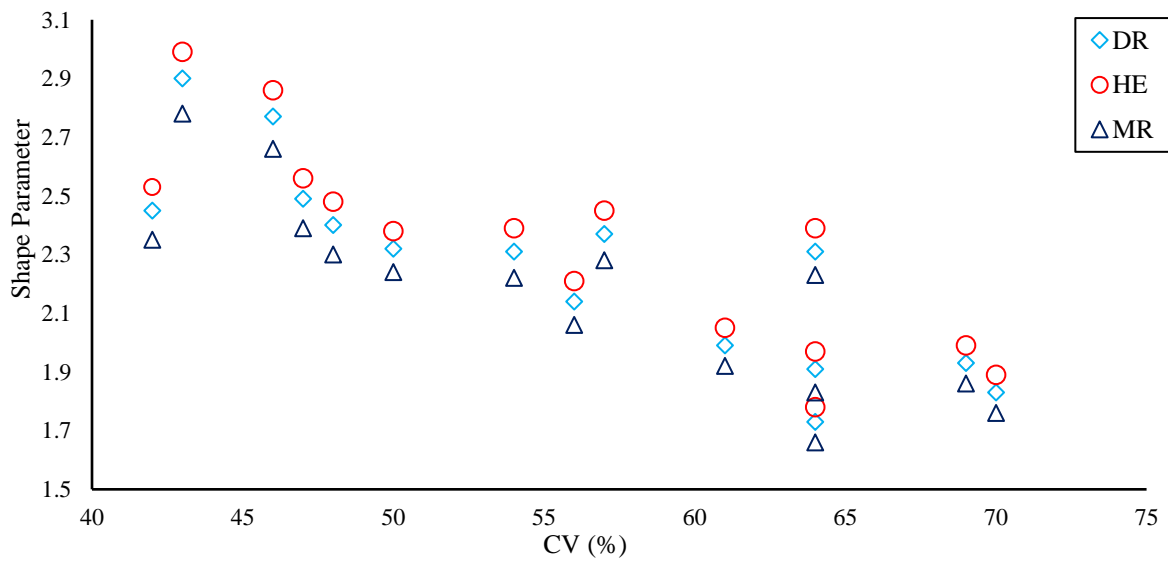


Figure 3.23: Relationship between shape parameter and coefficient of variation (%) of modulus

The scale parameter (β) for the three estimators is always higher than σ_{avg} and x_{modulus} for all five growth stages and lengths. β was the highest for the DR estimator, followed by HE and MR estimators, although the difference between the three estimators is very small (Figure 3.24). The difference between the β and \bar{x}_{modulus} is directly proportional to the coefficient of variation of the experimental averages: the larger the CV%, the higher the difference (Figure 3.24). For example, the largest differences were obtained for samples NF-L1 (CV%: 64, %difference: 8), F-L1 (CV%: 64, %difference: 10), LF-L2 (CV%: 69, %difference: 8) and LF-L3 (CV%: 70, %difference: 9), while the smallest differences were obtained for NF-L3 (CV%: 42, %difference: 2), F-L3 (CV%: 43, %difference: 1) and FM-L1 (CV%: 47, %difference: 3).

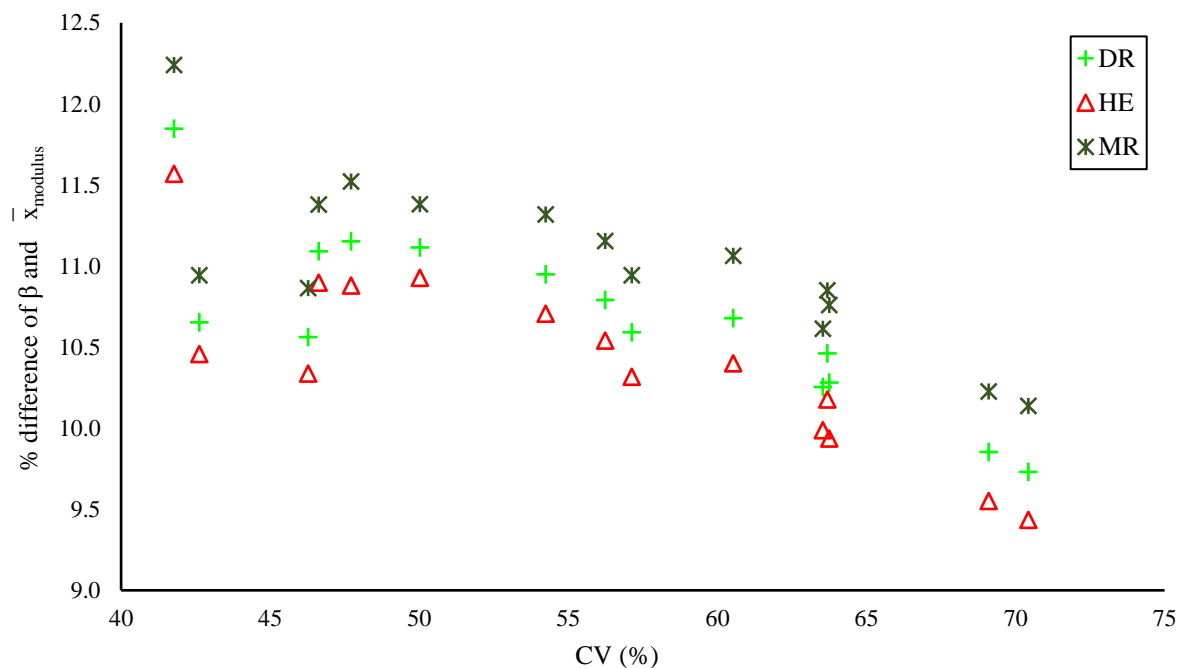


Figure 3.24: Relationship between CV% and the percentage difference between scale parameter and average experimental modulus

No relationship was obtained for CV% with the percentage difference between scale parameters and Weibull average (Figure 3.25). The percentage difference ranged from 4.90% to 9.19%, except for the F-L1 batch.

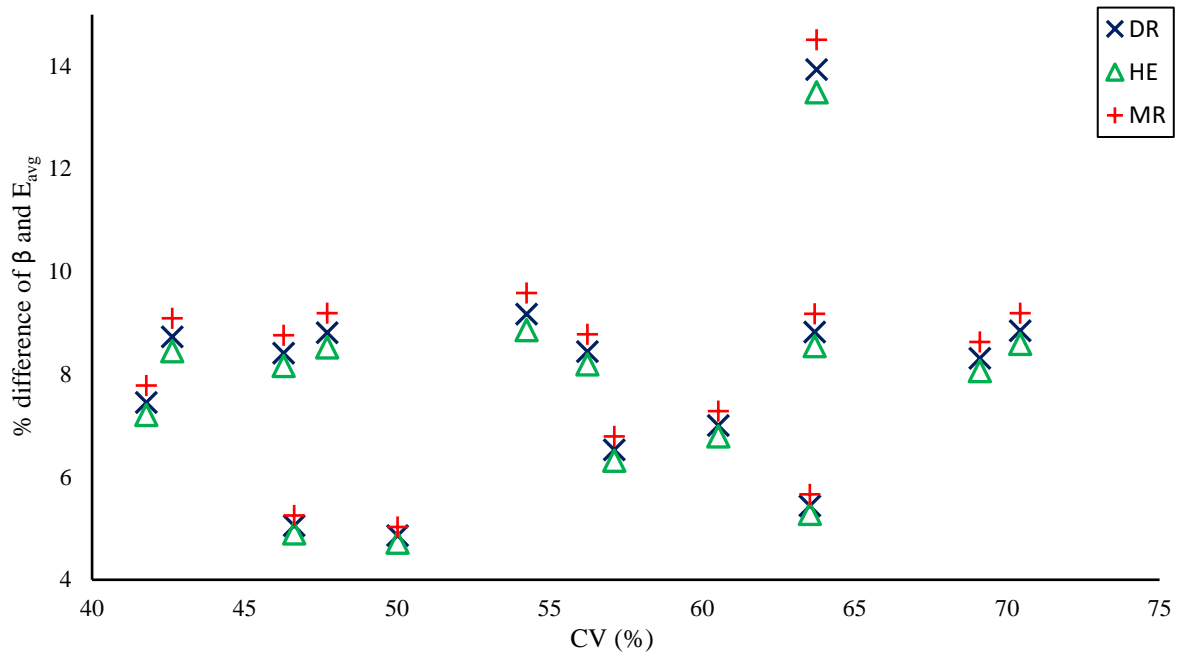


Figure 3.25: Relationship between CV% and the percentage difference between scale parameter and average Weibull modulus

However, there is a direct relationship between the standard deviation and the percentage differences between scale parameters and the Weibull average (Figure 3.26). An extreme difference of 15% was obtained for the standard deviation of 42 GPa for the sample F-L1.

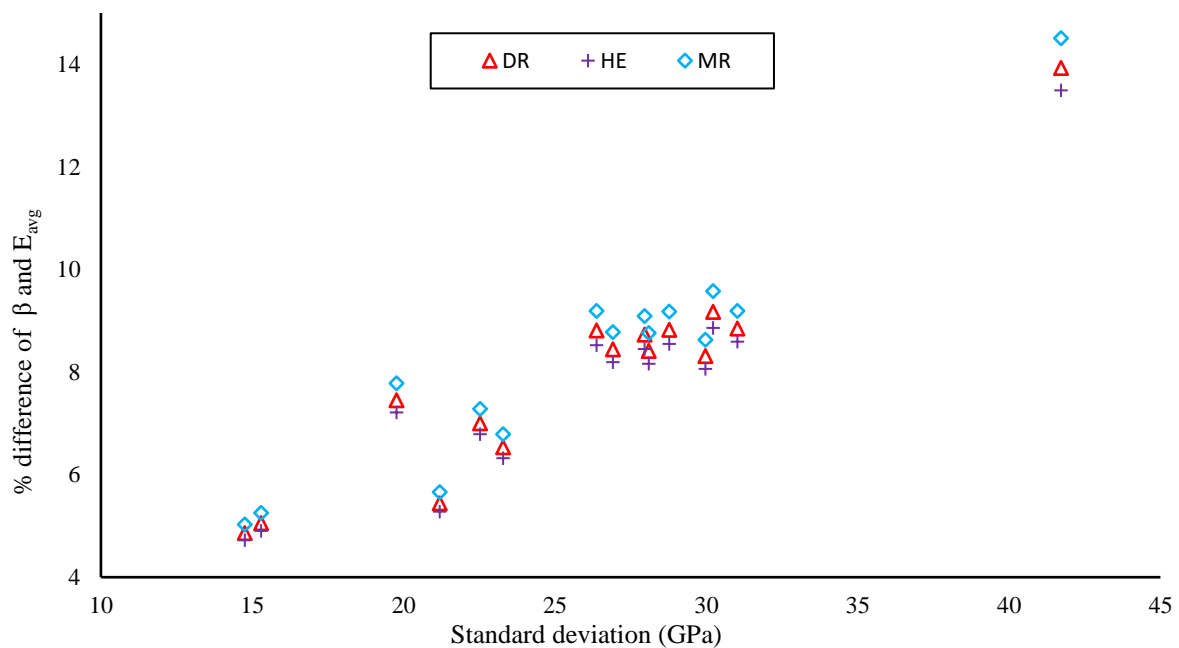


Figure 3.26: Relationship between CV% and the percentage difference between scale parameter and standard deviation of modulus

Weibull graph for modulus using linear regression method is shown in Figure 3.27 to Figure 3.35. Two parameters of Weibull distribution were calculated using these Weibull lines in the figures.

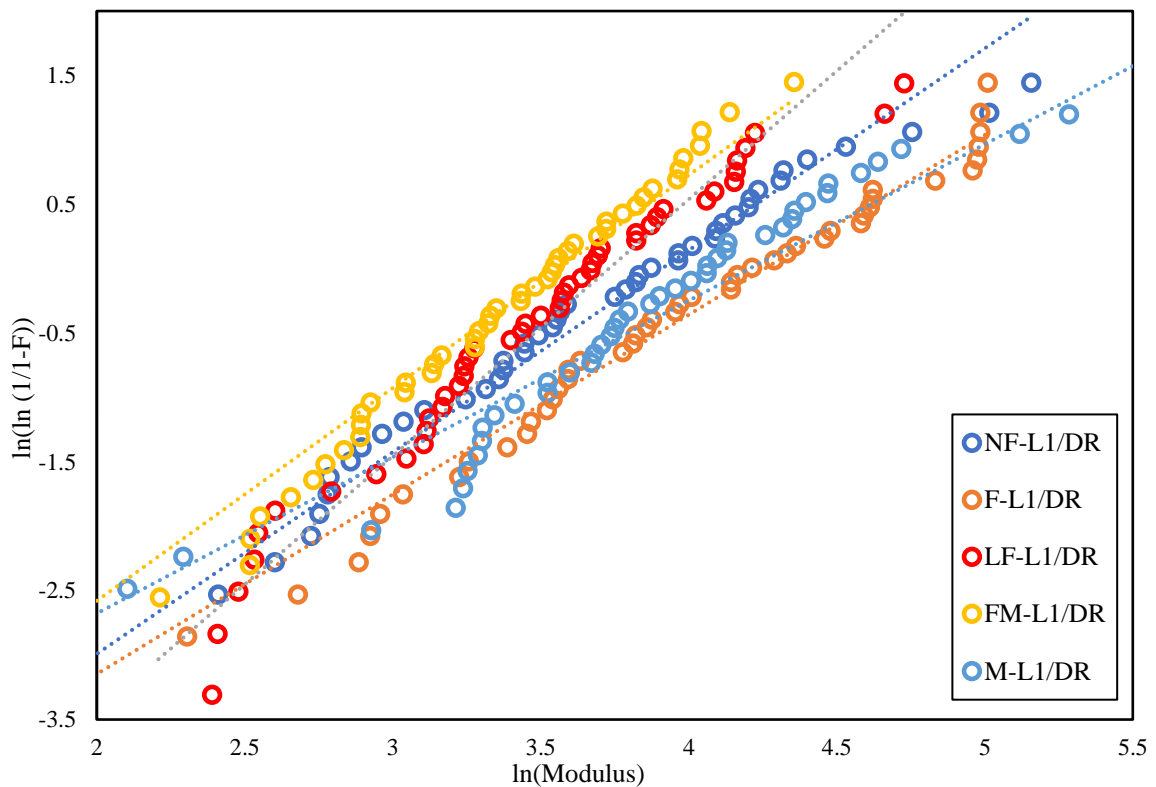


Figure 3.27: $\ln(\ln(1/(1-F)))$ vs $\ln(\text{modulus})$ curve of 5 growth stages with L1 length and the DR estimator

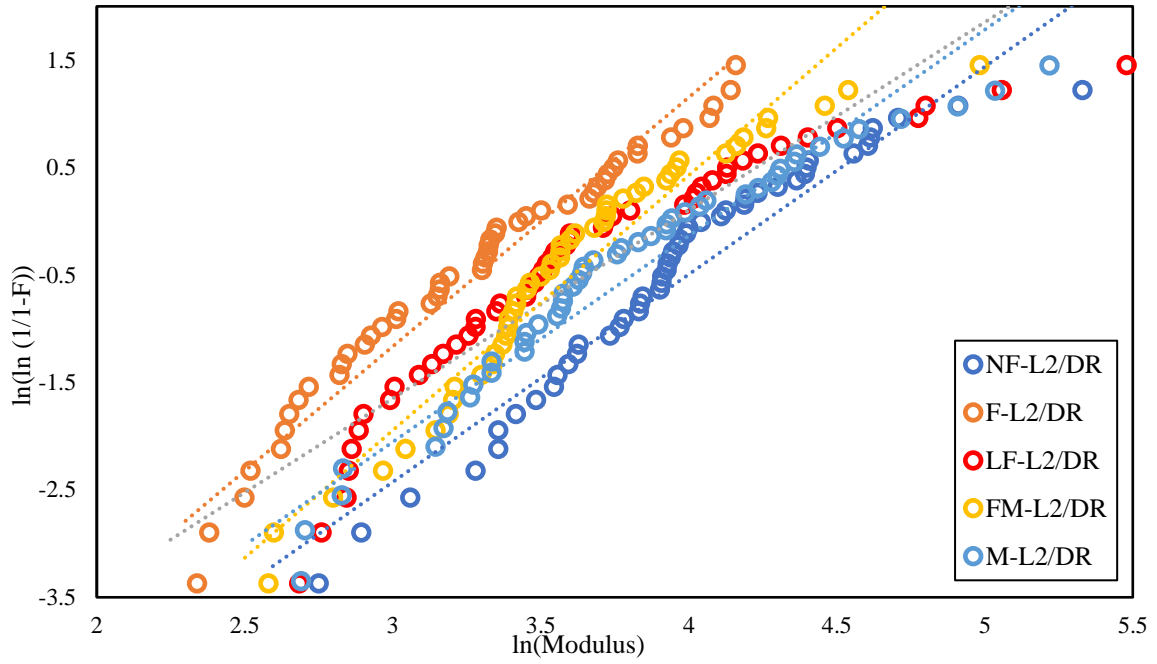


Figure 3.28: $\ln(\ln(1/(1-F)))$ vs $\ln(\text{modulus})$ curve of 5 growth stages with L2 length and the DR estimator

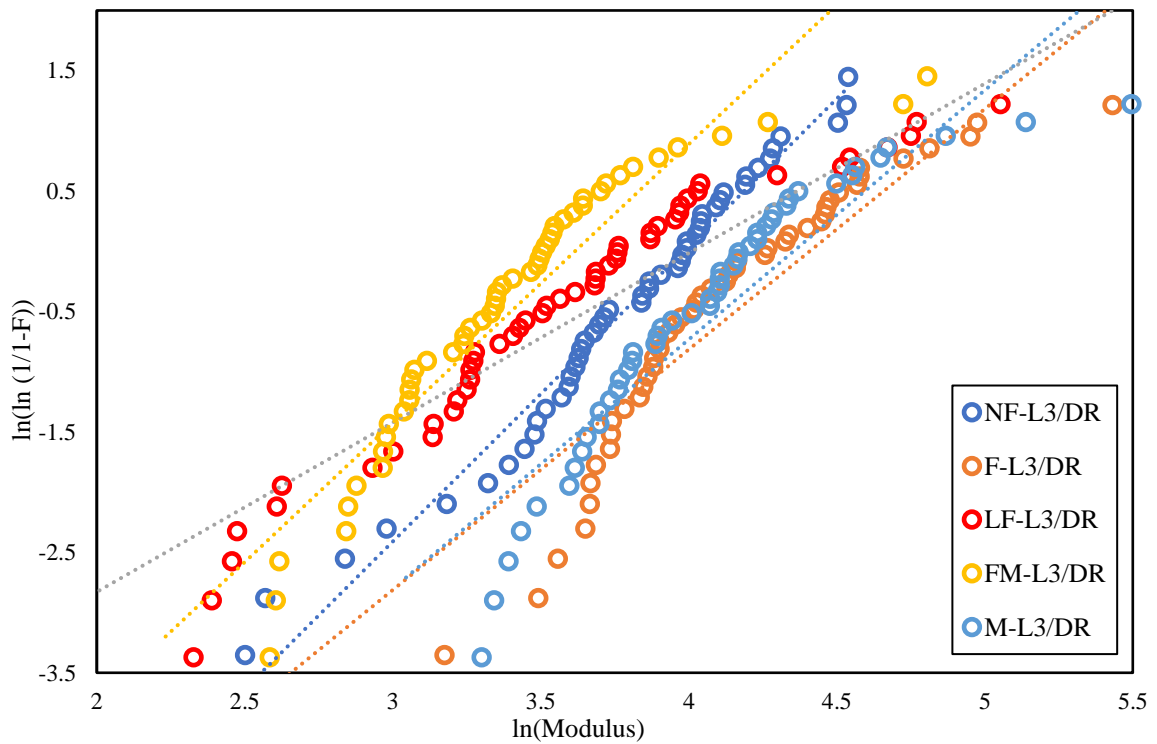


Figure 3.29: $\ln(\ln(1/(1-F)))$ vs $\ln(\text{modulus})$ curve of 5 growth stages with L3 length and the DR estimator

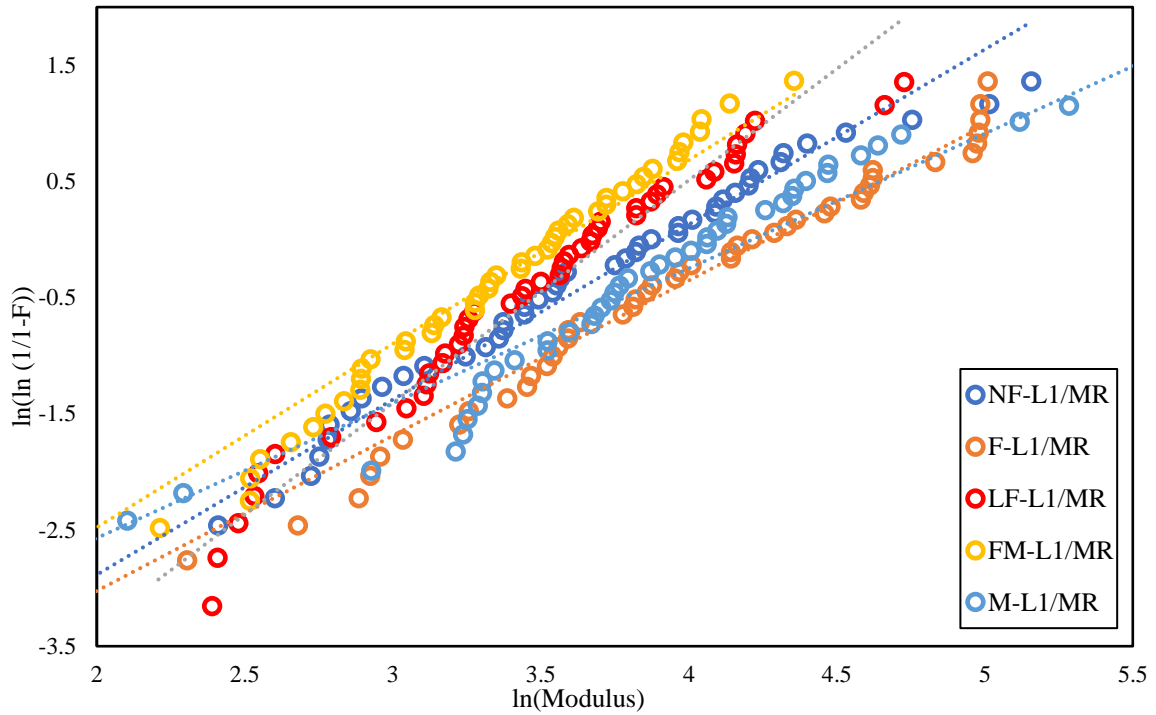


Figure 3.30: $\ln(\ln(1/1-F))$ vs $\ln(\text{modulus})$ curve of 5 growth stages with L1 length and the MR estimator

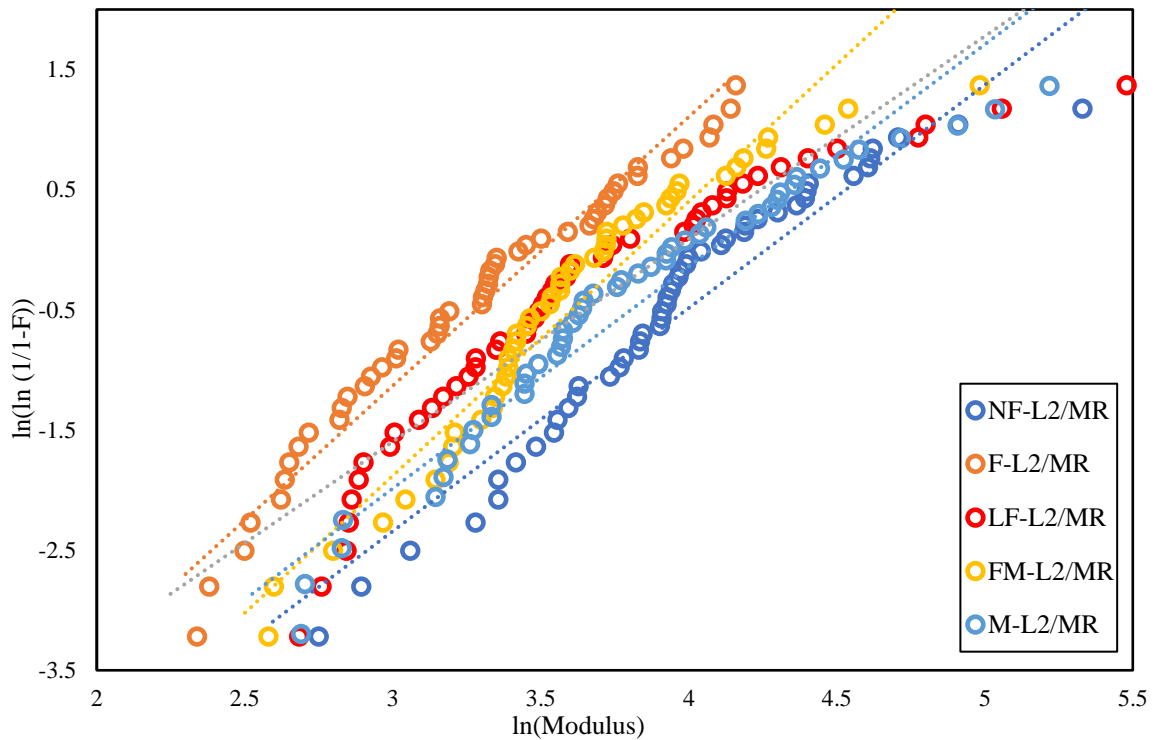


Figure 3.31: $\ln(\ln(1/1-F))$ vs $\ln(\text{modulus})$ curve of 5 growth stages with L2 length and the MR estimator

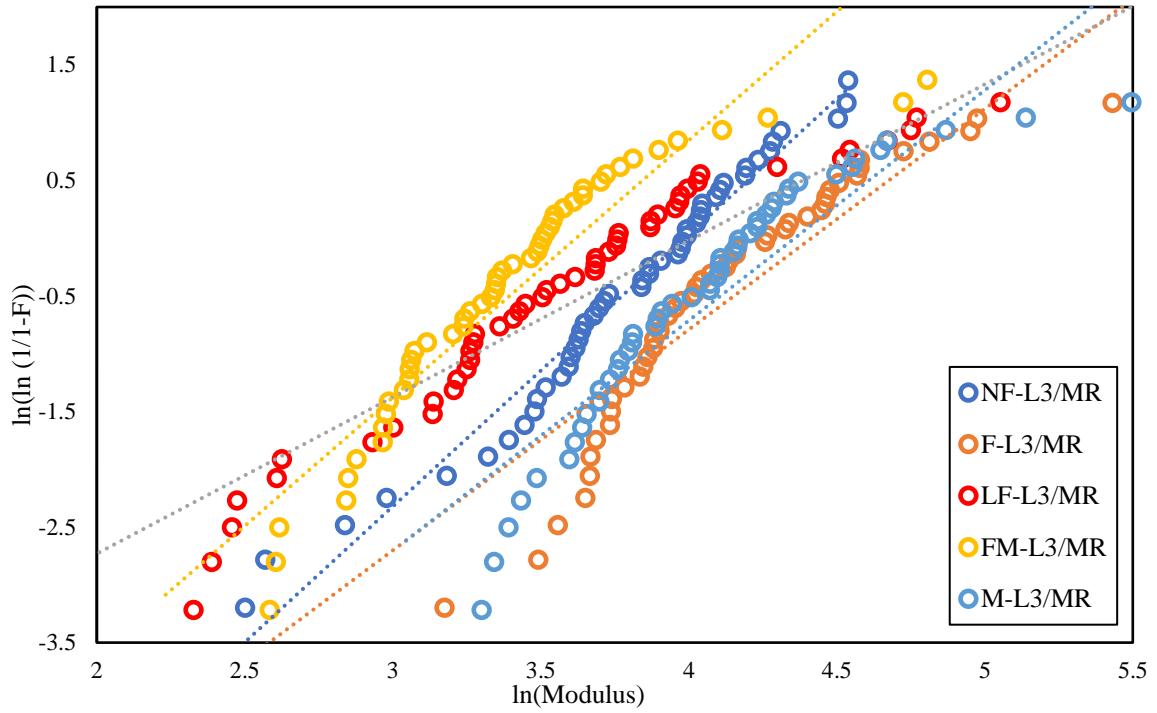


Figure 3.32: $\ln(\ln(1/1-F))$ vs $\ln(\text{modulus})$ curve of 5 growth stages with L3 length and the MR estimator

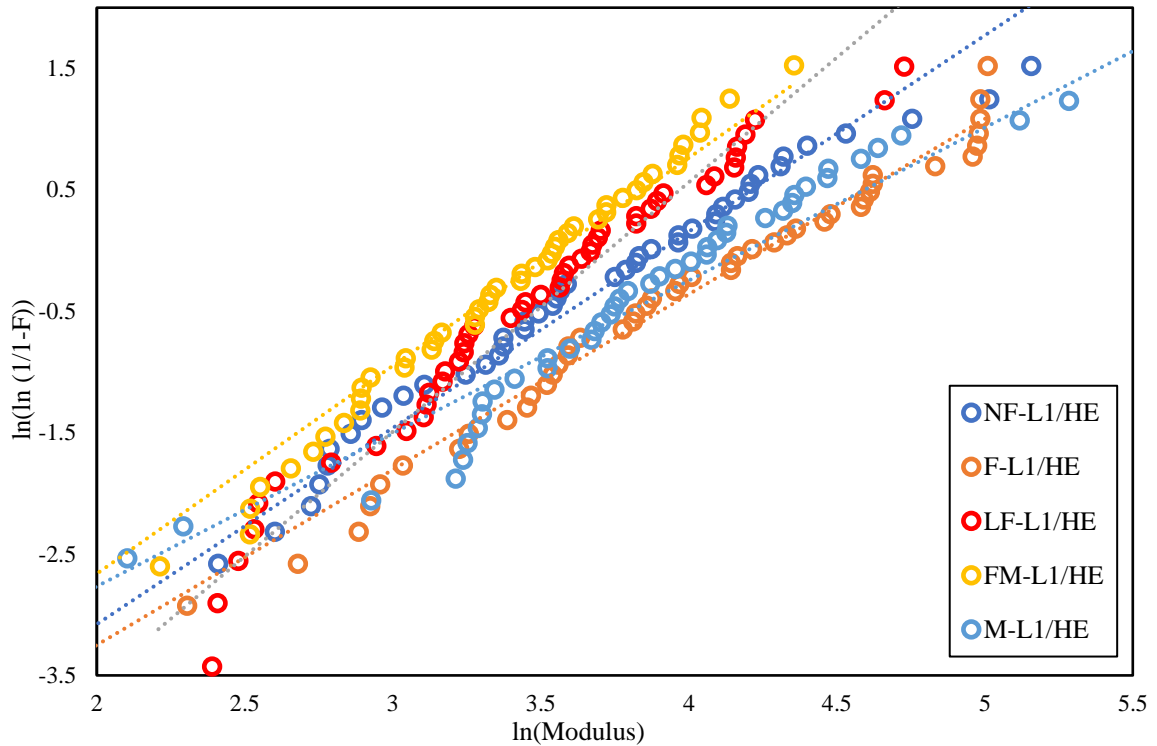


Figure 3.33: $\ln(\ln(1/1-F))$ vs $\ln(\text{modulus})$ curve of 5 growth stages with L1 length and the HE estimator

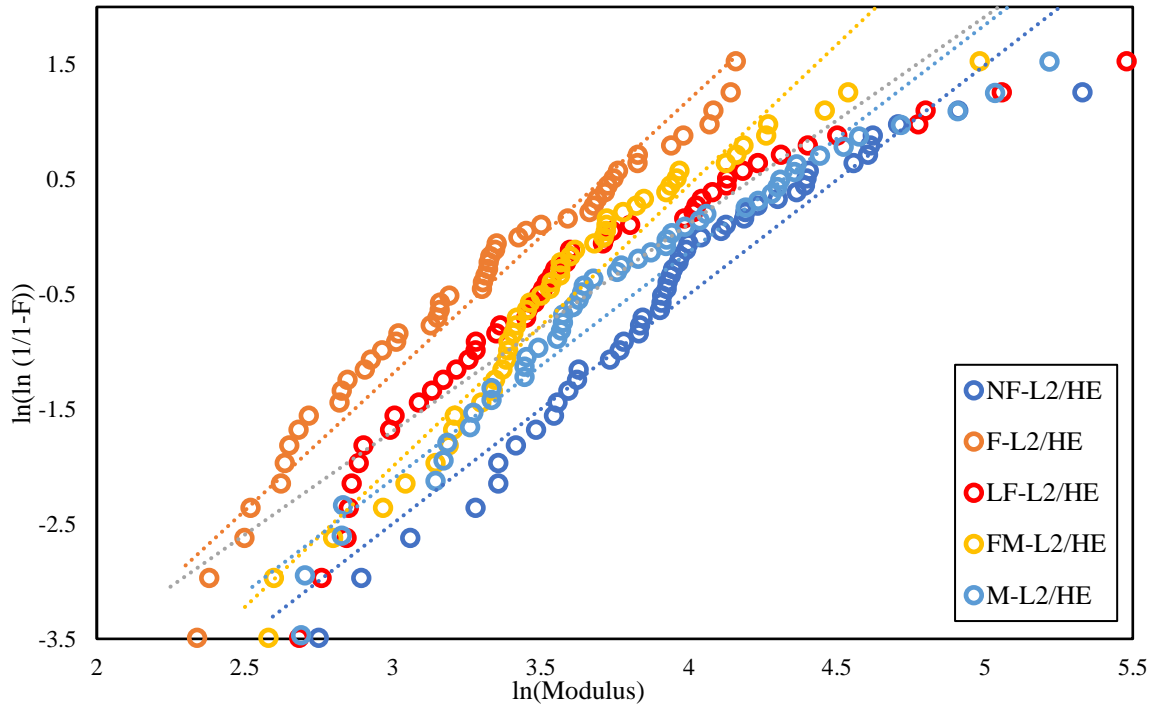


Figure 3.34: $\ln(\ln(1/(1-F)))$ vs $\ln(\text{modulus})$ curve of 5 growth stages with L2 length and the HE estimator

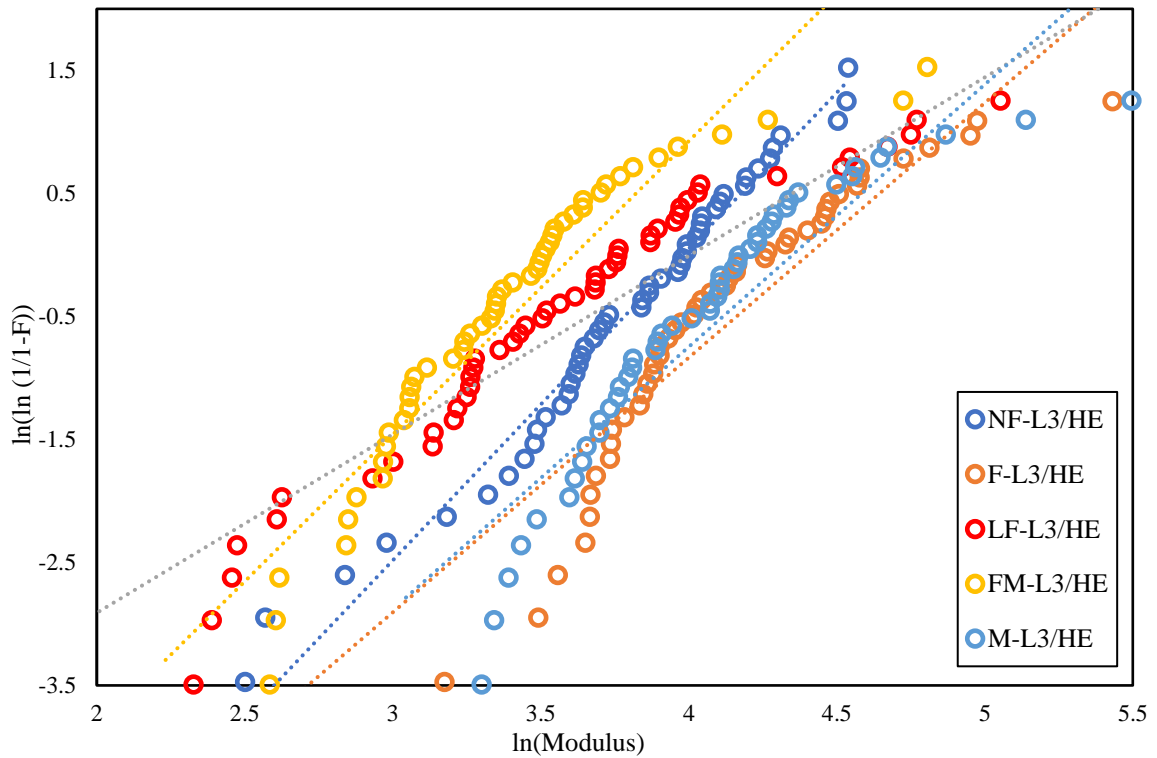


Figure 3.35: $\ln(\ln(1/(1-F)))$ vs $\ln(\text{modulus})$ curve of 5 growth stages with L3 length and the HE estimator

Figure 3.36 to Figure 3.44 delineate the curves of the modulus vs probability of survival for five growth stages of three different lengths using three estimators separately. The curves indicate the inversely proportional relationship between the modulus and the probability of survival which means the probability of survival or reliability decreases with the positive change in modulus. The rate of decrease in the probability of survival with an increase of modulus varies from batch to batch and estimator to estimator; however, a common trend is noticed here.

In Figure 3.36, it can be noticed that the F-L1 batch has the highest probability of survival among the five growth stages of L1 length using the DR estimator, followed by the M-L1 and NF-L1. In addition, when the DR estimator was used, the NF-L2 batch had the best probability of survival among the growth stages of L2 length (Figure 3.37), followed by batches M-L2 and LF-L2. Moreover, in Figure 3.38, the reliability was found to be better at the F-L3 batch than at any other batches of L3 length when the DR estimator was used.

The probability of survival of the F-L1 batch was the highest (Figure 3.39) among the five growth stages of L1 length when the MR estimator was implemented in the Weibull distribution. The second highest batch was the M-L1, followed by the NF-L1 batch (Figure 3.39). Moreover, in the case of the L2 length of five growth stages and the MR estimator, the NF-L2 batch was the top-ranked dataset of reliability, followed by the M-L2 and LF-L2 (Figure 3.40). Furthermore, the F-L3 batch has the highest reliability among the growth stages of L3 length when the MR estimator was used, followed by the M-L3 and NF-L3 (Figure 3.41).

In Figure 3.42, the minimum probability of failure was at the dataset of the F-L1 batch among the L1 length using the HE estimator in Weibull distribution, followed by batches M-L1 and NF-L1 (Figure 3.42), as with the other estimators. In addition, when the HE estimator was implemented, the NF-L2, M-L2, and LF-L2 were the top-ranked batches of

the probability of survival among the five growth stages of L2 length (Figure 3.43). Further, the best batch of the five growth stages of L3 length was the F-L1 which has the highest reliability, followed by the M-L3 and NF-L3 batches (Figure 3.44).

Figure 3.36 to Figure 3.44 conclude a finding that the flower (F) stage has the best dataset of modulus for the L1 and L3 length, but for L2, the non-flower (NF) stage has the values with the highest reliability.

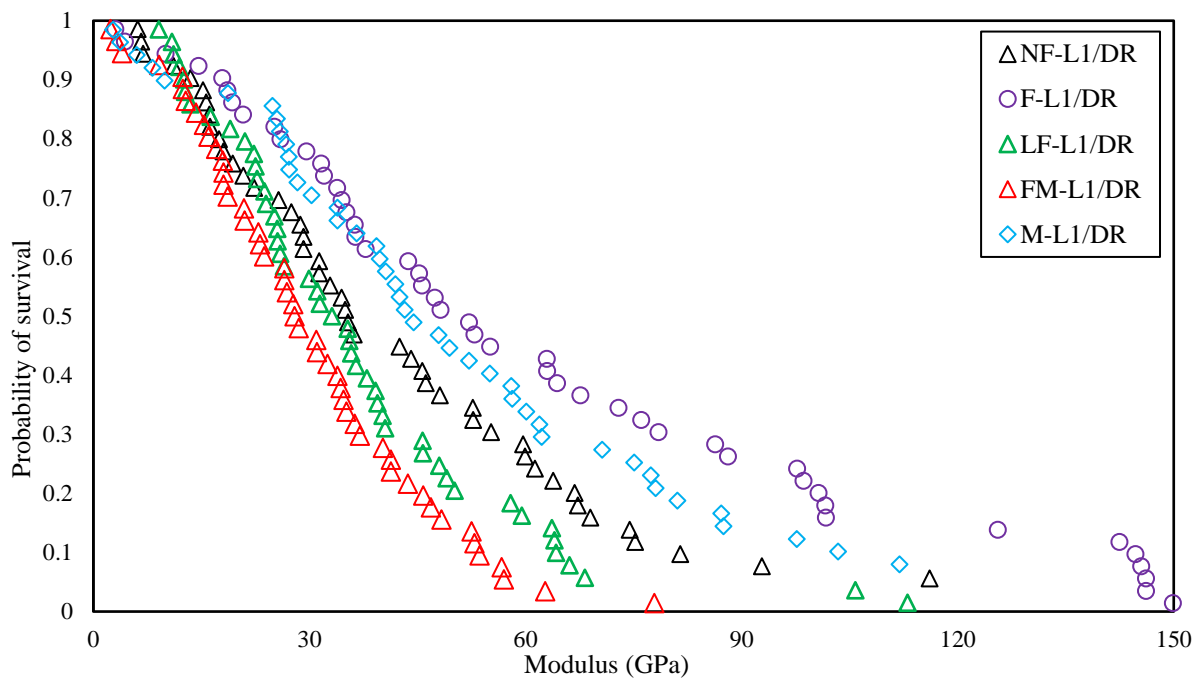


Figure 3.36: Modulus vs Probability of survival curve of 5 growth stages with L1 length and the DR estimator

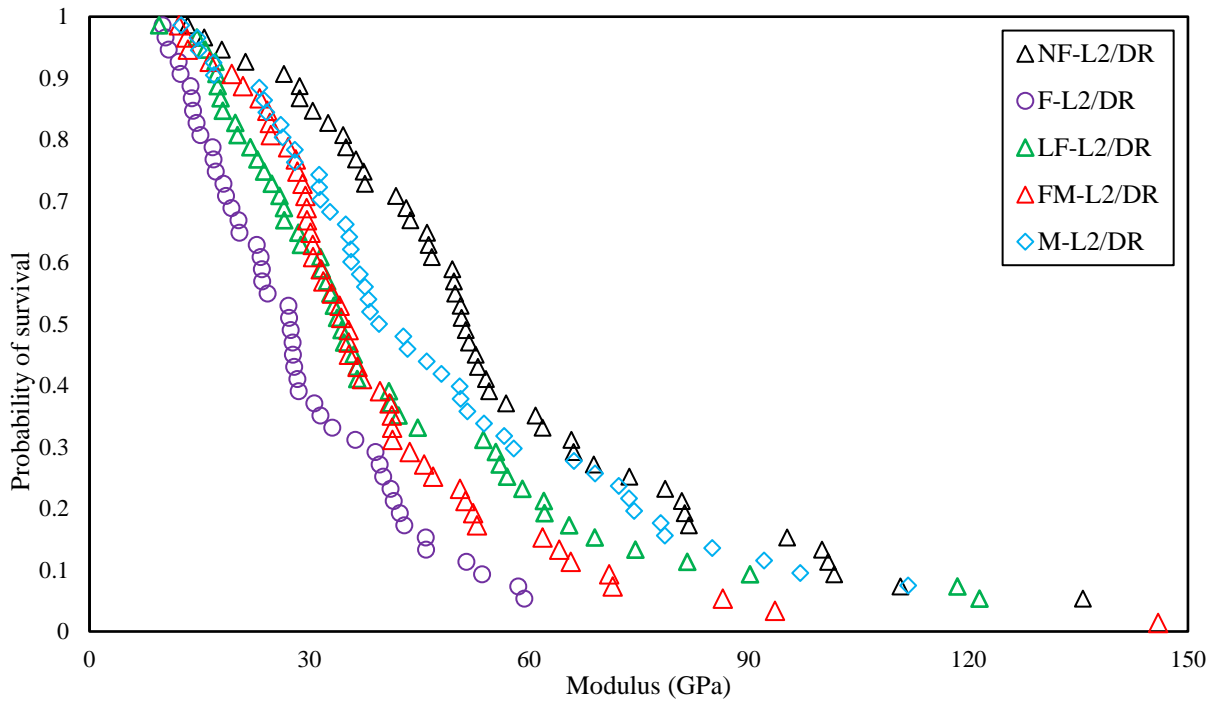


Figure 3.37: Modulus vs Probability of survival curve of 5 growth stages with L2 length and the DR estimator

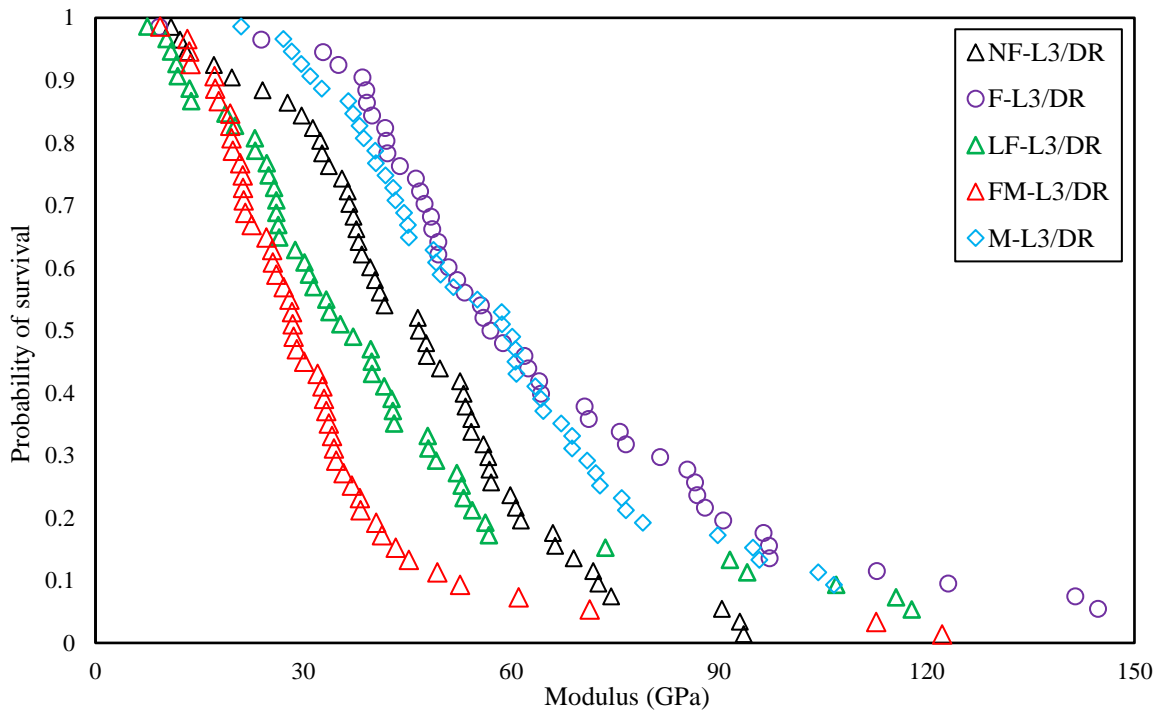


Figure 3.38: Modulus vs Probability of survival curve of 5 growth stages with L3 length and the DR estimator

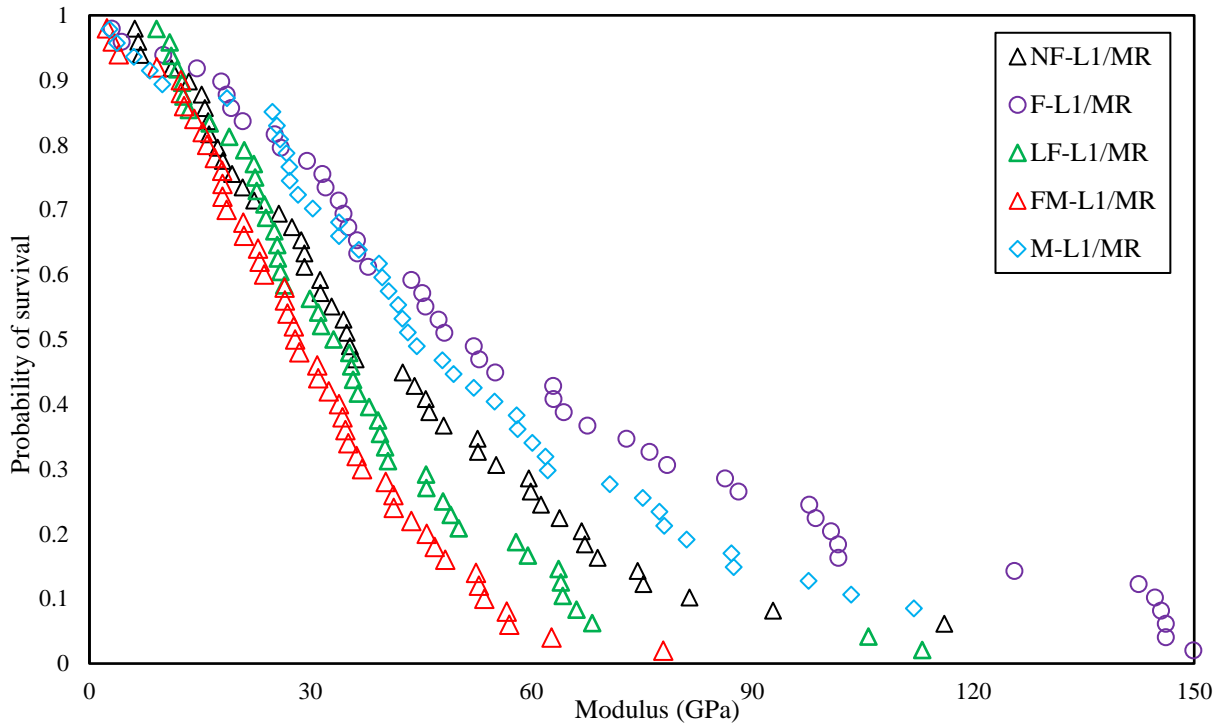


Figure 3.39: Modulus vs Probability of survival curve of 5 growth stages with L1 length and the MR estimator

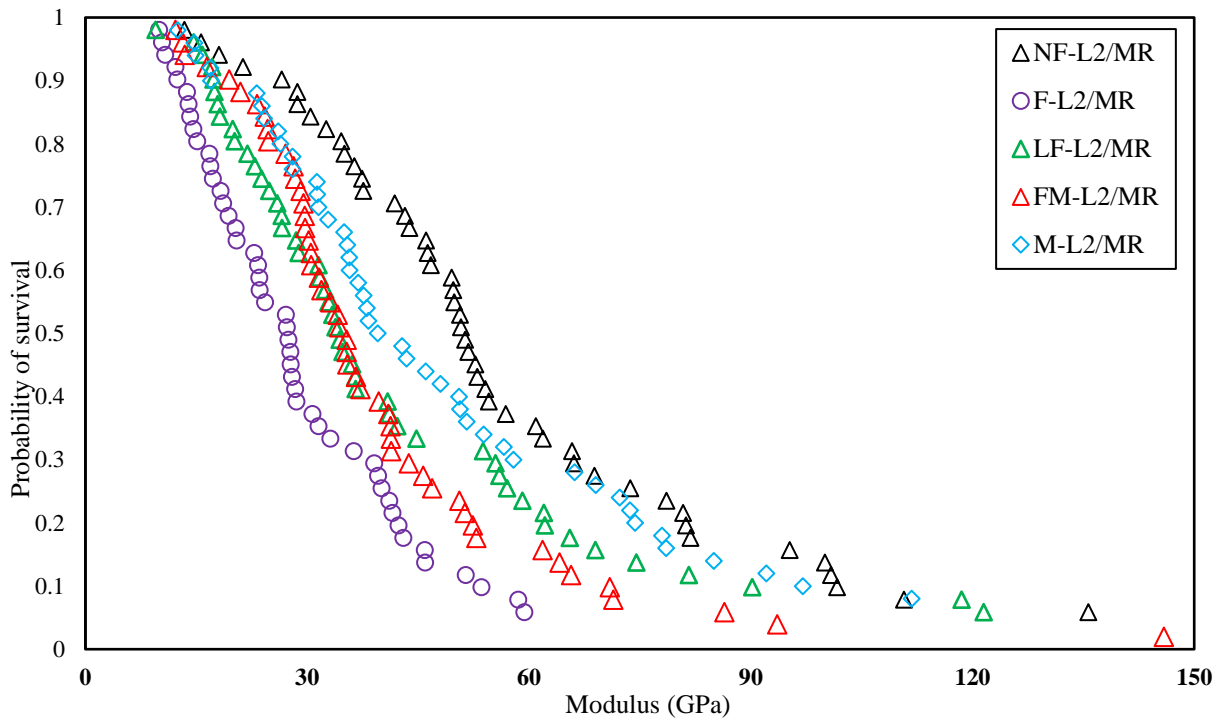


Figure 3.40: Modulus vs Probability of survival curve of 5 growth stages with L2 length and the MR estimator

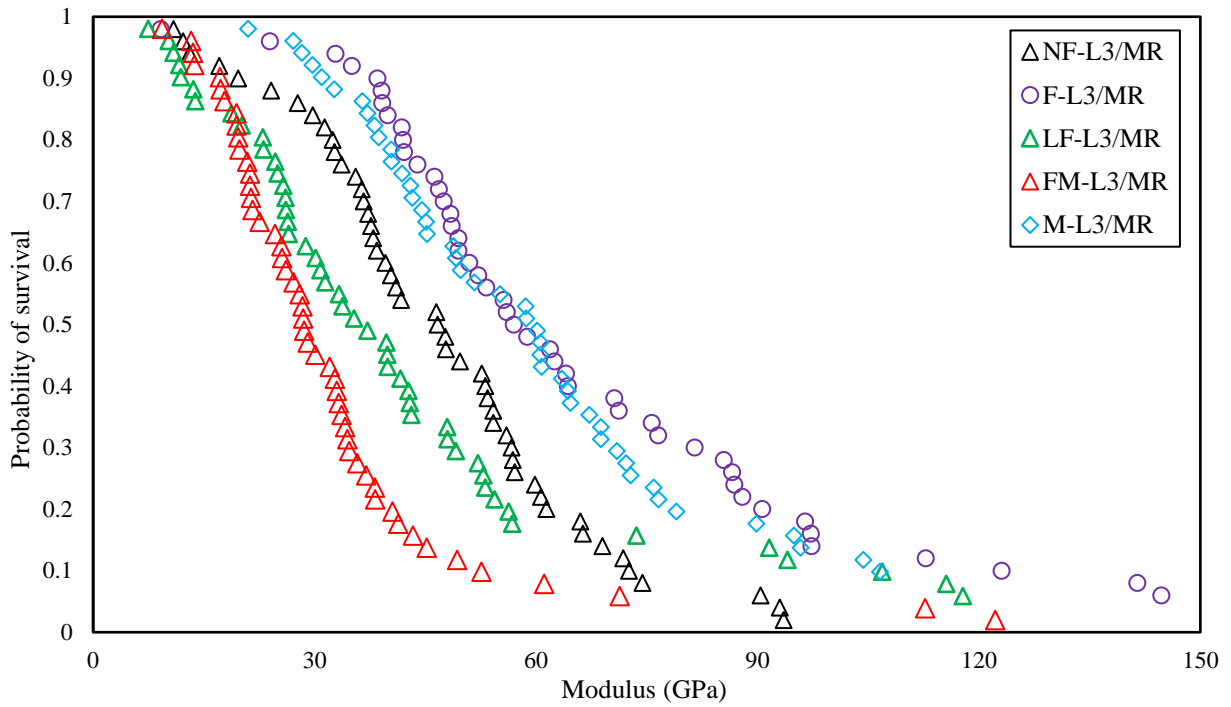


Figure 3.41: Modulus vs Probability of survival curve of 5 growth stages with L3 length and the MR estimator

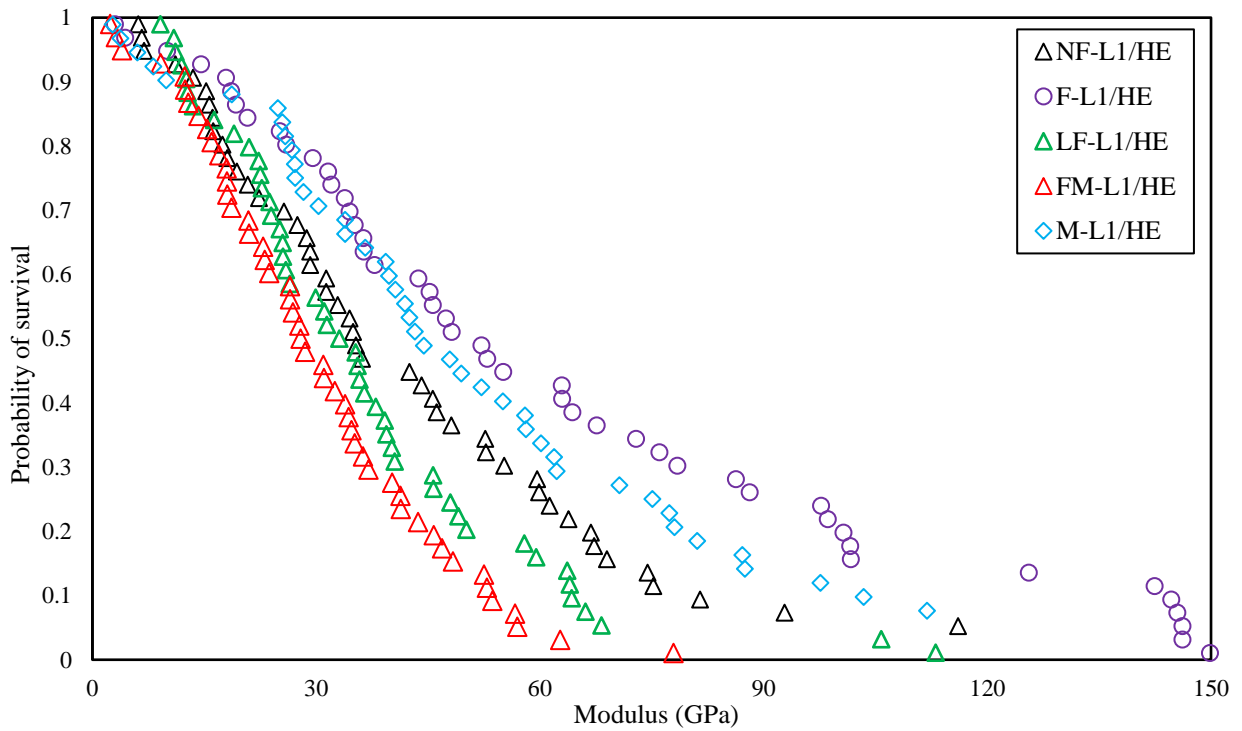


Figure 3.42: Modulus vs Probability of survival curve of 5 growth stages with L1 length and the HE estimator

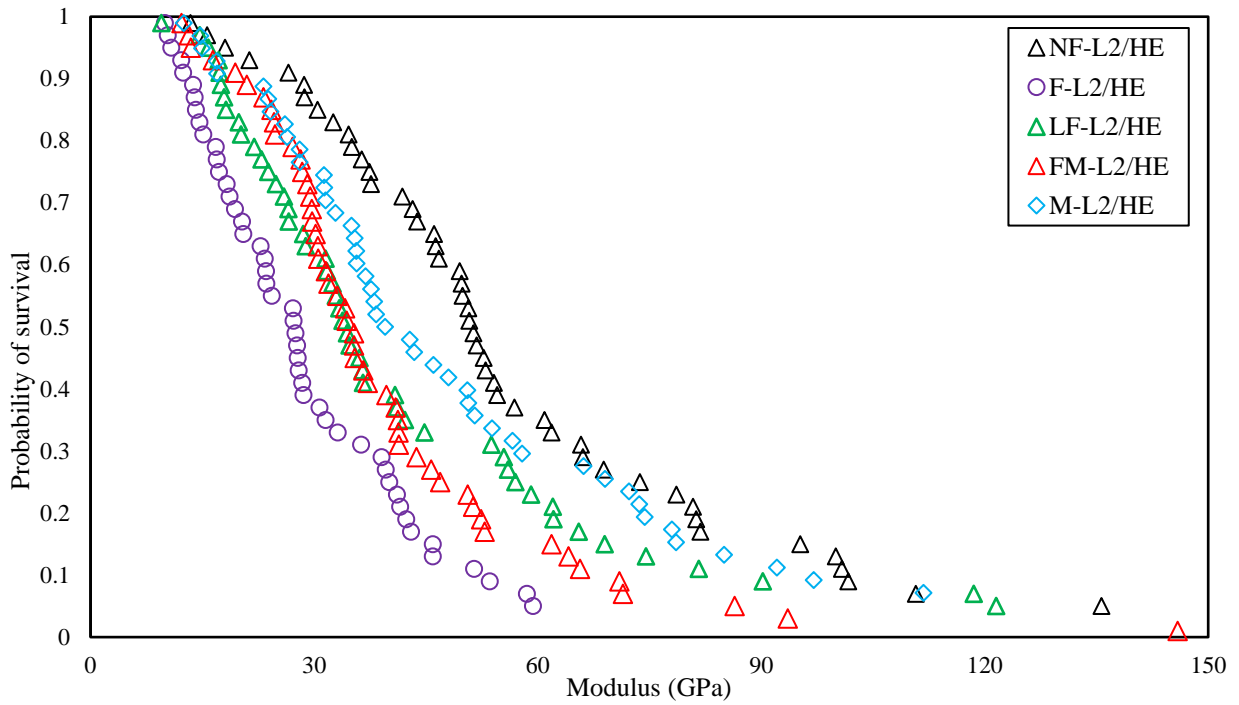


Figure 3.43: Modulus vs Probability of survival curve of 5 growth stages with L2 length and the HE estimator

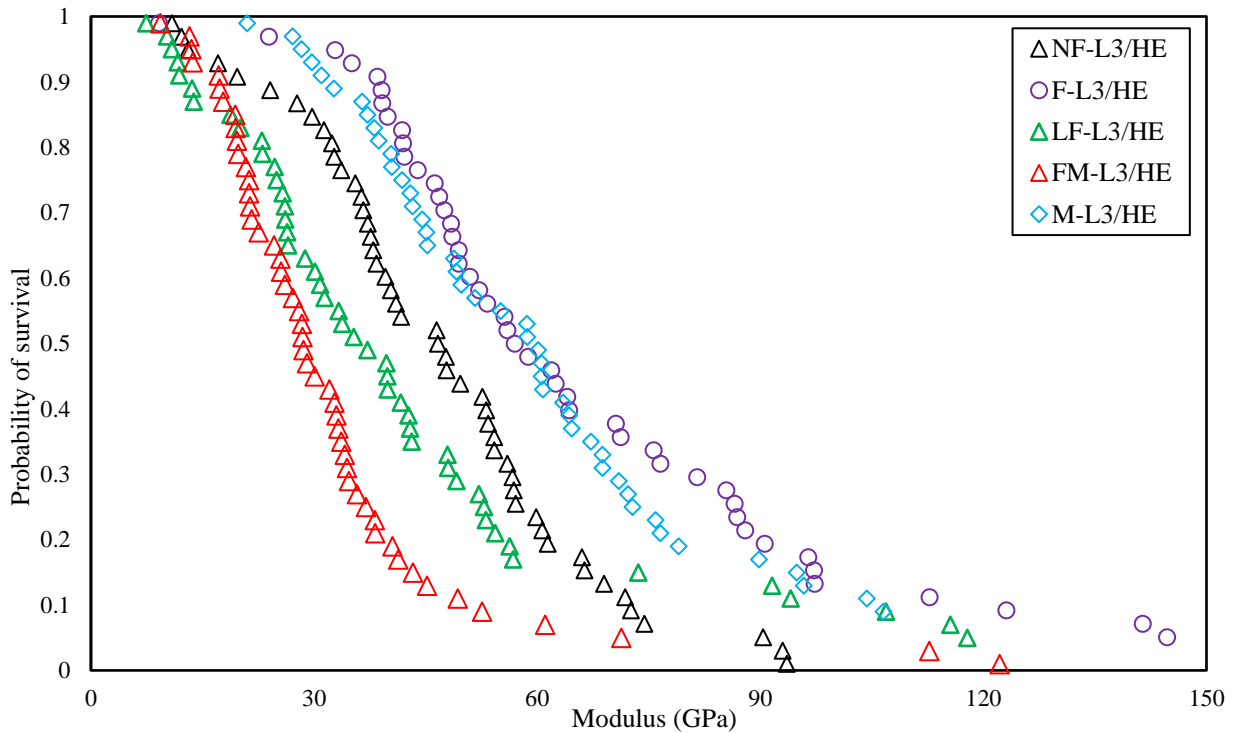


Figure 3.44: Modulus vs Probability of survival curve of 5 growth stages with L3 length and the HE estimator

3.2.4 Weibull Analysis of Modulus Using Python

In Table 3.4, the Weibull parameters of modulus obtained from Python programming Linear Regression (LR) and Maximum Likelihood Estimation (MLE) is presented.

Table 3.4: Weibull parameters for modulus using Python

ID	LR method (estimator: DR)			MLE method		
	α	β (GPa)	R^2_{σ}	α	β (GPa)	E_{avg} (GPa)
NF-L1	2.03	49.60	0.94	1.72	51.00	41.21
NF-L2	2.45	61.90	0.98	2.25	62.60	53.19
NF-L3	2.50	53.40	0.98	2.59	53.30	46.27
F-L1	1.79	72.10	0.97	1.67	73.60	59.10
F-L2	2.47	32.72	0.94	2.17	33.50	28.29
F-L3	3.19	72.14	0.91	2.51	74.11	64.04
LF-L1	2.10	41.09	0.95	1.79	42.09	34.30
LF-L2	2.13	46.82	0.91	1.62	48.89	38.99
LF-L3	1.98	47.73	0.93	1.58	49.52	39.27
FM-L1	2.63	36.42	0.94	2.32	37.14	31.71
FM-L2	2.59	44.71	0.92	1.91	46.20	38.13
FM-L3	2.79	34.68	0.91	1.91	35.93	29.66
M-L1	2.54	61.24	0.91	2.00	63.21	52.63
M-L2	2.25	53.00	0.95	1.93	54.28	44.89
M-L3	2.97	66.97	0.93	2.29	68.68	58.52

The shape parameter (α) calculated by Python program using LR method (DR estimator) is greater than 1.0 for all three lengths and five growth stages. The fibre length does not have any impact on the shape parameters (Table 3.4). The shape parameters in Python (LR) are always larger than the shape parameters calculated using Excel (Figure 3.45).

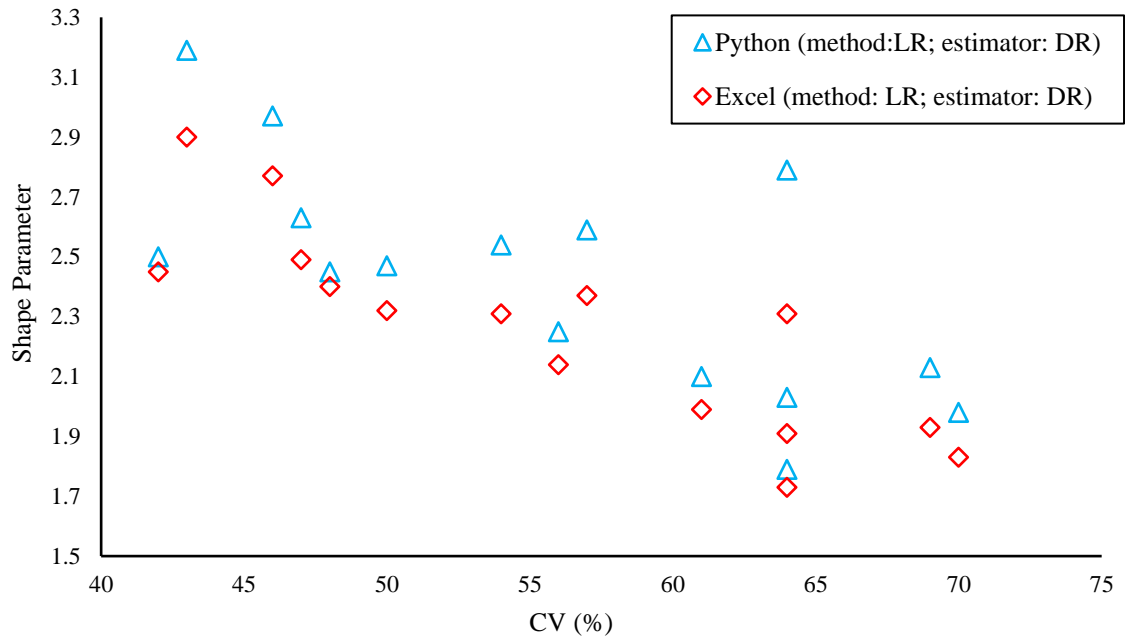


Figure 3.45: Relationship between shape parameter of modulus and CV% - Python (LR method with DR estimator) and Excel (LR method with DR estimator)

The shape parameters calculated by MLE using Python programming are also greater than one for all three lengths and five growth stage fibres (Table 3.4). The shape parameters in MLE method are lower than the shape parameters in LR methods except one sample (NF-L3, Table 3.4, Figure 3.46).

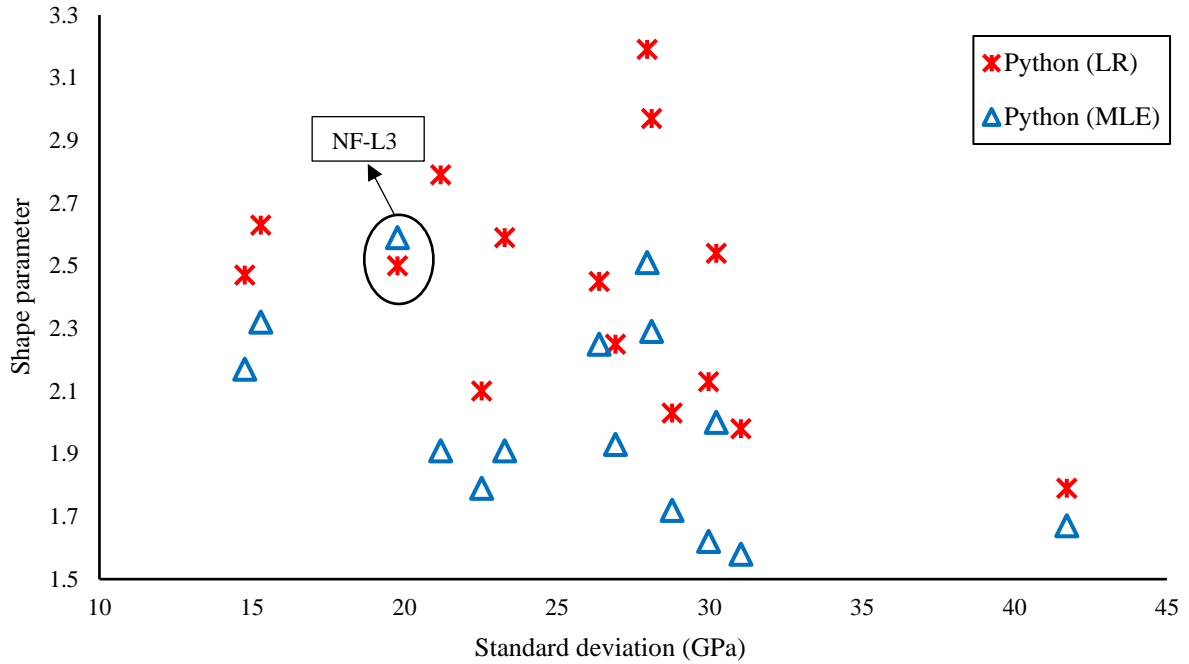


Figure 3.46: Relationship between the shape parameters of modulus by Python programming (LR and MLE) and standard deviation

The shape parameters are found inversely proportional with the CV% for both LR (DR estimator) and MLE methods (Figure 3.47). It seems that the shape parameters and CV% relationship for MLE estimator is more pronounced than the LR method (Figure 3.47).

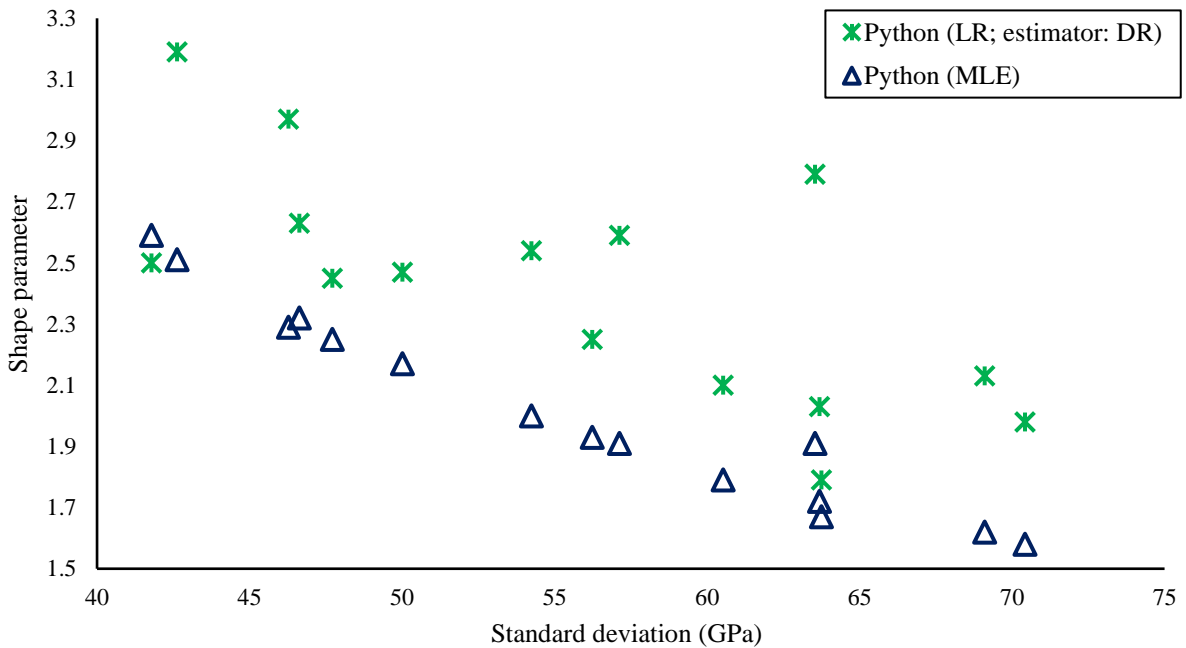


Figure 3.47: Relationship between shape parameter of modulus by Python programming (LR and MLE) and CV%

A slight difference was noticed between the β value using two methods of Python (Table 3.4). It was also remarkable that the difference percentage of β values using these two methods, range from 0.19% to 4.23%, increases with an increase of CV% (Figure 3.48).

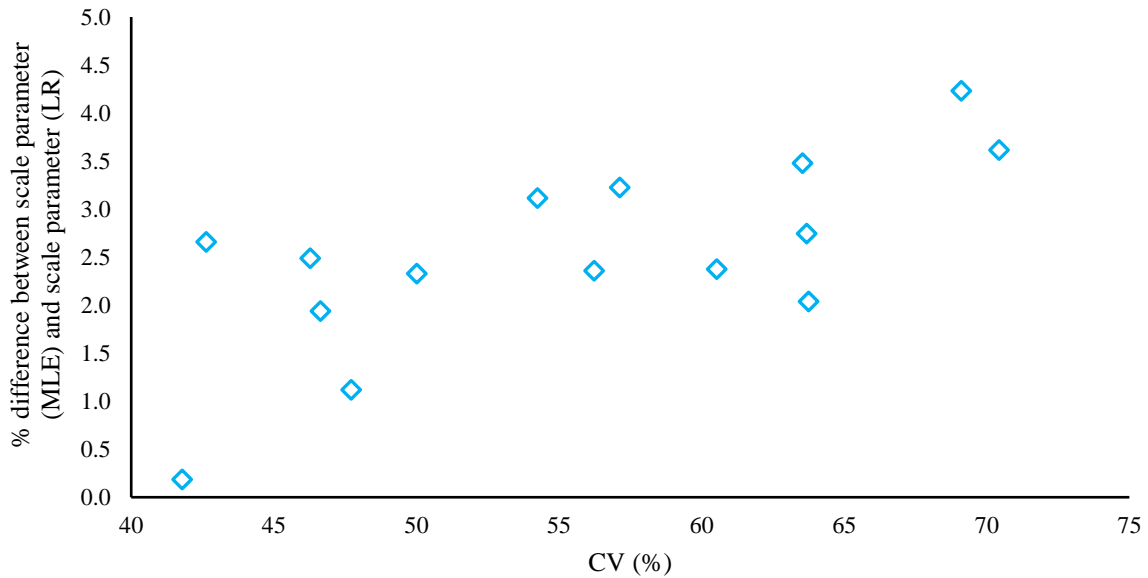


Figure 3.48: Relationship between the (%) difference of scale parameters from MLE and LR of modulus with the CV%.

On the other hand, a directly proportional relationship was also observed with scale parameters obtained from Python (both LR and MLE method) and standard deviation as shown in Figure 3.49. In addition, the value of β in MLE method is always higher than the value obtained from LR methods using Python except for the NF-L3 batch.

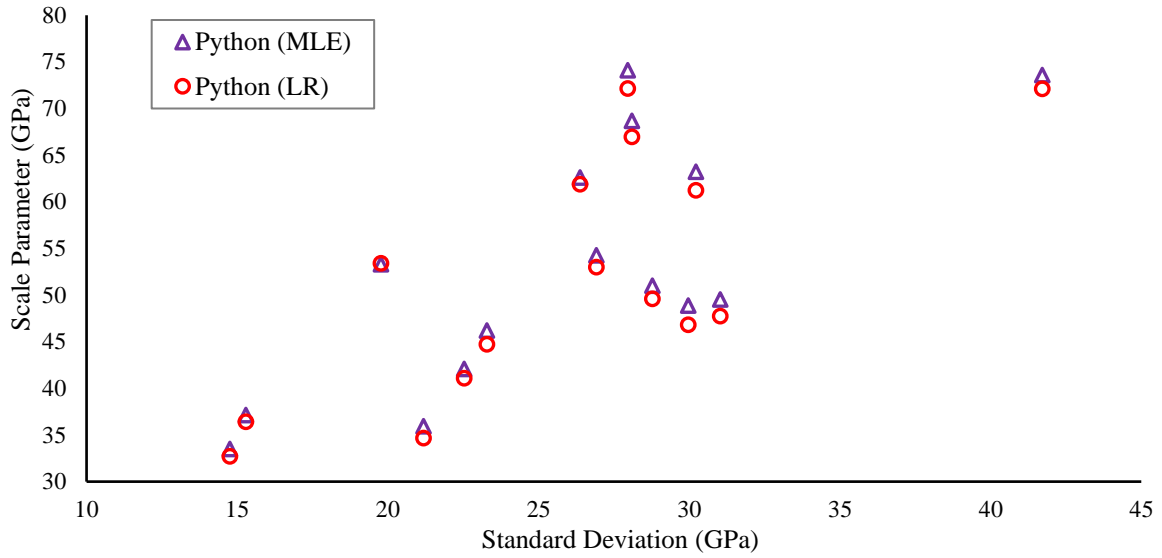


Figure 3.49: Relationship between scale parameters of modulus obtained from Python and standard deviation

A similar proportional relationship was found with the standard deviation and the difference percentage of β value obtained from LR and MLE method as shown in Figure 3.50.

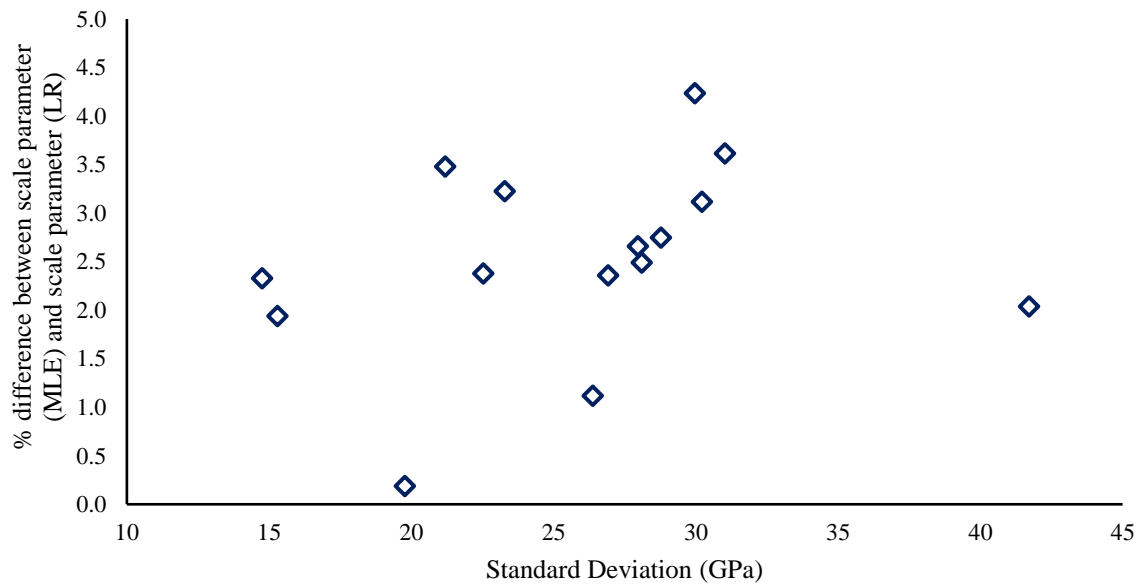


Figure 3.50: Relationship between the difference percentage of scale parameters of modulus from MLE and LR with the standard deviation.

To conclude, the α value for tensile stress and modulus was always greater than 1.0 which indicates the data are evenly and closely distributed and can be used for composite applications. In addition, an inverse relationship was noticed between the α and β for both tensile stress and modulus and growth stage does not have any impact on α and β values. Moreover, fibre length has a positive impact on the α value (Figure 3.51).

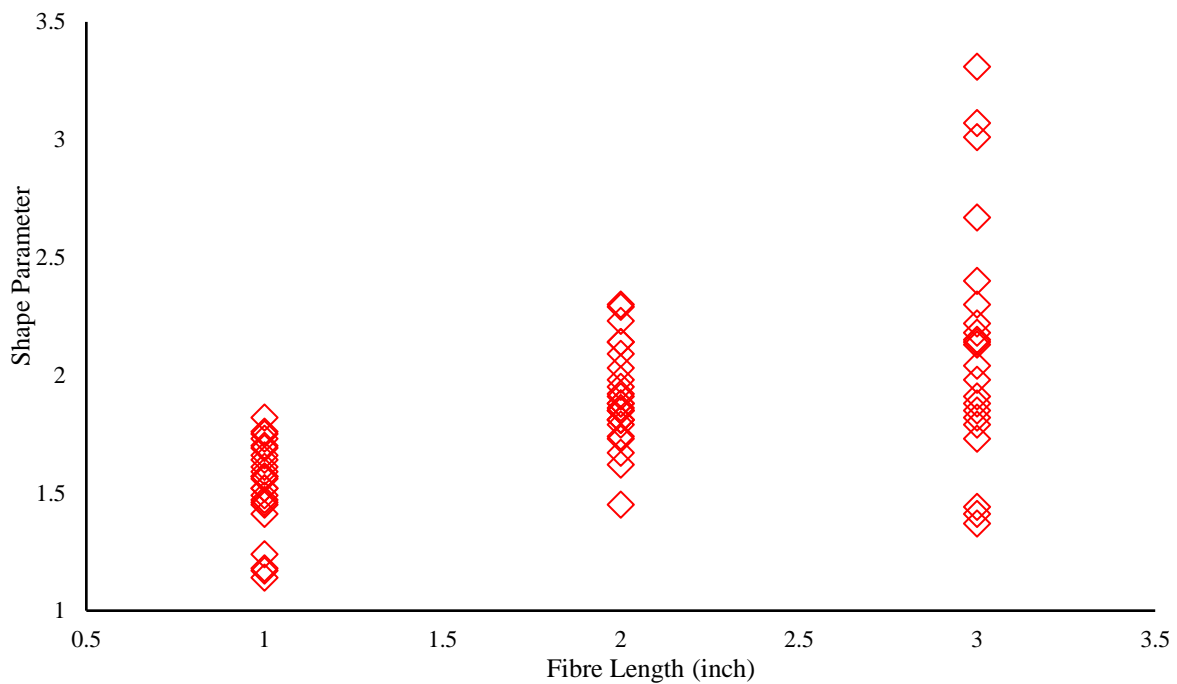


Figure 3.51: Relationship between the shape parameters and fibre lengths

The value of α tends to go higher with an increase of fibre lengths (Figure 3.51). However, it is contradictory to the Weibull distribution and weak-link theory. Zok (2017) mentioned the difference between the weak-link theory and Weibull statistics for the strength distribution of brittle fibre. He suggested that the Weibull model might have to be modified while various fibre gauge length is measured, since Weibull model is combination of weak-link theory and Weibull's power law of survival probability (Zok, 2017). However, lower fluctuation of α value was observed at shorter fibre lengths while a high range of α values are found at L3 (Figure 3.51). For this reason, the result of the Weibull distribution is confusing and not precise.

Finally, a concrete decision cannot be made from the Weibull parameters regarding the preferable and suitable growth stages of cattail plant for composite application. Therefore, a customized analysis using computer programming may be useful to find a perfectly suited growth stage or length of fibre with a comparison of existing natural fibre properties.

Chapter 4 Suitability Analysis – Results and Discussion

Since ANOVA and Weibull distribution could not suggest any proper decision on growth stages as described in Chapter 3, another decision-making method was required. Suitability of cattail fibre in fibre-reinforced composite application based on the standard values of mechanical properties of flax fibre were carried out to discover the suitable growth stage and length of fibre. A computer programming language (Python) was used to compare mechanical properties of cattail fibres with the three thresholds (LLV, ALV, and HLV) values of flax fibres. The suitability (%) for 15 batches (5 growth stages \times 3 lengths) is determined for 3 parameters (S/R/Y), 2 parameters (S/R, Y/R, S/Y) and 1 parameter (S, R, Y) for stress (S), modulus (Y) and strain (R) of LLV, ALV and HLV as shown in Table 2.4. The detailed programming process is described in Chapter 2. The results of suitability (%) were then ranked in 4 different ways to obtain a decision: growth stage wise ranking, length wise ranking, combination of length and growth stage wise ranking, and the parameter wise ranking.

4.1 Suitability (%)

The suitability is calculated based on the percentage of individual data set (Appendices A1 to A15) that satisfy the limit values. The three limit (LLV, ALV and HLV) values are given in Table 2.6. To calculate the suitability (%), the required high or low values of stress, modulus and strain were established for the intended application (which is composite application for the current research).

For composite application, high tensile stress, high modulus, and low strain is preferable. Using Python programming language, every fibre of each batch (50 samples) is examined for calculating the percentages of fibre that can fulfill the limit requirements using the LLV, ALV and HLV as a threshold. In addition, 3 parameters (tensile stress & tensile

strain & modulus), 2 parameters (tensile stress & strain, modulus & tensile strain, and tensile stress & modulus), and 1 parameter (tensile stress, tensile strain, modulus) are considered as conditions for examining the suitability percentage for composites. The suitability (%) results are shown in Table 4.1.

Table 4.1: Suitability (%) of cattail fibre

Limit value	Growth stage	Suitability (%)																				
		1 Parameter						2 Parameter						3 Parameter								
		S			R			Y			S/R			Y/R			S/Y			S/R/Y		
		L1	L2	L3	L1	L2	L3	L1	L2	L3	L1	L2	L3	L1	L2	L3	L1	L2	L3	L1	L2	L3
LLV	NF	90	92	94	15	80	100	90	98	94	13	74	94	15	78	94	88	92	94	13	74	94
	F	96	98	96	35	8	100	95	82	100	35	6	96	35	8	100	96	80	96	35	6	96
	LF	81	82	68	38	96	98	85	96	86	23	76	66	34	92	84	72	80	68	23	76	66
	FM	80	76	67	73	100	100	91	94	92	58	76	67	69	94	92	80	76	67	58	76	67
	M	80	96	94	18	15	96	82	94	100	16	11	90	16	13	96	80	91	94	16	11	90
ALV	NF	33	32	2	4	10	53	31	42	37	0	2	2	0	4	27	25	26	2	0	2	2
	F	43	26	28	2	4	85	48	8	55	0	0	19	2	0	43	39	8	25	0	0	19
	LF	9	6	6	9	42	70	19	30	22	0	4	2	4	16	14	6	6	6	0	4	2
	FM	7	8	4	40	78	82	9	16	6	2	4	2	7	10	4	4	8	4	2	4	2
	M	32	53	10	5	2	92	39	30	55	0	0	10	5	0	55	23	23	10	0	0	10
HLV	NF	16	2	0	0	2	2	6	8	0	0	0	0	0	2	0	4	2	0	0	0	0
	F	20	8	4	0	0	2	15	0	11	0	0	0	0	0	2	15	0	4	0	0	0
	LF	2	2	2	0	2	14	4	8	10	0	0	0	0	0	0	2	2	2	0	0	0
	FM	0	2	0	0	6	4	0	2	2	0	0	0	0	0	0	0	2	0	0	0	0
	M	5	19	2	2	2	8	7	4	10	0	0	0	0	0	2	0	4	2	0	0	0

S: tensile stress; R: tensile strain; Y: Modulus

4.1.1 Single Parameter – Tensile Stress

Considering LLV and individual parameter of tensile stress (S), all the data fall within 80% level for all growth conditions except for the L2 and L3 lengths of FM stage (Table 4.1). For ALV, the stress suitability (%) values for LF and FM lie below 10%, while for all other growth stages, the values fall between 26 and 53% except NF-L3 and M-L3 for which the suitability found 2.0% and 10% respectively. For HLV, the stress values fluctuated from 0 to

20%. Further, using HLV, the suitability of stresses were found to be 20%, 19%, and 16%, respectively for F-L1, M-L2, and NF-L1.

4.1.2 Single Parameter – Tensile Strain

It can be seen in Table 4.1, when considered individually, the growth stages of the cattail plant does not have any impact on the tensile strain (R). However, L3 of each growth stages and for all three limit values were noticed to have the highest suitability (%). Considering LLV, the tensile strain values fall between 15 to 100% except for the F-L2 (8%). However, for ALV, the strain suitability (%) values fluctuated between 2 to 92%. In contrast, 0 to 8% suitability (%) of tensile strain was noticed while HLV is considered, whereas a 14% suitability (%) for LF-L3 was observed.

4.1.3 Single Parameter – Modulus

Considering LLV and individual parameter of Young's modulus (Y), all the suitability (%) data fall between 82 to 100% for all growth conditions (Table 4.1). For ALV, the values for the FM growth stage were less than or equal to 16%; whereas, for other growth stages, the suitability (%) value of single parameter (Y) was between 19 and 55% except for the F-L2 (8%). For HLV, the values fall from 0 to 15% for modulus.

4.1.4 Two Parameters – S/R

Considering S/R and LLV, all the suitability (%) data fall between 6 and 96% for all growth stages and lengths (Table 4.1). However, in the case of ALV, the suitability (%) of most of the samples lies between 0 and 4% except F-L3 (19%) and M-L3 (10%). On the other hand, in the case of HLV, the suitability (%) was found 0% for all growth stages and lengths that means not a single fibre (50 fibres from each batch) from 15 batches could exceed the higher limit value.

4.1.5 Two Parameters – Y/R

If LLV is considered, the suitability percentage of Y/R is fall between 15 to 100% except for the F-L2 batch (8%); whereas, if ALV is considered, the values are 2 to 55% except NF-L1, F-L2, and M-L2 and whose values are always 0% (Table 4.1). For HLV, the percentage is always zero for all growth stages and lengths except for the NF-L2, F-L3, and M-L3 and their values are 2%.

4.1.6 Two Parameters – S/Y

Considering S/Y as combination and LLV as limit value, the percentages of the suitability of different growth stage found above 70% except for LF-L3 and FM-L3 (Table 4.1). However, if ALV is considered, the values lie between 2 and 39%. Moreover, the values are $\leq 15\%$ for every growth stage if HLV is considered.

4.1.7 Three Parameters - S/R/Y

The suitability (%) of all the growth stages are fluctuating from 6% to 96% in the case of S/R/Y and LLV (Table 4.1). However, the values of all growth stages fall between 0% and 19% if ALV is considered. In this case, the suitability (%) of all the growth stages of L1 length is zero except FM-L1(2%). On the other hand, for HLV, the suitability of five growth stages and three lengths are zero percent.

4.1.8 Average suitability (%)

The average suitability (%) which was calculated ‘row-wise’ using the suitability (%) data in Table 4.1 that comprises of three lengths (L1, L2, L3) of three individual parameters (S, R, Y), three 2-parameter combinations (S/R, Y/R, S/Y) and a three-parameter combination (S/R/Y) for five different growth stages and three limit values (LLV, ALV HLV). The average and overall average suitability (%) are shown in Table 4.2. The overall average (%) was calculated using the average LLV, ALV and HLV data for each growth stage.

Table 4.2: Average suitability (%) of different growth stages

Growth stage	Suitability (%) using different limit values			Overall (%)
	HLV	ALV	LLV	
NF	2.10	16.00	75.05	31.05
F	3.86	21.62	66.62	30.70
LF	2.38	13.19	70.95	28.84
FM	0.86	14.43	78.71	31.33
M	3.19	21.62	61.86	28.89

For HLV, the average suitability of fibres from the F stage is the highest (3.86%), and the second-highest value is 3.19%, which belongs to the M stage, while the average suitability (%) value of the fibres from the LF stage is 2.38%; for NF, the value is 2.10%, followed by the lowest value (0.86%) obtained for FM stages' fibres (Table 4.2). In the case of ALV, the top average value is 21.62% that belong to both the M and F growth stages and the result is similar to HLV. For NF, the suitability (%) is 16, and for the FM stage, the value is 14.43%; whereas the lowest value, 13.19%, belongs to the LF . However, the FM stage is noted the highest position for LLV, i.e., 78.71%, and the NF stage is at the second position with 75.05% followed by the LF stage (70.95%). While F stage fibres showed the highest suitability (%) in HLV and ALV limit values, in case of LLV this sample fell in the fourth position with 66.62%, where M stages represent 61.86% of suitability. It can be noted that for LLV, the suitability (%) is consistently above 60% for all growth stages. Further, the overall suitability (%) was also noted between about 29 and 31 for all growth stages with FM, NF, and F stages are in the top three positions.

4.2 Ranking

The suitability (%) of three lengths (L1, L2, and L3), five different growth stages, and seven parameter as well as parameter combinations (S, Y, R, S/R, Y/R, S/Y, S/R/Y), which is given in Table 4.1, does not provide any separate ranking for length, growth stages, combination of length and growth stages and combination of parameters due to the imbalance variables of length, growth stages, length x growth stages and parameter

combinations which are three, five, fifteen and seven, respectively. Therefore, to rank the suitability (%), a 1 to 3 ranking is provided for three lengths (L1, L2, L3), 1 to 5 ranking is given for five growth stages (NF, F, LF, FM, M), 1 to 15 is for the combination of five growth stages x three lengths, and 1 to 7 is provided for parameters and their interactions (S, R, Y, Y/R, S/Y, S/R, S/R/Y), where 1 is worst and the highest numerical value represents the best. The ranking was conducted using the suitability (%) data in Table 4.1.

4.2.1 Ranking along the fibre length (L1, L2 and L3)

The lengthwise rank of 1 (red highlighted colour), 2 (yellow highlighted colour), and 3 (green highlighted colour) (1 being the lowest and 3 being the highest) for three lengths with seven parameters was conducted for each growth stage for all threshold values (LLV, ALV, HLV) as shown in Table 4.3. Therefore, each growth stage contains seven set of lengthwise ranking due to the seven parameters for each limit value. If samples are found with same suitability (%), the ranking score is equal and samples remain ranked in the same position, If the tie were for the highest ranking, both samples would have awarded the highest ranking of 3. The ranking values were generated from the suitability (%) provided in Table 4.1.

Table 4.3: Ranking along the length

Limit value	Growth stage	Ranking																				
		1 Parameter									2 Parameter									3 Parameter		
		S			R			Y			S/R			Y/R			S/Y			S/R/Y		
		L1	L2	L3	L1	L2	L3	L1	L2	L3	L1	L2	L3	L1	L2	L3	L1	L2	L3	L1	L2	L3
LLV	NF	1	2	3	1	2	3	1	3	2	1	2	3	1	2	3	1	2	3	1	2	3
	F	1	3	1	2	1	3	2	1	3	2	1	3	2	1	3	3	1	3	2	1	3
	LF	2	3	1	1	2	3	1	3	2	1	3	2	1	3	2	2	3	1	1	3	2
	FM	3	2	1	1	3	3	1	3	2	1	3	2	1	3	2	3	2	1	1	3	2
	M	1	3	2	2	1	3	1	2	3	2	1	3	2	1	3	1	2	3	2	1	3
ALV	NF	3	2	1	1	2	3	1	3	2	1	3	3	1	2	3	2	3	1	1	3	3
	F	3	1	2	1	2	3	2	1	3	1	1	3	2	1	3	3	1	2	1	1	3
	LF	3	1	1	1	2	3	1	3	2	1	3	2	1	3	2	3	3	3	1	3	2
	FM	2	3	1	1	2	3	2	3	1	1	3	1	2	3	1	1	3	1	1	3	1
	M	2	3	1	2	1	3	2	1	3	1	1	3	2	1	3	3	3	1	1	1	3
HLV	NF	3	2	1	1	3	3	2	3	1	1	1	1	1	3	1	3	2	1	1	1	1
	F	3	2	1	1	1	3	3	1	2	1	1	1	1	1	3	3	1	2	1	1	1
	LF	3	3	3	1	2	3	1	2	3	1	1	1	1	1	1	3	3	3	1	1	1
	FM	1	3	1	1	3	2	1	3	3	1	1	1	1	1	1	1	3	1	1	1	1
	M	2	3	1	1	1	3	2	1	3	1	1	1	1	1	3	1	3	2	1	1	1

1 Low 2 Medium 3 High

In case of the single parameter of tensile stress (S), L2 got the highest rank of 3 in majority of the cases (3 times out of 5) for LLV, whereas L1 and L3 got once for each (Table 4.3). However, L1 got the highest rank of 3 maximum time (3 times out of 5) followed by L2 (2 times) for ALV (Table 4.3). In contrast, both L1 and L2 were marked as the highest rank of 3 in most of the cases (3 times out of 5) followed by L3 (once) for HLV (Table 4.3).

When considering strain (R) as a single parameter, L3 got the highest rank of 3 in most of cases for all the three limit values followed by L2 (Table 4.3). Moreover, the lowest rank of 1 were noticed in most of the cases at L1 length.

If modulus is considered as single parameter, L2 hold the highest rank in most of the cases followed by L3 for LLV and ALV, whereas an inverse result was found for ALV (Table 4.3). However, the lowest rank belonged to L1 length in most of the cases.

Considering S/R as 2-parameter, L3 hold the highest ranking in maximum case for LLV, followed by L2 and L1 (Table 4.3). However, for ALV, both L2 and L3 had the

maximum times of highest ranking (3 times each out of 5) followed by L1. On the other hand, all the batches ranked as 1 since their suitability (%) was zero percent (Table 4.1) for each batch for HLV.

If Y/R is considered as 2-parameter, the maximum times of highest ranking of 3 goes to the side of L3 for all the three limit values followed by L2 and L1 (Table 4.3).

In case of 2-parameter of S/Y, L3 had the maximum times (3 times out of 5) of highest ranking of 3 for LLV followed by L1 (2 times out of 5) and L2 (once out of 5) (Table 4.3). However, L2 got the highest ranking in most of the cases (4 times out of 5) for ALV followed by L1 (3 times out of 5) and L3 (once out of 5). On the other hand, both L1 and L2 got the maximum times of highest ranking (3 times each out of 5) for HLV followed by L3.

When all the three parameters (S/R/Y) is considered, L3 had the maximum times (3 times out of 5) of highest ranking of 3 for LLV followed by L2 (2 times out of 5) and L1 (Table 4.3). However, both L2 and L3 got the maximum times of highest ranking (3 times each out of 5) for ALV followed by L1. On the other hand, all the batches got rank 1 for HLV due to their suitability (%) (0% for all the batches).

The average ranking for L1 was 1.46, 1.63, and 1.51 for LLV, ALV, and HLV, respectively. For L2, these values were 2.11 (LLV), 2.14 (ALV), and 1.77 (HLV); while for L3 the values were 2.43, 2.17, and 1.74 (Table 4.4). Considering all factors, the average ranking of fibre quality is L3>L2>L1 (Table 4.4) which supports the results of Weibull parameters for maximum cases

Table 4.4: Average Ranking of lengths

Fibre length	Limit Value			Final ranking
	LLV	ALV	HLV	
L1	1.46	1.63	1.51	1.53
L2	2.11	2.14	1.77	2.01
L3	2.43	2.17	1.74	2.11

4.2.2 Ranking along the five growth stages

Fibre maturity and quality affect the maturity of the plant and are interrelated to each other. Therefore, to identify the suitable growth stage for making a composite, the ranking of 5 growth stages will enlighten the path.

4.2.2.1 Ranking for individual parameter, parameter combinations and limit values (fixed length)

This analysis was conducted to determine the most suitable growth stage to fibres of a specific length. The ranking is 1 (lowest ranking) to 5 (highest ranking) for five growth stages for each length, and comparison is made only among growth stages within the same lengths, i.e., L1 or L2 or L3 for each parameter and limit values (Table 4.5).

Table 4.5: Ranking of 5 growth stages

Limit value	Growth stage	Ranking																				
		1 Parameter									2 Parameter									3 Parameter		
		S			R			Y			S/R			Y/R			S/Y			S/R/Y		
		L1	L2	L3	L1	L2	L3	L1	L2	L3	L1	L2	L3	L1	L2	L3	L1	L2	L3	L1	L2	L3
LLV	NF	4	3	4	1	3	5	3	5	3	1	3	4	1	3	3	4	5	4	1	3	4
	F	5	5	5	3	1	5	5	1	5	4	1	5	4	1	5	5	3	5	4	1	5
	LF	3	2	2	4	4	2	2	4	1	3	5	1	3	4	1	1	3	2	3	5	1
	FM	1	1	1	5	5	5	4	3	2	5	5	2	5	5	2	3	1	1	5	5	2
	M	2	4	4	2	2	1	1	3	5	2	2	3	2	2	4	3	4	4	2	2	3
ALV	NF	4	4	1	2	3	1	3	5	3	1	3	1	1	3	3	4	5	1	1	3	1
	F	5	3	5	1	2	4	5	1	5	1	1	5	2	1	4	5	2	5	1	1	5
	LF	2	1	3	4	4	2	2	4	2	1	5	1	3	5	2	2	1	3	1	5	1
	FM	1	2	2	5	5	3	1	2	1	5	5	1	5	4	1	1	2	2	5	5	1
	M	3	5	4	3	1	5	4	3	5	1	1	4	4	1	5	3	4	4	1	1	4
HLV	NF	4	1	1	1	4	1	3	5	1	1	1	1	1	1	5	1	4	4	1	1	1
	F	5	4	5	1	1	1	5	1	5	1	1	1	1	1	5	5	1	5	1	1	1
	LF	2	1	4	1	4	5	2	5	4	1	1	1	1	1	1	3	4	4	1	1	1
	FM	1	1	1	1	5	3	1	2	2	1	1	1	1	1	1	1	4	1	1	1	1
	M	3	5	4	5	4	4	4	3	4	1	1	1	1	1	5	1	5	4	1	1	1

1 Lowest 2 Low 3 Medium 4 High 5 Highest

As seen in Table 4.5, for LLV-L1, fibres from the flower (F) stage produced the highest rank of 5 for all three individual parameters and four parameter combinations (S-L1,

R-L1, Y-L1, S/R-L1, Y/R-L1, S/Y-L1, S/R/Y-L1), followed by FM (4), LF (3), NF (2) and M (1) [F>FM>LF>NF>M]. For ALV-L1 considering all seven parameter combinations, the ranking is FM>F>M>NF>LF; and for HLV-L1, the ranking is F>M>NF>LF>FM.

For LLV-L2 considering all parameter combinations, the fibres from the late-flower (LF) stage hold the highest ranking of 5, followed by the NF stage and FM stage (both have the same rank of 4). The other stages M and F have a rank of 2, and 1, respectively [LF>NF=FM>M>F]. However, for ALV-L2, the ranking can be declared as LF=FM>NF>M>F; for HLV-L2, it is NF>M>LF>FM>F.

In the case of LLV-L3, considering all parameter combinations, the highest-ranking fibre was from the flower stage (F) (rank 5), followed by NF (4), M (3), FM (2), LF (1) [F>NF>M>FM>LF]. For ALV-L3, the ranking was F>M>LF>NF=FM; and for HLV-L3, the ranking was F>M>LF>FM>NF.

4.2.2.1.1 Rank for average of lengths and limit values (fixed parameter and parameter combination)

The average suitability percentage of different growth stages for low, average, and high limit values was calculated. The values of the ranking were taken from Table 4.5; the average ranking was calculated for each parameter (S/R/Y, S/R, Y/R, S/Y, S, R, Y) shown in Figure 4.1.

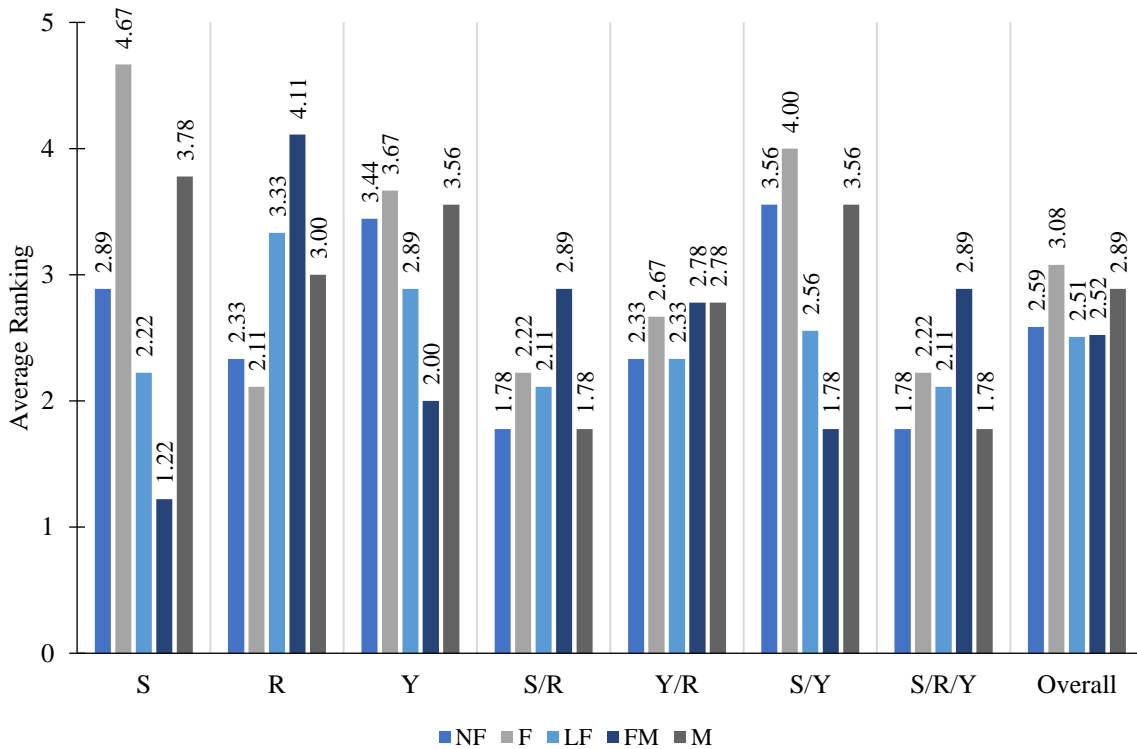


Figure 4.1: Average ranking of different growth stages considering different parameters (average of length and average limit value data)

The F stage possesses the highest average ranking value (3.08/5.00), and the M stage (2.89/5.00) slightly lower than that of the flower (F) stage. Further, the NF stage also had a moderate ranking value (2.59/5.00), but lower than the mature stage (M). The lowest ranking was found in the FM stage and LF stage. A detailed graphical representation of this data with different parameter combination is also found in Figure 4.1.

4.2.2.1.2 Ranking for average length and parameter combinations (fixed limit value)

The average ranking was calculated for different growth stages considering 3 limit values (LLV, ALV, HLV) and presented the results in Figure 4.2.

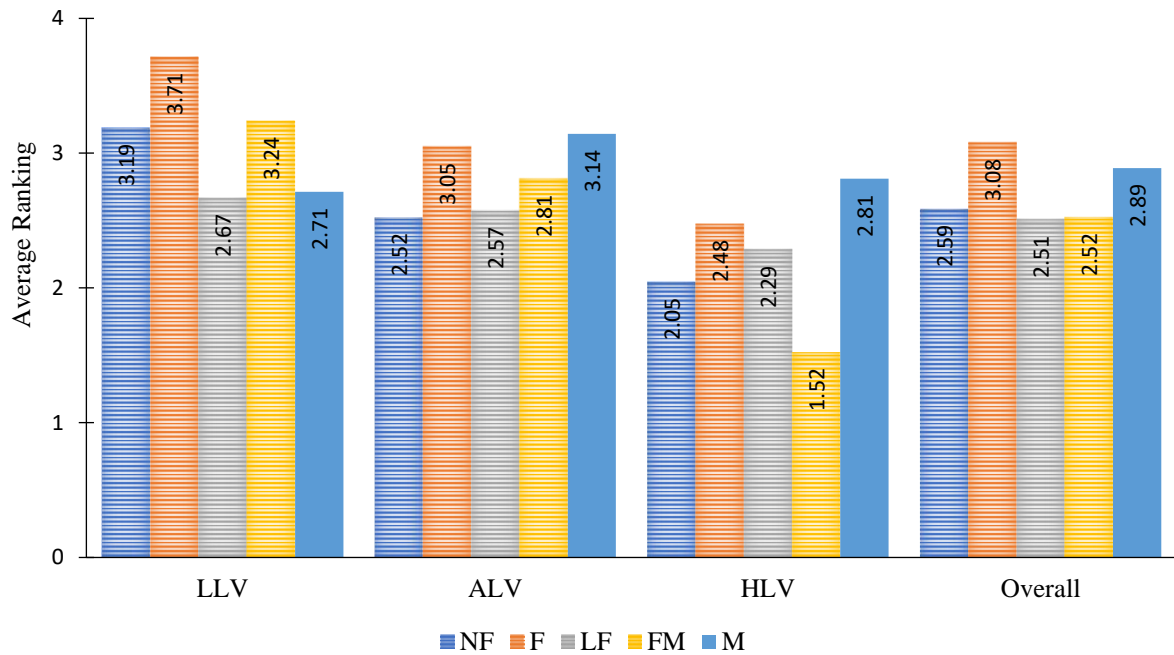
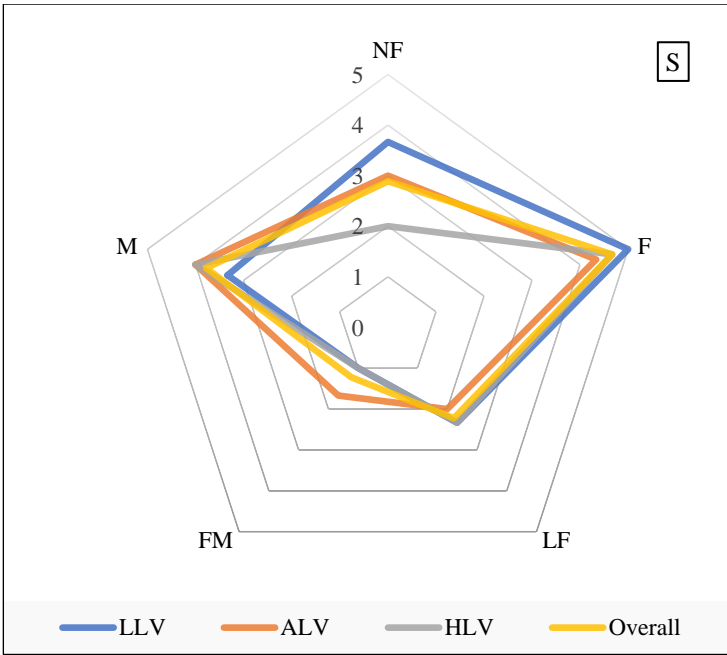


Figure 4.2: Ranking of growth stages considering all conditions with different limit value for average length (average of lengths and parameter combinations)

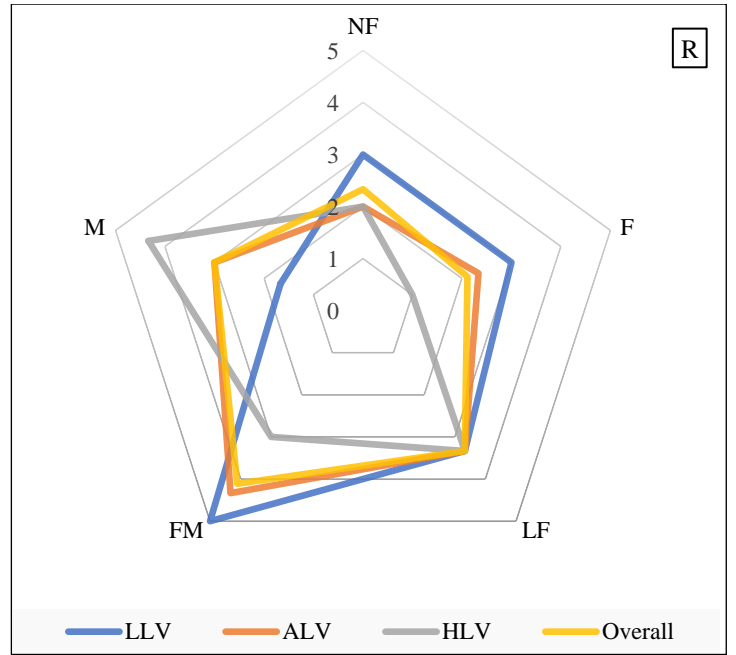
The F stage takes the first position for LLV, shown in Figure 4.2. The FM and NF stage secured the second and third positions, respectively; followed by the M stage and the last rank to the LF stage. In case of ALV, the highest rank goes to the F stage followed by the M stage, FM stage, LF stage, and NF stage respectively. However, the M stage secures the highest ranking while considered HLV followed by the F stage, LF stage, NF stage, and FM stage respectively.

4.2.2.1.3 Ranking for average of lengths and limit values (fixed parameters and parameter combinations)

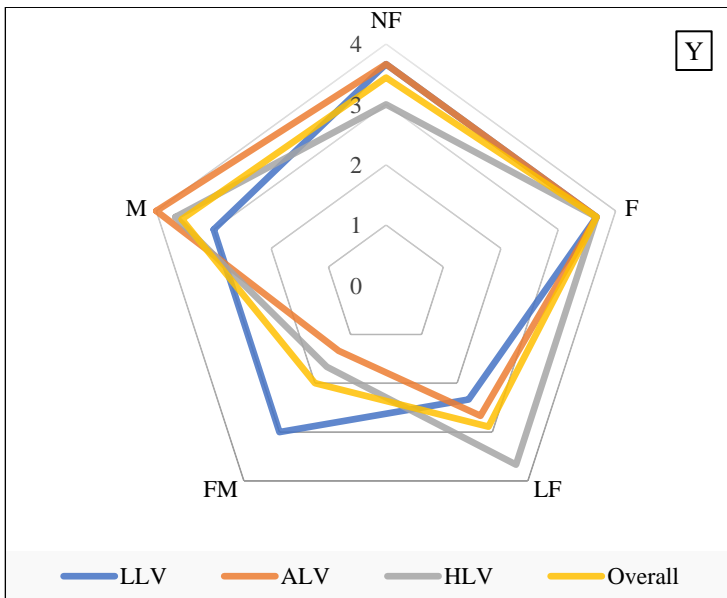
The average ranking of three lengths was taken for the five growth stages considering different parameters (S, R, Y, S/R, Y/R, S/Y, S/R/Y) separately along with the limit value to clarify the ranking with different conditions where average of lengths was calculated, shown in Figure 4.3.



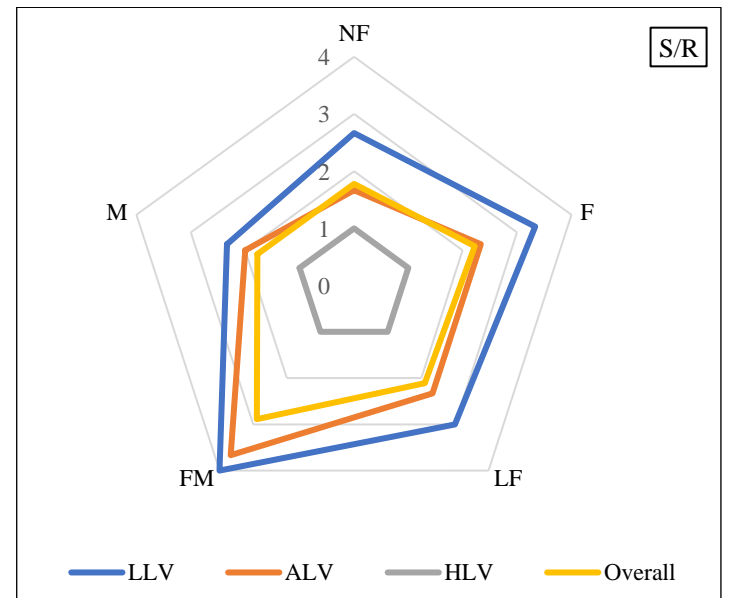
(a)



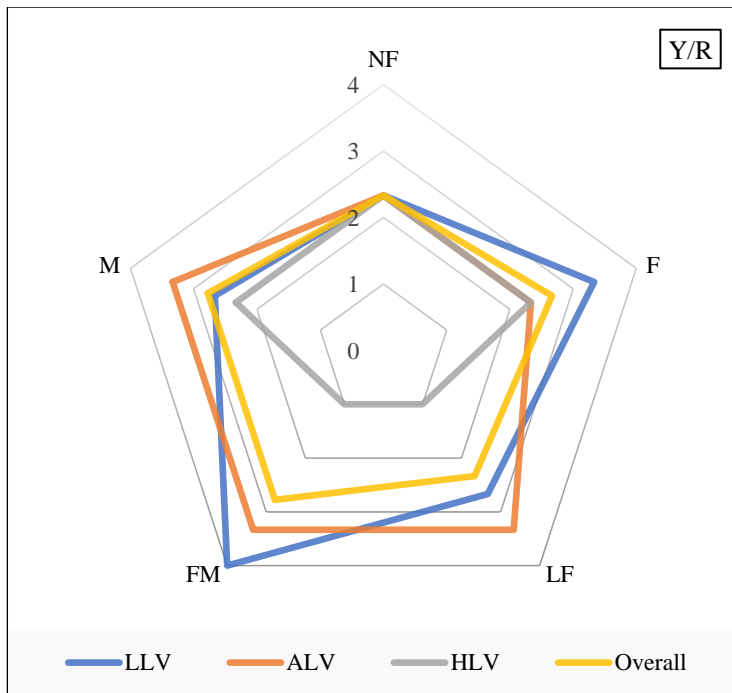
(b)



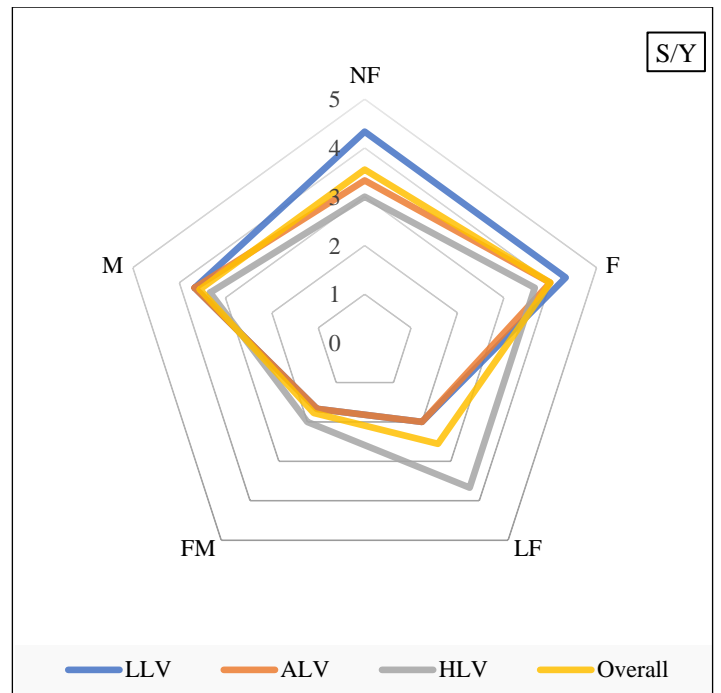
(c)



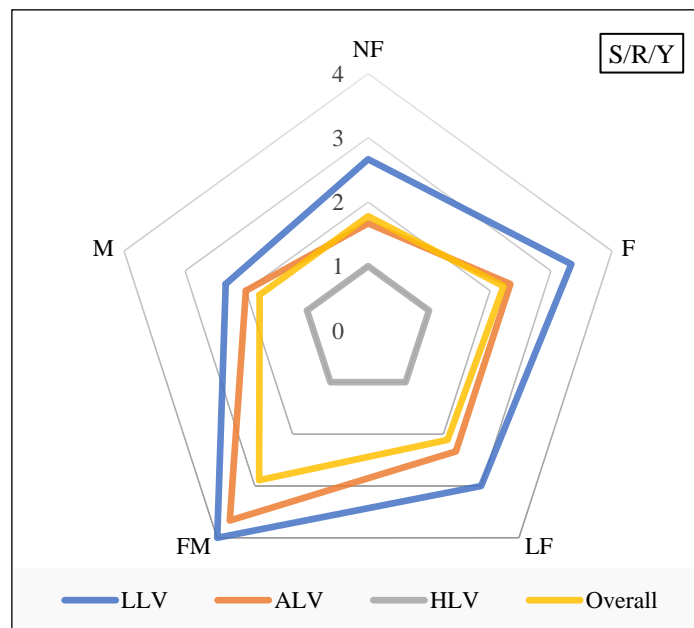
(d)



(e)



(f)



(g)

Figure 4.3: Ranking of growth stage considering (a) 1 parameter-S; (b) 1 parameter-R; (c) 1 parameter-Y; (d) 2 parameters-S/R; (e) 1 parameter-S; (f) 2 parameters-Y/R; (g) 3 parameters-S/R/Y

If S/R/Y is considered as the parameter with different limit values, the overall highest-ranking was found at the FM stage, followed by the F and LF stages as seen in Figure 4.3a.

The last two stages are NF and M as seen in previous rankings. When two parameters (S/R)

are considered, the FM stage ranks highest (Figure 4.3b), and the F stage is second. The following orders belong to LF, NF, and M, respectively. In addition, the highest-ranking is found at the FM stage when considering the two parameters (Y/R) as shown in Figure 4.3c, the second highest to the F stage, followed by M, NF, and LF stages. However, if the two parameters (S/Y) are considered, the flower (F) stage holds the overall highest ranking, the NF and M stages the second-highest combinedly (Figure 4.3d), with LF and FM stages following. When only the one parameter (S) is considered, the highest overall ranking of different limit values goes with the F stage; whereas the M stage has fallen to the second-highest position as shown in Figure 4.3e, with the last positions to the NF, LF, and FM stages. In contrast, the FM stage holds the highest average ranking when 1-parameter (R) is considered followed by the LF, M, NF, and F stage (Figure 4.3f). On the other hand, if 1-parameter (Y) is considered, the flower (F) stage stands in the highest position, and the M, NF, LF, and FM stages follow (Figure 4.3g).

4.2.3 Ranking (5x3) for the combination of five growth stages and three lengths

The suitability ranking was done along the combination of 5 growth stages and 3 lengths to decide for the 15 (5x3) batches, i.e., growth stage-length. From the 7 different combinations of parameters and 3 limit values, 21 groups with distinct colour were formed in which each group contained a total of 15 batches that were ranked from the lowest to highest on a scale of 1 to 15. Python coding (Appendix A 44) was used on data in Table 4.1 as input and the ranking is shown in Table 4.6.

Table 4.6: Ranking along combination of growth stage and length

Limit value	Growth stage	Ranking																				
		1 Parameter									2 Parameter									3 Parameter		
		S			R			Y			S/R			Y/R			S/Y			S/R/Y		
		L1	L2	L3	L1	L2	L3	L1	L2	L3	L1	L2	L3	L1	L2	L3	L1	L2	L3	L1	L2	L3
LLV	NF	8	9	10	2	8	15	5	13	8	3	10	14	3	8	12	9	11	12	3	10	14
	F	12	15	12	5	1	15	11	1	15	6	1	15	6	1	15	15	5	15	6	1	15
	LF	6	7	2	6	9	11	3	12	4	5	11	8	5	10	9	3	5	2	5	11	8
	FM	4	3	1	7	15	15	6	8	7	7	11	9	7	12	10	5	4	1	7	11	9
	M	4	12	10	4	2	9	1	8	15	4	2	13	4	2	14	5	10	12	4	2	13
ALV	NF	13	11	1	13	11	1	9	12	10	1	7	7	1	5	13	12	14	1	1	7	7
	F	14	9	10	14	9	10	13	2	15	1	1	15	4	1	14	15	7	12	1	1	15
	LF	7	3	3	7	3	3	5	7	6	1	12	7	5	12	11	4	4	4	1	12	7
	FM	5	6	2	5	6	2	3	4	1	7	12	7	9	10	5	2	7	2	7	12	7
	M	11	15	8	11	15	8	11	7	15	1	1	14	8	1	15	10	10	9	1	1	14
HLV	NF	13	4	1	1	6	6	8	10	1	1	1	1	1	15	1	12	6	1	1	1	1
	F	15	12	10	1	1	6	15	1	14	1	1	1	1	1	15	15	1	12	1	1	1
	LF	4	4	4	1	6	15	6	10	12	1	1	1	1	1	1	6	6	6	1	1	1
	FM	1	4	1	1	13	12	1	4	4	1	1	1	1	1	1	1	6	1	1	1	1
	M	11	14	4	6	6	14	9	6	12	1	1	1	1	1	15	1	12	6	1	1	1

same colour indicates the same batch, ranked 1 to 15 within the batch

In Table 4.6, only two groups (HLV-S/R, HLV-S/R/Y) do not have any batches without having the ranking 1. It is due to the suitability (%) of each batch of this group is zero, i.e., no group could fulfill the threshold conditions. Apart from these 3 groups, among the 19 groups, F-L3 (LLV-R, LLV-Y, LLV-S/R, LLV-Y/R, LLV-S/Y, LLV-S/R/Y, ALV-Y, ALV-S/R, ALV-S/R/Y, HLV-Y/R) obtained the maximum number (10) of the highest rank, whereas F-L1 (LLV-S/Y, ALV-S/Y, HLV-S, HLV-Y, HLV-S/Y) got the second highest number (5) of highest ranking of 15 followed by M-L3 (LLV-Y, ALV-Y, ALV-Y/R, HLV-Y/R), M-L2 (ALV-S, ALV-R), NF-L2 (HLV-Y/R), NF-L3 (LLV-R), F-L2 (LLV-S), LF-L3 (HLV-R), FM-L2 (LLV-R), FM-L3 (LLV-R).

Figure 4.4 represents the number of highest rankings taken from Table 4.6. When considering only growth stages, flower (F) stage holds 16 (F-L3: 10; F-L1: 5; F-L2: 1) highest rank and mature (M) stage has 6 (M-L3: 4; M-L2: 2) highest rank for a total of 19 batches.

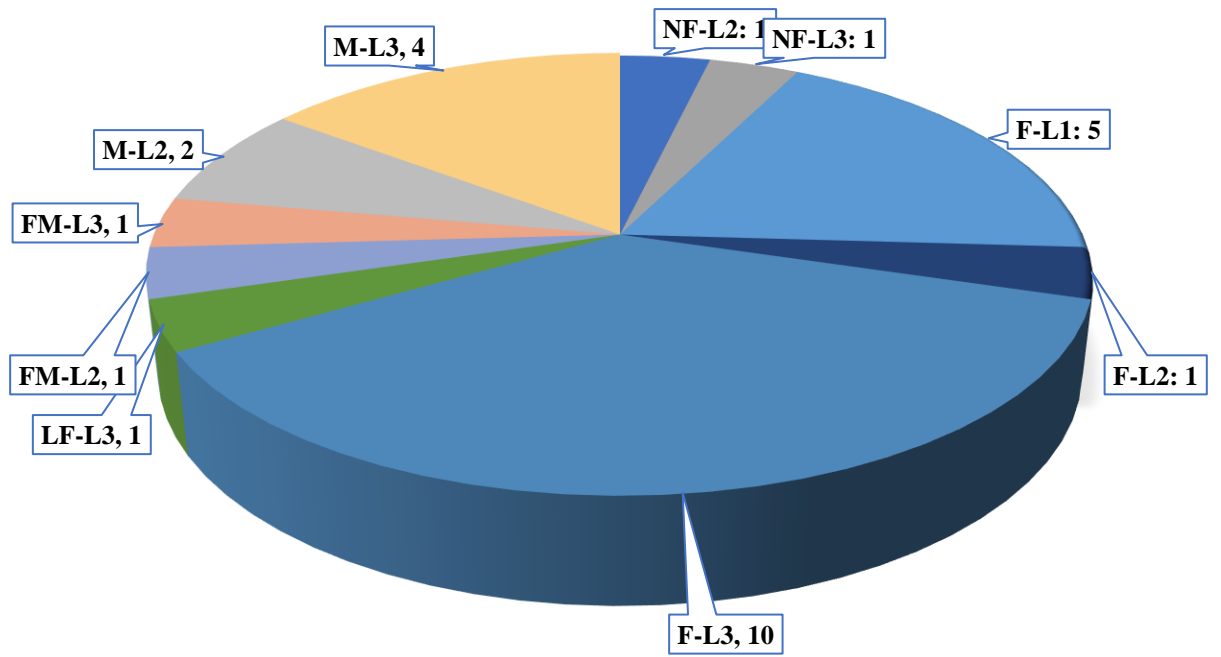


Figure 4.4: No. of the highest ranking of growth stages from the ranking along both length and growth stages

Since F-L3 and F-L1 are the highest number of top ranks holders, a calculation of the average of the ranking of each group from Table 4.6 was done; can show that F-L3 is the highest (average rank: 12/15) in the average hierarchy (Figure 4.5). At the same time, M-L3 (10.57/15), NF-L2 (8.52/15), and F-L1 (8.19/15) are in the positions shown in Figure 4.5.

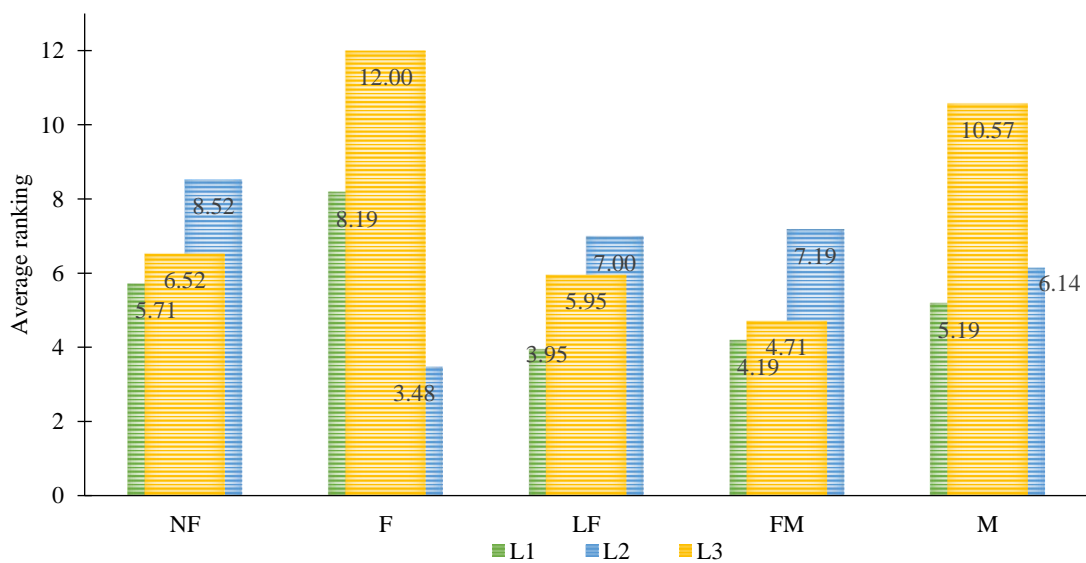


Figure 4.5: Average combined ranking of growth stage and length

4.2.4 Ranking within parameters and parameter combination

The average suitability (%) of three lengths (L1, L2, and L3) was calculated for different parameters (S/R/Y, S/R, Y/R, S/Y, S, R, Y) and the 7 parameters ranked 1 to 7 (low to high) within the same growth stages and for 3 different limit values (Table 4.7). Finally, the average ranking was calculated for every growth stage and limit value.

Table 4.7 Ranking of different parameters

Limit value	Growth stage	Ranking						
		1 Parameter			2 Parameter			3 Parameter
		S	R	Y	S/R	Y/R	S/Y	S/R/Y
LLV	NF	6	4	7	1	3	5	1
	F	7	4	6	1	4	5	1
	LF	6	6	7	1	3	4	1
	FM	4	6	7	1	5	4	1
	M	6	4	7	3	1	5	1
ALV	NF	6	6	7	1	3	4	1
	F	6	5	7	1	3	4	1
	LF	4	6	7	1	5	3	1
	FM	4	6	7	1	5	3	1
	M	5	6	7	1	4	3	1
HLV	NF	7	4	6	1	4	5	1
	F	7	4	6	1	4	5	1
	LF	5	6	7	1	1	5	1
	FM	6	7	6	1	1	6	1
	M	5	7	6	1	3	4	1

1 Lowest 2 Low 3 Moderately low 4 Medium 5 Moderately high 6 High 7 Highest

In the case of a single parameter, modulus (Y) is on the top of the ranking, noted from Table 4.7 and Figure 4.6 for all the three limit values. Tensile stress (S) and strain (R) are in the second and third positions among the single parameters for LLV and HLV, whereas a reverse second and third position was remarked for ALV. However, when 2 parameters are considered, S/Y holds the top position followed by Y/R and S/Y for LLV and HLV. In the case of ALV, Y/R got the highest rank followed by S/Y and S/R, respectively.

On the other hand, S/R/Y is the lowest ranked among the 7 parameter combination. Obviously, the more conditions you apply on checking, the less possibility of matching the

requirements. Nevertheless, while taking the rank average gives $Y > S > R > S/Y > Y/R > S/R > S/R/Y$ as shown in Figure 4.6.

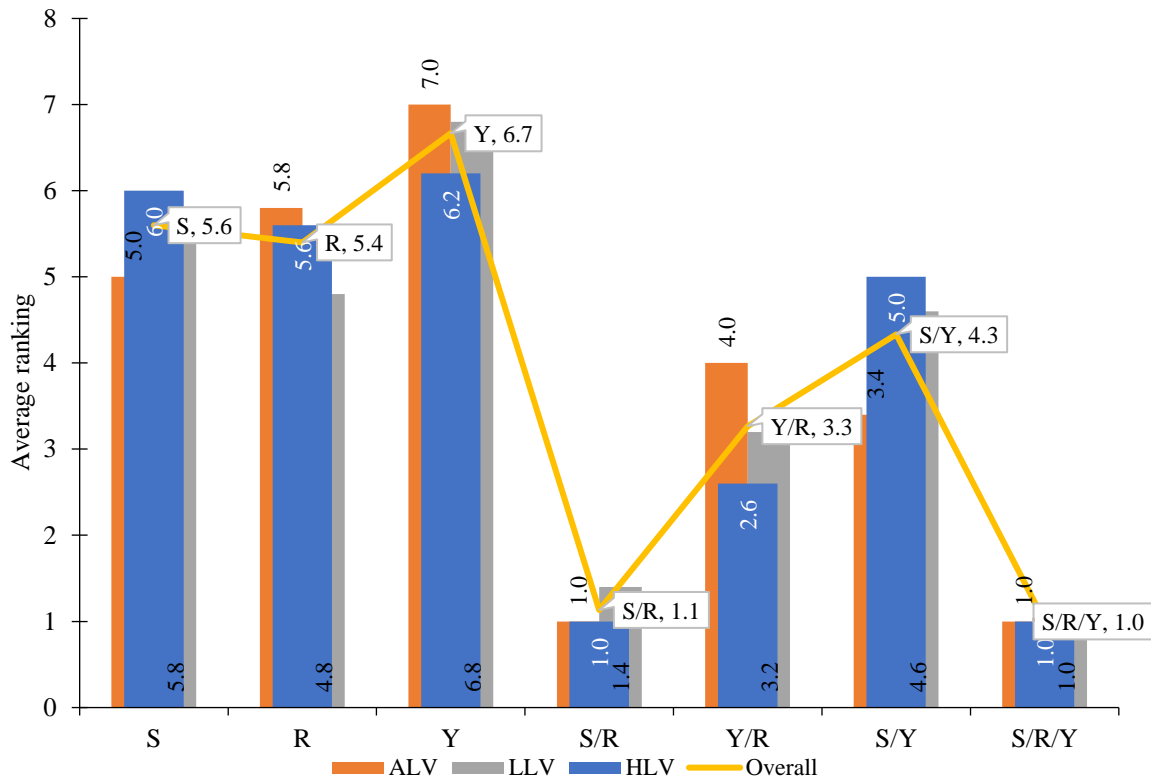


Figure 4.6: Average ranking of parameters with different limit value

Finally, considering only growth stages, the flower (F) stage showed the highest average ranking (3.08/5) followed by the mature (M) stage (2.89/5) among the five. It might be due the presence of lowest amount of nonstructural carbohydrates as mentioned by Beule (1979) and Linde et al., (1976). In addition, L3 got the highest average ranking (2.11/3) if length is considered separately. However, when both growth stage and length is considered combined, F-L3 exhibited the highest average ranking (12/15); whereas M-L3 (10.57/15) was its closest competitor batch. Moreover, Young's modulus (Y) holds the top position (6.67/7) among the 7 parameter combinations. A summary table of ranking shown in Table 4.8

Table 4.8: Summary table of ranking

Ranking Type	Method	Table / Figure #	Result (Ranking)
Along fibre lengths	Ranked three lengths from 1 to 3 for each growth stage, parameter combination, and limit value individually		L3>L2>L1
Ranking for individual parameter, parameter combinations and limit values (fixed length)	Ranked five growth stages from 1 to 5 for each length, parameter combination, and limit value individually	Table 4.5	F>FM>LF>NF>M (LLV-L1) FM>F>M>NF>LF (ALV-L1) F>M>NF>LF>FM (HLV-L1) LF>NF=FM>M>F (LLV-L2) LF=FM>NF>M>F (ALV-L2) NF>M>LF>FM>F (HLV-L2) F>NF>M>FM>LF (LLV-L3) F>M>LF>NF=FM (ALV-L3) F>M>LF>FM>NF (HLV-L3)
Rank for average of lengths and limit values (fixed parameter and parameter combination)	Calculated the average of three lengths and three limit values so that the average ranking of growth stages were found for different parameter and parameter combinations using the ranking from Table 4.5	Figure 4.1	F>M>NF>LF>FM (S) FM>LF>M>NF>F (R) F>M>NF>LF>FM (Y) FM>F>LF>NF=M (S/R) FM=M>F>NF=LF (Y/R) F>NF=M>LF>FM (S/Y) FM>F>LF>NF=M (S/R/Y) F>M>NF>FM>LF (Overall)
Along growth stages Ranking for average length and parameter combinations (fixed limit value)	Calculated the average of three lengths and 7 parameter combinations to find out the average ranking of growth stages for different limit values using the ranking data from Table 4.5	Figure 4.2	F>FM>NF>M>LF (LLV) M>F>FM>LF>NF (ALV) M>F>LF>NF>FM (HLV) F>M>NF>FM>LF (Overall)
Ranking for average of lengths and limit values (fixed parameters and parameter combinations)	Calculated the average ranking of three length to find out the ranking of growth stages for three limit values with each of seven parameter combinations individually using the data from Table 4.5	Figure 4.5	F>NFM>LF>FM (LLV-S) F>M>NF>LF>FM (ALV-S) F>M>LF>NF>FM (HLV-S) FM>LF>NF=F>M (LLV-R) FM>LF>M>F>NF (ALV-R) M>LF>FM>NF>F (HLV-R) NF=F>FM=M>LF (LLV-Y) M>NF=F>LF>FM (ALV-Y) F=LF=M>NF>FM (HLV-Y) FM>LF>F>NF>M (LLV-S/R) FM>F=LF>M>NF (ALV-S/R) NF=F=LF=FM=M (HLV-S/R) FM>F>LF=M>NF (LLV-Y/R) LF=FM=M>NF=F (ALV-Y/R) NF=F=M>LF=FM (HLV-Y/R) NF=F>M>LF>FM (LLV-S/Y) F>M>NF>LF>FM (ALV-S/Y) F=LF>M>NF>FM (HLV-S/Y) FM>F>LF>NF>M (LLV-S/R/Y) FM>F=LF>M>NF (ALV-S/R/Y) NF=F=LF=FM=M (HLV-S/R/Y)
Combination of growth stages and lengths	Ranked the suitability (%) values (Table 4.1) from 1 to 15 among the 15 batches (5 growth stages × 3 lengths) for specific parameters combinations and limit values separately.	Table 4.6	F-L3>M-L3>NF-L2>F-L1>FM-L2>LF-L2>NF-L3>M-L2>LF-L3>NF-L1>M-L1>FM-L3>FM-L1>LF-L1>F-L3

Within parameters and parameter combination

Ranked the parameter values (using data from Table 4.1) based on the average suitability (%) of three lengths of each parameter combination and limit values

Table 4.7

Y>S>R>S/Y>Y/R>S/Y>S/R/Y

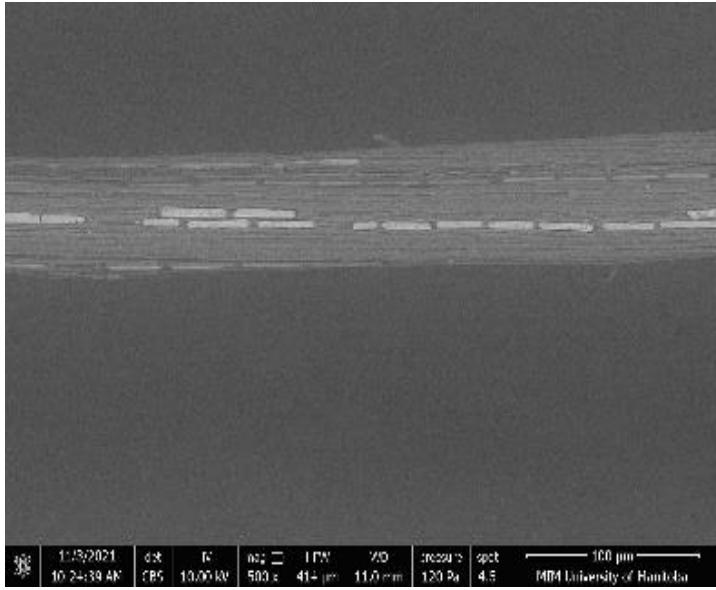
Chapter 5 Image Analysis and Chemical Composition – Results and Discussion

5.1 ESEM Analysis of Fibres from Different Growth Stages

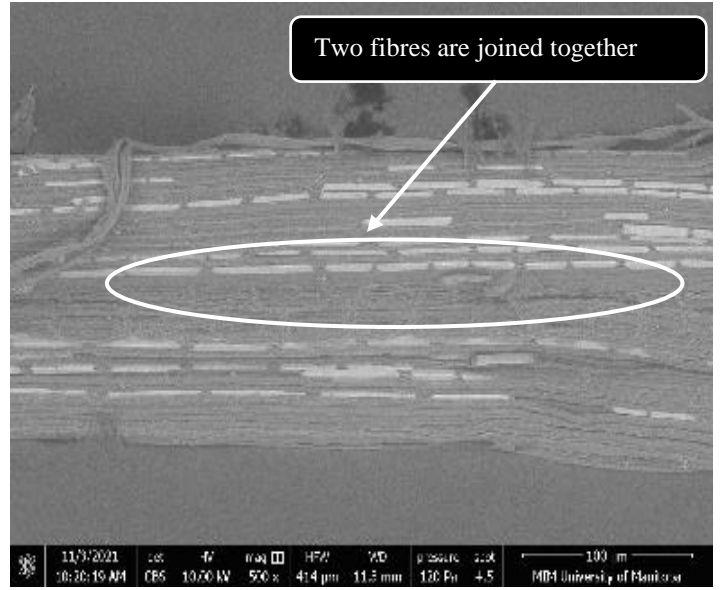
Environmental scanning electron microscopy (ESEM) was conducted using four fibres (Fibre 1, Fibre 2, Fibre 3 and Fibre 4) from each of the growth stages. Although the length of fibre in the ESEM mount was 20000 μm , the captured image length was only 415 μm . The captured image contains the most plates from the 50 different images within the total mount length of a single fibre and these ESEM pictures are shown here.

Figure 5.1 to Figure 5.5 represent the ESEM image of different growth stages and Table 5.1 shows the surface features with the diameter of the fibre in the parentheses. The effects of diameter on the surface features are discussed in Section 5.2 Effect of fibre diameter on the formation of calcium oxalate plates.

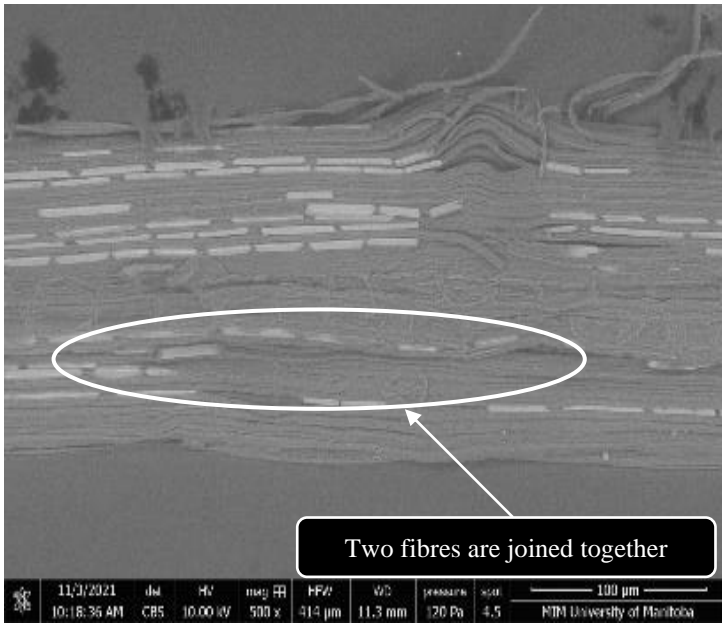
It can be seen from these figures that fibres from all five maturities contain the calcium oxalate plates (Figure 5.1 to Figure 5.5), with a few exceptions. For example, Fibres 3 and 4 of FM stage (Figure 5.4c and Figure 5.4d), and Fibre 3 of mature stage (Figure 5.5c) contain very few to no calcium oxalate plates. The plates are mostly rectangular in shape, in a series of lines which are parallel to one another in the longitudinal direction. Similar oxalate plates were reported by Yu (2021) and (Shadhin et al., 2022). Different shaped calcium oxalate plates were also noticed such as quadrilateral, parallelogram, rhombus, trapezium and so forth. The number of plates and plate dimensions vary for different maturity stages as well as for different fibres within same maturity level.



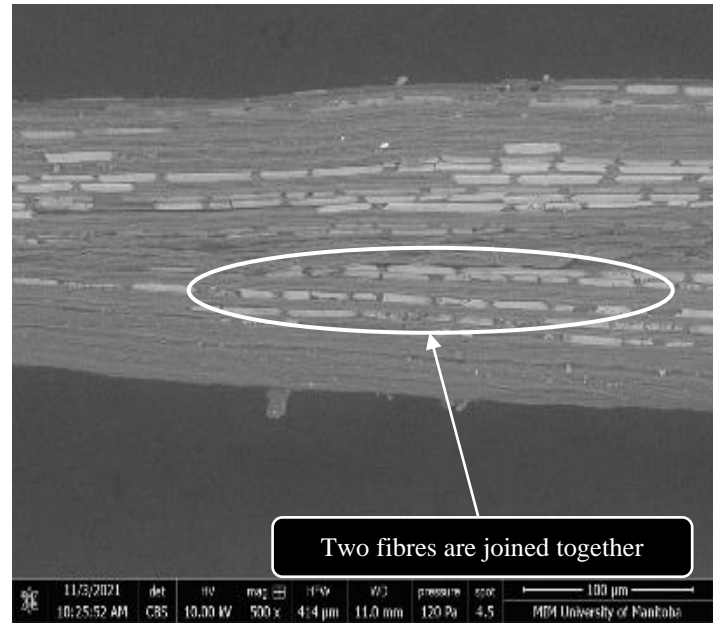
(a)



(b)

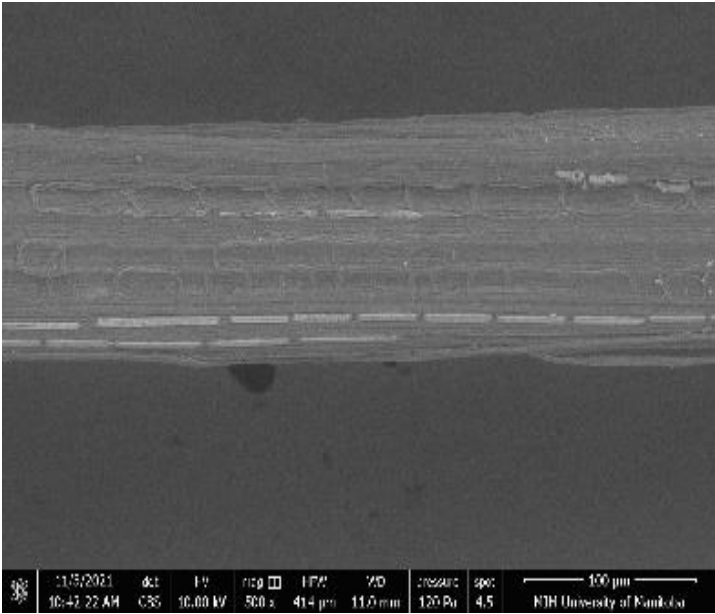


(c)

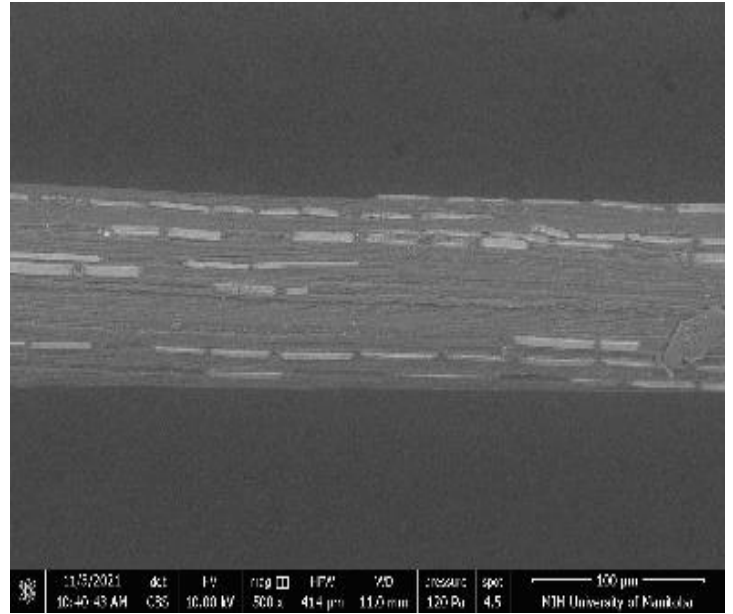


(d)

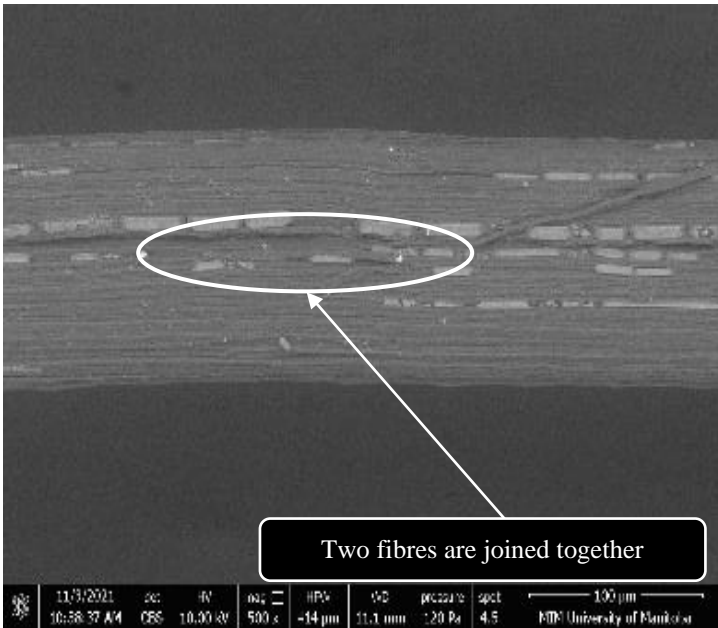
Figure 5.1: ESEM image of fibres from NF stage - (a) Fibre 1 (b) Fibre 2 (c) Fibre 3 (d) Fibre



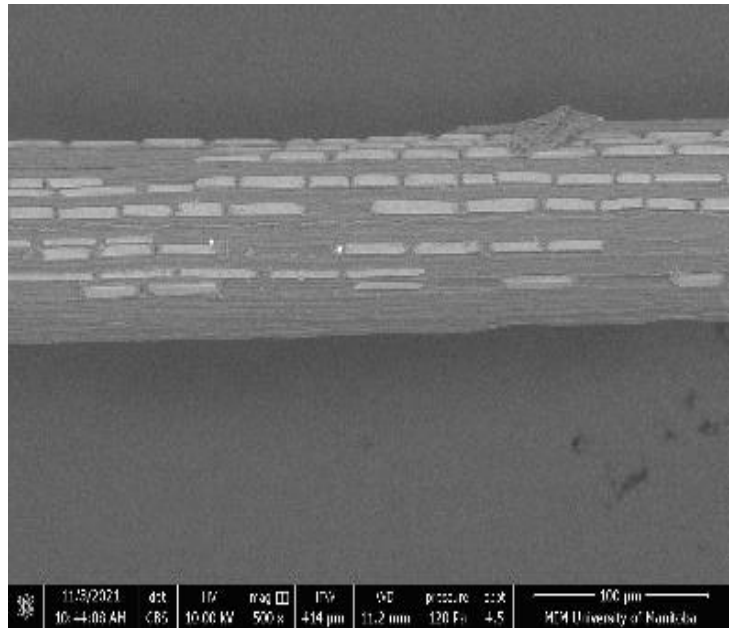
(a)



(b)

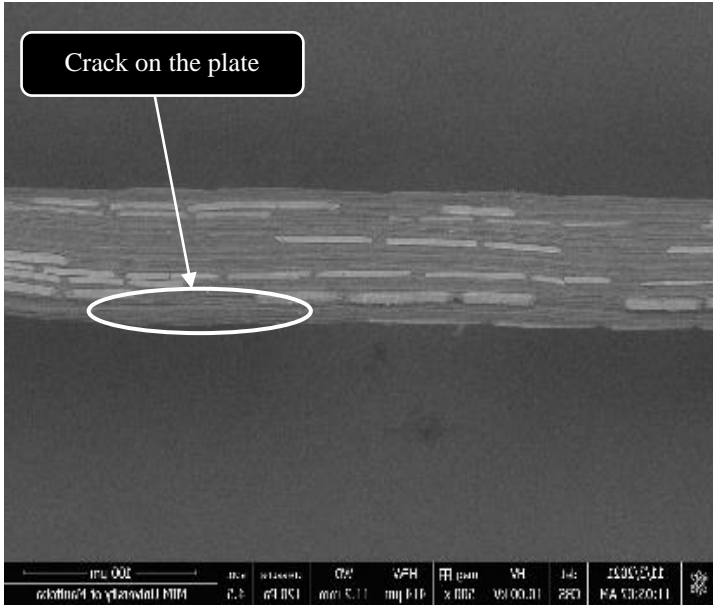


(c)

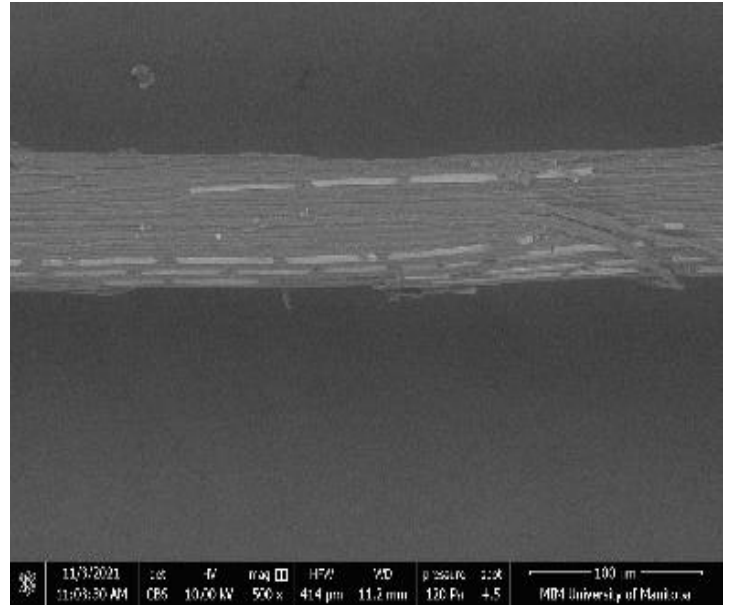


(d)

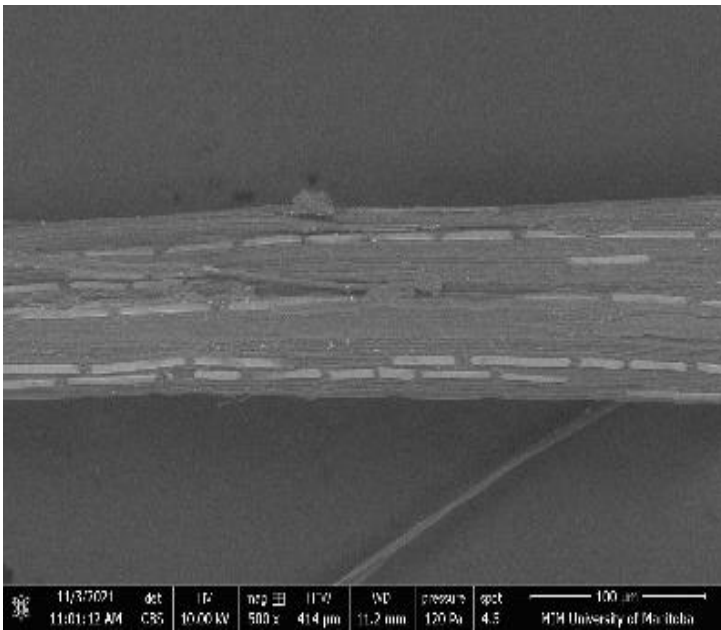
Figure 5.2: ESEM image of fibre from F stage - (a) Fibre 1 (b) Fibre 2 (c) Fibre 3 (d) Fibre 4



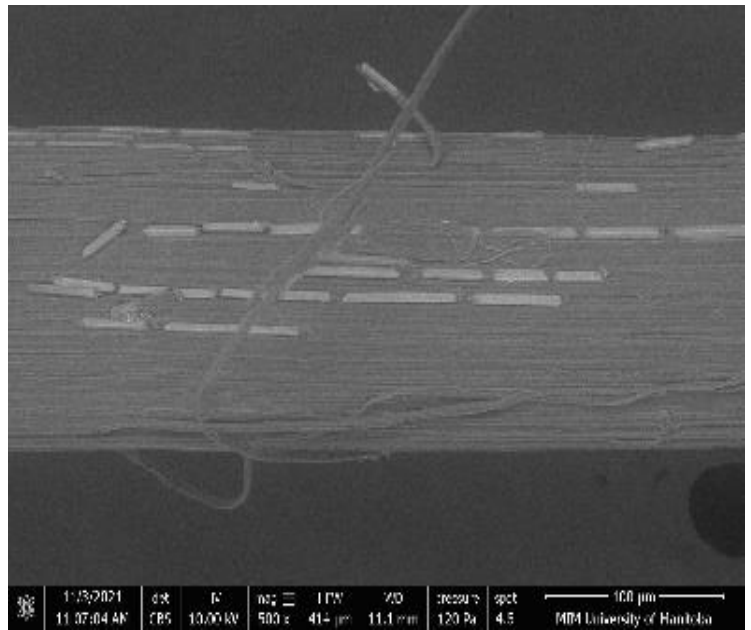
(a)



(b)

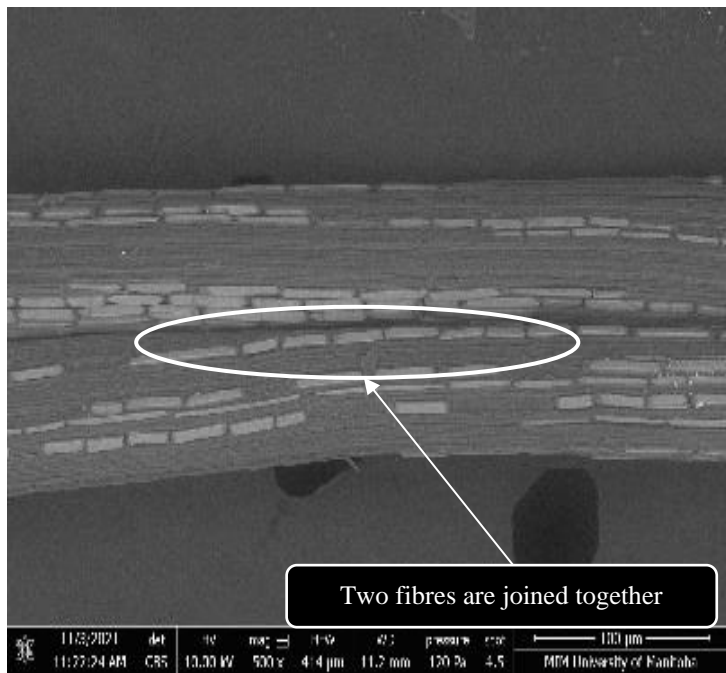


(c)

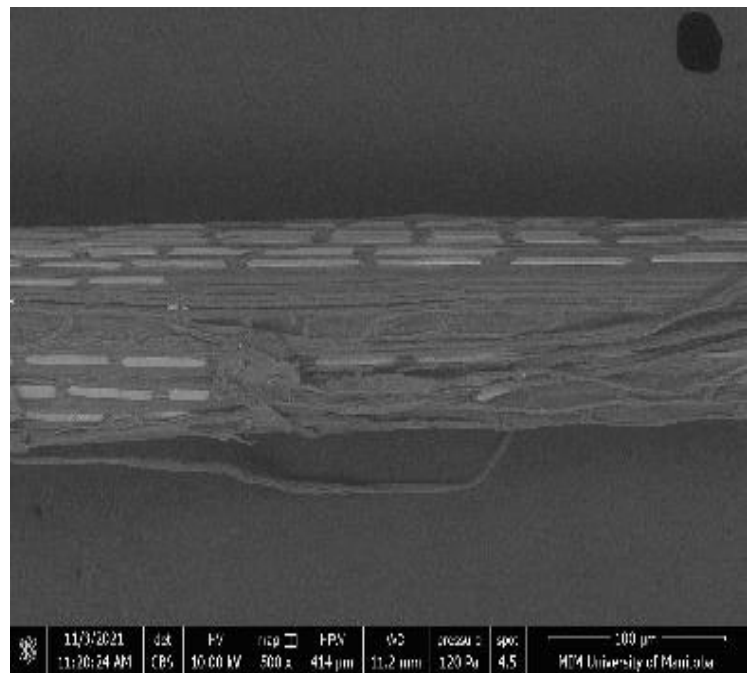


(d)

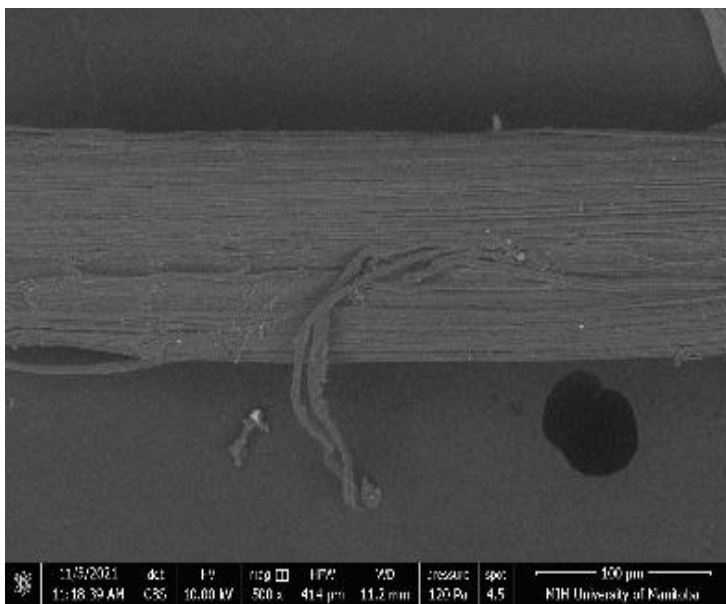
Figure 5.3: ESEM image of fibre from LF stage - (a) Fibre 1 (b) Fibre 2 (c) Fibre 3 (d) Fibre



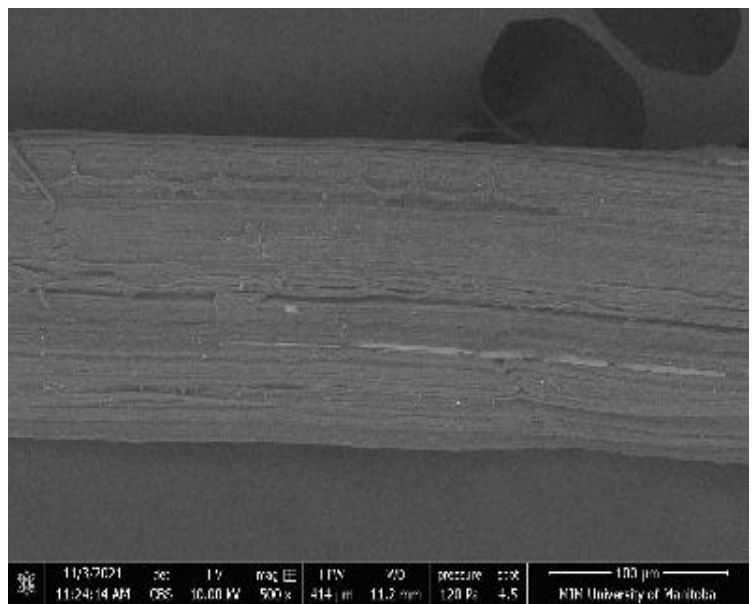
(a)



(b)

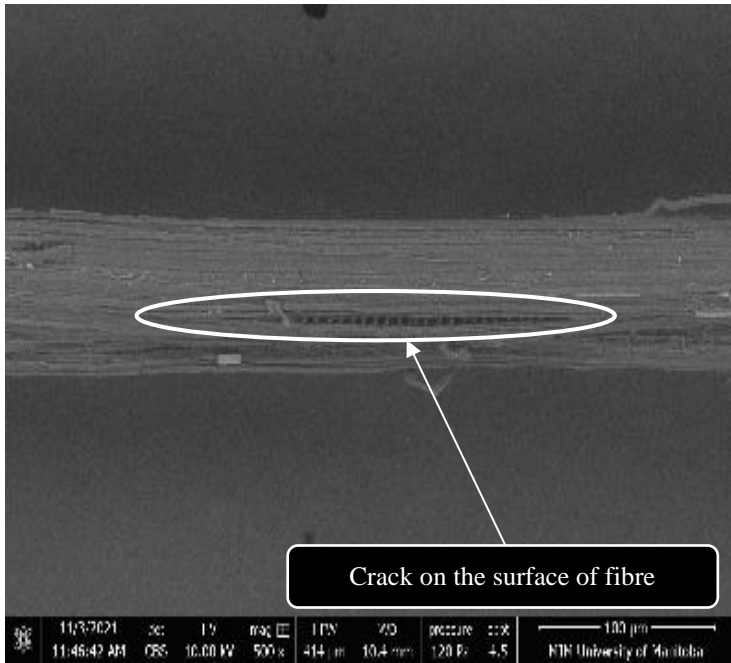


(c)

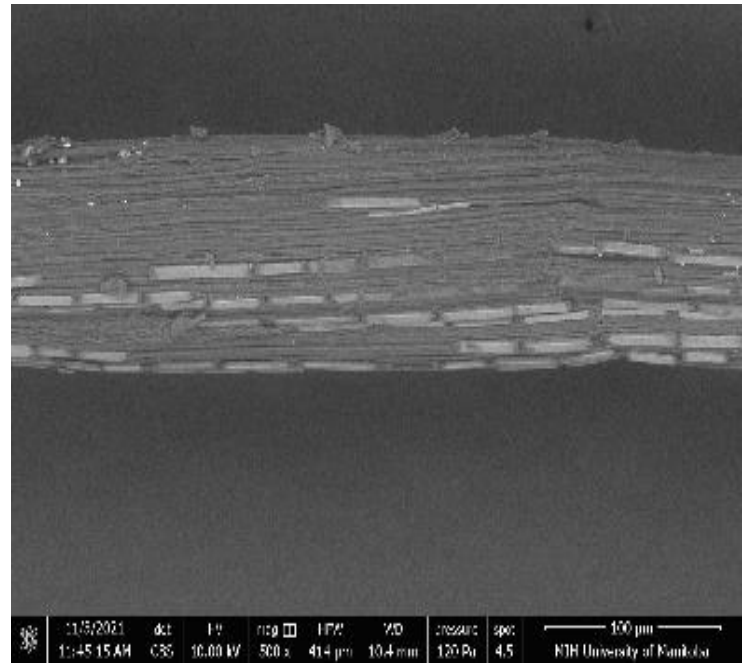


(d)

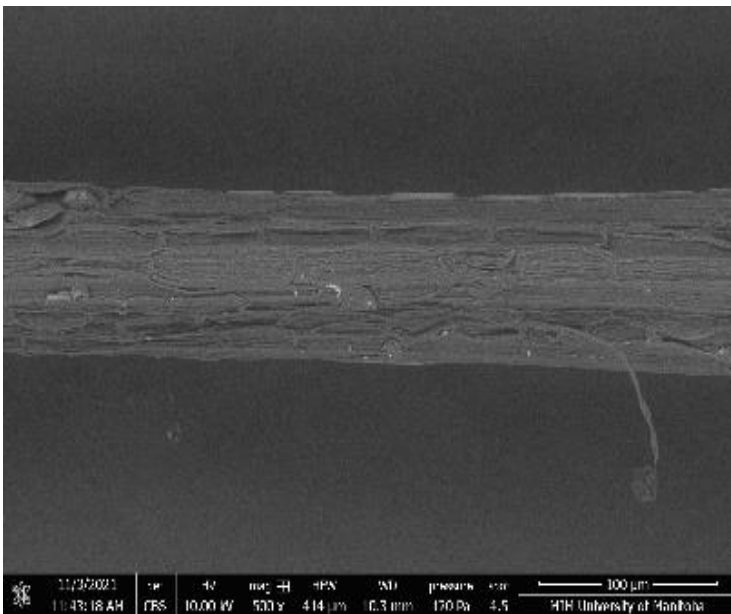
Figure 5.4: ESEM image of fibre from FM stage - (a) Fibre 1 (b) Fibre 2 (c) Fibre 3 (d) Fibre



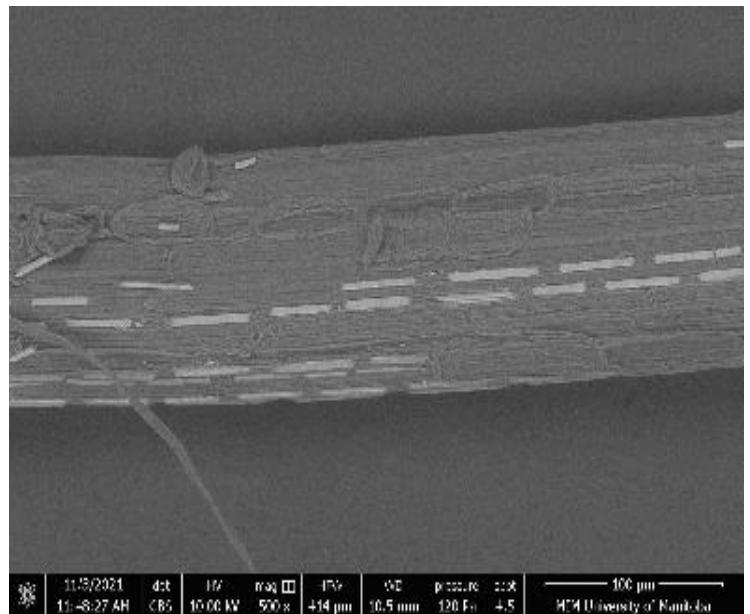
(a)



(b)



(c)



(d)

Figure 5.5: ESEM image of fibre from M stage - (a) Fibre 1 (b) Fibre 2 (c) Fibre 3 (d) Fibre 4

A few samples were noticed to have very little or no plates in the mature stage fibre (Figure 5.5a and Figure 5.5c) while one fibre from each of the FM stage and M stage showed no plates at all (Figure 5.4c and Figure 5.5c). The most consistent number (34 ± 4.8) of plates

was noticed in the four fibres of LF stage, varying between 27 (Fibre 2) and 38 (Fibre 3); while the most variation in plates was found in the FM fibres [Range: 0 (Fibre 3) – 106 (Fibre 1), 37.8±48.6] as shown in Table 5.1. For the NF stage, the number of plates (66.8±35.1) varies between 15 (Fibre 1) and 90 (Fibre 4) and for F stage, the number of plates (45.5±24.2) was found between 15 (Fibre 1) to 73 (Fibre 4). Meanwhile, in case of the M stage, the number of plates (23.0±26.2) was noticed between 0 (Fibre 3) and 53 (Fibre 2).

Table 5.1: Dimensions and frequency of Calcium Oxalate plates at various growth stages

Growth stage	No. of plates				Plate average dimensions (visually more frequent size)			Plate Largest dimension			
	Fibre 1	Fibre 2	Fibre 3	Fibre 4	Avg. [SD]	Length (µm)	Width (µm)	Longitudinal Distance (µm)	Length (µm)	Width (µm)	Longitudinal Distance (µm)
NF	15 (55.3)	87 (149)	75 (155)	90 (149)	66.75 [35.10]	31.09 [6.91]	3.97 [0.11]	3.26 [0.92]	73.91 (F4)	4.78 (F1)	32.61 (F1)
F	15 (115)	53 (91.5)	41 (119)	73 (93.6)	45.50 [24.24]	34.24 [2.08]	5.60 [2.62]	5.43 [4.16]	73.48 (F1)	6.30 (F4)	8.70 (F3)
LF	35 (63.8)	27 (61.7)	38 (89.4)	36 (148.9)	34.00 [4.83]	39.67 [5.65]	3.64 [1.09]	6.25 [1.63]	89.13 (F1)	4.35 (F4)	5.43 (F3)
FM	106 (119)	39 (91.5)	0 (110.6)	6 (154)	37.75 [48.62]	42.75 [6.99]	4.71 [0.63]	7.61 [2.88]	73.91 (F1)	2.61 (F4)	15.22 (F2)
M	2 (64.9)	53 (107)	0 (80.9)	37 (123)	23.00 [26.24]	34.94 [25.37]	3.18 [2.21]	6.76 [4.00]	52.17 (F4)	5.61 (F2)	10.87 (F4)

Fibre diameter (µm) in parentheses; Standard deviations are shown in square bracket; N = 4 for NF, F & LF; N = 3 for FM & M

It appears that the average number of plates decreases with maturity; for example, the average number of plates in NF fibres is 66.75, while for mature fibres the average number of plates is only 23 (Table 5.1). However, due to the larger standard deviation, the differences in plate count are not statistically significant. It is worth mentioning here that, cracks appear almost in the middle of the plates (Figure 5.3a), as well as cracks on the fibre surface (Figure 5.5a).

The dimensions of the plates (length, width and longitudinal distance i.e. the distance between two adjacent plates) were taken using a representative from the visually most frequent plates in each of the four fibres. Since one of the FM (Fibre 3, Figure 5.4c) and M

(Fibre 3, Figure 5.5c) stage fibres do not contain any plates, these two fibres are omitted from the dimension calculation. The average length of the plate varies between the $31.09 \pm 6.91 \mu\text{m}$ (NF stage, N=4) and $42.75 \pm 6.99 \mu\text{m}$ (FM stage, N=3), while the average width from $3.97 \pm 0.11 \mu\text{m}$ (NF stage, N=4) to $5.60 \pm 2.62 \mu\text{m}$ (F stage, N=4). The average longitudinal distances (head to tail, visually more frequent plates) between two plates are $3.26 \pm 0.92 \mu\text{m}$ (NF stage, N=4) to $7.61 \pm 2.88 \mu\text{m}$ (FM stage, N=3), while the transverse distance between two plates in all fibres is approximately $4.07 \pm 1.99 \mu\text{m}$ (N=16). Since the most frequent plates were based on the naked eye observation, the data may not be very accurate.

Other dimensions, such as the longest distance, largest width and the longest longitudinal distance were also measured. For each growth stage in four fibres (Fibre 1, Fibre 2, Fibre 3 and Fibre 4), the longest plate length found was $89.1 \mu\text{m}$ in LF, $74.0 \mu\text{m}$ in NF, F, and FM stage and $52 \mu\text{m}$ in mature stage fibres. The width of the plates also varies widely within the fibre of a growth stage and in different growth stages. The width of the widest plates was found $4.78 \mu\text{m}$, $6.3 \mu\text{m}$, $4.35 \mu\text{m}$, $2.61 \mu\text{m}$ and $5.61 \mu\text{m}$ for NF, F, LF, FM and M growth stage fibres, respectively. The longest longitudinal distance (maximum value of the longest dimension of Fibre 1, Fibre 2, Fibre 3 and Fibre 4) between the adjacent two plates was $32.61 \mu\text{m}$ in NF stage, $8.70 \mu\text{m}$ in F stage, $5.43 \mu\text{m}$ in LF stage, $15.22 \mu\text{m}$ in FM stage, and $10.87 \mu\text{m}$ in mature (M) stage (Table 5.1)

One of the reasons for variation in the plates within a maturity stage is due to fibres sticking together as shown in Figure 5.1b (Fibre 2/NF), Figure 5.1c (Fibre 3/NF), Figure 5.1d (Fibre 4/NF), Figure 5.2c (Fibre 2/F), and Figure 5.4a (Fibre 1/FM). The number of plates on these fibres is higher than on the other fibres within the same growth stage, which are – 87 in Fibre 2/NF, 75 in Fibre 3/NF and 90 in Fibre 4/NF, while the number of plates are 41 in Fibre 3/F and 106 in Fibre 1/FM stage fibres. The attachment of two or more fibres was not visible by unaided eyes, however, was visible only in ESEM.

Each sample was examined using EDS (Energy Dispersive X-ray Spectroscopy) and made the elemental analysis of the calcium oxalate plate and pit areas of the surface of the cattail fibre. Figures in Appendices (A19a, A19b, A19c, A19d, A19e) show the EDS spots of all fibres from various growth stages. Four spots were selected from each ESEM image: two were at the calcium oxalate plate, and the other two were at the pit areas (non-plate areas).

Table 5.2: Atomic % of cattail fibre at different growth stages

Growth stage	Elements							
	Carbon (C)		Oxygen (O)		Aluminum (Al)		Calcium (Ca)	
	Plate area	Non-plate area	Plate area	Non-plate area	Plate area	Non-plate area	Plate area	Non-plate area
NF	59.5 [2.3]	75.1 [0.7]	31.1 [1.4]	21.8 [0.6]	^b 0.95 [0.1]	^c 1.18 [0.1]	8.48 [0.9]	^g 1.44 [0.3]
F	62.2 [1.6]	77.5 [0.9]	27.7 [2.2]	19.9 [2.0]	^b 1.25 [0.1]	^{de} 1.42 [0.4]	8.78 [0.6]	1.17 [0.7]
LF	67.0 [4.9]	76.7 [0.6]	27.5 [2.7]	22.8 [0.7]	^b 0.18 [0.1]	^{df} 0.18 [0.1]	5.29 [2.2]	^g 0.36 [0.1]
FM	^a 61.0 [0.1]	76.7 [0.3]	29.9 [0.1]	21.8 [0.9]	^b 0.14 [0.1]	^e 0.16 [0.1]	8.93 [0.1]	1.30 [0.5]
M	^a 62.3 [0.1]	76.4 [0.1]	29.3 [0.7]	22.1 [0.4]	^b 0.77 [0.1]	^{cf} 0.82 [0.2]	7.63 [0.9]	0.70 [0.4]

*^{abcdefg}: pairs with same alphabet are statistically significant; standard deviation is shown in square brackets

Table 5.2 shows that the cattail fibre consists of carbon, oxygen, aluminum, calcium, potassium, and a minuscule amount of chlorine (not shown in Table 5.2). It can be seen that the plates contain less carbon and aluminum, and higher oxygen than non-plate areas; however, all plates contain a significantly higher amount of calcium than the non-plate areas. In every growth stage, the plate areas contain an average of 59.53% to 67.02% carbon, 27.75 to 31.05% oxygen, 0.14% to 1.25% aluminum, and 5.29% to 8.93% calcium; whereas, the non-plate areas contain an average of 75.14% to 77.53% carbon, 19.88% to 22.75% oxygen, 0.16% to 1.42% aluminum, and 0.30% to 1.44% calcium. Carbon (%) of plate areas of the FM and M stage are statistically significant. In addition, aluminum (%) of plate areas of all five growth stages have significant differences; whereas, for non-plate areas, the NF and M stage, the F and LF stage, the F and FM stage, and the LF and M stages are all statistically significant. Moreover, calcium (%) of the non-plate areas of NF and LF stage are statistically significant.

5.2 Effect of fibre diameter on the formation of calcium oxalate plates

A few fibres from the mature and FM stages contained zero calcium oxalate plates: FM/Fibre 3 (Figure 5.4c); M/Fibre 3 (Figure 5.5c). Additionally, some fibres had lower plate counts in all growth stages: for example, 15 in NF/Fibre 1, F/Fibre 1, 6 and 2 in FM/Fibre 4, and M/Fibre 1 (Table 5.1), respectively. To identify whether the effect is due to chemical treatment or growth stage, a mechanical extraction was performed. The different sizes in fibre diameter in a cattail leaf is reported by (Witztum & Wayne, 2014) that might have an impact on plate count.

The mechanical fibre extraction was carried out for the mature plant only, by a process described by Yu (2021). The details of the chemical extraction process are given in Chapter 2. Only fine fibres (diameter: 21.74 – 28.26 μm) could be removed from the central area of cattail leaf by mechanical extraction, while both fine (diameter: 29.79 – 40.43 μm) and coarse fibres (diameter: 51.06 – 129.79 μm) were found in the chemically-extracted fibre (Figure 5.7 to Figure 5.9). The coarse fibre in the leaf broke during mechanical extraction due to the fibre attachment to the dorsal (convex surface) and ventral surface (concave surface) as shown in Figure 5.6. The diameter of the mechanically extracted fibre was similar to Yu's, (2021) findings.

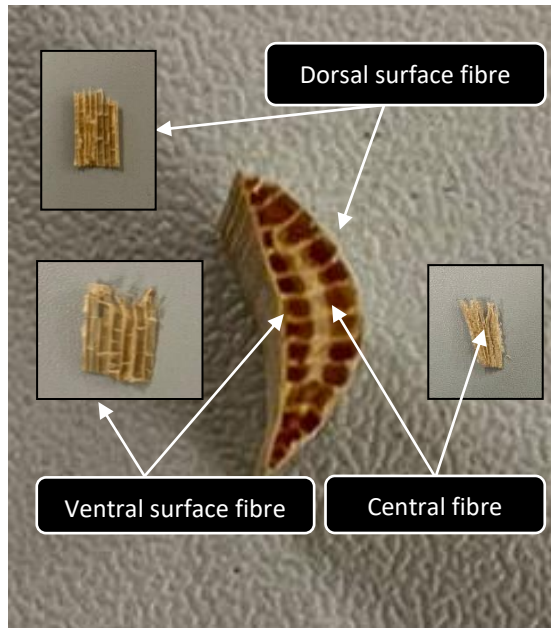
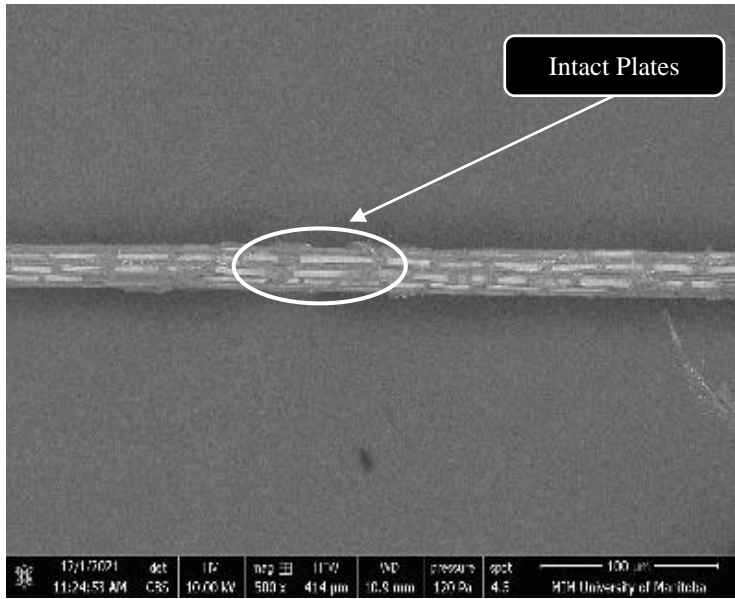
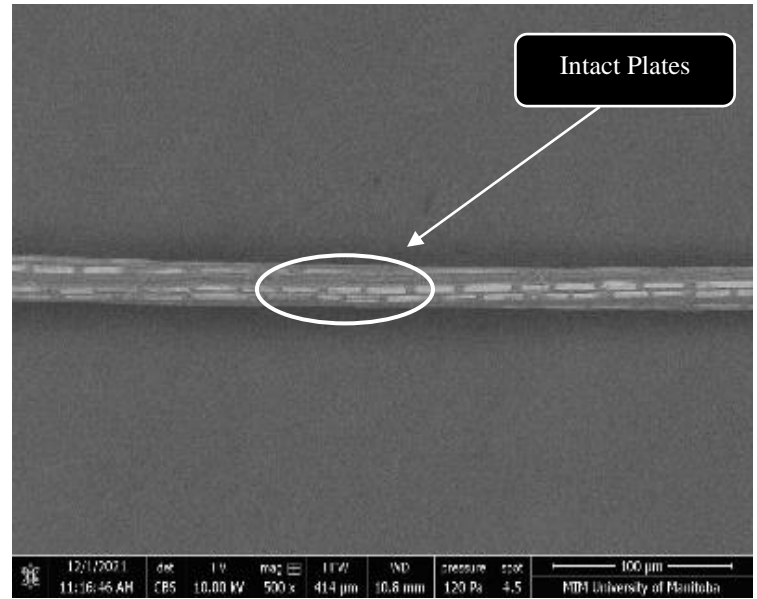


Figure 5.6: Different parts of cattail leaf and locations of fibre

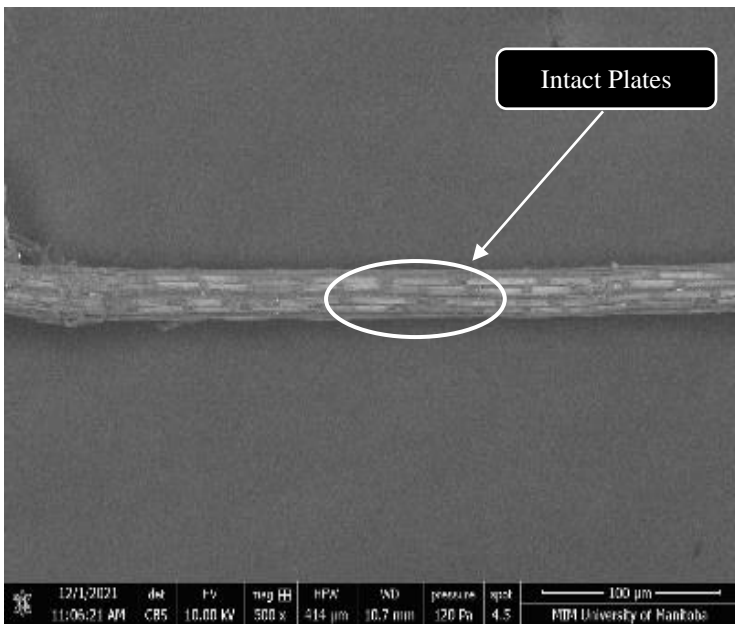
ESEM Figure 5.7 shows the mechanically extracted fine fibre from the center of the cattail leaf (Figure 5.7a –Figure 5.7d), and chemically extracted fine fibre from the centre of leaf (Figure 5.8a – Figure 5.8d), and chemically extracted coarse fibre from the surfaces (dorsal and ventral) of leaf (Figure 5.9a – Figure 5.9d).



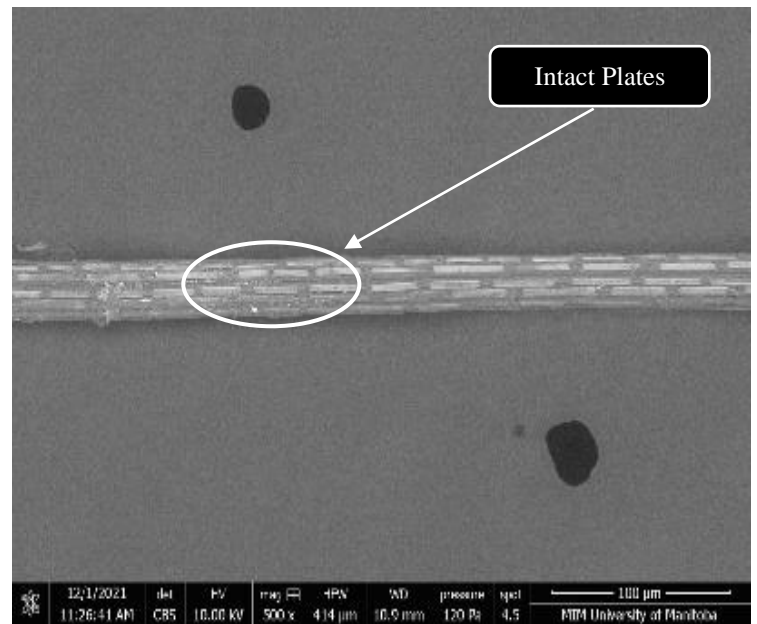
(a)



(b)

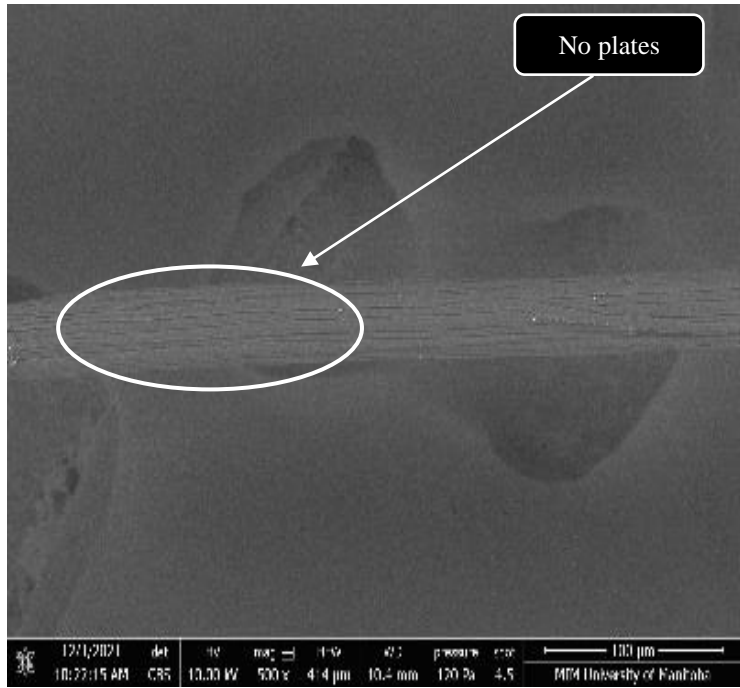


(c)

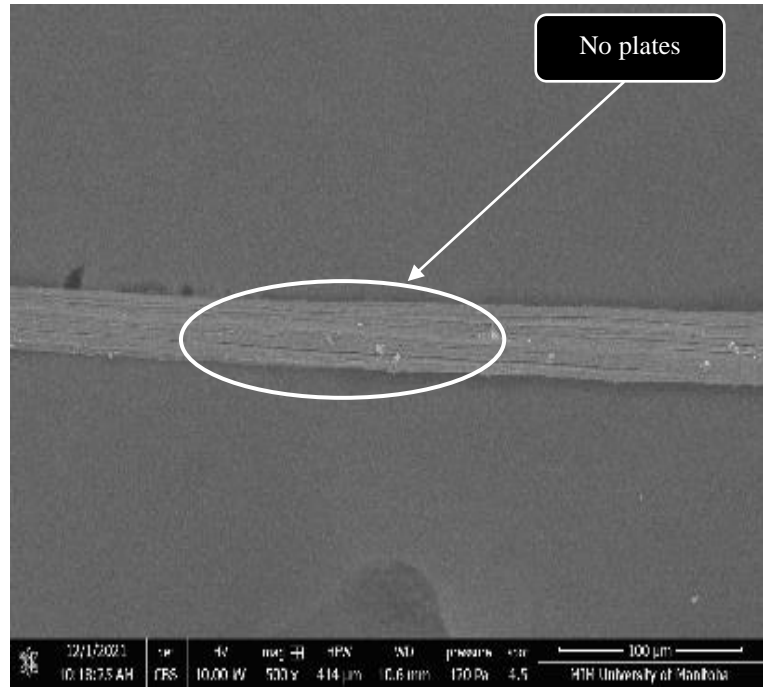


(d)

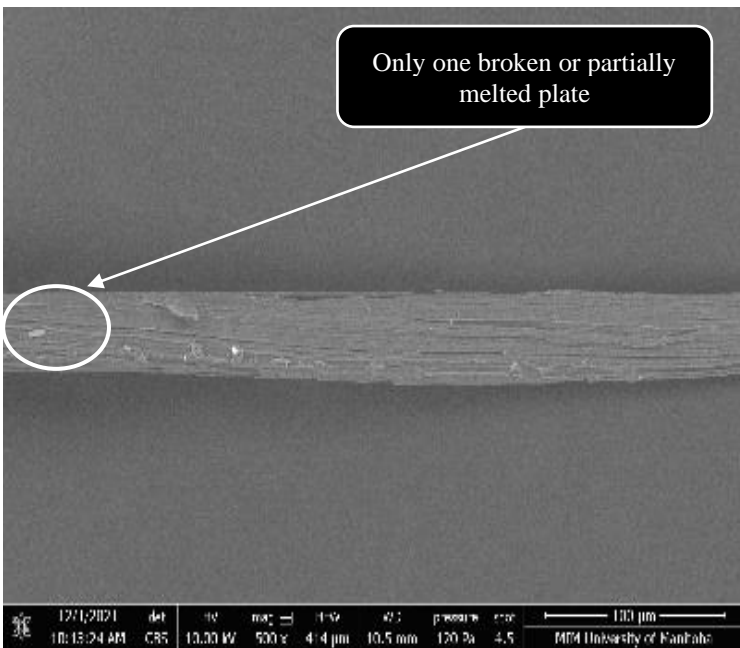
Figure 5.7: ESEM image of mechanically extracted mature fine fibre from the center of leaf
 (a) Fibre 1; (b) Fibre 2; (c) Fibre 3; (d) Fibre 4



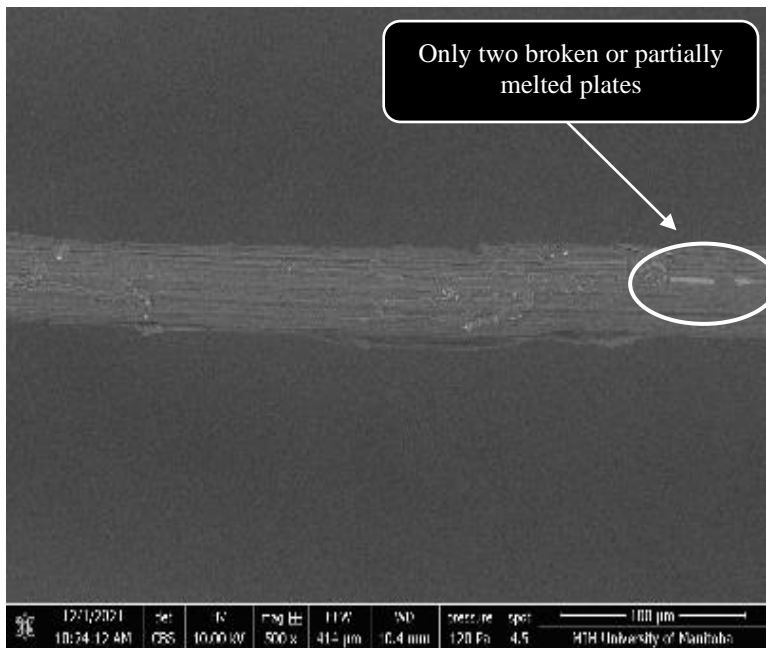
(a)



(b)

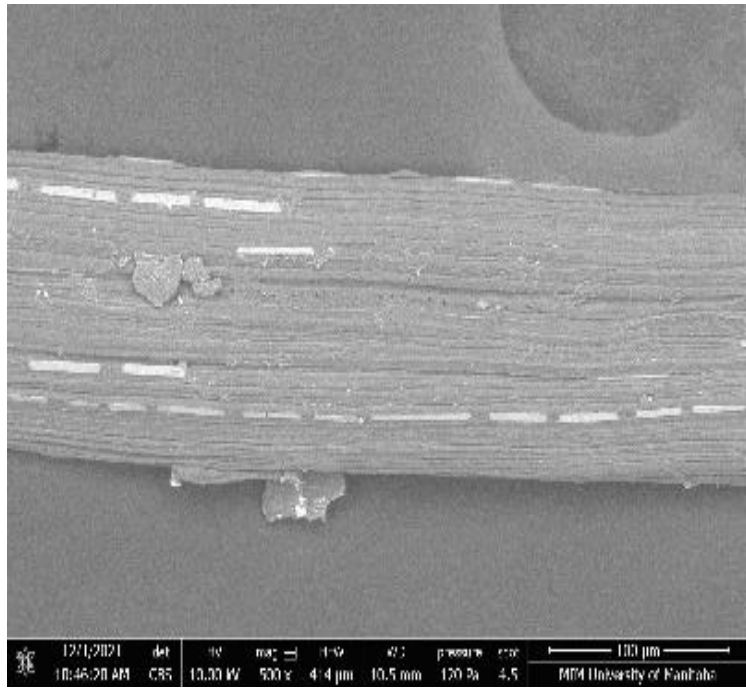


(c)

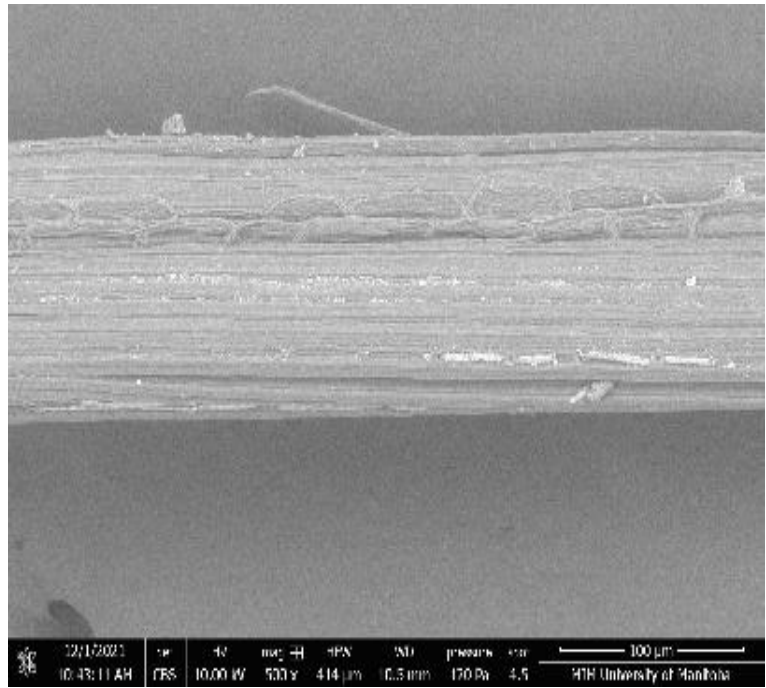


(d)

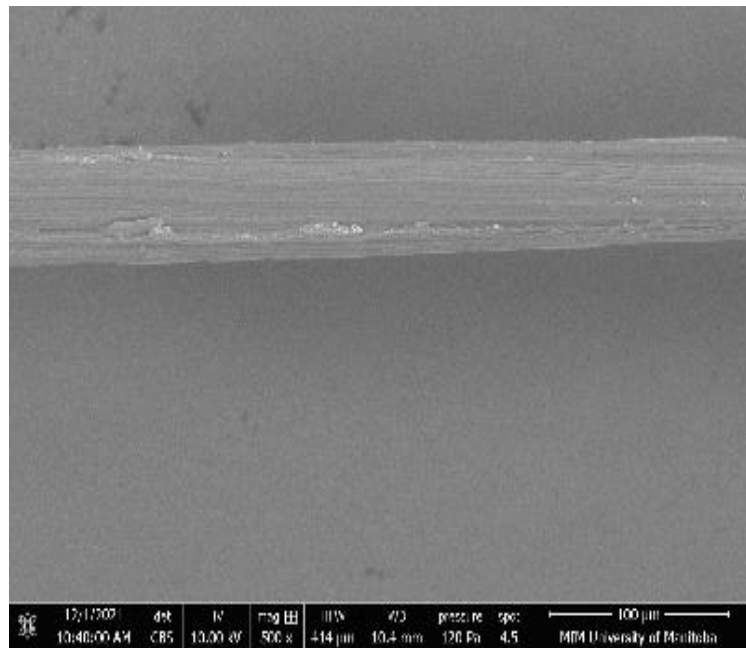
Figure 5.8: ESEM image of chemically extracted mature fine fibre (a) Fibre 1; (b) Fibre 2; (c) Fibre 3; (d) Fibre 4



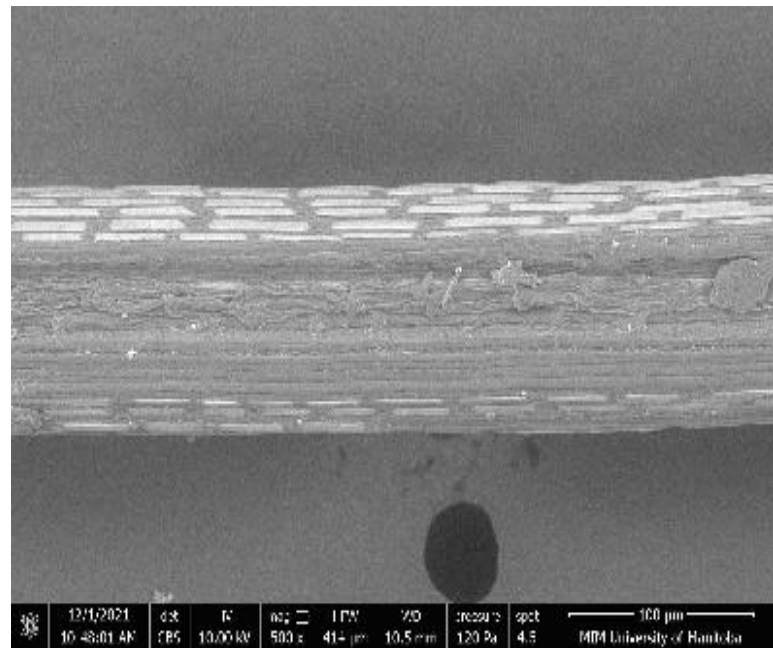
(a)



(b)



(c)



(d)

Figure 5.9: ESEM image of chemically extracted mature coarse fibre (a) Fibre 1; (b) Fibre 2; (c) Fibre 3; (d) Fibre 4

Very few calcium oxalate plates (0.75 ± 0.96 , $N=4$) were noticed on the chemically extracted fine fibre (Figure 5.8a to Figure 5.8d & Table 5.3) whose diameters were $34\mu\text{m}$, $30\mu\text{m}$, $40\mu\text{m}$, and $40\mu\text{m}$; however, numerous plates (53.75 ± 9.74 , $N=4$) were found in the

mechanically extracted fine fibre (Figure 5.7a to Figure 5.7d) which is also statistically significant ($p=0.0001$) with chemically extracted fine fibre. Further, chemically extracted coarse fibres (Figure 5.9a – Figure 5.9d) contain fewer plates (25.75 ± 34.97 , $N=4$) than the mechanically extracted fine fibres (53.75 ± 9.74 , $N=4$).

Table 5.3: Dimensions and frequency of Calcium Oxalate plates from different extraction methods

Fibre type	No. of plates				Plate average dimensions (visually more frequent size)			Plate's largest dimension			
	Fibre 1	Fibre 2	Fibre 3	Fibre 4	Avg. [SD]	Length (μm)	Width (μm)	Longitudinal distance (μm)	Length (μm)	Width (μm)	Longitudinal distance (μm)
Mechanically extracted fine fibre	48 (23.9)	47 (21.7)	52 (25.0)	68 (28.3)	^a 53.75 [9.74]	25.27 [1.04]	3.21 [1.09]	5.60 [1.85]	43.48 (F4)	4.35 (F4)	7.61 (F3)
Chemically extracted fine fibre	0 (34.0)	0 (29.8)	1 (40.4)	2 (40.0)	^a 0.75 [0.96]	17.39 [12.83]	3.15 [1.42]	5.43 [5.82]	26.09 (F4)	3.91 (F3)	0.00
Chemically extracted coarse fibre	23 (130)	4 (120)	0 (51.1)	76 (114)	25.75 [34.97]	38.41 [10.04]	3.77 [0.82]	8.70 [2.17]	65.22 (F4)	3.48 (F2)	19.57 (F4)

^a: statistically significant; fibre diameter (μm) in the parentheses in columns of no. of plates; standard deviation is shown in square bracket; F1, F2, F3, F4 indicates the Fibre1, Fibre 2, Fibre 3, Fibre 4 accordingly.

The dimensions of the ‘visually more frequent plates’ were different for the different extraction methods. The average length of the plates was measured $17.39 \pm 12.83 \mu\text{m}$ for chemically extracted fine fibre ($N=2$) to $38.41 \pm 10.04 \mu\text{m}$ for chemically extracted coarse fibre, ($N=3$), while the average width was noted between $3.15 \pm 1.42 \mu\text{m}$ for chemically extracted fine fibre ($N=2$) and $3.77 \pm 0.82 \mu\text{m}$ for chemically extracted coarse fibre ($N=2$) as shown in Table 5.3. The average longitudinal distance between the adjacent two plates was $5.43 \pm 5.82 \mu\text{m}$ for chemically extracted fine fibre, ($N=2$; Figure 5.8d) to $8.70 \pm 2.17 \mu\text{m}$ for chemically extracted coarse fibre, ($N=3$; Figure 5.9a, Figure 5.9b, Figure 5.9d). The average length of plates of the mechanically extracted fine fibre was $25.27 \pm 1.04 \mu\text{m}$ ($N=4$), width of fibre $3.21 \pm 1.09 \mu\text{m}$ ($N=4$) and the distance between the adjacent plates $5.60 \pm 1.85 \mu\text{m}$ ($N=4$).

However, if the longest plates (maximum value among the largest value of the four samples, Table 5.3) were considered, the longest length was $26.09 \mu\text{m}$ for the chemically

extracted fine fibre (Figure 5.8d), 43.48 μm for mechanically extracted fine fibre (Figure 5.7d) and 65.22 μm for chemically extracted coarse fibre (Figure 5.9d) as shown in Table 5.3. The largest width was 3.48 μm for chemically extracted coarse fibre (Figure 5.9b), while the value was 4.35 μm for mechanically extracted fine fibre (Figure 5.9d) and 3.91 μm for chemically extracted fine fibre (Figure 5.8c). The longest longitudinal distance between the adjacent two plates was between zero for chemically extracted thin fibre (this was due to the presence of 0, 0, 1, and 2 plates on the each of the four fibres investigated), 19.57 μm for chemically extracted coarse fibre (Figure 5.9d) and 7.61 μm mechanically extracted fine fibre (Figure 5.8c).

The length and width of the plates on the surface of the chemically extracted fine fibre (Figure 5.8a – Figure 5.8d) were less than the mechanically extracted fine fibre (Figure 5.7a – Figure 5.7d). The plate dimensions were highest for the chemically extracted coarse fibre (Figure 5.9a – Figure 5.9d) in both the most frequent plate size and the largest size. Similar occurrence was found in the case of longitudinal distance between the plates.

5.2.1 Relation between the number of plates and the fibre diameter

The mechanically extracted fibres contained a higher number of plates [number of plates: 48 (Figure 5.7a), 47 (Figure 5.7b), 52 (Figure 5.7c), 68 (Figure 5.7d)] than the chemically extracted fine [number of plates: 0 (Figure 5.8a), 0 (Figure 5.8b), 1 (Figure 5.8c), 2 (Figure 5.8d)] and coarse [number of plates: 23 (Figure 5.9a), 4 (Figure 5.9b), 0 (Figure 5.9c), 76 (Figure 5.9d)] fibres that have the similar diameter. Further, in most cases the lowest number of plates were found in the chemically extracted fine fibres [number of plates: 0 (Figure 5.8a), 0 (Figure 5.8b), 1 (Figure 5.8c), 2 (Figure 5.8d)] than in the chemically extracted coarse fibres [number of plates: 23 (Figure 5.9a), 4 (Figure 5.9b), 0 (Figure 5.9c), 76 (Figure 5.9d)] as shown in Table 5.3. The fluctuation in plate counts in the chemically extracted coarse fibres is higher than the plate counts in the fine fibres from the mechanical

and chemically extracted fibres. The plate count consistency in the mechanically extracted fine fibres (average plate count: 53.75 ± 9.74 , $N=4$) is far greater than both fine (0.75 ± 0.96 , $N=4$) and coarse (25.75 ± 34.97 , $N=4$) fibres extracted by the chemical method (Table 5.3).

Moreover, in the case of mechanically extracted fibres, the number of plates increases with the increase in fibre diameter (Table 5.3). No such trend is observed for chemically extracted fibres. It can be stated that calcium oxalate plates might have been removed during the alkali extraction and therefore, chemically extracted fibres contain fewer or in some cases zero oxalate plates. It is not known how the plates are attached to the fibre surface or the bond breaking mechanism caused by alkali treatment. Although mechanical extraction used the mature plant, an analysis of the relationship between fibre diameter and number plates revealed a similar phenomenon in the chemically extracted fibres from other growth stages.

For example, Fibre 1 from the NF stage had just 15 calcium oxalate plates (Figure 5.1a), and a diameter of $55.32 \mu\text{m}$ (Table 5.2). In addition, from the LF stage, Fibre 1 had 35 plates (Figure 5.3a) with $63.83 \mu\text{m}$ of diameter, and Fibre 2 contained 27 plates (Figure 5.3b) with $61.70 \mu\text{m}$ diameter. Fibres 1 and 3 of mature stage had 2 plates (Figure 5.5a) and plates (Figure 5.5c), respectively although their diameters were $64.89 \mu\text{m}$ and $80.85 \mu\text{m}$, respectively, and Fibre 3 of the FM stage (diameter: $110.64 \mu\text{m}$) had zero plates (Figure 5.4c). In addition, 15 (Figure 5.2a) and 37 (Figure 5.5d) plates were found in Fibre 1 of the F stage and Fibre 4 of the mature stage, respectively, but their diameters were $114.89 \mu\text{m}$ and $123.40 \mu\text{m}$, respectively. On the other hand, a higher number of plates was found in the coarser fibres: 106 plates (Figure 5.4a) in Fibre 1 of FM stage with diameter $119.15 \mu\text{m}$, and 90 (Figure 5.5b), 87 (Figure 5.5c), and 75 (Figure 5.5d) plates were found in mature Fibres 2, 3, and 4, respectively, with diameters $149.15 \mu\text{m}$, $148.94 \mu\text{m}$, and $155.32 \mu\text{m}$, respectively.

A summary of atomic percentage of different elements from the EDS report (Appendix A 31 to A 36) was also constructed as shown in Table 5.4. Both mechanically and

chemically extracted fibres contain carbon, oxygen, calcium, and aluminum; however, the amounts are different for different fibres as well as for plate and non-plate areas.

Table 5.4: Average atomic % of elements from different extraction method

Fibre Extraction method	Element							
	Carbon (C)		Oxygen (O)		Aluminum (Al)		Calcium (Ca)	
	Plate area	Non-plate area	Plate area	Non-plate area	Plate area	Non-plate area	Plate area	Non-plate area
Mechanically extracted fine fibre	^a 69.6 [2.1]	^c 81.7 [0.0]	24.6 [1.7]	^f 17.6 [0.0]	^g 0.06 [0.1]	0.05 [0.0]	5.72 [0.4]	ⁱ 0.67 [0.0]
Chemically extracted fine fibre	^b 71.4 [0.0]	^d 81.58 [0.6]	23.4 [0.0]	^e 17.7 [0.2]	^g 0.04 [0.0]	0.11 [0.1]	5.25 [0.0]	^j 0.22 [0.1]
Chemically extracted coarse fibre	^{ab} 64.0 [0.9]	^{cd} 76.6 [0.1]	27.2 [3.9]	^{ef} 22.0 [0.3]	^h 0.04 [0.0]	0.13 [0.1]	8.76 [3.0]	^j 0.64 [0.0]

*^{abcdefghij}: Pairs with same alphabets are statistically significant (N= 2); Standard deviation is presented in square bracket

Table 5.4 shows the average atomic percentage of elements of the fibre extracted by mechanical and chemical methods. Mechanically extracted fine fibres consist of an average of 69.61 % carbon, 24.60% oxygen, 0.06% aluminum, and 5.72% calcium in the plate area; whereas the non-plate area consists of 81.70% carbon which is greater than the plate area, 17.58% oxygen, or slightly less than the plate area, 0.05% aluminum, and 0.67% calcium which is much less than the plate area. In contrast, the fine fibres from both the chemical and mechanical extractions have almost similar atomic percentage at the plate and non-plate areas for each element (Table 5.4).

On the other hand, carbon (%) of plate and non-plate areas of mechanically extracted fine and chemically extracted coarser fibres are statistically significant; whereas, chemically extracted fine and coarse fibres have significant differences as well. A similar trend was noticed for oxygen (%) in non-plate areas, whereas plate areas are not statistically significant. However, aluminum (%) of plate areas of fine fibres from both mechanical and chemical extraction methods and for mechanically extracted fine and chemically extracted coarse fibres are statistically significant. Aluminum (%) of non-plate areas and calcium (%) of plate

areas are not statistically significant. In contrast, calcium (%) of non-plate areas of fine fibres from mechanical and chemical extraction methods is statistically significant as well as fine and coarse fibres from the chemical extraction method.

Chapter 6 Sources of Variation on Mechanical Properties –

Results and Discussion

The variation in the mechanical properties of cattail fibres might have specific reasons. To establish possible causes, we investigated yield (%), moisture regain (%), diameter variation, breakage category, and location of fibre in the leaf. In this chapter, these possible sources of variation in mechanical properties have been reported, although there might be many other factors.

6.1 Yield (%) of growth stages

Yield (%) of fibre was calculated using Equation 2.1 and the result is presented in Table 6.1.

Table 6.1: Fibre yield (%) of different growth stages

Growth stage	Weight of plant (grams)	Weight of extracted fibre (grams)	Yield (%)
NF	35	2.61	7.46
F	35	2.87	8.2
LF	35	4.15	11.86
FM	35	3.46	9.89
M	35	10.12	28.91

The yield (%) was found highest at the mature stage (28.91%); whereas the lowest (7.46%) was found at the NF stage. It seems that the yield (%) of fibre increases with the plant maturity except for the LF stage (11.86%). Since the mature plants contain less water than the green plants, this could account for the relation between the plant growth stage and yield (%).

To determine the relationship between water content and yield (%), the cattail leaves and barks were oven-dried at 100°C to vaporize the constituent water. Using the oven dry

weight, water content (%) was calculated for five growth stages of cattail plant and results are visualized in Figure 6.1.

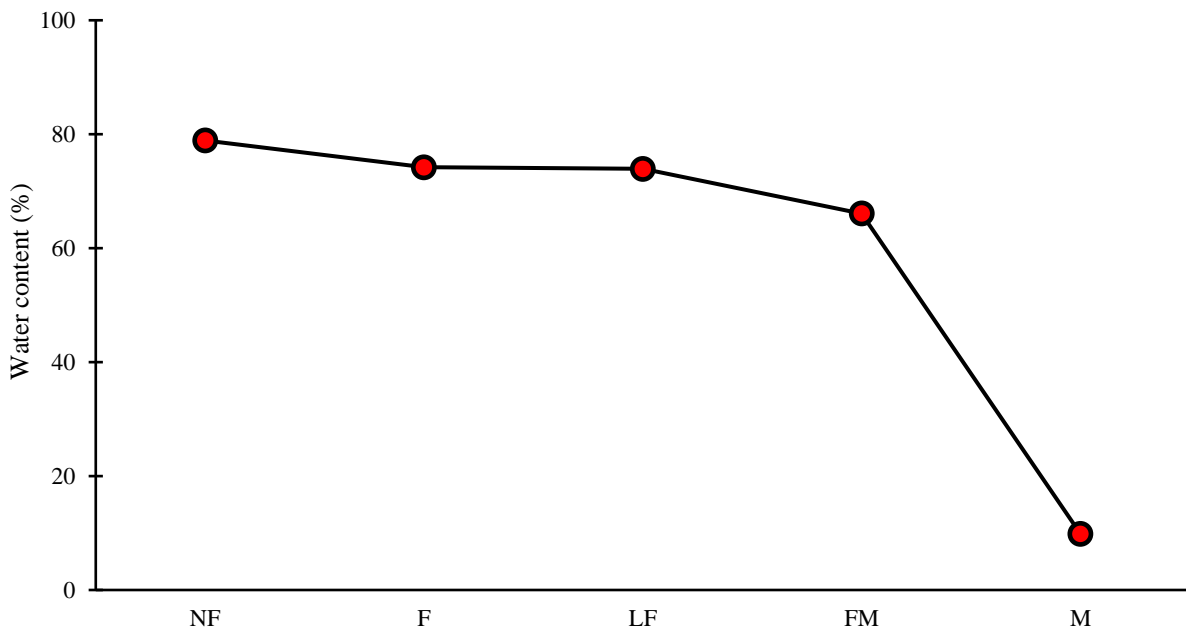


Figure 6.1: Water content (%) of cattail plant from 5 different growth stages

In Figure 6.1, an inversely proportional relationship was found with the maturity of cattail plant and water content (%) which is lowest at mature stage. The reduction of water content (%) indicates the decrease in leaf weight, having a positive impact on yield (%) (Table 6.1).

6.2 Moisture regain (%)

Moisture regain (%) was calculated by separating the fibres into two parts in each growth stage at 75.5% relative humidity (RH) as stated in chapter 2. The results of the moisture regain test of fibres from 5 growth stages are shown in Table 6.2.

Table 6.2: Moisture Regain (%) of different growth stages at 75.5% RH

Growth stage	Sample ID	Moisture regain (%)	Average moisture regain (%)	Time to obtain constant oven dry weight (hours)	Time to obtain constant weight in desiccator (hours)
NF	Sample 1	9.51	^a 9.58 [0.10]	96	120
	Sample 2	9.65			
F	Sample 1	8.66	8.83 [0.24]	96	120
	Sample 2	9.01			
LF	Sample 1	8.22	8.57 [0.39]	72	96
	Sample 2	8.92			
FM	Sample 1	8.77	^{ab} 8.87 [0.14]	72	96
	Sample 2	8.97			
M	Sample 1	9.63	^b 9.56 [0.09]	96	120
	Sample 2	9.5			

^{ab}: pairs with the same alphabets are statistically significant; Standard deviation is presented in square bracket; N=2

As shown in Table 6.2, the moisture regain (%) of 5 different growth stages was between 8.22% and 9.65%. The lowest moisture regain, 8.22% was found in the fibre from the LF stage (sample 1). However, the highest moisture regain is just 1.43% higher than the lowest one. Although the difference was small among the growth stages, the moisture regain of the NF and FM stages, and the FM and M stages are statistically significant. It seems that the fibre from LF and FM stages takes 24 hours less time to obtain a stable weight both in the oven and the desiccator than the other three growth stages.

Since moisture regain has a positive impact on natural fibre strength (Placet et al., 2012), it can be expected that the fibre tensile strength might be highest at the NF, would decrease with the maturity of cattail fibre until the LF stage, and would increase afterwards until the M stage.

6.3 Diameter variations and their effect on mechanical properties

Since it is a natural fibre, cattail has a wide range of diameters leading to a variety of tensile stresses. An inversely proportional relation was noticed between the diameter and tensile stress of the fibre (Figure 6.2). In addition, majority of fibres diameter was between 20 μm and 45 μm with a wide range of tensile stress (around 500 MPa to 3500 MPa). The fibres with diameter 70 μm or higher had tensile stress less than 1000MPa.

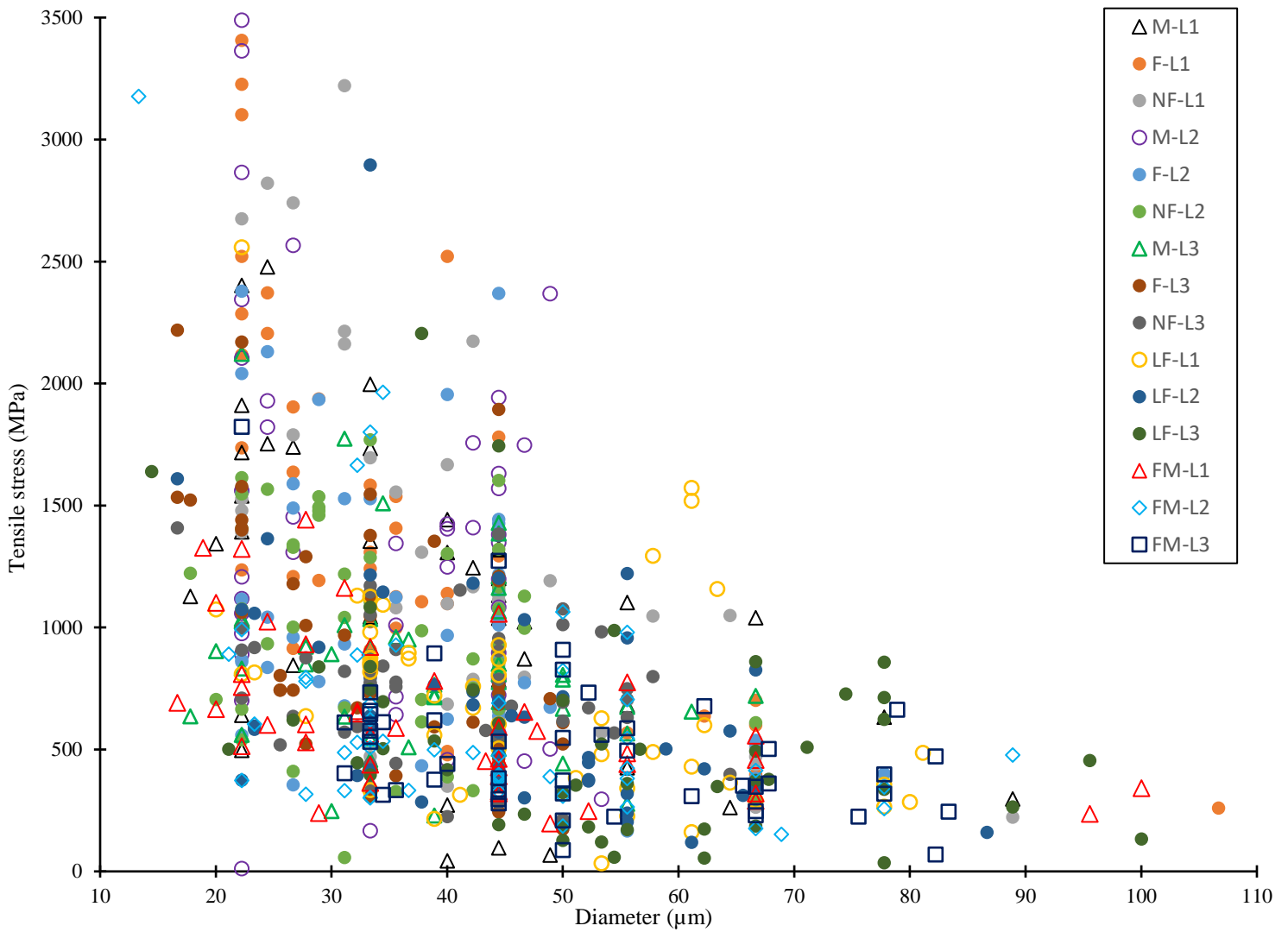


Figure 6.2: Relation between diameter and tensile stress

Figure 6.3 shows the relationship between the diameter of the cattail fibre and modulus. Numerous fibres with lower diameter (10μm to 45μm) have a wide range of modulus varying from 10 GPa to 200 GPa; whereas lower modulus was found in the fibres with higher diameter.

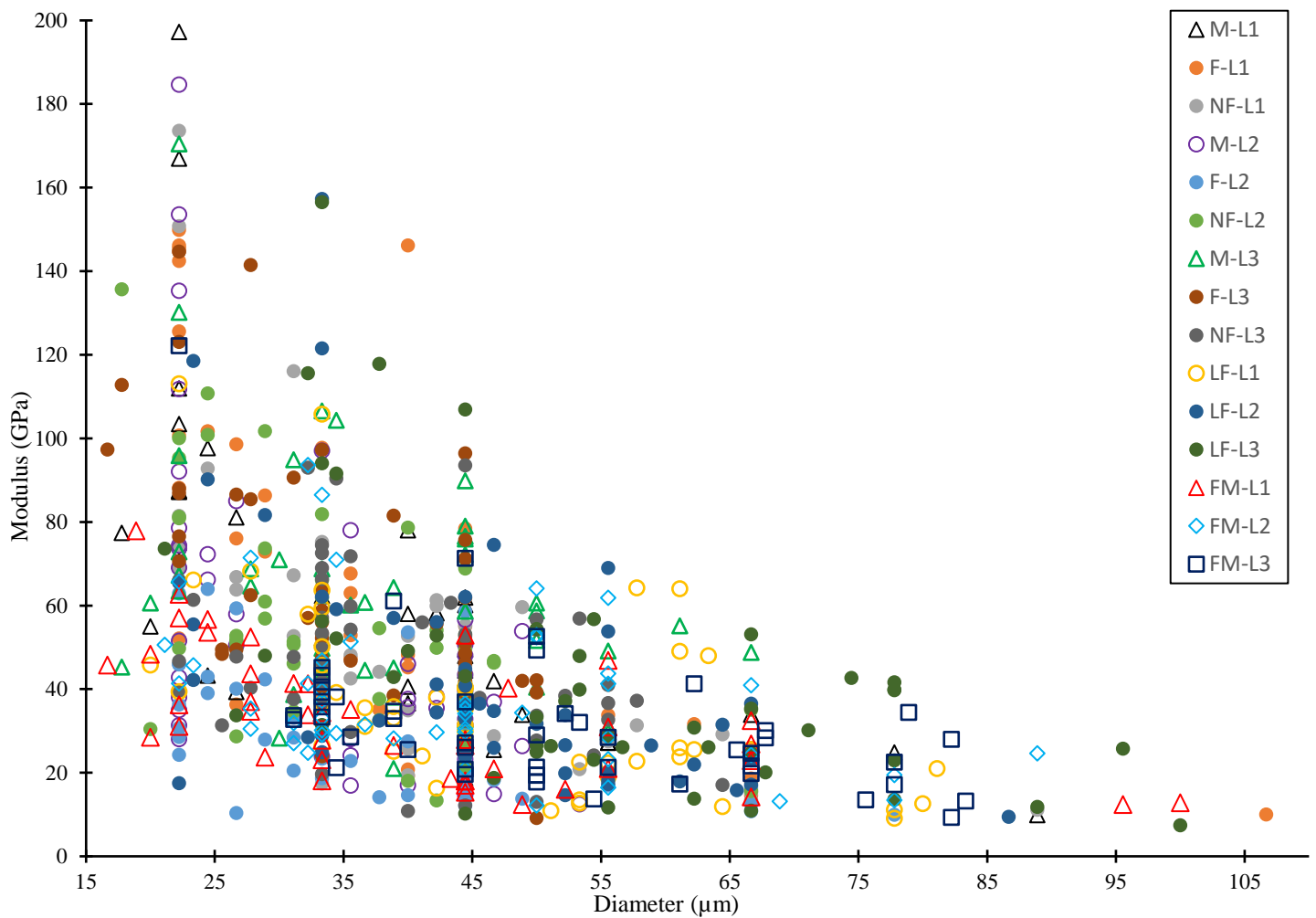


Figure 6.3: Relation between diameter and modulus

6.4 Fibre breakage point and causes of mechanical properties variations

6.4.1 Types of breakage

Fibres break into various forms during tensile testing depending on the fibre properties (W. E. Morton et al., 1996). After tensile testing, each fibre from each batch was examined using a microscope to identify the type of fibre breakage. Various kinds of fibre fractures were detected: granular failure, brittle fracture, tensile fatigue, independent fibrillar failure, ductile fracture, stake-and-socket break. Figure 6.4 depicts a few examples of distinct types of fibre breakage found during the tensile testing of cattail fibres.

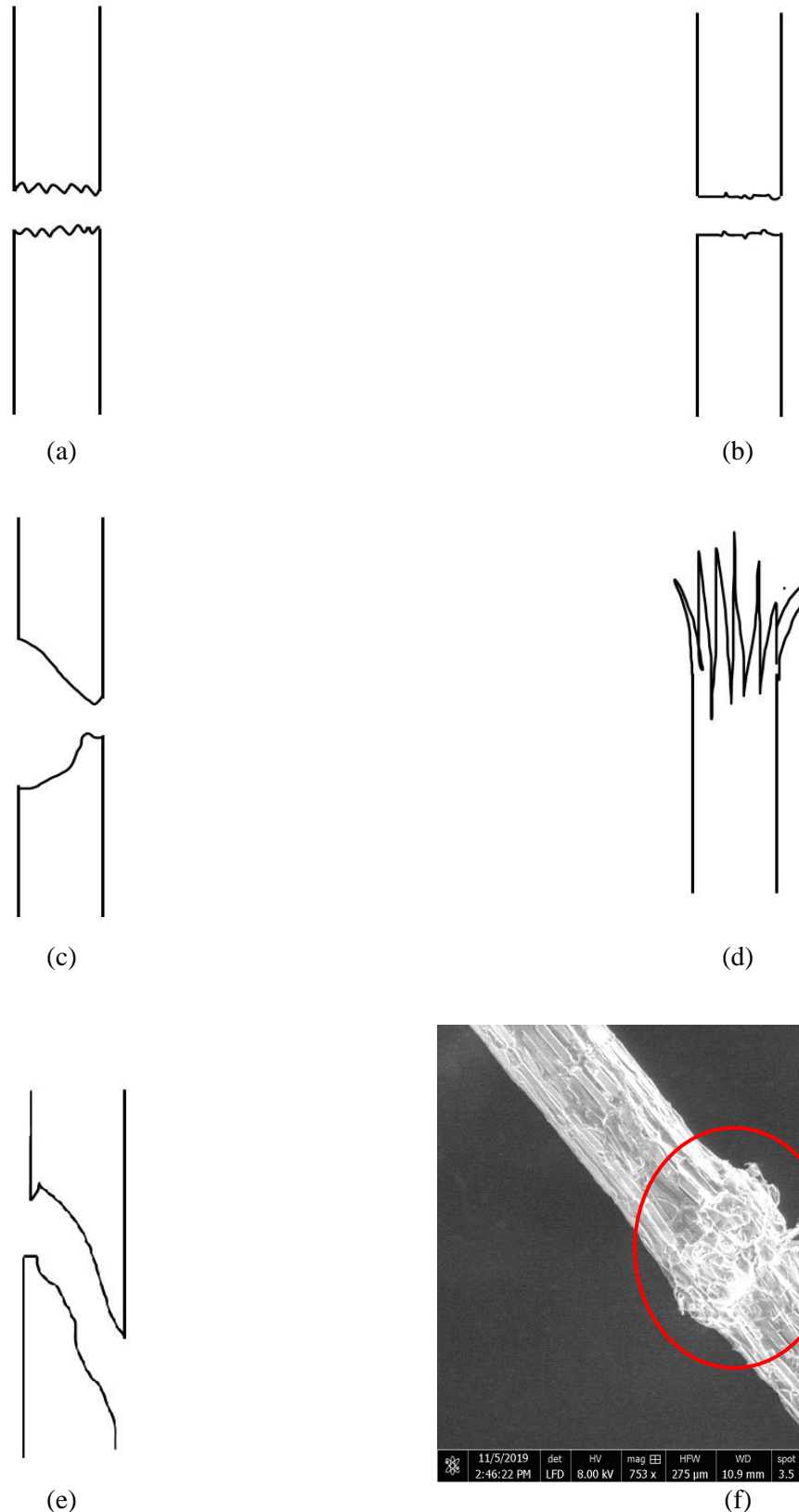


Figure 6.4: (a) Schematic diagram of granular failure; (b) Schematic diagram of brittle fracture; (c) Schematic diagram of ductile fracture; (d) Schematic diagram of fibrillar failure; (e) Schematic diagram of tensile fatigue (f) ESEM image of Node point on fibre

Table 6.3 summarizes breakage with breaking point on the fibre and types of breakage for all the 15 batches (5 growth stages \times 3 lengths). Most of the fibres (among 50 samples) were found to be broken at node point (Figure 6.4f). Chen & Luo (2021) suggested that nodes consist of sporadic fibres that affect the nature of fibre fracture due to the presence of two-way blend. In addition, a surprising number of fibres broke at the thick place; but less breakage at the thin place was observed. A few fibres broke close to the frame (Table 6.3)

Table 6.3: Fibre breaking point and types of breakage for different growth stage

ID	# of total sample	# of breaks at thin place	# of breaks at node point	# of breaks close to frame	# of breaks at thick place	Breakage type				
						Granular failure	Brittle fracture	Tensile fatigue	Fibrillar failure	*Others
NF-L1	50	8	13	3	26	30	4	8	7	1
NF-L2	50	6	23	9	12	29	5	6	6	4
NF-L3	50	6	29	6	9	17	11	12	9	1
F-L1	50	11	22	2	15	28	6	4	5	7
F-L2	50	9	32	2	7	28	6	6	6	4
F-L3	50	15	35	0	0	24	5	8	9	4
LF-L1	50	13	20	0	17	23	8	8	6	5
LF-L2	50	8	19	0	25	24	12	5	9	0
LF-L3	50	9	19	3	19	25	8	9	5	3
FM-L1	50	19	13	2	16	20	10	6	13	1
FM-L2	50	7	20	2	21	15	14	14	6	1
FM-L3	50	12	8	2	28	22	6	19	2	1
M-L1	50	10	31	6	3	22	15	5	4	4
M-L2	50	9	27	6	8	28	4	9	5	4
M-L3	50	5	35	2	8	21	7	6	13	3

*Others category of breakage includes ductile fracture, stake-and-socket break, and peeling and splitting

Granular failure was the most common type of fracture observed during the tensile testing of the fibre from five growth stages (Table 6.3). Brittle fracture, tensile fatigue, and fibrillar failures were also noticed.

6.4.2 Effect of breakage type on mechanical properties

According to the location of the breakage, mechanical properties of 15 batches (5 growth stages \times 3 lengths) are calculated separately into three groups: broken at the thin

places, did not break at the thin places, and broke near to the frame. The individual breakage results are given in Table 6.4.

Table 6.4: Mechanical properties of fibre at different breaking point

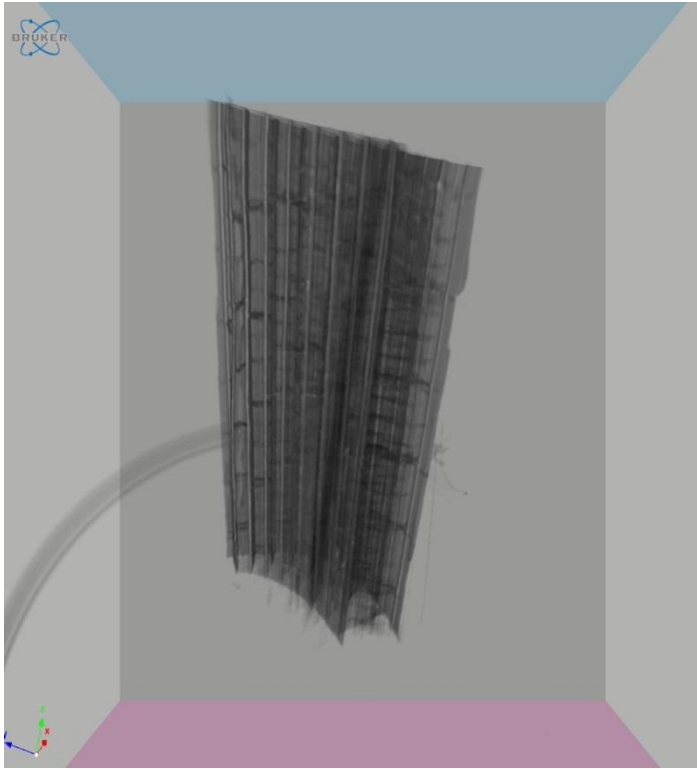
ID	Tensile stress (MPa)			Modulus (GPa)		
	At the thin place	Not at the thin place*	Near to the frame	At the thin place	Not at the thin place*	Near to the frame
NF-L1	1591 [819.9]	1128 [915.3]	1114 [938.9]	47.48 [50.22]	37.80 [32.23]	49.39 [20.44]
NF-L2	1311 [1194]	881.0 [377.6]	885.1 [565.1]	74.90 [63.07]	76.29 [54.77]	58.67 [34.74]
NF-L3	631.6 [298.1]	1141 [273.0]	712.7 [171.9]	51.55 [15.84]	40.33 [21.09]	48.68 [13.72]
F-L1	555.1 [796.9]	975.1 [4474]	283.0 [643.1]	33.66 [51.31]	53.02 [40.63]	50.44 [50.72]
F-L2	1064 [349.3]	1961 [565.4]	459.2 [415.7]	29.62 [7.990]	44.64 [16.20]	22.35 [7.690]
F-L3	1420 [367.6]	1099 [1064]	-	87.42 [22.88]	69.08 [63.69]	-
LF-L1	758.8 [667.3]	690.7 [369.4]	-	37.00 [29.98]	37.30 [19.45]	-
LF-L2	587.4 [166.4]	707.1 [474.1]	-	57.06 [12.70]	45.43 [31.70]	-
LF-L3	614.7 [298.7]	525.9 [415.1]	488.1 [298.7]	130.5 [255.7]	41.63 [28.01]	43.74 [18.38]
FM-L1	652.5 [356.4]	340.3 [304.7]	589.5 [13.72]	34.67 [18.89]	27.85 [14.02]	38.62 [1.600]
FM-L2	576.3 [221.8]	656.4 [558.5]	318.8 [62.10]	45.78 [13.37]	39.96 [24.17]	14.93 [1.490]
FM-L3	551.7 [480.6]	459.2 [243.1]	326.8 [0.000]	44.54 [33.10]	29.89 [13.45]	19.70 [0.000]
M-L1	834.2 [544.8]	731.7 [297.5]	1764 [880.9]	57.02 [50.99]	34.85 [113.1]	82.43 [32.12]
M-L2	3931 [1985]	1306 [1250]	1021 [1729]	111.4 [48.45]	36.31 [30.37]	35.70 [46.11]
M-L3	626.8 [495.8]	554.4 [894.5]	1377 [1051]	45.82 [21.22]	46.04 [60.01]	84.42 [64.68]

*Fibre broke either at the thick place or the other place except the thinnest place; standard deviation is resented in square bracket

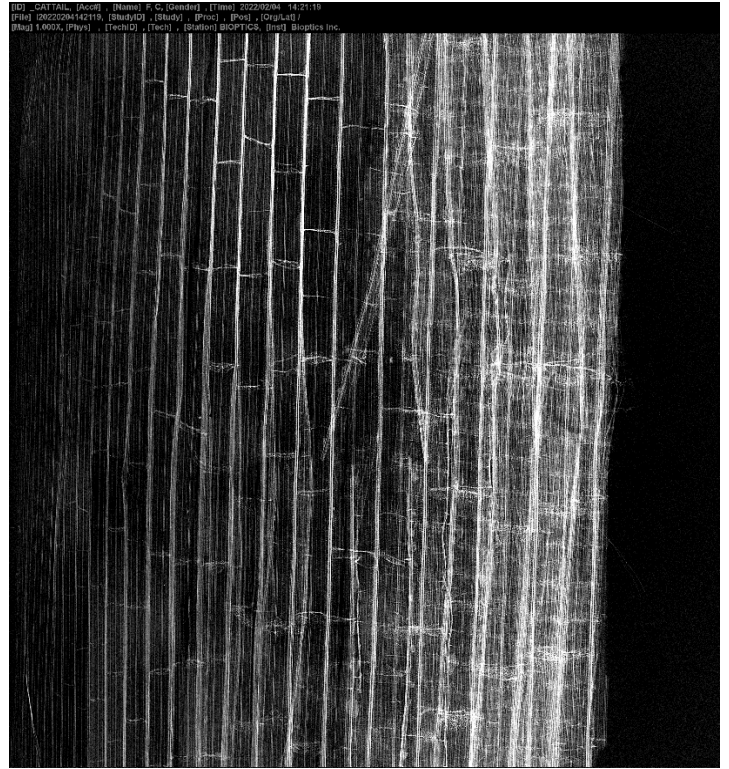
It can be noticed that the standard deviation and CV% have reduced in most of the cases after categorizing the mechanical properties data according to the breakage location. It is worth mentioning that the results of fibres that broke at the thin place are likely to be more accurate; since the diameter of the thin place was used in calculating the mechanical properties.

6.5 Fibre Location Effect

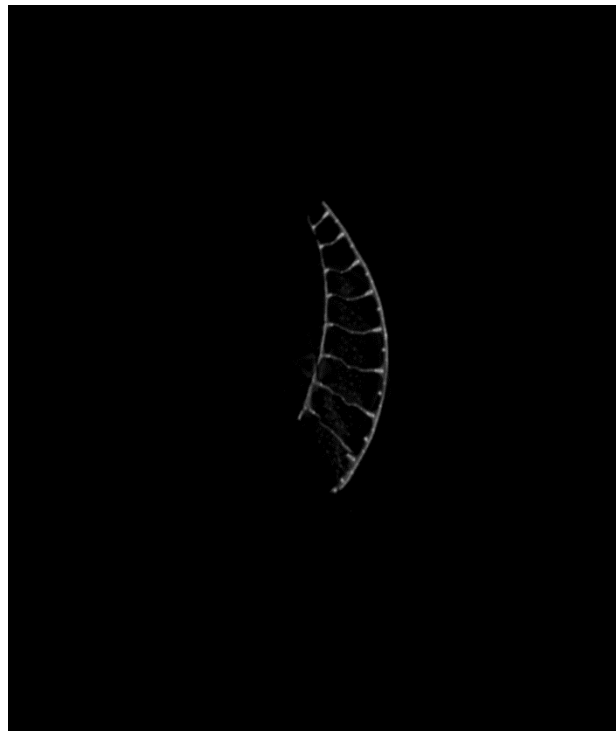
An X-Ray of the mature cattail leaf identifies the fibre locations and diameter (Figure 6.5). Three types of fibre (dorsal, ventral, and central fibre) of various diameters are present in a single leaf.



(a)



(b)



(c)

Figure 6.5: (a) Three-dimensional (3D) X-Ray image of cattail leaf; (b) X-Ray image of longitudinal section of cattail leaf; (c) X-Ray image of cross-section of cattail leaf

(Yu, 2021) mentioned that the dorsal (convex i.e., outer surface) and ventral surfaces (concave i.e., inner surface) of a cattail leaf contain fibres. However, after careful

observation, a third layer, the central surface was also found to contain fibre, as shown in Figure 5.7 in the previous chapter.

Further X-ray examinations of these three components of cattail leaf reveal the existence of fibre inside: dorsal (Figure 6.6a), ventral (Figure 6.6b) and central fibres (Figure 6.6c).

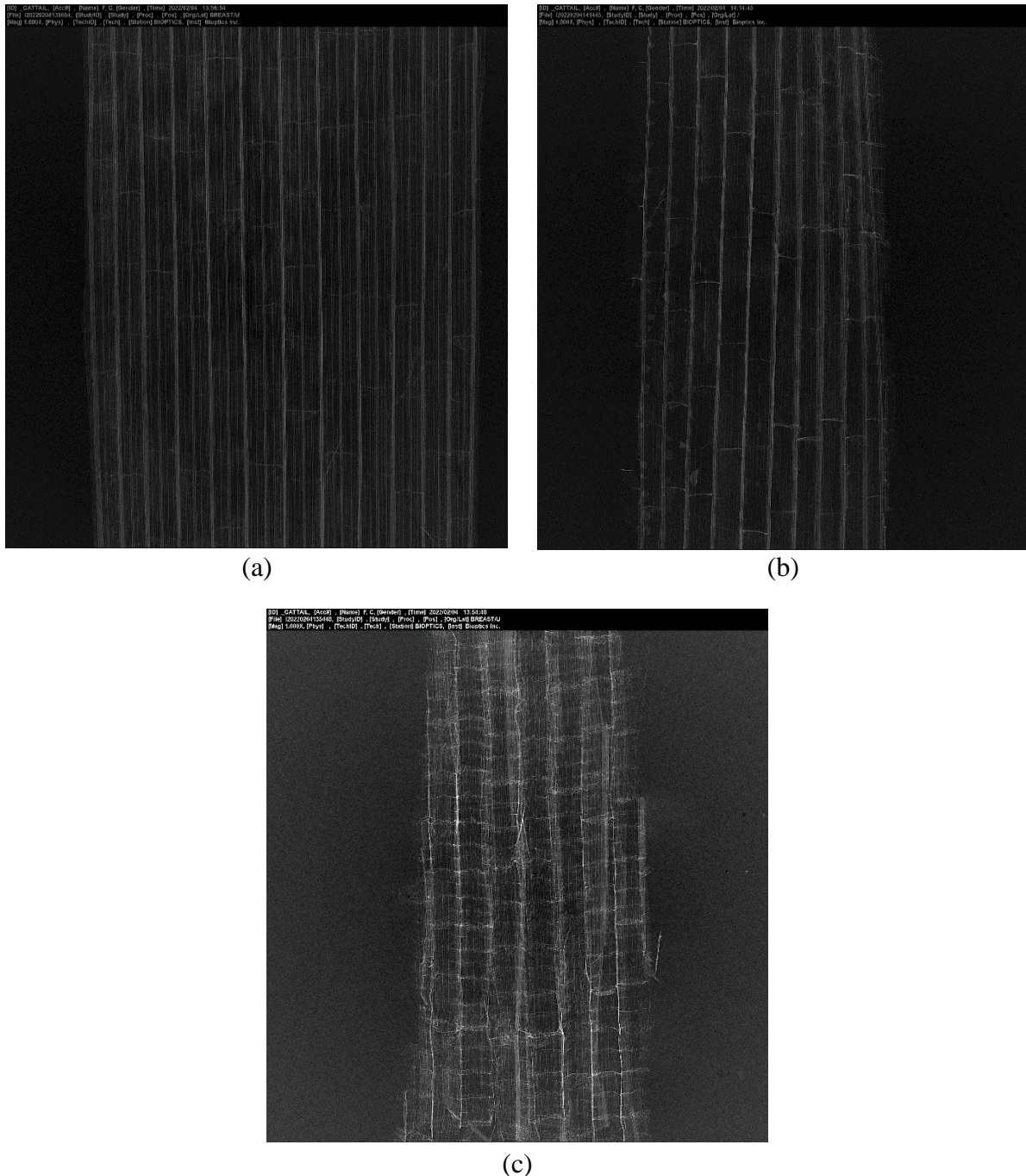


Figure 6.6: X-Ray image of (a) Dorsal fibre (b) Ventral fibre (c) Central fibre

Each of these cattail leaf components were mechanically separated into the three parts: dorsal, ventral, and central. If a chemical extraction method had been used on the whole leaf, the origin (location in leaf) of the fibres could not have been identified and separated. For this reason, a mechanical method was the best solution. After this mechanical separation, the fibres from the three parts were extracted individually by chemical means. However, separating the ventral part of cattail leaf was challenging due to the fibre tenderness, and extracting the central fine fibres was very difficult due to their low strength. In contrast, the fibres from the dorsal surface were easier to extract since they had higher strength.

The result of the mechanical properties of the fibres from the three locations is shown in Table 6.5.

Table 6.5: Mechanical properties of fibres from different locations

Location	Diameter (μm)	Tensile Stress (MPa)	Modulus (GPa)
Dorsal (N=36)	^a 47.7 [19.66]	^c 501.70 [331.56]	^e 38.70 [27.73]
Ventral (N=41)	^b 42.92 [11.02]	^d 512.58 [203.33]	^f 31.17 [15.53]
Central (N=27)	^{ab} 18.02 [3.71]	^{cd} 249.88 [136.52]	^{ef} 15.68 [10.55]

^{Abcdef}: pairs with the same alphabets are statistically significant; standard deviation is presented in square bracket

In Table 6.5, it can be noticed that the diameter, tensile stress and modulus of fibres from three different locations are identical (Figure 6.6). The average diameter of dorsal fibre was $47.71 \pm 19.66 \mu\text{m}$ (N = 36), which is the highest among the three fibre locations followed by the ventral fibre ($42.92 \pm 11.02 \mu\text{m}$, N=41) and the central fibres $18.02 \pm 3.71 \mu\text{m}$ (N= 27) as shown in Table 6.5.

The ventral fibres had the highest average of tensile stress ($512.58 \text{ MPa} \pm 203.33$, N = 41) followed by the fibres from dorsal part ($501.70 \text{ MPa} \pm 331.56$, N = 36). The lowest tensile stress was for the central fibres: 249.88 MPa with a standard deviation of 136.52 MPa (N = 27).

Dorsal fibres exhibited the highest Young's modulus with an average of $38.70 \text{ GPa} \pm 27.73$ ($N = 36$), followed by the ventral fibre ($31.17 \text{ GPa} \pm 15.53$, $N= 41$), and central fibres the lowest, at $15.68 \pm 10.55 \text{ GPa}$ ($N=27$).

The data of diameter, tensile stress and modulus of central fibres are statistically significant individually with the dorsal and ventral fibres. However, dorsal and ventral fibres have similar mechanical properties (Table 6.5).

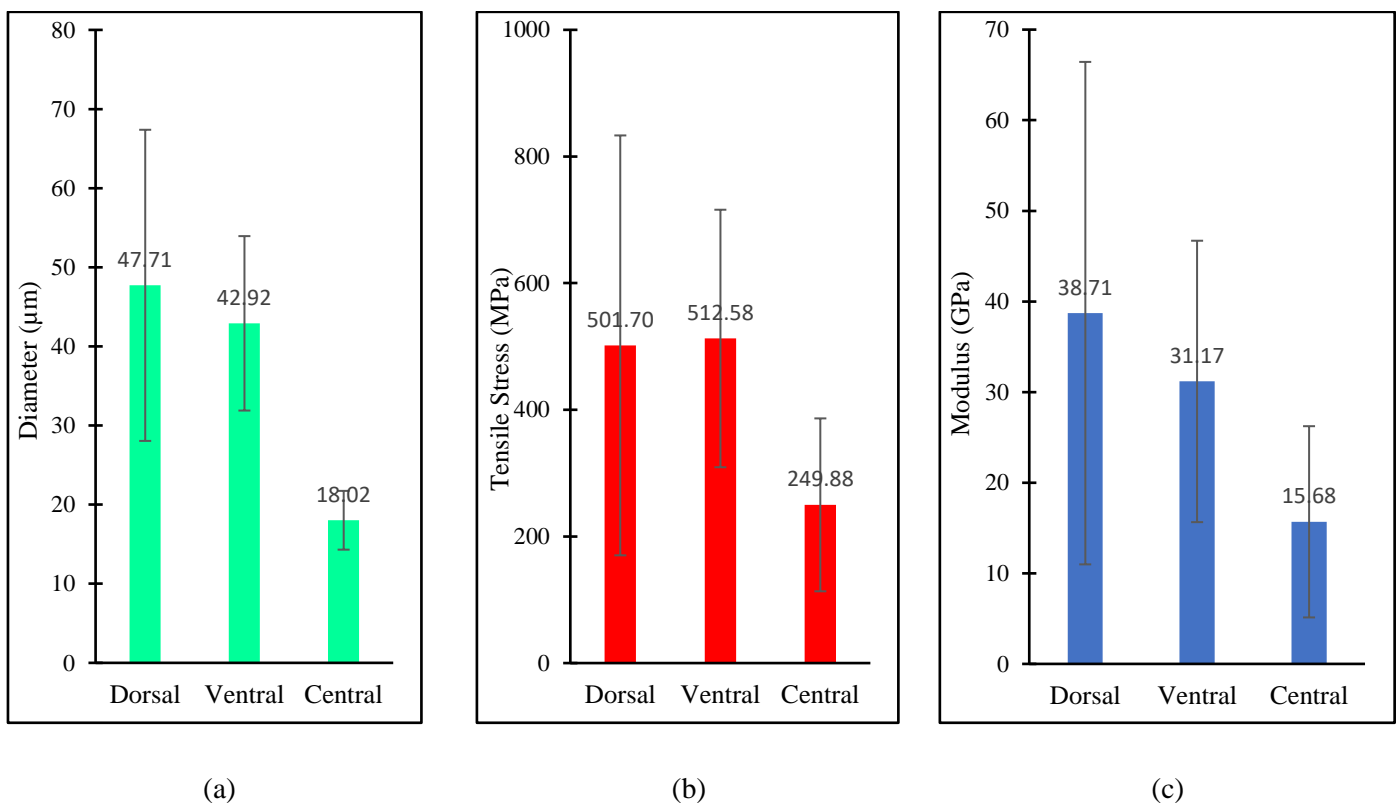


Figure 6.7: Variation of (a) Diameter; (b) Tensile stress; (c) Modulus of fibres from different locations

6.6 Effect of Outliers

Mechanical properties obtained from the 5 growth stages were found to be sporadic. The locations and variations in diameter (discussed in previous section) create numerous outliers in data sets and makes analysis difficult. Removal of the 10% percentile of the upper and lower values of each data set through quantile of Python programming language, gave a better interpretation of the results.

6.6.1 Effect of outliers on Tensile Stress

Figure 6.8(a) presents the average tensile stress with standard deviation of 15 batches (5 growth stages \times 3 lengths) of cattail fibre before removing the outliers; whereas Figure 6.8b shows the changes after removing outliers.

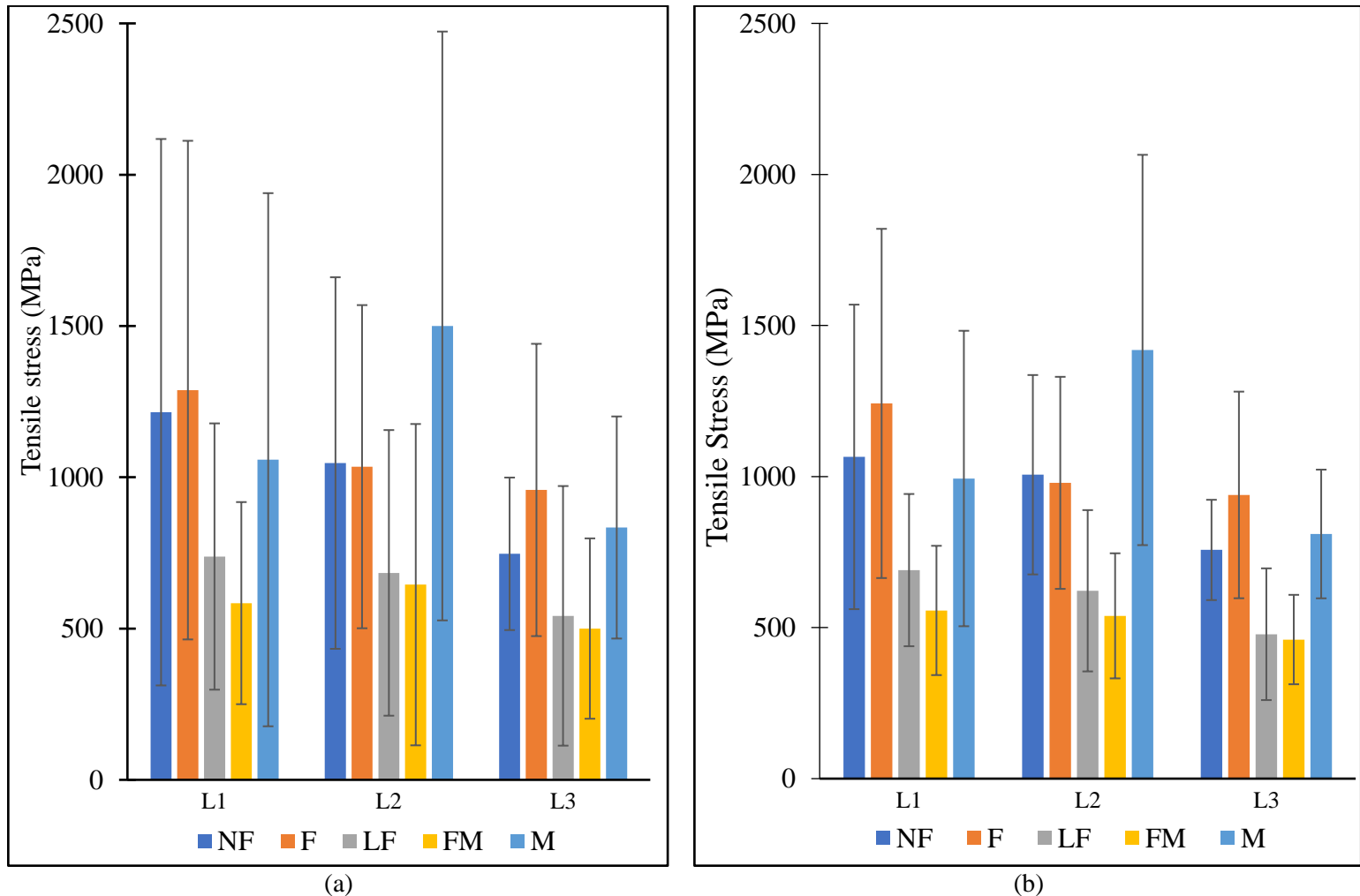


Figure 6.8: Average tensile stress (a) before removing outliers; (b) after removing outliers

It is clearly noticeable that a few batches have a high standard deviation before the removal of outliers. For example, NF-L1 (1215 MPa \pm 903 MPa), F-L1 (1288 MPa \pm 824 MPa), M-L1 (1058 MPa \pm 881 MPa), M-L2 (1500 MPa \pm 973), F-L3 (958 MPa \pm 483 MPa), M-L3 (834 MPa \pm 367 MPa), all have high standard deviations (Figure 6.8a). In contrast, the data sets were found to be more stable after removing the outliers. For example, the standard deviation of tensile stress was reduced to 504 MPa from 903 MPa for the NF-L1; and was as

low as 578 MPa from 824 MPa for the F-L1 which is an excellent improvement for this data set. In addition, for M-L1, standard deviation was lowered to 489 MPa from 881 MPa after removing the outliers. Moreover, the value was reduced to 646 MPa from 973 MPa for M-L2 and to 342 MPa from 483 MPa for F-L3 after removing outliers. Further, due to the removal of outliers, the standard deviation of M-L3 was reduced from 367 MPa to 213 MPa.

6.6.2 Effect of outliers on Modulus

Figure 6.9a presents the average Young's modulus with standard deviation of 15 batches (5 growth stages \times 3 lengths) of cattail fibre before removing the outliers; Figure 6.9b shows the changes after removing outliers.

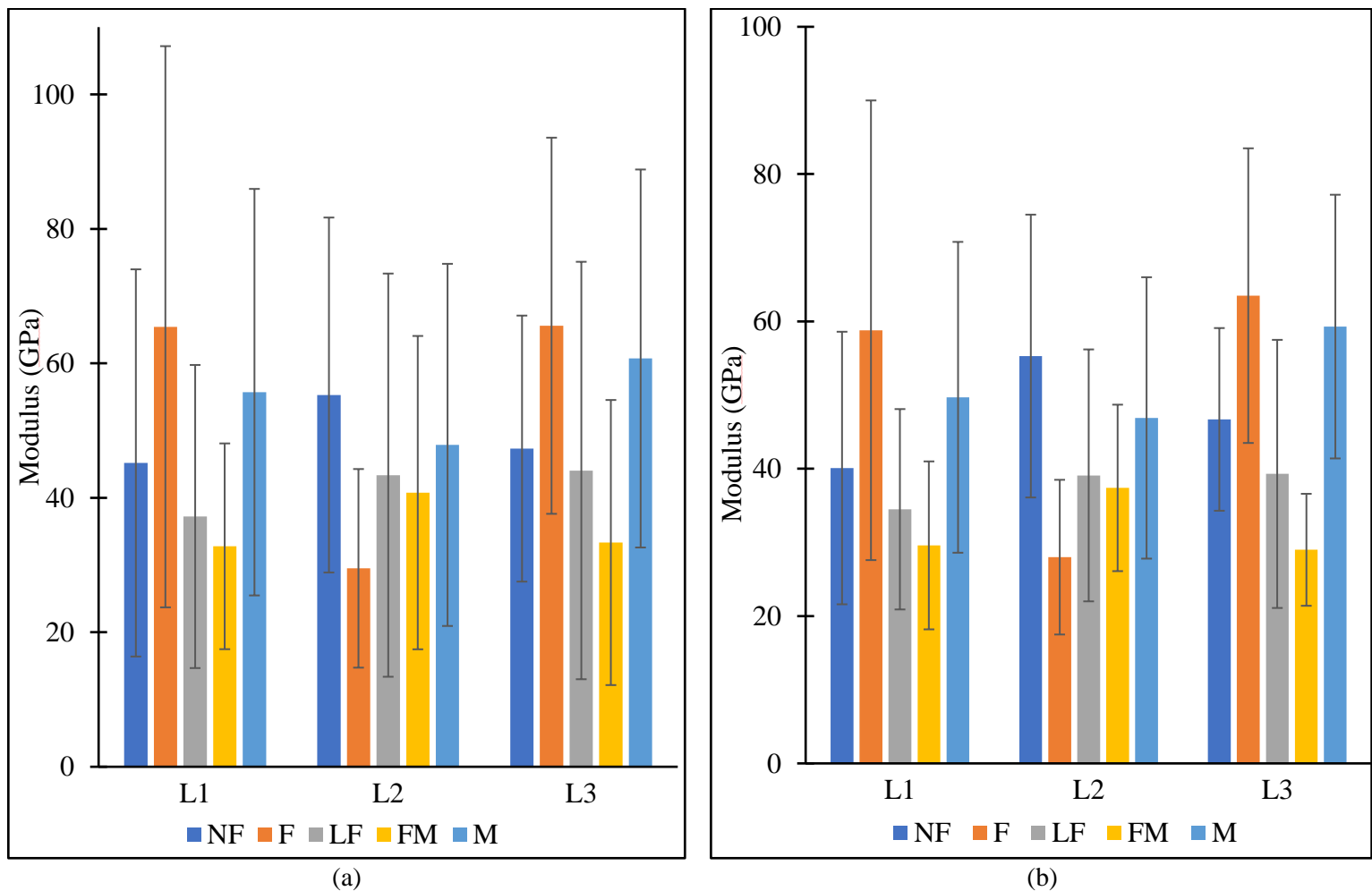


Figure 6.9: Average modulus (a) before removing outliers; (b) after removing outliers

In Figure 6.9a, excessive standard deviations of modulus were spotted for the specific batches F-L1 and LF-L3 before removing outliers. The average modulus of fibre from the F-L1 was 65.44 GPa \pm 41.73 GPa; and the value was 44.06 GPa \pm 31.04 GPa for LF-L3. On the other hand, after removing the outliers, the average modulus dropped to 58.80 GPa \pm 31.20 GPa and 39.3 GPa \pm 18.2 GPa for F-L1 and LF-L3, respectively. The effect of outlier removal was not limited to these two batches; it affected all the other batches to lower their standard deviation and CV (%).

The standard deviation of tensile stress and Young's modulus of a few batches dropped to the extent that the value was lower than the mean after removal of the outliers, giving excellent efficiency on the result and decision making.

6.6.3 Effect of outliers on Weibull Parameters

After removing the outliers from the raw data, the result of Weibull parameters are presented in Appendix A 46. The α value of tensile stress after removing outliers was higher than 2.0 in most cases which indicates the data are closer to one another than before (Appendix A 46) for both LR and MLE methods. In some cases, the value climbed to more than 4.0. In addition, the β values of the 15 batches were either lower than the β values before removing outliers, or equal for both LR and MLE methods which indicates less variability among the data. Moreover, the correlation (R^2_σ) values always fluctuate between 84% and 98% , which is almost similar to the values before removing outliers.

On the other hand, Weibull parameters of modulus (after removing outliers) are shown in Appendix A 47. In Appendix A 47, the α value of modulus is always more than 2.0, that indicating that the data got closer to one another after removing outliers. Sometimes the value jumped to over 4.0. Moreover, the β values were found to be mostly lower than the values before removing outliers. In addition, the correlation (R^2_σ) values are always more than 85%.

The Weibull parameters of tensile stress and modulus to interpret the data sets are more likely to be more suitable for composite application after removing outliers. Separating the three different layers could be a great solution for minimizing variation on the mechanical properties.

Chapter 7 Conclusions

In this study, cattail fibres of five different growth stages with three different lengths were used to determine suitability of cattail in composite applications. Mechanical properties, especially tensile stress, strain, and modulus of cattail fibres were measured to make decisions over the growth stage and length.

Two-parameter Weibull distribution was conducted on the mechanical properties of 15 batches (5 growth stages \times 3 lengths). The shape parameter of tensile stress and modulus were always greater than 1.0 for all the 15 batches. The values of shape parameters indicates the data are evenly and closely distributed. The lower scale parameter values compared to average experimental values were also identified for both tensile stress and modulus that show lower variability among the data.

Despite the data reliability obtained by Weibull distribution model, a decision on the ranking of growth stages or length could be made from the result. Therefore, a new method of ranking the cattail fibre properties from the five different growth stages with three different lengths was developed using a computer programming language that used the highest, average, and lowest values of flax fibre as threshold limits. Although the suitability of cattail fibres varied according to the limit values, L3 (3-inch) was ranked as the best among the three lengths, the F (flower) stage was the best among the five growth stages, F-L3 was the best among the 15 batches, and Y (modulus) was the best among the 7 parameter combinations. If lengthwise ranking is considered, the position was highest at L3 (3-inch), followed by L2 and L1. In addition, when growth stage-wise ranking was conducted, the F stage got the highest rank followed by the M stage, NF stage, FM stage, and LF stage. When growth stages and lengths are considered together, F-L3 was the highest-ranked fibres, followed by M-L3, NF-L2, F-L1 and so forth. Moreover, for parameter-wise ranking within themselves, modulus (Y) showed the highest ranking, which means the suitability of modulus

is the largest among the seven parameters combinations, followed by the tensile stress (S) and tensile strain (R).

The exact suitable batch might be selected based on the applications of the fibre. For example, if an application requires a high tensile stress the F-L1 batch can be used; whereas M-L2 might be the best choice when average stress is required and F-L2 where lower stress is required. However, if an application requires only high strain value, then fibres from LF-L3 batch can be used; whereas M-L2 can be used when average strain is required. In addition, any of NF-L3, F-L3, FM-L2, and FM-L3 might be used when an application requires lower strain. In contrast, if an application requires a high modulus, then the F-L1 batch can be used; whereas F-L3 and M-L3 can be used if an average or lower limit value of modulus is required. However, if any application needs average stress, strain, and modulus, F-L3 can be selected.

Surface structure characteristics by ESEM showed that the number of calcium oxalate plates decreased with the increase in the growth stages; however, no differences were found in the chemical compositions as revealed by EDS report. This indicates that the chemical makeup of fibres from all growth stages is similar. These findings will have an implication for wet processing of cattail fibres in that similar processing methods can be applied for fibres extracted from all growth stages.

Fibre diameter and extraction methods have an effect on the removal of calcium oxalate plates. While chemical extraction completely removed the plates from the fine fibres and partially from the coarse fibres, mechanical extraction did not remove any plates at all from the fine fibres. No plates from the coarse fibres could be removed by mechanical extraction method.

While the average plate count declines with the maturity of the cattail fibre, the average of 'more frequent size' lengths increased from the NF to FM stages, then slightly

decreased at the mature stage. In addition, the longitudinal distance between the plates increased with the growth of the cattail plant.

It was found that the location of fibre within a leaf has an impact on the fibre diameter and mechanical properties. The dorsal, central, and ventral fibres were separated. The dorsal and ventral fibres contained coarser fibres with high tensile stress, strain, and modulus, whereas the central fibres were finer with low tensile strain and modulus. When calculated separately, the standard deviation of these fibres was much lower than when the standard deviation for all fibres from the whole leaf was calculated.

A summary of the research outcomes is presented in Table 7.1.

Table 7.1: Summary table

Analysis	Analytical method	Outcomes	Value type	Major results obtained	Table / Figure #
Suitability Percentage	Python	(%) of Fibres fulfil the flax's threshold values	Absolute	Input data for ranking	Table 2.1
Ranking (growth stage wise)	Objective	1 to 5 ranking within the growth stages	Relative	F is the best growth stage	Figure 4.1 & Figure 4.2
Ranking (length wise)	Objective	1 to 3 ranking within the lengths	Relative	L3 is the best lengths	Table 4.4
Ranking (Combination of growth stages and lengths)	Python	1 to 15 ranking within groups: five growth stages and three lengths	Relative	F-L3 is the best batch	Figure 4.5
Ranking (parameter wise)	Objective	1 to 7 ranking within parameter combination	Relative	modulus is the best parameter	Figure 4.6
Image analysis	ESEM	Images of fibres surface with 500x magnification	Absolute	Decreasing the number of calcium oxalate plate with the maturity of plant	Table 5.1
Chemical Composition	EDS	Chemical composition of fibre	Absolute	Same chemical composition of five growth stages	Table 5.2

7.1 Limitations and Future Work

Since the breakage pattern of cattail fibre is uneven, the breakage point cannot be predicted before the tensile testing. For this reason, measured diameter might have errors that lead to the error in the mechanical properties. Moreover, the broken surface of fibre was not plane, so the cross-sectional area could not be measured accurately. A few researchers had measured the diameter after breakage using an electron microscope and software, but in this research, it could not be done. However, the objectives of this work were not to acquire any absolute values, rather a comparison of the fibre's mechanical properties among the phenological development stages of cattail plants.

On the other hand, the length of a cattail fibre used in this research was 1 to 3 inches (25.4 to 76.2mm); in contrast, the reference flax fibre length was 10 to 30mm (Yan et al., 2014). In addition, the diameter of cattail fibre was 30 to 180 μ m; whereas the flax fibre was 40 to 80 μ m (Li & Dai, 2006). For this reason, there might be a question of whether the values of these two fibres are comparable. Future work should be done to resolve these limitations.

The plants from different growth stages were collected randomly from the open field. The regrowth of cattail plants was not monitored and evaluated. Future work can be done on the regrowth pattern and time of cattail plants after harvesting in a controlled environment.

References

- Abdelbary, A., & Mohamed, Y. S. (2021). Tribological behavior of fiber-reinforced polymer composites. In *Tribology of polymer composites* (pp. 63–94). Elsevier.
- Akkol, E. K., Süntar, I., Keles, H., & Yesilada, E. (2011). The potential role of female flowers inflorescence of *Typha domingensis* Pers. in wound management. *Journal of Ethnopharmacology*, *133*(3), 1027–1032.
- Amaniampong, G., & Burgoyne, C. J. (1994). Statistical variability in the strength and failure strain of aramid and polyester yarns. *Journal of Materials Science*, *29*(19), 5141–5152.
- Ashik, K. P., & Sharma, R. S. (2015). A review on mechanical properties of natural fiber reinforced hybrid polymer composites. *Journal of Minerals and Materials Characterization and Engineering*, *3*(05), 420.
- Avril, C., Bailly, P. A., Njuguna, J., Nassiopoulos, E., & de Larminat, A. (2012). Development of flax-reinforced bio-composites for high-load bearing automotive parts. *Proceeding of European Conference on Composite Materials (ECCM), Venice, Italy*, 2428.
- Bajwa, D. S., Sitz, E. D., Bajwa, S. G., & Barnick, A. R. (2015). Evaluation of cattail (*Typha* spp.) for manufacturing composite panels. *Industrial Crops and Products*, *75*, 195–199.
- Barber, A., & Pellow, G. (2006). LCA: New Zealand merino wool total energy use. *5th Australian Life Cycle Assessment Society (ALCAS) Conference, Melbourne*, 22–24.
- Bergman, B. (1984). On the estimation of the Weibull modulus. *Journal of Materials Science Letters*, *3*(8), 689–692.
- Beule, J. D. (1979). Control and management of cattails in southeastern Wisconsin wetlands. *Wisconsin. Dept. of Natural Resources. Technical Bulletin (USA)*.

- Cao, S., Dong, T., Xu, G., & Wang, F. (2018). Cyclic filtration behavior of structured cattail fiber assembly for oils removal from wastewater. *Environmental Technology*, 39(14), 1833–1840.
- Chakma, K. (2018). *Extraction efficiency, quality and characterization of Typha latifolia L. fibres for textile applications*. University of Manitoba.
- Charlet, K., Jernot, J.-P., Gomina, M., Bizet, L., & Bréard, J. (2010). Mechanical properties of flax fibers and of the derived unidirectional composites. *Journal of Composite Materials*, 44(24), 2887–2896.
- Chen, G., & Luo, H. (2021). Asymmetric flexural process and fracture behaviors of natural bamboo node with gradient discontinuous fibers. *Composites Communications*, 24, 100647.
- Clegg, J. (1967). *observer's book of pond life*.
- Cotton Incorporated. (n.d.). *Cotton Fibre Development & Maturation*. Retrieved November 27, 2021, from <https://www.cottonworks.com/topics/sourcing-manufacturing/Fibre-science/cotton-Fibre-development-maturation/>
- Dalziel, J. M. (1937). The useful plants of west tropical Africa. *The Useful Plants of West Tropical Africa*.
- Dubbe, D. R., Garver, E. G., & Pratt, D. C. (1988). Production of cattail (*Typha* spp.) biomass in Minnesota, USA. *Biomass*, 17(2), 79–104.
- Grace, J. B., & Harrison, J. S. (1986). The biology of Canadian weeds.: 73. *Typha latifolia* L., *Typha angustifolia* L. and *Typha xglauca* Godr. *Canadian Journal of Plant Science*, 66(2), 361–379.
- Harris, W. (1999). The domestication of New Zealand plants. *New Zealand Plants and Their Story. Proceedings of a Conference Held in Wellington*, 1–3.

- Hasan, M. (2019). *Optimization of Typha fibre extraction and properties for composite applications using desirability function analysis*. University of Manitoba.
- Hasan, M., Rahman, M., Chen, Y., & Cicek, N. (2022). Optimization of Typha Fibre Extraction and Properties for Bio-Composite Applications Using Desirability Function Analysis. *Polymers*, *14*(9), 1685.
- Hernandez, A., Westerhuis, W., & van Dam, J. E. G. (2007). Microscopic study on hemp bast fibre formation. *Journal of Natural Fibers*, *3*(4), 1–12.
- Houlahan, J. E., Keddy, P. A., Makkay, K., & Findlay, C. S. (2006). The effects of adjacent land use on wetland species richness and community composition. *Wetlands*, *26*(1), 79–96.
- Hughes, M. (2012). Defects in natural fibres: their origin, characteristics and implications for natural fibre-reinforced composites. *Journal of Materials Science*, *47*(2), 599–609.
- Jiang, R. (2014). A drawback and an improvement of the classical Weibull probability plot. *Reliability Engineering & System Safety*, *126*, 135–142.
- Joshi, S. v, Drzal, L. T., Mohanty, A. K., & Arora, S. (2004). Are natural fiber composites environmentally superior to glass fiber reinforced composites? *Composites Part A: Applied Science and Manufacturing*, *35*(3), 371–376.
- Khan, M. R. I. (2016). *Evaluation of Brassica fibre for textile and spinning properties*. University of Manitoba.
- Koga, J., Rahman, M., & Mann, D. (2022). The effect of harvest time on cattail (*Typha latifolia* L.) fiber quality for nonwoven applications [Manuscript submitted for publication]. *Journal of Natural Fibre*. Biosystems Engineering. University of Manitoba
- Krus, M., Theuerkorn, W., Großkinsky, T., & Künzel, H. (2014). New sustainable and insulating building material made of cattail. *Full Papers NSB*, *156*, 1252–1260.

- Lafranche, E., Oliveira, V. M., Martins, C. I., & Krawczak, P. (2015). Prediction of injection-moulded flax fibre reinforced polypropylene tensile properties through a micro-morphology analysis. *Journal of Composite Materials*, 49(1), 113–128.
- Langlois, R. (1991). Estimation of Weibull parameters. *Journal of Materials Science Letters*, 10(18), 1049–1051.
- Lee, C. H., Khalina, A., Lee, S., & Liu, M. (2020). A comprehensive review on bast fibre retting process for optimal performance in fibre-reinforced polymer composites. *Advances in Materials Science and Engineering*, 2020.
- Li, Y., & Dai, D. X. Q. (2006). *Biomechanical engineering of textiles and clothing*. Woodhead Publishing.
- Linde, A. F., Janish, T., & Smith, D. (1976). Cattail [*Typha* spp.]-the significance of its growth, phenology and carbohydrate storage to its control and management. *Cattail [Typha Spp.]-the Significance of Its Growth, Phenology and Carbohydrate Storage to Its Control and Management.*, 94.
- Maiden, J. H. (1889). *The useful native plants of Australia:(including Tasmania)*. Turner and Henderson.
- Martin, N., Davies, P., & Baley, C. (2016). Evaluation of the potential of three non-woven flax fiber reinforcements: Spunlaced, needlepunched and paper process mats. *Industrial Crops and Products*, 83, 194–205.
- McLellan, J. D., & Moustafa, E. (2011). Management accounting practices in the gulf cooperative countries. *International Journal for Business, Accounting and Finance*, 6(1).
- Miao, M., & Finn, N. (2008). Conversion of natural fibres into structural composites. *Journal of Textile Engineering*, 54(6), 165–177.

- Mokshina, N., Chernova, T., Galinousky, D., Gorshkov, O., & Gorshkova, T. (2018). Key stages of fiber development as determinants of bast fiber yield and quality. *Fibers*, 6(2), 20.
- Monteiro, S. N., Lopes, F. P. D., & Ferreira, A. S. (2013). Weibull analysis for the diameter dependence of the elastic modulus of curaua fibers. *Matéria (Rio de Janeiro)*, 18, 46–54.
- Mortazavi, S. M., & Moghadam, M. K. (2009). Introduction of a new vegetable fiber for textile application. *Journal of Applied Polymer Science*, 113(5), 3307–3312.
- Morton, J. F. (1975). Cattails (*Typha* spp.)—weed problem or potential crop? *Economic Botany*, 29(1), 7–29.
- Morton, W. E., Hearle, J. W. S., & Gupta, V. B. (1996). Physical properties of textile fibres. *INDIAN JOURNAL OF FIBRE AND TEXTILE RESEARCH*, 21, 233.
- Naik, D. L., & Fronk, T. H. (2016). Weibull distribution analysis of the tensile strength of the kenaf bast fiber. *Fibers and Polymers*, 17(10), 1696–1701.
- Nair, G. R., Rho, D., Yaylayan, V., & Raghavan, V. (2013). Microwave assisted retting—A novel method of processing of flax stems. *Biosystems Engineering*, 116(4), 427–435.
- Othman, M., Ruzaidi, G., Khalisanni, K., & Nazarudin, Z. (2012). Morphology and water absorption analysis on single fibre and leaf of *Typha latifolia*. *Advanced Materials Research*, 576, 492–495.
- Pan, N., Chen, H. C., Thompson, J., Inglesby, M. K., Khatua, S., Zhang, X. S., & Zeronian, S. H. (1997). The size effects on the mechanical behaviour of fibres. *Journal of Materials Science*, 32(10), 2677–2685.
- Pandey, R. (2016). Fiber extraction from dual-purpose flax. *Journal of Natural Fibers*, 13(5), 565–577.

- Pickering, K. L., Efendy, M. G. A., & Le, T. M. (2016). A review of recent developments in natural fibre composites and their mechanical performance. *Composites Part A: Applied Science and Manufacturing*, 83, 98–112.
- Pickering, K. L., & Murray, T. L. (1999). Weak link scaling analysis of high-strength carbon fibre. *Composites Part A: Applied Science and Manufacturing*, 30(8), 1017–1021.
- Placet, V., Cisse, O., & Boubakar, M. L. (2012). Influence of environmental relative humidity on the tensile and rotational behaviour of hemp fibres. *Journal of Materials Science*, 47(7), 3435–3446.
- Preisner, M., Kulma, A., Zebrowski, J., Dymińska, L., Hanuza, J., Arendt, M., Starzycki, M., & Szopa, J. (2014). Manipulating cinnamyl alcohol dehydrogenase (CAD) expression in flax affects fibre composition and properties. *BMC Plant Biology*, 14(1), 1–18.
- Quinn, J. B., & Quinn, G. D. (2010). A practical and systematic review of Weibull statistics for reporting strengths of dental materials. *Dental Materials*, 26(2), 135–147.
- Rahman, M., Cicek, N., & Chakma, K. (2021). The optimum parameters for fibre yield (%) and characterization of *Typha latifolia* L. fibres for textile applications. *Fibers and Polymers*, 22(6), 1543–1555.
- Ramaswamy, G. N., Ruff, C. G., & Boyd, C. R. (1994). Effect of bacterial and chemical retting on kenaf fiber quality. *Textile Research Journal*, 64(5), 305–308.
- Reddit. (2018, February 28). *What is the difference between linear regression computed simply in an application like Excel, and linear regression created in a programming environment such as python with machine learning?* .
https://www.reddit.com/r/datascience/comments/80yw17/what_is_the_difference_between_linear_regression/
- Sadrmanesh, V., & Chen, Y. (2019). Bast fibres: structure, processing, properties, and applications. *International Materials Reviews*, 64(7), 381–406.

- Sana, R., Mounir, J., & Slah, M. (2014). Study of structure and properties of Tunisian Typha leaf fibers. *International Journal of Engineering Research & Technology (IJERT)*, 3.
- Shadhin, M. (2021). *Comparative evaluation of flax, cattail, and hemp fiber composites*. University of Manitoba.
- Shadhin, M., Mann, D., & Rahman, M. (2022). Probabilistic model for cattail and canola fibers: Effect of environmental conditions, structural parameters, fiber length, and estimators. *Textile Research Journal*, 00405175221086891.
- Shadhin, M., Rahman, M., Jayaraman, R., & Mann, D. (2021). Novel cattail fiber composites: converting waste biomass into reinforcement for composites. *Bioresources and Bioprocessing*, 8(1), 1–12.
- Shioya, M., & Kikutani, T. (2015). Synthetic textile fibres: non-polymer fibres. In *Textiles and Fashion* (pp. 139–155). Elsevier.
- Sobrero, M. T., Sabbatini, M. R., & Fernandez, O. A. (1997). Phenology and biomass dynamics of cattail (*Typha subulata*) in southern Argentina. *Weed Science*, 45(3), 419–422.
- Stacey, A. G. (2020). Robust parameterisation of ages of references in published research. *Journal of Informetrics*, 14(3), 101048.
- Steen, M., Sinnema, S., & Bressers, J. (1992). Statistical analysis of bend strength data according to different evaluation methods. *Journal of the European Ceramic Society*, 9(6), 437–445.
- Stuckey, R. L., & Salamon, D. P. (1987). Typha-Angustifolia in North-America-a foreigner masquerading as a native. *Ohio Journal of Science*, 87(2), 4.
- Sullivan, J. D., & Lauzon, P. H. (1986). Experimental probability estimators for Weibull plots. *Journal of Materials Science Letters*, 5(12), 1245–1247.

- Thiripura Sundari, M., & Ramesh, A. (2012). Catalysis of cellulose-New perspectives in preparation of biogenic material. *Recent Patents on Catalysis (Discontinued)*, 1(1), 85–92.
- Timmons, F. L., Bruns, V. F., Lee, W. O., Yeo, R. R., Hodgson, J. M., Weldon, L. W., & Comes, R. D. (1963). *Studies on the control of common cattail in drainage channels and ditches*.
- Trustum, K., & Jayatilaka, A. D. S. (1979). On estimating the Weibull modulus for a brittle material. *Journal of Materials Science*, 14(5), 1080–1084.
- Vetayasuporn, S. (2007). Using cattails (*Typha latifolia*) as a substrate for *Pleurotus ostreatus* (Fr.) Kummer cultivation. *J Biol Sci*, 7, 218–221.
- Wambua, P., Ivens, J., & Verpoest, I. (2003). Natural fibres: can they replace glass in fibre reinforced plastics? *Composites Science and Technology*, 63(9), 1259–1264.
- Witztum, A., & Wayne, R. (2014). Fibre cables in the lacunae of *Typha* leaves contribute to a tensegrity structure. *Annals of Botany*, 113(5), 789–797.
- Wuzella, G., Mahendran, A. R., Bätge, T., Jury, S., & Kandelbauer, A. (2011). Novel, binder-free fiber reinforced composites based on a renewable resource from the reed-like plant *Typha* sp. *Industrial Crops and Products*, 33(3), 683–689.
- Yan, L., Chou, N., & Jayaraman, K. (2014). Flax fibre and its composites—A review. *Composites Part B: Engineering*, 56, 296–317.
- Yu, C. H. (2021). *A study on the extraction methods and characterizations of Typha leaf fibers*. University of Manitoba.
- Yukseloglu, S. M., & Yoney, H. (2016). The mechanical properties of flax fibre reinforced composites. In *Natural Fibres: Advances in Science and Technology Towards Industrial Applications* (pp. 255–266). Springer.

Zafeiropoulos, N. E., & Baillie, C. A. (2007). A study of the effect of surface treatments on the tensile strength of flax fibres: Part II. Application of Weibull statistics. *Composites Part A: Applied Science and Manufacturing*, 38(2), 629–638.

Zhang, Y., Wang, X., Pan, N., & Postle, R. (2002). Weibull analysis of the tensile behavior of fibers with geometrical irregularities. *Journal of Materials Science*, 37(7), 1401–1406.

Zok, F. W. (2017). On weakest link theory and Weibull statistics. *Journal of the American Ceramic Society*, 100(4), 1265–1268.

Appendix

Appendix A 1: Raw data of NF-L1

ID	Tensile stress at Break (Standard)	Tensile strain at Break (Standard)	Modulus (Automatic Young's)
L1-NF1	701.35559	0.0433	27.49356
L1-NF2	1,528.21	0.03215	69.00737
L1-NF3	1,191.44	0.03742	59.64576
L1-NF4	2,674.60	0.04109	81.46809
L1-NF5	1,696.00	0.03739	75.21164
L1-NF6	1,667.15	0.04987	52.75351
L1-NF7	1,080.27	0.03604	42.52317
L1-NF8	1,098.56	0.03612	55.21979
L1-NF9	891.77	0.03783	35.34378
L1-NF10	786.93	0.03543	34.47791
L1-NF11	1,390.36	0.03442	150.7713
L1-NF12	469.95	0.03896	15.66593
L1-NF13	1,789.65	0.04017	66.82628
L1-NF14	684.92	0.03823	25.69145
L1-NF15	1,479.63	0.03288	74.45277
L1-NF16	1,112.65	0.04015	46.14637
L1-NF17	570.33	0.03807	20.82192
L1-NF18	438.10803	0.03969	15.2312
L1-NF19	2,173.65	0.04853	61.29961
L1-NF20	145.86	0.046	
L1-NF21	607.68	0.04073	18.08613
L1-NF22	4,692.60	0.04276	173.59878
L1-NF23	3,221.05	0.0383	116.08633
L1-NF24	471.13	0.02933	17.42511
L1-NF25	1,049.19	0.04793	29.19066
L1-NF26	349.32608	0.01983	19.36928
L1-NF27	2,821.02	0.04136	92.80516
L1-NF28	1,166.95	0.03469	59.91311
L1-NF29	1,033.17	0.03954	45.65469
L1-NF30	1,097.47	0.03894	34.93815
L1-NF31	417.32	0.0228	31.33864
L1-NF32	2,740.34	0.04382	63.84611
L1-NF33	843.39	0.04007	29.1835
L1-NF34	159.44	0.0378	6.63945
L1-NF35	2,162.56	0.04545	67.26477
L1-NF36	1,308.74	0.04479	44.12478
L1-NF37	913.42	0.04274	22.35462
L1-NF38	796.36	0.04007	28.73849
L1-NF39	819.93	0.03285	36.14753
L1-NF40	1,131.08	0.04195	
L1-NF41	222.12	0.03314	11.13588
L1-NF42	1,046.93	0.04321	31.3441
L1-NF43	934.52	0.03449	16.12543
L1-NF44	1,148.02	0.04137	32.87825
L1-NF45	157.58	0.03931	6.91647
L1-NF46	163.55379	0.04382	6.163
L1-NF47	2,214.34	0.04498	52.68458
L1-NF48	263.52158	0.02878	16.21777
L1-NF49	1,555.49	0.04947	48.11519
L1-NF50	508.56	0.04386	13.48626

Appendix A 2: Raw data of NF-L2

ID	Tensile stress at Break (Standard)	Tensile strain at Break (Standard)	Modulus (Automatic Young's)
L2-NF1	933.84	0.03328	110.75147
L2-NF2	292.53	0.02592	15.63786
L2-NF3	1,535.69	0.02689	73.70385
L2-NF4	613.25	0.03048	32.57665
L2-NF5	855.05	0.0269	37.4397
L2-NF6	1,076.24	0.02552	49.77656
L2-NF7	1,222.18	0.03126	135.67469
L2-NF8	1,566.67	0.02594	100.84843
L2-NF9	1,602.38	0.03535	68.87384
L2-NF10	870.95	0.02294	49.91439
L2-NF11	410.10	0.02675	28.6753
L2-NF12	664.97	0.02981	95.26546
L2-NF13	996.77	0.03074	46.72113
L2-NF14	1,076.93	0.03532	43.81682
L2-NF15	1,287.13	0.02771	66.08361
L2-NF16	1,405.49	0.02799	65.81622
L2-NF17	986.89	0.02762	54.5582
L2-NF18	327.21	0.00922	354.71011
L2-NF19	665.55	0.02957	26.55386
L2-NF20	751.43	0.02816	54.11045
L2-NF21	4,169.29	0.03059	206.51078
L2-NF22	1,768.67	0.04195	61.87429
L2-NF23	1,128.00	0.03481	46.30747
L2-NF24	1,328.92	0.02909	52.73949
L2-NF25	704.38	0.02398	37.61579
L2-NF26	331.15	0.0291	13.38847
L2-NF27	432.57	0.02405	21.31635
L2-NF28	388.09	0.0267	18.0493
L2-NF29	1,320.65	0.03471	49.52977
L2-NF30	924.45	0.03176	36.36679
L2-NF31	1,613.60	0.02526	80.86572
L2-NF32	57.10	0.05868	34.62632
L2-NF33	1,477.56	0.02498	101.70499
L2-NF34	1,040.89	0.02729	51.38845
L2-NF35	1,302.48	0.02701	78.62123
L2-NF36	608.97	0.02889	35.03435
L2-NF37	1,165.68	0.02945	53.03432
L2-NF38	442.83	0.02535	28.67969
L2-NF39	539.24	0.02501	81.26535
L2-NF40	1,460.30	0.03627	56.87197
L2-NF41	1,492.66	0.03995	60.9206
L2-NF42	705.10	0.02889	30.45978
L2-NF43	1,338.79	0.03163	51.79801
L2-NF44	671.10	0.02767	46.10585
L2-NF45	1,103.87	0.02512	81.85758
L2-NF46	1,001.65	0.02528	50.80585
L2-NF47	1,085.76	0.03707	43.23507
L2-NF48	1,219.31	0.03099	50.69127
L2-NF49	1,547.30	0.02608	100.02323
L2-NF50	828.25	0.0256	41.83808

Appendix A 3: Raw data of NF-L3

ID	Tensile stress at Break (Standard)	Tensile strain at Break (Standard)	Modulus (Automatic Young's)
L3-NF1	875.75	0.0249	40.32841
L3-NF2	917.92	0.01585	61.39535
L3-NF3	635.54	0.01505	47.80668
L3-NF4	798.77	0.02977	37.23348
L3-NF5	1,052.62	0.02246	53.41651
L3-NF6	518.44	0.01644	31.35073
L3-NF7	820.52	0.02042	47.72032
L3-NF8	710.04	0.01862	46.65469
L3-NF9	590.03	0.01974	36.38003
L3-NF10	224.43	0.0241	10.88324
L3-NF11	594.21	0.02108	93.00891
L3-NF12	1,075.93	0.0276	54.22445
L3-NF13	747.53	0.01872	72.5902
L3-NF14	756.67	0.01847	54.22671
L3-NF15	631.24	0.02506	36.63948
L3-NF16	775.83	0.02292	59.85234
L3-NF17	212.79	0.02034	13.0493
L3-NF18	443.61	0.01981	29.74246
L3-NF19	773.22	0.01901	57.12013
L3-NF20	1,382.60	0.02311	93.55462
L3-NF21	767.77	0.02472	46.49347
L3-NF22	571.50	0.02085	37.63268
L3-NF23	787.28	0.0293	35.55368
L3-NF24	551.72	0.02648	32.4204
L3-NF25	693.75	0.02633	33.66793
L3-NF26	907.03	0.01483	66.01288
L3-NF27	615.95	0.02971	27.71859
L3-NF28	705.84	0.02616	32.68984
L3-NF29	1,011.24	0.0248	56.67702
L3-NF30	795.78	0.02661	49.68232
L3-NF31	1,171.02	0.03145	69.00292
L3-NF32	397.92	0.03008	17.08337
L3-NF33	954.95	0.02779	53.133
L3-NF34	982.54	0.02492	56.85404
L3-NF35	282.12	0.0261	12.19159
L3-NF36	438.34	0.02586	19.65999
L3-NF37	677.79	0.02528	37.94803
L3-NF38	578.26	0.01736	60.67529
L3-NF39	567.43	0.03073	24.11393
L3-NF40	670.21	0.02502	38.40873
L3-NF41	841.40	0.02712	90.39904
L3-NF42	996.34	0.02755	39.60835
L3-NF43	1,152.92	0.03298	55.99997
L3-NF44	748.62	0.02509	41.03524
L3-NF45	345.43	0.00991	41.6974
L3-NF46	903.78	0.02981	52.63672
L3-NF47	885.18	0.02069	74.42097
L3-NF48	909.95	0.01884	71.82126
L3-NF49	1,145.10	0.02735	66.35551
L3-NF50	1,407.83	0.01904	

Appendix A 4: Raw data of F-L1

ID	Tensile stress at Break (Standard)	Tensile strain at Break (Standard)	Modulus (Automatic Young's)
L1-F1	396.43042	0.03301	17.91071
L1-F2	1,293.34	0.03782	55.1025
L1-F3	599.60315	0.03692	18.61845
L1-F4	2,285.00	0.03871	125.58492
L1-F5	1,097.36	0.03762	45.20515
L1-F6	1,536.54	0.0354	62.99556
L1-F7	1,406.77	0.03671	52.92793
L1-F8	701.02533	0.04495	25.96463
L1-F9	1,139.96	0.03495	48.18535
L1-F10	1,023.09	0.03125	62.94116
L1-F11	3,226.59	0.03306	145.48913
L1-F12	2,117.69	0.02952	144.66486
L1-F13	1,780.89	0.03505	78.45051
L1-F14	2,521.44	0.02795	146.15004
L1-F15	2,521.44	0.02795	146.15004
L1-F16	1,937.18	0.03935	72.89147
L1-F17	1,208.73	0.03412	
L1-F18	76.59165	0.03654	3.02512
L1-F19	1,583.78	0.04639	43.71262
L1-F20	3,102.10	0.03591	149.87429
L1-F21	2,205.39	0.03157	101.63538
L1-F22	440.60492	0.0271	34.48126
L1-F23	283.08411	0.03309	14.57985
L1-F24	1,192.51	0.04001	86.30941
L1-F25	1,241.81	0.03734	37.82017
L1-F26	567.67719	0.03496	33.8238
L1-F27	800.31781	0.02478	97.71826
L1-F28	492.04636	0.03238	20.79428
L1-F29	913.64624	0.03186	36.30921
L1-F30	28,183.51	0.10461	
L1-F31	3,407.04	0.04049	142.45272
L1-F32	908.45386	0.03251	45.63136
L1-F33	661.73358	0.03946	32.04054
L1-F34	848.21448	0.0405	29.55859
L1-F35	2,371.99	0.04267	101.68829
L1-F36	1,105.02	0.04445	35.14809
L1-F37	1,736.24	0.03279	100.69559
L1-F38	480.11078	0.03045	25.13966
L1-F39	1,126.45	0.03882	47.38522
L1-F40	617.10724	0.0325	36.37153
L1-F41	1,636.07	0.03183	98.61674
L1-F42	997.01227	0.03182	67.63093
L1-F43	636.8833	0.04132	31.61679
L1-F44	477.89313	0.03518	19.24546
L1-F45	1,307.88	0.03341	64.37503
L1-F46	260.12906	0.03973	10.03043
L1-F47	1,235.98	0.03353	52.16362
L1-F48	87.11272	0.03971	4.38093
L1-F49	1,904.22	0.04218	76.05277
L1-F50	1,553.91	0.03283	88.12936

Appendix A 5: Raw data of F-L2

ID	Tensile stress at Break (Standard)	Tensile strain at Break (Standard)	Modulus (Automatic Young's)
L2-F1	911.81311	0.0466	27.71403
L2-F2	1,552.48	0.05965	30.7154
L2-F3	399.85	0.05643	9.97119
L2-F4	1,123.22	0.05741	22.82649
L2-F5	432.64	0.05033	14.15104
L2-F6	1,588.59	0.04737	59.35904
L2-F7	835.74	0.02924	42.99593
L2-F8	637.06	0.04801	17.24471
L2-F9	558.94	0.0259	24.30578
L2-F10	679.15	0.0457	20.47142
L2-F11	967.67	0.05332	27.47533
L2-F12	773.21	0.0594	18.27555
L2-F13	2,040.95	0.05851	45.9183
L2-F14	656.93	0.05334	20.31895
L2-F15	1,934.25	0.06147	42.35234
L2-F16	1,077.35	0.06444	27.22767
L2-F17	382.37	0.08196	10.80467
L2-F18	1,443.06	0.05637	41.53777
L2-F19	1,426.37	0.08496	19.38305
L2-F20	623.92	0.05199	14.60314
L2-F21	1,042.60	0.03554	39.06235
L2-F22	813.41	0.0509	23.3634
L2-F23	1,116.17	0.0356	36.28346
L2-F24	1,527.45	0.05202	33.15793
L2-F25	1,153.70	0.0489	39.60226
L2-F26	2,129.96	0.04955	63.9776
L2-F27	858.66	0.02499	45.94381
L2-F28	354.94	0.04467	10.37173
L2-F29	486.28	0.05225	12.1665
L2-F30	1,528.13	0.05259	41.10885
L2-F31	1,010.43	0.0546	27.13699
L2-F32	1,954.53	0.05846	53.5827
L2-F33	536.56	0.06415	12.42267
L2-F34	1,042.73	0.04967	23.52938
L2-F35	753.22	0.05124	27.78309
L2-F36	778.78	0.03908	27.92598
L2-F37	931.87	0.04934	28.39234
L2-F38	2,378.47	0.05439	62.92351
L2-F39	729.96	0.05854	18.65283
L2-F40	672.46	0.05359	13.75915
L2-F41	958.92	0.04419	51.4476
L2-F42	165.19	0.01707	16.91227
L2-F43	881.69	0.0546	13.95084
L2-F44	866.60	0.03866	28.54695
L2-F45	523.82	0.05221	16.78426
L2-F46	790.06195	0.04456	23.5662
L2-F47	664.56	0.06022	15.11665
L2-F48	1,217.46	0.05843	31.52624
L2-F49	1,489.64	0.05514	40.0845
L2-F50	2,369.55	0.06066	58.55608

Appendix A 6: Raw data of F-L3

ID	Tensile stress at Break (Standard)	Tensile strain at Break (Standard)	Modulus (Automatic Young's)
L3-F1	1,191.43	0.02114	75.67939
L3-F2	1,441.01	0.01979	87.9617
L3-F3	391.76	0.01346	46.84027
L3-F4	882.38	0.01921	64.30393
L3-F5	728.75	0.0238	43.92938
L3-F6	1,046.38	0.02584	56.01077
L3-F7	522.43	0.02181	39.16011
L3-F8	1,353.47	0.02028	81.49974
L3-F9	1,377.51	0.02741	53.26357
L3-F10	1,209.81	0.02468	71.21437
L3-F11	671.14	0.01586	56.99971
L3-F12	707.57	0.02249	41.97671
L3-F13	1,522.38	0.01544	112.78442
L3-F14			
L3-F15	243.79	0.01551	48.57934
L3-F16	567.78	0.0171	41.81931
L3-F17	1,179.14	0.02064	86.5484
L3-F18	6,352.10	0.02298	351.0256
L3-F19	611.70	0.01539	55.59578
L3-F20	1,118.28	0.02647	58.79453
L3-F21	743.24	0.01756	49.46158
L3-F22	743.24	0.01756	49.46158
L3-F23	1,577.66	0.01947	123.08485
L3-F24	1,290.57	0.02793	85.416
L3-F25	683.97	0.02138	39.06717
L3-F26	729.43	0.02424	47.50523
L3-F27	592.26	0.02222	38.50869
L3-F28	2,170.51	0.03097	144.70558
L3-F29	803.24	0.01972	48.40566
L3-F30	763.96	0.0241	46.24278
L3-F31	968.37	0.01578	90.61641
L3-F32	305.96	0.01725	23.92557
L3-F33	1,546.32	0.02173	97.2272
L3-F34	2,218.22	0.0143	228.5126
L3-F35	521.85	0.00903	141.45218
L3-F36	366.18	0.01579	32.82443
L3-F37	463.30	0.01627	50.96684
L3-F38	516.18	0.01507	61.88826
L3-F39	1,060.92	0.01634	70.58008
L3-F40	554.73	0.02032	35.06195
L3-F41	1,893.56	0.02761	96.44794
L3-F42	805.44	0.01934	52.18914
L3-F43	1,127.97	0.02561	64.03195
L3-F44	618.77	0.01874	39.88807
L3-F45	1,406.80	0.01281	76.5546
L3-F46	173.61345	0.02154	9.1724
L3-F47	609.36	0.01719	42.11561
L3-F48	1,533.73	0.01878	97.3233
L3-F49	1,008.31	0.02033	62.47944
L3-F50	1,400.30	0.02124	86.87942

Appendix A 7: Raw data of LF-L1

ID	Tensile stress at Break (Standard)	Tensile strain at Break (Standard)	Modulus (Automatic Young's)
L1-LF1	759.20	0.03368	37.98178
L1-LF2	480.38	0.04236	22.51775
L1-LF3	873.11	0.03276	45.69937
L1-LF4	599.39	0.03934	25.51521
L1-LF5	636.44	0.03143	68.25411
L1-LF6	1,157.11	0.04345	48.00797
L1-LF7	870.29	0.05111	40.5312
L1-LF8	980.64	0.03323	63.68436
L1-LF9	2,558.19	0.045	113.05755
L1-LF10	314.11	0.02553	23.9785
L1-LF11	808.29	0.02647	39.42809
L1-LF12	341.62	0.03241	18.98953
L1-LF13	1,519.40	0.04022	49.05979
L1-LF14	558.64	0.03401	33.12618
L1-LF15	290.48	0.02448	25.56667
L1-LF16	1,125.36	0.02308	105.77479
L1-LF17	265.17	0.04242	11.11446
L1-LF18	1,130.27	0.03115	57.91139
L1-LF19	355.73	0.03919	9.09594
L1-LF20	815.80	0.02229	66.11432
L1-LF21	720.14	0.03641	25.11744
L1-LF22	670.89	0.04167	16.30951
L1-LF23	227.27	0.0292	22.30264
L1-LF24	602.91	0.03172	40.15042
L1-LF25	486.18	0.03815	21.02442
L1-LF26	363.35	0.04539	11.926
L1-LF27	429.14	0.03756	23.763
L1-LF28	503.93	0.0332	29.92088
L1-LF29	857.58	0.04093	50.14354
L1-LF30	852.13	0.03151	36.45113
L1-LF31	895.68	0.03694	35.5463
L1-LF32	383.34	0.04501	10.90802
L1-LF33	804.07	0.03655	35.29223
L1-LF34	488.98	0.03605	22.72246
L1-LF35	817.62	0.02571	59.50594
L1-LF36	1,293.42	0.03031	64.25171
L1-LF37	628.09	0.0412	12.74658
L1-LF38	1,073.61	0.03067	45.73675
L1-LF39	872.15	0.03939	31.07778
L1-LF40	32.91	0.02906	13.49631
L1-LF42	927.30	0.04576	31.44322
L1-LF43	160.93	0.05018	25.93714
L1-LF44	215.81	0.01217	35.79818
L1-LF45	284.66	0.0329	12.58978
L1-LF46	842.26	0.04263	26.45418
L1-LF47	1,093.36	0.03828	39.18356
L1-LF49	1,571.58	0.03984	64.01563

Appendix A 8: Raw data of LF-L2

ID	Tensile stress at Break (Standard)	Tensile strain at Break (Standard)	Modulus (Automatic Young's)
L2-LF1	1,181.67	0.02964	56.01836
L2-LF2	422.73	0.02232	33.3766
L2-LF3	370.35	0.03145	14.64315
L2-LF4	764.63	0.03094	57.02155
L2-LF5	374.42	0.02239	17.48272
L2-LF6	2,895.33	0.03166	157.27498
L2-LF7	1,609.30	0.01842	239.59152
L2-LF8	736.14	0.03142	34.40036
L2-LF9	480.63	0.02223	36.08376
L2-LF10	571.55	0.02583	40.8698
L2-LF11	637.93	0.02829	36.53822
L2-LF12	359.66	0.02531	22.93501
L2-LF13	1,363.59	0.02268	90.20231
L2-LF14	683.11	0.03038	41.12601
L2-LF15	1,074.34	0.02235	65.50754
L2-LF16	416.32	0.02388	24.88437
L2-LF17	715.56	0.04321	31.70198
L2-LF18	826.28	0.02755	36.52989
L2-LF19	239.29	0.02731	18.18566
L2-LF20	918.67	0.02436	81.6264
L2-LF21	502.33	0.0268	26.55441
L2-LF22	357.56	0.01848	32.89374
L2-LF23	420.32	0.02498	21.94429
L2-LF24	405.17	0.02663	23.82872
L2-LF25	318.08	0.02841	17.31134
L2-LF26	587.49	0.01764	121.53074
L2-LF27	582.12	0.0129	55.46441
L2-LF28	338.54	0.02883	17.17824
L2-LF29	301.37	0.01787	25.94512
L2-LF30	1,215.22	0.02349	62.13716
L2-LF31	446.17	0.02515	26.60473
L2-LF32	159.86	0.02457	9.47613
L2-LF33	957.34	0.02575	53.79591
L2-LF34	575.33	0.03243	31.52314
L2-LF35	376.14	0.02876	19.9109
L2-LF36	1,145.32	0.02793	59.12991
L2-LF37	632.47	0.03132	34.77278
L2-LF38	1,201.80	0.03447	62.04155
L2-LF39	595.82	0.01661	118.52727
L2-LF40	203.12	0.01337	20.19737
L2-LF41	699.80	0.02525	44.79535
L2-LF42	637.03	0.02889	28.86186
L2-LF43	1,220.76	0.03066	68.97895
L2-LF44	466.55	0.02804	33.8159
L2-LF45	312.26	0.02286	15.79797
L2-LF46	1,031.61	0.0266	74.54035
L2-LF47	393.77	0.01616	28.51182
L2-LF48	1,057.69	0.0301	42.17743
L2-LF49	118.77	0.01126	17.89355
L2-LF50	284.77	0.01262	32.45841

Appendix A 9: Raw data of LF-L3

ID	Tensile stress at Break (Standard)	Tensile strain at Break (Standard)	Modulus (Automatic Young's)
L3-LF1	503.35	0.02771	91.59607
L3-LF2	621.39	0.02207	33.76213
L3-LF3	987.95	0.02572	56.75804
L3-LF4	353.83	0.01981	26.36209
L3-LF5	264.33	0.0312	11.86347
L3-LF6	1,638.38	0.01404	759.14117
L3-LF7	521.82	0.02191	47.95364
L3-LF8	322.61	0.01932	26.50357
L3-LF9	132.66	0.02411	7.45269
L3-LF10	185.61	0.02121	10.89226
L3-LF11	234.74	0.01573	18.74889
L3-LF12	336.74	0.02378	22.97303
L3-LF13	743.80	0.02074	52.85774
L3-LF14	377.53	0.02813	20.11423
L3-LF15	695.21	0.01993	52.14354
L3-LF16	501.21	0.0276	26.10505
L3-LF17	1,083.23	0.02443	94.06557
L3-LF18	2,204.55	0.03191	117.8434
L3-LF19	622.90	0.02535	39.86124
L3-LF20	701.30	0.03565	33.31125
L3-LF21	55.13	0.02225	30.81054
L3-LF22	454.48	0.02586	25.76656
L3-LF23	607.35	0.02099	43.10205
L3-LF24	445.34	0.01285	115.57726
L3-LF25	1,743.75	0.02721	106.89952
L3-LF26	127.25	0.00817	24.97722
L3-LF27	859.46	0.02765	53.10587
L3-LF28	185.26	0.01133	54.3715
L3-LF29	839.40	0.02366	156.48877
L3-LF30	712.95	0.02586	41.64398
L3-LF31	57.77	0.00786	23.05971
L3-LF32	857.63	0.02766	39.73038
L3-LF33	838.39	0.02465	48.02184
L3-LF34	347.69	0.02188	26.07469
L3-LF35	726.81	0.02697	42.70625
L3-LF36	372.48	0.02028	24.6832
L3-LF37	360.82	0.01421	28.80728
L3-LF38	173.52	0.01847	13.81434
L3-LF39	500.43	0.0118	73.57979
L3-LF40	191.19	0.02187	10.25178
L3-LF41	508.48	0.02952	30.13439
L3-LF42	119.83	0.00876	39.90166
L3-LF43	35.80	0.00664	13.57553
L3-LF44	182.21	0.00743	37.17987
L3-LF45	493.24	0.02184	35.35184
L3-LF46	746.58	0.02298	56.28077
L3-LF47	534.25	0.0228	42.89483
L3-LF48	396.04	0.01524	31.43398
L3-LF49	171.27	0.01704	11.66911
L3-LF50	416.53	0.01385	49.1359

Appendix A 10: Raw data of FM-L1

ID	Tensile stress at Break (Standard)	Tensile strain at Break (Standard)	Modulus (Automatic Young's)
L1-FM1	426.14	0.03433	18.07853
L1-FM2	575.78	0.02909	40.21196
L1-FM3	588.07	0.02598	35.15297
L1-FM4	556.33	0.0438	22.89791
L1-FM5	513.39	0.0181	31.05782
L1-FM6	931.67	0.02544	52.49398
L1-FM7	1,326.77	0.02433	77.90459
L1-FM8	1,162.57	0.03768	41.33021
L1-FM9	603.22	0.02136	37.02115
L1-FM10	56.83	0.0289	3.97588
L1-FM11	319.10	0.03451	14.24194
L1-FM12	451.77	0.03002	18.63742
L1-FM13	1,321.96	0.02884	62.72813
L1-FM14	456.41	0.02675	32.49624
L1-FM15	461.34	0.03658	27.92916
L1-FM16	59.62	0.04094	3.15845
L1-FM17	320.04	0.02401	18.00038
L1-FM18	288.97	0.02343	26.87331
L1-FM19	389.42	0.03331	15.36043
L1-FM20	437.80	0.03185	18.04586
L1-FM21	653.44	0.03357	20.9073
L1-FM22	341.03	0.04439	12.8329
L1-FM23	920.29	0.03769	34.35488
L1-FM24	327.51	0.01595	26.49939
L1-FM25	755.38	0.01809	56.99434
L1-FM26	247.58	0.01902	15.99501
L1-FM27	529.02	0.01861	34.73175
L1-FM28	774.59	0.0292	46.87222
L1-FM29	1,055.83	0.03149	52.88919
L1-FM30	362.09	0.01795	27.74992
L1-FM31	440.07	0.03224	20.9841
L1-FM32	483.45	0.02702	30.94436
L1-FM33	67.28	0.04741	2.37646
L1-FM34	235.35	0.03148	12.39313
L1-FM35	1,441.42	0.03565	43.68458
L1-FM36	656.70	0.02644	33.87436
L1-FM37	195.87	0.01836	12.4137
L1-FM38	590.92	0.04758	17.02704
L1-FM39	162.02	0.03897	9.14491
L1-FM40	647.40	0.02426	41.29076
L1-FM41	239.35	0.01323	23.7018
L1-FM42	600.18	0.01288	56.67552
L1-FM43	1,100.98	0.02328	48.32754
L1-FM44	1,023.53	0.02712	53.62248
L1-FM45	664.81	0.02277	28.51032
L1-FM46	690.71	0.01556	45.78975
L1-FM47	563.21	0.02673	23.11843
L1-FM48	781.02	0.03698	26.51713
L1-FM49	808.40	0.02317	36.27778

Appendix A 11: Raw data of FM-L2

ID	Tensile stress at Break (Standard)	Tensile strain at Break (Standard)	Modulus (Automatic Young's)
L2-FM1	686.94	0.0204	39.67444
L2-FM2	372.49	0.00866	41.3774
L2-FM3	263.72	0.0156	23.20305
L2-FM4	1,665.40	0.02224	93.58797
L2-FM5	308.29	0.01227	52.39683
L2-FM6	529.39	0.02378	24.75306
L2-FM7	603.86	0.01557	45.70848
L2-FM8	330.49	0.01298	31.91309
L2-FM9	823.73	0.01995	52.89386
L2-FM10	705.06	0.02761	41.25965
L2-FM11	778.83	0.02672	35.3583
L2-FM12	301.51	0.01245	29.09618
L2-FM13	991.11	0.01842	65.69749
L2-FM14	396.46	0.01751	30.5371
L2-FM15	927.48	0.02355	51.32816
L2-FM16	890.87	0.02218	50.59298
L2-FM17	413.20	0.02185	40.96083
L2-FM18	3,176.83	0.02399	145.90979
L2-FM19	538.43	0.01673	46.89788
L2-FM20	376.34	0.01718	35.43771
L2-FM21	486.93	0.02181	27.09667
L2-FM22	332.29	0.01493	31.5842
L2-FM23	395.92	0.02052	29.70944
L2-FM24	386.82	0.02309	20.95437
L2-FM25	506.45	0.01895	33.11903
L2-FM26	327.20	0.01292	36.60432
L2-FM27	545.11	0.02375	43.74543
L2-FM28	345.57	0.02427	19.43688
L2-FM29	887.47	0.02478	41.33944
L2-FM30	1,063.08	0.02171	64.12317
L2-FM31	315.78	0.01095	30.49172
L2-FM32	533.49	0.02143	29.48716
L2-FM33	690.10	0.02538	35.36467
L2-FM34	388.31	0.02053	34.36219
L2-FM35	622.40	0.02609	30.18579
L2-FM36	152.40	0.01682	13.19071
L2-FM37	486.79	0.02528	29.66866
L2-FM38	1,963.63	0.03035	70.95762
L2-FM39	423.05	0.0236	28.37746
L2-FM40	380.99	0.0268	16.41948
L2-FM41	186.11	0.02318	12.18629
L2-FM42	302.82	0.00839	37.19738
L2-FM43	979.50	0.02563	61.86864
L2-FM44	498.53	0.02137	28.17579
L2-FM45	1,800.76	0.02695	86.45496
L2-FM46	176.08	0.01298	24.25752
L2-FM47	256.79	0.02558	13.43736
L2-FM48	794.92	0.01541	71.42453
L2-FM49	477.43	0.02714	24.63186
L2-FM50	474.52	0.01888	34.14806

Appendix A 12: Raw data of FM-L3

ID	Tensile stress at Break (Standard)	Tensile strain at Break (Standard)	Modulus (Automatic Young's)
L3-FM1	244.44	0.02475	13.25431
L3-FM2	551.77	0.01432	45.20839
L3-FM3	1,821.94	0.02031	122.19613
L3-FM4	586.44	0.02527	21.25902
L3-FM5	893.99	0.02093	61.08602
L3-FM6	1,272.77	0.02561	71.32689
L3-FM7	611.71	0.01726	38.16776
L3-FM8	658.64	0.02053	40.52742
L3-FM9	733.70	0.02654	33.27825
L3-FM10	533.04	0.02362	36.97309
L3-FM11	531.68	0.01554	38.21999
L3-FM12	620.22	0.02336	32.99191
L3-FM13	318.02	0.02135	17.1586
L3-FM14	296.34	0.01315	27.1587
L3-FM15	381.49	0.02426	26.08971
L3-FM16	645.05	0.02121	35.7833
L3-FM17	314.03	0.01655	21.24017
L3-FM18	278.87	0.01492	20.8454
L3-FM19	360.33	0.01399	30.10155
L3-FM20	372.38	0.02176	19.41169
L3-FM21	87.89	0.00549	17.76032
L3-FM22	308.64	0.01821	17.28191
L3-FM23	826.40	0.0252	49.31214
L3-FM24	502.34	0.02226	28.36219
L3-FM25	326.84	0.01974	19.62956
L3-FM26	209.20	0.01262	19.44297
L3-FM27	397.45	0.02659	22.54251
L3-FM28	247.17	0.01663	19.8075
L3-FM29	677.44	0.02261	41.31984
L3-FM30	319.83	0.01856	21.37538
L3-FM31	230.08	0.01578	21.6065
L3-FM33	346.94	0.0207	24.63415
L3-FM34	333.21	0.01505	28.5655
L3-FM35	376.24	0.01428	34.70618
L3-FM36	440.51	0.01995	25.57548
L3-FM37	559.14	0.02736	32.0423
L3-FM38	576.55	0.01561	43.3099
L3-FM39	547.73	0.02173	29.0575
L3-FM40	68.96	0.01034	9.32021
L3-FM41	351.56	0.01756	25.49717
L3-FM42	224.00	0.02073	13.69553
L3-FM43	495.09	0.02726	28.46087
L3-FM44	471.06	0.02273	27.97235
L3-FM45	224.59	0.02246	13.52307
L3-FM46	733.43	0.02918	34.1342
L3-FM47	402.36	0.01347	32.73126
L3-FM48	908.06	0.02491	52.596
L3-FM49	662.33	0.02698	34.4226
L3-FM50	610.42	0.02075	33.66151

Appendix A 13: Raw data of M-L1

ID	Tensile stress at Break (Standard)	Tensile strain at Break (Standard)	Modulus (Automatic Young's)
L1-M1	425.46326	0.02921	27.20025
L1-M2	1,306.84	0.04678	40.6201
L1-M3	640.36066	0.11657	166.93319
L1-M4	496.61	0.11462	103.39936
L1-M5	1,127.28	0.0199	77.37934
L1-M6	151.53	0.04708	3.73236
L1-M7	66.62538	0.11644	33.87418
L1-M8	784.40436	0.0377	25.86909
L1-M9	1,101.72	0.05486	28.31288
L1-M10	1,325.55	0.04429	44.44579
L1-M11	1,538.96	0.02515	111.92113
L1-M12	1,342.97	0.04483	55.02686
L1-M13	1,734.22	0.02897	
L1-M14	1,753.65	0.05252	43.24368
L1-M15	844.92	0.04324	39.31579
L1-M16	283.86	0.05105	8.19079
L1-M17	1,442.06	0.03827	78.04568
L1-M18	632.14642	0.04154	24.85259
L1-M19	435.61	0.0286	18.67781
L1-M20	60.24	0.03148	2.72361
L1-M21	1,040.26	0.04487	33.89982
L1-M22	1,131.27	0.03672	
L1-M23	1,022.66	0.04543	41.92317
L1-M24	1,212.29	0.04078	39.74493
L1-M25	1,717.59	0.02974	87.15973
L1-M26	413.98547	0.00816	60.13033
L1-M27	360.28784	0.11753	26.76867
L1-M28	96.79947	0.11781	30.30456
L1-M29	140.38969	0.04052	6.02063
L1-M30	2,477.61	0.03947	97.64249
L1-M31	5,105.43	0.04287	197.2612
L1-M32	1,318.53	0.04673	49.44972
L1-M33	1,996.88	0.04349	62.24107
L1-M34	17,615.28	0.11496	656.52267
L1-M35	1,201.00	0.03552	61.92623
L1-M36	271.66	0.11693	58.00732
L1-M37	1,910.20	0.0389	70.65779
L1-M38	2,402.13	0.03591	87.47448
L1-M39	681.03	0.04311	27.13375
L1-M40	1,739.67	0.04127	81.09687
L1-M41	1,353.00	0.04786	
L1-M42	1,245.23	0.03904	58.15055
L1-M43	1,042.95	0.03442	52.16904
L1-M44	262.20944	0.02761	
L1-M45	850.22	0.03462	47.9383
L1-M46	43.70625	0.118	36.56455
L1-M47	871.40	0.03632	25.46831
L1-M48	297.3172	0.03792	9.89758
L1-M49	1,391.95	0.02535	75.10672
L1-M50	1,038.02	0.03855	42.49616

Appendix A 14: Raw data of M-L2

ID	Tensile stress at Break (Standard)	Tensile strain at Break (Standard)	Modulus (Automatic Young's)
L2-M1	1,404.01	0.05778	37.62332
L2-M2	1,197.85	0.04137	56.61331
L2-M3	3,363.55	0.06619	74.35706
L2-M4	3,489.16	0.05651	92.10687
L2-M5	896.17	0.05349	23.19956
L2-M6	641.87	0.03251	24.15446
L2-M7	1,928.64	0.0547	66.15863
L2-M8	890.09	0.03175	38.08009
L2-M9	1,453.05	0.04473	57.9127
L2-M10	4,080.29	0.05583	97.05379
L2-M11	1,308.22	0.03507	50.54904
L2-M12	2,566.55	0.05386	85.02903
L2-M13	795.34	0.03304	35.71479
L2-M14	1,009.40	0.02795	77.99711
L2-M15	1,747.30	0.0649	36.91881
L2-M16	11.09	0.03902	
L2-M17	2,104.51	0.03769	111.79452
L2-M18	458.08	0.05117	16.97712
L2-M19	2,344.69	0.04354	73.6532
L2-M20	1,560.24	0.04405	51.57417
L2-M21	1,117.89	0.03452	42.83424
L2-M22	1,057.68	0.03863	69.03313
L2-M23	1,347.34	0.05523	31.34153
L2-M24	700.25	0.02877	28.03662
L2-M25	2,865.82	0.04761	78.57347
L2-M26	1,423.44	0.04289	46.03021
L2-M27	2,368.54	0.05986	53.85995
L2-M28	722.80	0.03876	26.0935
L2-M29	1,344.08	0.11399	16.91256
L2-M30	975.45	0.03635	31.3381
L2-M31	783.81	0.0397	31.5351
L2-M32	1,408.82	0.0594	35.44405
L2-M33	1,756.60	0.05695	38.30883
L2-M34	501.93	0.02904	26.37871
L2-M35	1,942.21	0.05884	48.04868
L2-M36	1,630.71	0.04959	43.43903
L2-M37	1,570.13	0.05222	50.68267
L2-M38	566.67	0.04931	14.73186
L2-M39	1,821.76	0.04438	72.27411
L2-M40	1,381.25	0.057	32.85563
L2-M41	1,083.23	0.04247	39.53329
L2-M42	166.73	0.00904	23.85175
L2-M43	4,815.28	0.04924	135.35057
L2-M44	452.14	0.03796	14.92917
L2-M45	6,801.90	0.05809	153.60704
L2-M46	716.30261	0.03367	28.0425
L2-M47	295.80	0.03189	12.49214
L2-M48	6,971.54	0.0661	184.61183
L2-M49	1,247.71	0.05101	35.67725
L2-M50	1,207.99	0.04809	35.00028

Appendix A 15: Raw data of M-L3

ID	Tensile stress at Break (Standard)	Tensile strain at Break (Standard)	Modulus (Automatic Young's)
L3-M1	442.30	0.01455	40.43828
L3-M2	276.82	0.01036	49.15095
L3-M3	850.12	0.01756	58.60746
L3-M4	1,161.70	0.01898	79.02609
L3-M5	445.63	0.01054	49.78416
L3-M6	565.66	0.02129	29.69475
L3-M7	719.49	0.02622	48.78527
L3-M8	635.10	0.01569	45.23902
L3-M9	229.13	0.01264	20.99523
L3-M10	561.86	0.01858	37.16341
L3-M11	713.72	0.01583	45.08635
L3-M12	654.55	0.01767	55.10838
L3-M13	1,066.15	0.01933	75.94017
L3-M14	673.55	0.02044	30.98404
L3-M15	1,023.87	0.0137	95.83226
L3-M16	1,009.62	0.01561	243.49042
L3-M17	902.30	0.0206	60.60379
L3-M18	805.61	0.02038	60.60143
L3-M19	543.82	0.01571	43.25645
L3-M20	786.01	0.01793	58.67366
L3-M21	508.32	0.01678	44.52296
L3-M22	921.44	0.0163	68.78425
L3-M23	921.44	0.0163	68.78425
L3-M24	889.94	0.02027	70.95741
L3-M25	1,034.25	0.01841	67.20901
L3-M26	6,333.65	0.02499	364.08466
L3-M27	634.40	0.01955	38.68238
L3-M28	559.87	0.01028	170.44041
L3-M29	1,428.37	0.0225	89.83785
L3-M30	960.78	0.02077	60.13244
L3-M31	721.90	0.0341	38.10166
L3-M32	695.00	0.02058	40.38027
L3-M33	456.42	0.01355	36.47273
L3-M34	764.54	0.01753	64.31906
L3-M35	246.91	0.01089	28.29589
L3-M36	1,025.83	0.02001	63.48979
L3-M37	1,774.10	0.02449	94.90848
L3-M38	831.68	0.02333	72.82037
L3-M39	950.00	0.02197	60.75281
L3-M40	1,508.52	0.02157	104.33227
L3-M41	1,034.01	0.01338	106.58192
L3-M42	1,208.31	0.02181	76.57632
L3-M43	617.51	0.0175	42.9659
L3-M44	775.79	0.03756	27.10632
L3-M45	2,121.09	0.01994	130.14807
L3-M46	1,385.01	0.0235	72.20898
L3-M47	502.06	0.01922	32.64681
L3-M48	808.11	0.02643	41.84692
L3-M49	848.43	0.01728	64.64193
L3-M50	666.55	0.01963	51.63186

Appendix A 16: p value of tensile stress among groups from ANOVA (one-way)

ID	NF-L1	NF-L2	NF-L3	F-L1	F-L2	F-L3	LF-L1	LF-L2	LF-L3	FM-L1	FM-L2	FM-L3	M-L1	M-L2	M-L3
NF-L1		1.000	0.874	0.423	1.000	1.000	0.840	0.749	0.323	0.431	0.626	0.221	1.000	0.809	0.999
NF-L2	1.000		0.996	0.105	1.000	1.000	0.994	0.982	0.768	0.858	0.952	0.643	1.000	0.367	1.000
NF-L3	0.874	0.996		0.001	0.999	0.994	1.000	1.000	1.000	1.000	1.000	1.000	0.995	0.011	1.000
F-L1	0.423	0.105	0.001		0.064	0.126	0.001	0.000	0.000	0.000	0.000	0.000	0.121	1.000	0.030
F-L2	1.000	1.000	0.999	0.064		1.000	0.999	0.995	0.865	0.928	0.982	0.763	1.000	0.260	1.000
F-L3	1.000	1.000	0.994	0.126	1.000		0.990	0.973	0.724	0.823	0.935	0.593	1.000	0.413	1.000
LF-L1	0.840	0.994	1.000	0.001	0.999	0.990		1.000	1.000	1.000	1.000	1.000	0.991	0.009	1.000
LF-L2	0.749	0.982	1.000	0.000	0.995	0.973	1.000		1.000	1.000	1.000	1.000	0.975	0.005	0.999
LF-L3	0.323	0.768	1.000	0.000	0.865	0.724	1.000	1.000		1.000	1.000	1.000	0.734	0.000	0.950
FM-L1	0.431	0.858	1.000	0.000	0.928	0.823	1.000	1.000	1.000		1.000	1.000	0.831	0.001	0.979
FM-L2	0.626	0.952	1.000	0.000	0.982	0.935	1.000	1.000	1.000	1.000		1.000	0.939	0.002	0.997
FM-L3	0.221	0.643	1.000	0.000	0.763	0.593	1.000	1.000	1.000	1.000	1.000		0.605	0.000	0.890
M-L1	1.000	1.000	0.995	0.121	1.000	1.000	0.991	0.975	0.734	0.831	0.939	0.605		0.402	1.000
M-L2	0.809	0.367	0.011	1.000	0.260	0.413	0.009	0.005	0.000	0.001	0.002	0.000	0.402		0.149
M-L3	0.999	1.000	1.000	0.030	1.000	1.000	1.000	0.999	0.950	0.979	0.997	0.890	1.000	0.149	

Green marked pairs are statistically significant

Appendix A 17: p value of tensile strain among groups from ANOVA (one-way)

ID	NF-L1	NF-L2	NF-L3	F-L1	F-L2	F-L3	LF-L1	LF-L2	LF-L3	FM-L1	FM-L2	FM-L3	M-L1	M-L2	M-L3
NF-L1		0.003	0.000	1.000	0.000	0.000	0.903	0.000	0.000	0.000	0.000	0.000	0.000	0.360	0.000
NF-L2	0.003		0.379	0.064	0.000	0.003	0.531	0.908	0.019	1.000	0.006	0.005	0.000	0.000	0.001
NF-L3	0.000	0.379		0.000	0.000	0.959	0.000	1.000	0.999	0.700	0.986	0.982	0.000	0.000	0.796
F-L1	1.000	0.064	0.000		0.000	0.000	1.000	0.000	0.000	0.015	0.000	0.000	0.000	0.001	0.000
F-L2	0.000	0.000	0.000	0.000		0.000	0.000	0.000	0.000	0.000	0.000	0.000	1.000	0.899	0.000
F-L3	0.000	0.003	0.959	0.000	0.000		0.000	0.505	1.000	0.016	1.000	1.000	0.000	0.000	1.000
LF-L1	0.903	0.531	0.000	1.000	0.000	0.000		0.003	0.000	0.240	0.000	0.000	0.000	0.000	0.000
LF-L2	0.000	0.908	1.000	0.000	0.000	0.505	0.003		0.841	0.992	0.645	0.617	0.000	0.000	0.239
LF-L3	0.000	0.019	0.999	0.000	0.000	1.000	0.000	0.841		0.077	1.000	1.000	0.000	0.000	1.000
FM-L1	0.000	1.000	0.700	0.015	0.000	0.016	0.240	0.992	0.077		0.030	0.026	0.000	0.000	0.003
FM-L2	0.000	0.006	0.986	0.000	0.000	1.000	0.000	0.645	1.000	0.030		1.000	0.000	0.000	1.000
FM-L3	0.000	0.005	0.982	0.000	0.000	1.000	0.000	0.617	1.000	0.026	1.000		0.000	0.000	1.000
M-L1	0.000	0.000	0.000	0.000	1.000	0.000	0.000	0.000	0.000	0.000	0.000	0.000		0.908	0.000
M-L2	0.360	0.000	0.000	0.001	0.899	0.000	0.000	0.000	0.000	0.000	0.000	0.000	0.908		0.000
M-L3	0.000	0.001	0.796	0.000	0.000	1.000	0.000	0.239	1.000	0.003	1.000	1.000	0.000	0.000	

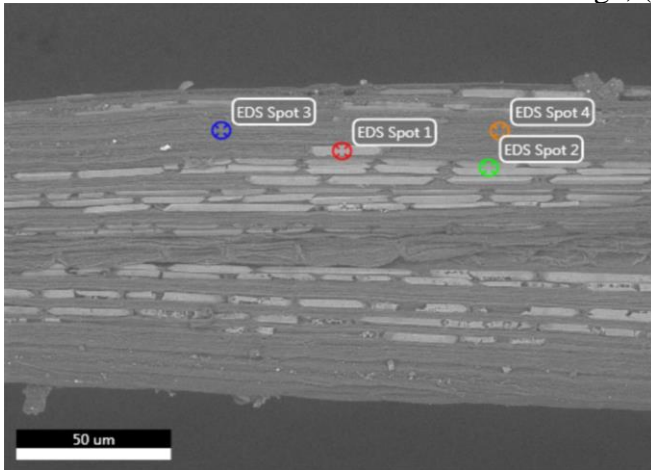
Green marked pairs are statistically significant

Appendix A 18: p value of modulus among groups from ANOVA (one-way)

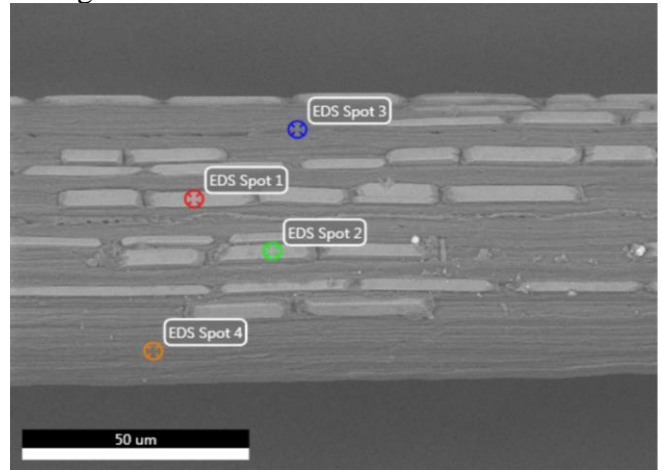
ID	NF-L1	NF-L2	NF-L3	F-L1	F-L2	F-L3	LF-L1	LF-L2	LF-L3	FM-L1	FM-L2	FM-L3	M-L1	M-L2	M-L3
NF-L1		0.918	1.000	0.977	0.957	0.429	1.000	1.000	0.995	0.983	1.000	0.996	0.851	1.000	0.470
NF-L2	0.918		0.908	1.000	0.059	1.000	0.352	0.977	1.000	0.093	0.662	0.165	1.000	0.993	1.000
NF-L3	1.000	0.908		0.973	0.963	0.408	1.000	1.000	0.994	0.986	1.000	0.997	0.836	1.000	0.449
F-L1	0.977	1.000	0.973		0.122	0.999	0.535	0.996	1.000	0.182	0.828	0.293	1.000	0.999	1.000
F-L2	0.957	0.059	0.963	0.122		0.004	1.000	0.873	0.209	1.000	0.998	1.000	0.036	0.774	0.005
F-L3	0.429	1.000	0.408	0.999	0.004		0.050	0.615	0.996	0.007	0.166	0.016	1.000	0.744	1.000
LF-L1	1.000	0.352	1.000	0.535	1.000	0.050		0.998	0.696	1.000	1.000	1.000	0.256	0.993	0.060
LF-L2	1.000	0.977	1.000	0.996	0.873	0.615	0.998		1.000	0.933	1.000	0.978	0.946	1.000	0.657
LF-L3	0.995	1.000	0.994	1.000	0.209	0.996	0.696	1.000		0.295	0.923	0.438	1.000	1.000	0.987
FM-L1	0.983	0.093	0.986	0.182	1.000	0.007	1.000	0.933	0.295		1.000	1.000	0.059	0.863	0.009
FM-L2	1.000	0.662	1.000	0.828	0.998	0.166	1.000	1.000	0.923	1.000		1.000	0.544	1.000	0.190
FM-L3	0.996	0.165	0.997	0.293	1.000	0.016	1.000	0.978	0.438	1.000	1.000		0.109	0.943	0.019
M-L1	0.851	1.000	0.836	1.000	0.036	1.000	0.256	0.946	1.000	0.059	0.544	0.109		0.980	1.000
M-L2	1.000	0.993	1.000	0.999	0.774	0.744	0.993	1.000	1.000	0.863	1.000	0.943	0.980		0.780
M-L3	0.470	1.000	0.449	1.000	0.005	1.000	0.060	0.657	0.987	0.009	0.190	0.019	1.000	0.780	

Green marked pairs are statistically significant

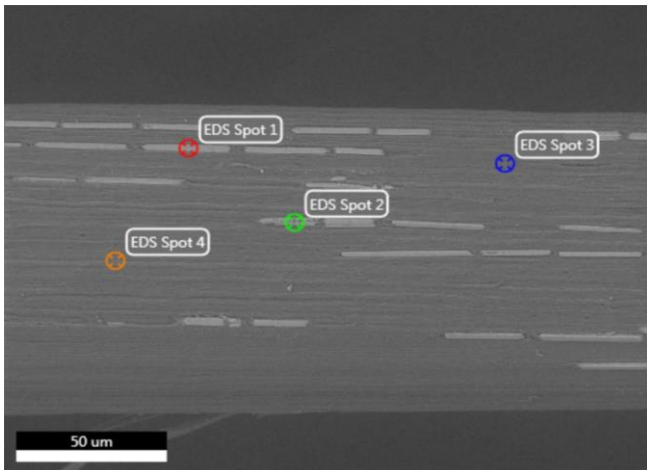
Appendix A 19: EDS spot of fibres from (a) NF stage; (b) F stage; (c) LF stage; (d) FM stage; (e) M stage



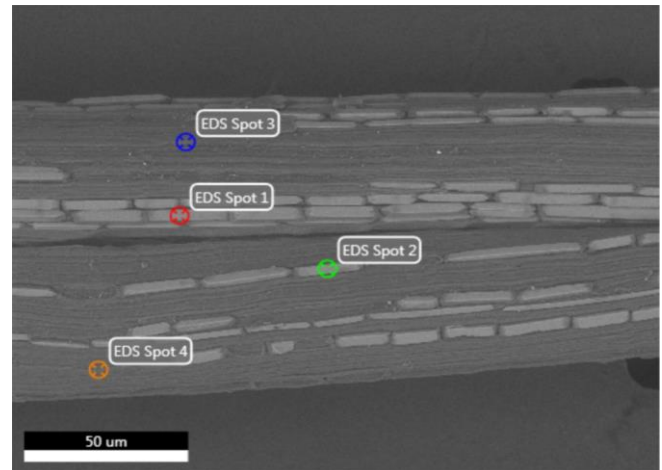
(a)



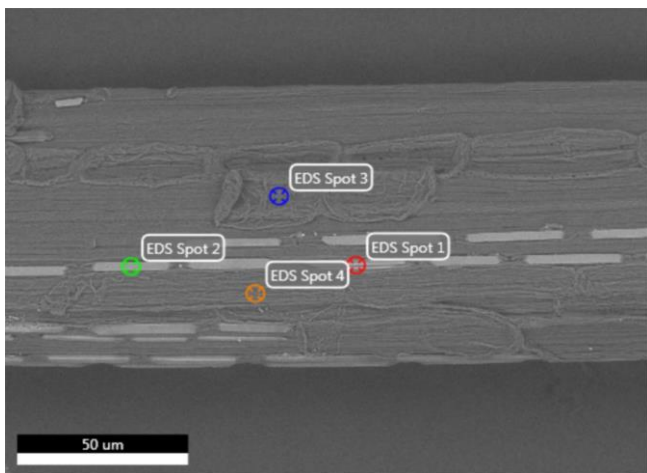
(b)



(c)

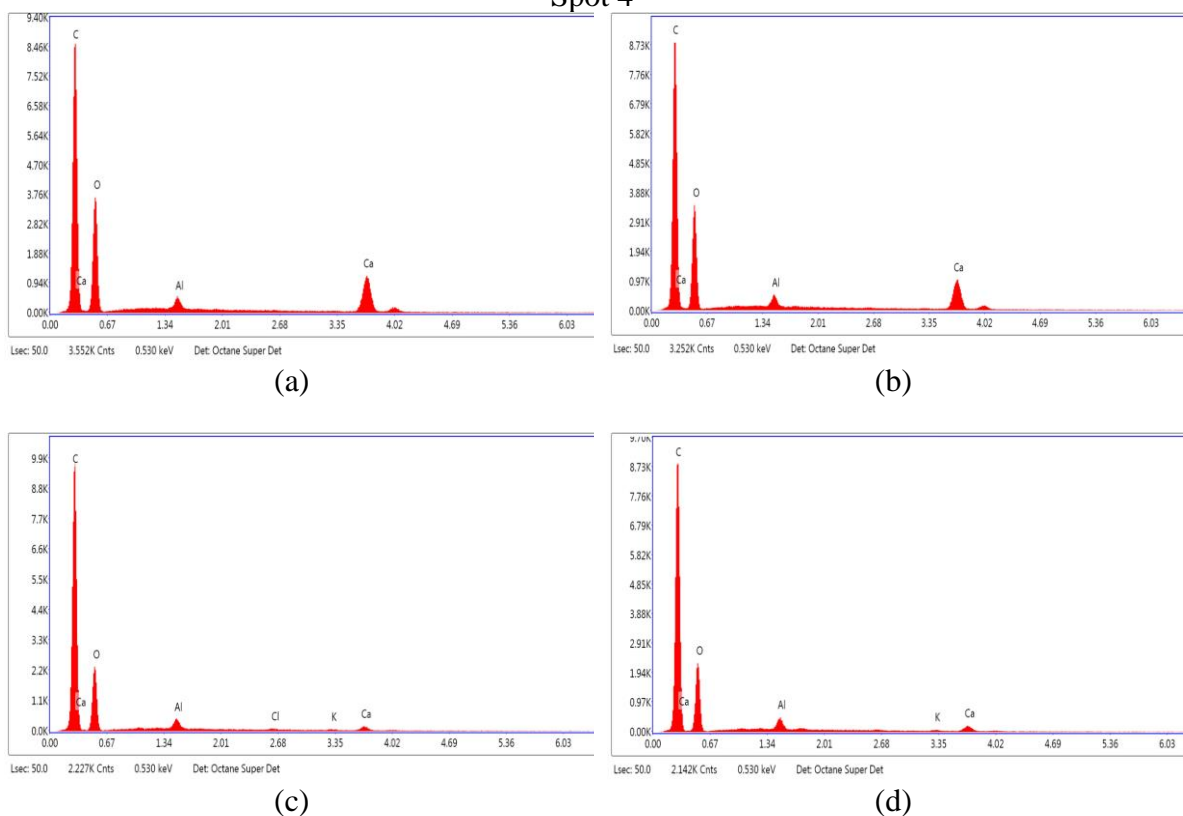


(d)



(e)

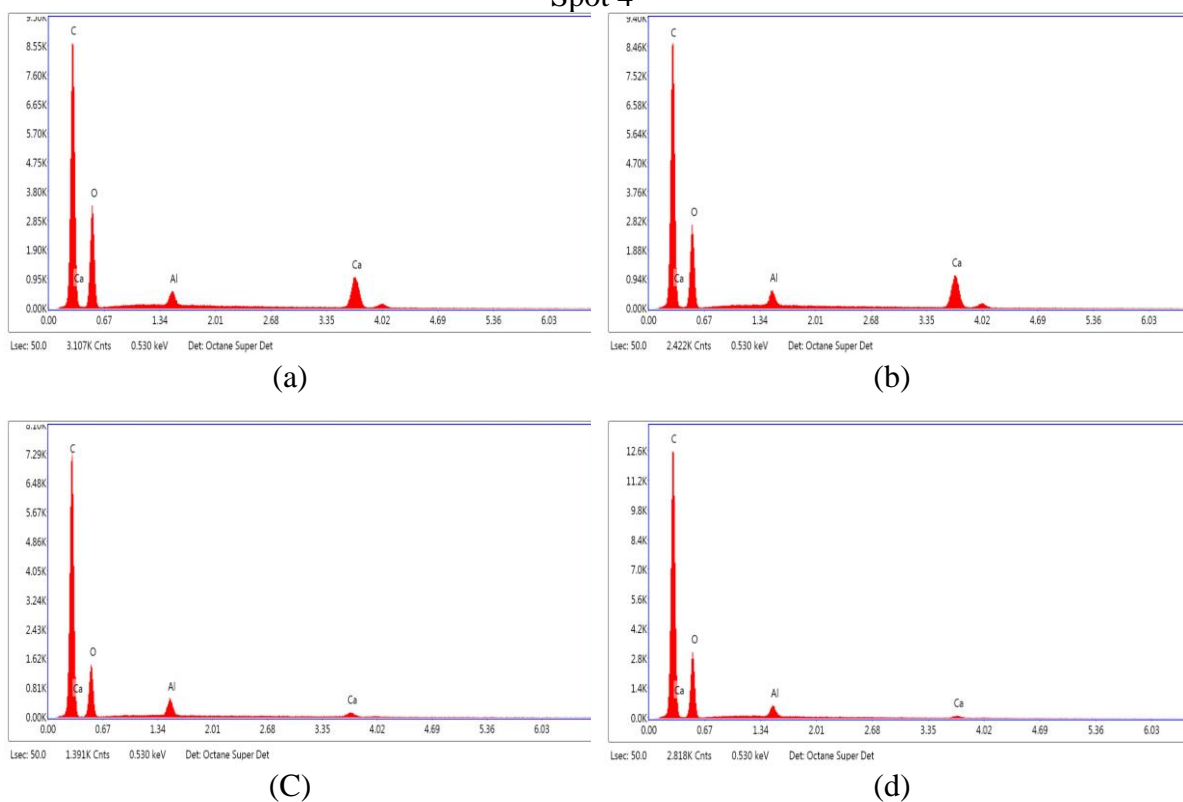
Appendix A 20: eZAF smart quant curve of NF stage of (a) spot 1; (b) Spot 2; (c) Spot 3; (d) Spot 4



Appendix A 21: Chemical composition of NF stage

Spot 1					Spot 2				
Element	Weight %	Atomic %	Net Int.	Error %	Element	Weight %	Atomic %	Net Int.	Error %
C K	43.53	57.93	913.36	5.11	C K	47.2	61.13	962.88	4.98
O K	32.04	32.01	429.75	9.4	O K	30.94	30.08	400.65	9.4
AlK	1.61	0.95	58.29	7.45	AlK	1.63	0.94	56.82	7.61
CaK	22.82	9.1	250.02	4.28	CaK	20.23	7.85	212.25	4.37
Spot 3					Spot 4				
Element	Weight %	Atomic %	Net Int.	Error %	Element	Weight %	Atomic %	Net Int.	Error %
C K	67.12	75.65	1090.03	4.8	C K	65.09	74.03	998.81	4.55
O K	25.22	21.34	272.52	9.32	O K	26.61	22.72	263.53	9.32
AlK	2.28	1.14	63.53	6.08	AlK	2.46	1.25	62.32	6.12
ClK	0.79	0.3	12.59	17.48	K K	0.86	0.3	8.84	22.78
K K	0.93	0.32	10.33	19.82	CaK	4.97	1.69	37.24	9.31
CaK	3.65	1.23	30.1	9.92					

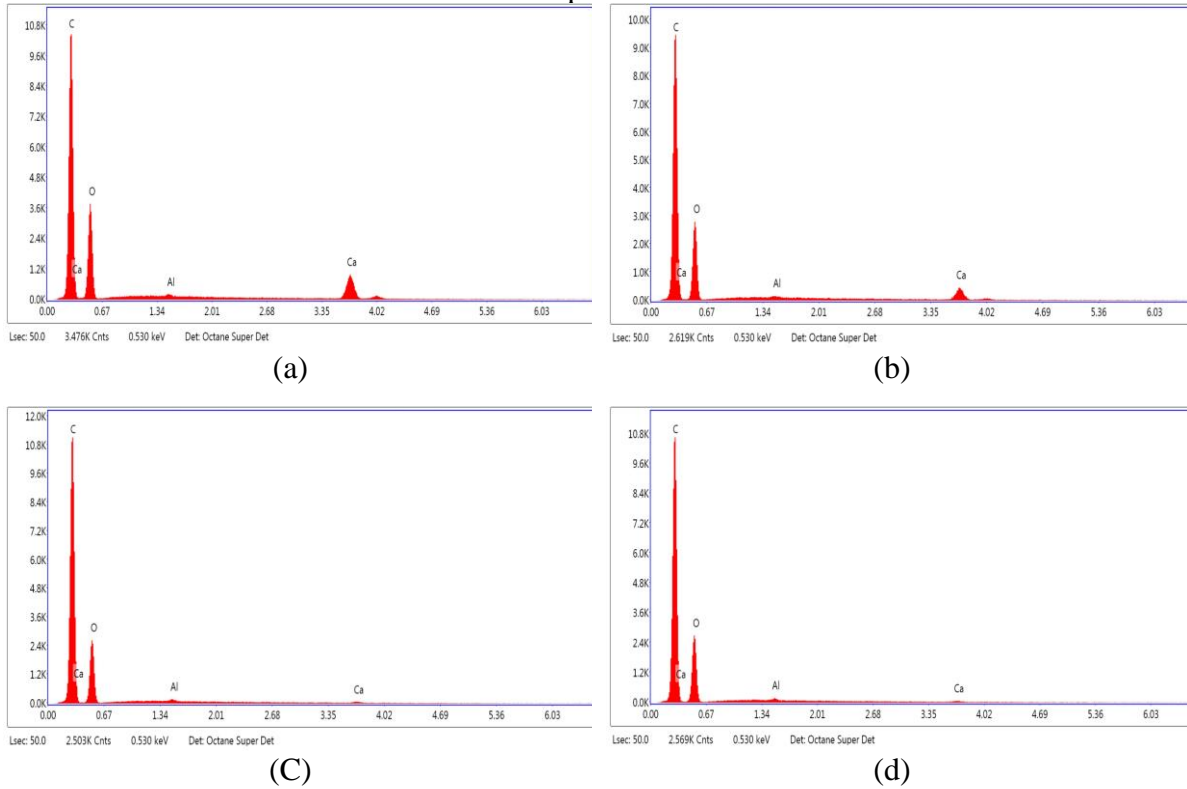
Appendix A 22: eZAF smart quant curve of F stage of (a) spot 1; (b) Spot 2; (c) Spot 3; (d) Spot 4



Appendix A 23: Chemical composition of F stage

Spot 1					Spot 2				
Element	Weight %	Atomic %	Net Int.	Error %	Element	Weight %	Atomic %	Net Int.	Error %
C K	46.71	61.09	942.28	5.09	C K	48.08	63.36	922.85	5.06
O K	29.87	29.33	382.36	9.46	O K	26.45	26.17	306.28	9.7
AlK	2.08	1.21	72.74	6.01	AlK	2.18	1.28	72.43	6.02
CaK	21.34	8.36	224	4.34	CaK	23.29	9.2	231.74	4.32
Spot 3					Spot 4				
Element	Weight %	Atomic %	Net Int.	Error %	Element	Weight %	Atomic %	Net Int.	Error %
C K	69.73	78.17	844.66	4.62	C K	69.81	76.88	1484.27	4.23
O K	21.96	18.48	166.65	9.91	O K	25.74	21.28	352.03	9.11
AlK	3.4	1.69	68.61	5.54	AlK	2.35	1.15	80.52	5.69
CaK	4.91	1.65	29.28	9.27	CaK	2.09	0.69	21.46	13.48

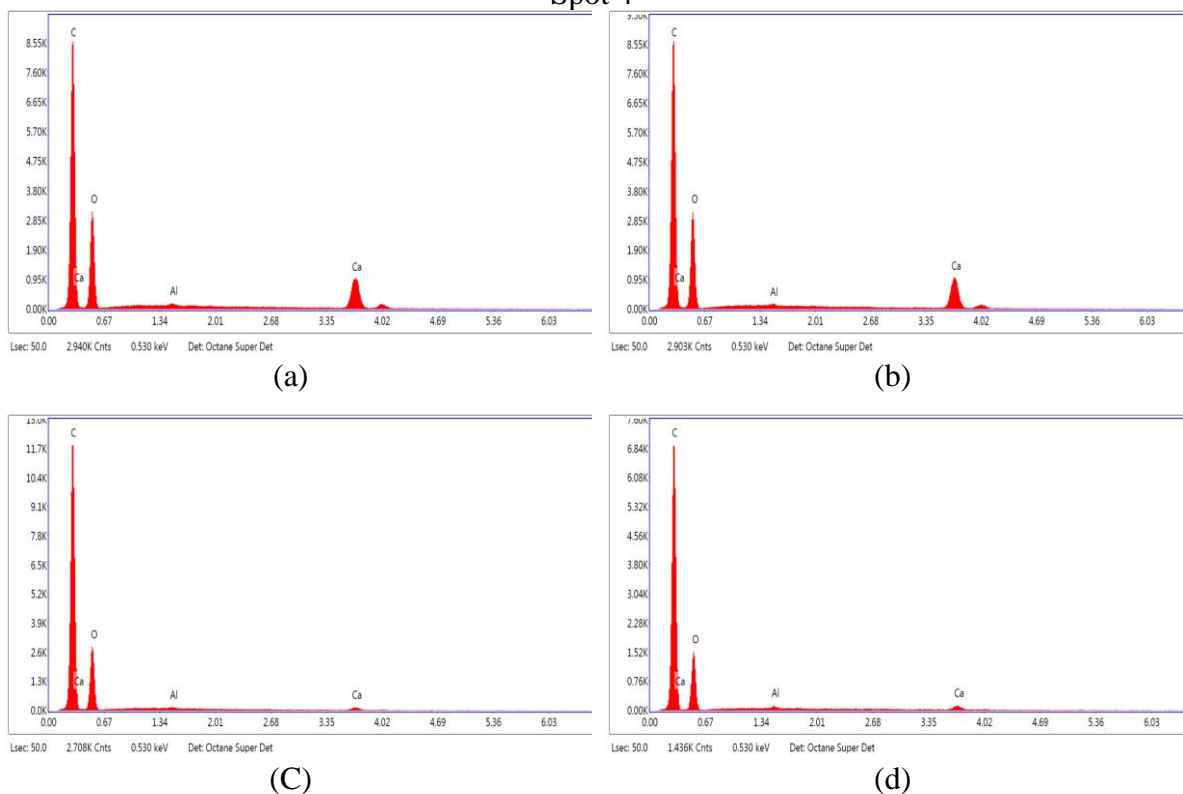
Appendix A 24: eZAF smart quant curve of LF stage of (a) spot 1; (b) Spot 2; (c) Spot 3; (d) Spot 4



Appendix A 25: Chemical composition of LF stage

Spot 1					Spot 2				
Element	Weight %	Atomic %	Net Int.	Error %	Element	Weight %	Atomic %	Net Int.	Error %
C K	50.41	63.52	1143.14	4.57	C K	60.04	70.51	1088.79	4.22
O K	31.14	29.45	430.02	9.35	O K	29.05	25.6	317.91	9.34
AlK	0.33	0.19	12.23	19.89	AlK	0.3	0.16	8.59	24.5
CaK	18.12	6.84	201.4	4.41	CaK	10.61	3.73	90.36	5.73
Spot 3					Spot 4				
Element	Weight %	Atomic %	Net Int.	Error %	Element	Weight %	Atomic %	Net Int.	Error %
C K	71.05	77.15	1305.8	3.74	C K	70.11	76.24	1255.36	3.77
O K	27.29	22.25	305.31	9.14	O K	28.46	23.24	315.51	9.07
AlK	0.4	0.19	11.11	16.59	AlK	0.34	0.17	9.3	22.8
CaK	1.26	0.41	10.63	22.23	CaK	1.09	0.36	8.99	24.62

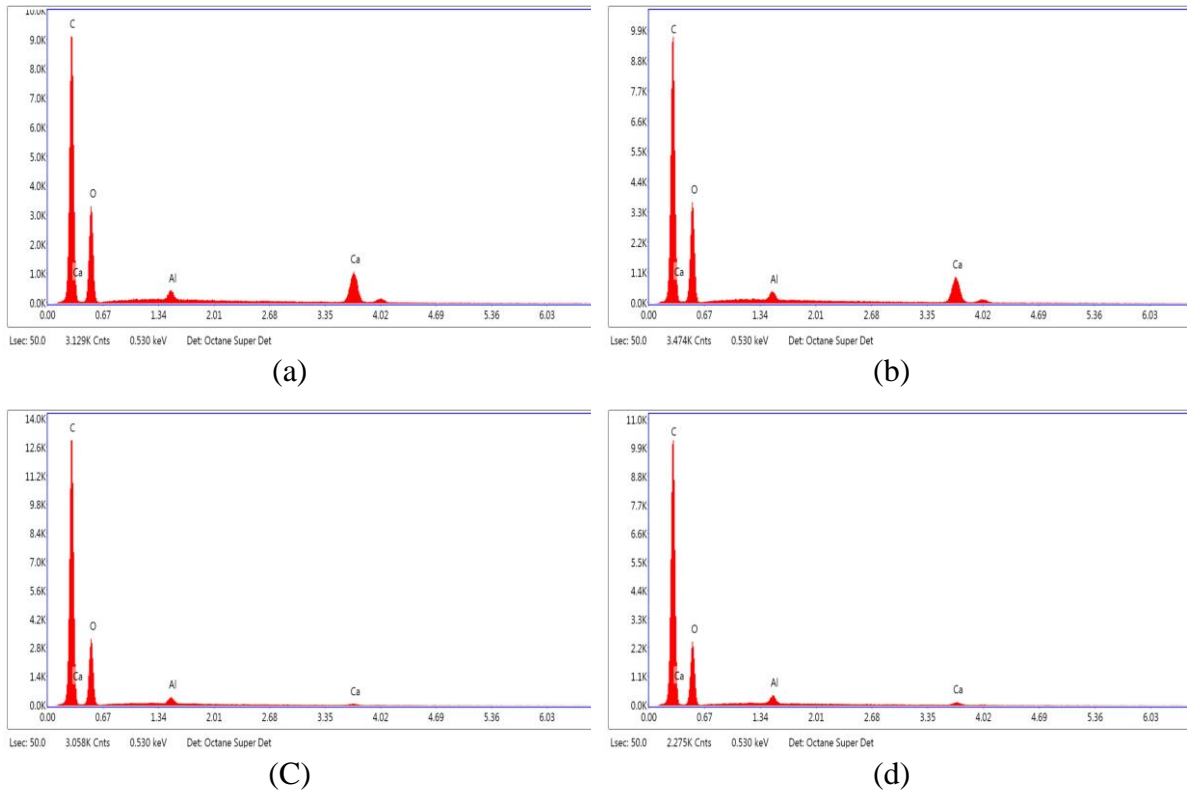
Appendix A 26: eZAF smart quant curve of FM stage of (a) spot 1; (b) Spot 2; (c) Spot 3; (d) Spot 4



Appendix A 27: Chemical composition of FM stage

Spot 1					Spot 2				
Element	Weight %	Atomic %	Net Int.	Error %	Element	Weight %	Atomic %	Net Int.	Error %
C K	46.43	60.9	926.95	4.73	C K	46.72	61.09	928.64	4.71
O K	30.41	29.94	360.64	9.54	O K	30.49	29.93	360.07	9.53
AlK	0.27	0.16	8.82	25.48	AlK	0.21	0.12	6.91	31.9
CaK	22.89	9	226.59	4.34	CaK	22.58	8.85	221.91	4.34
Spot 3					Spot 4				
Element	Weight %	Atomic %	Net Int.	Error %	Element	Weight %	Atomic %	Net Int.	Error %
C K	69.59	76.44	1401.02	3.77	C K	69.3	76.99	806.98	3.9
O K	27.22	22.45	331.79	9.14	O K	25.44	21.22	172.56	9.84
AlK	0.36	0.18	11.14	18.5	AlK	0.28	0.14	4.89	37.51
CaK	2.82	0.93	25.79	13.46	CaK	4.98	1.66	26.14	10.45

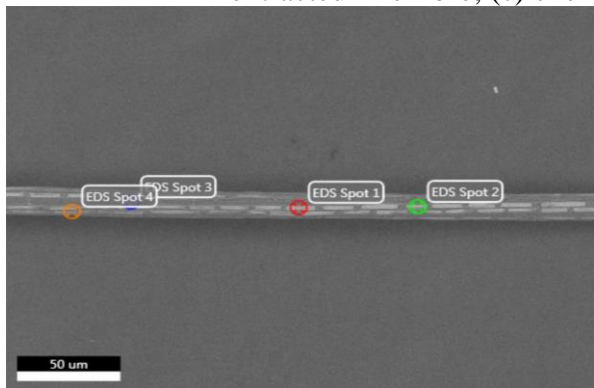
Appendix A 28: eZAF smart quant curve of M stage of (a) spot 1; (b) Spot 2; (c) Spot 3; (d) Spot 4



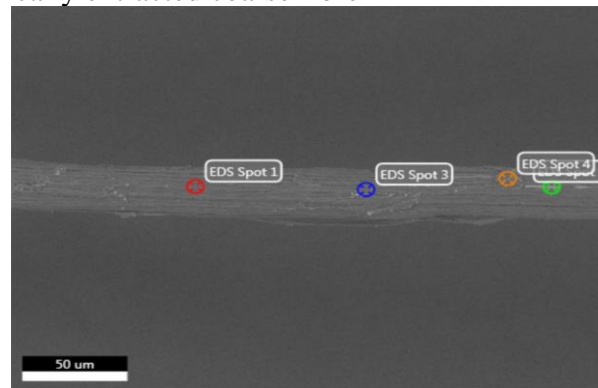
Appendix A 29: Chemical composition of M stage

Spot 1					Spot 2				
Element	Weight %	Atomic %	Net Int.	Error %	Element	Weight %	Atomic %	Net Int.	Error %
C K	47.87	62.13	1006.41	4.73	C K	49.06	62.43	1061.15	4.86
O K	29.62	28.86	381.08	9.54	O K	31.18	29.79	425.37	9.36
AlK	1.35	0.78	48.44	25.48	AlK	1.33	0.75	48.68	7.77
CaK	21.15	8.23	228.08	4.34	CaK	18.43	7.03	203.37	4.48
Spot 3					Spot 4				
Element	Weight %	Atomic %	Net Int.	Error %	Element	Weight %	Atomic %	Net Int.	Error %
C K	69.99	76.51	1534.49	4.02	C K	69.01	76.35	1199.43	4.22
O K	27.22	22.34	377.8	9.06	O K	26.21	21.77	286.98	9.25
AlK	1.46	0.71	50.38	7.2	AlK	1.87	0.92	52.18	6.37
CaK	1.33	0.43	13.85	17.19	CaK	2.91	0.96	24.28	12.07

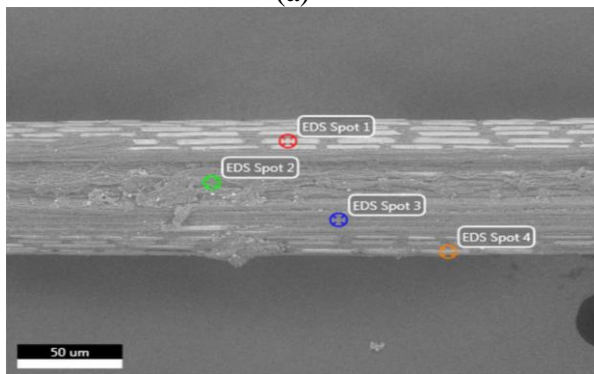
Appendix A 30: EDS spot of M stage (a) mechanically extracted fine fibre; (b) Chemically extracted fine fibre; (c) chemically extracted coarse fibre



(a)

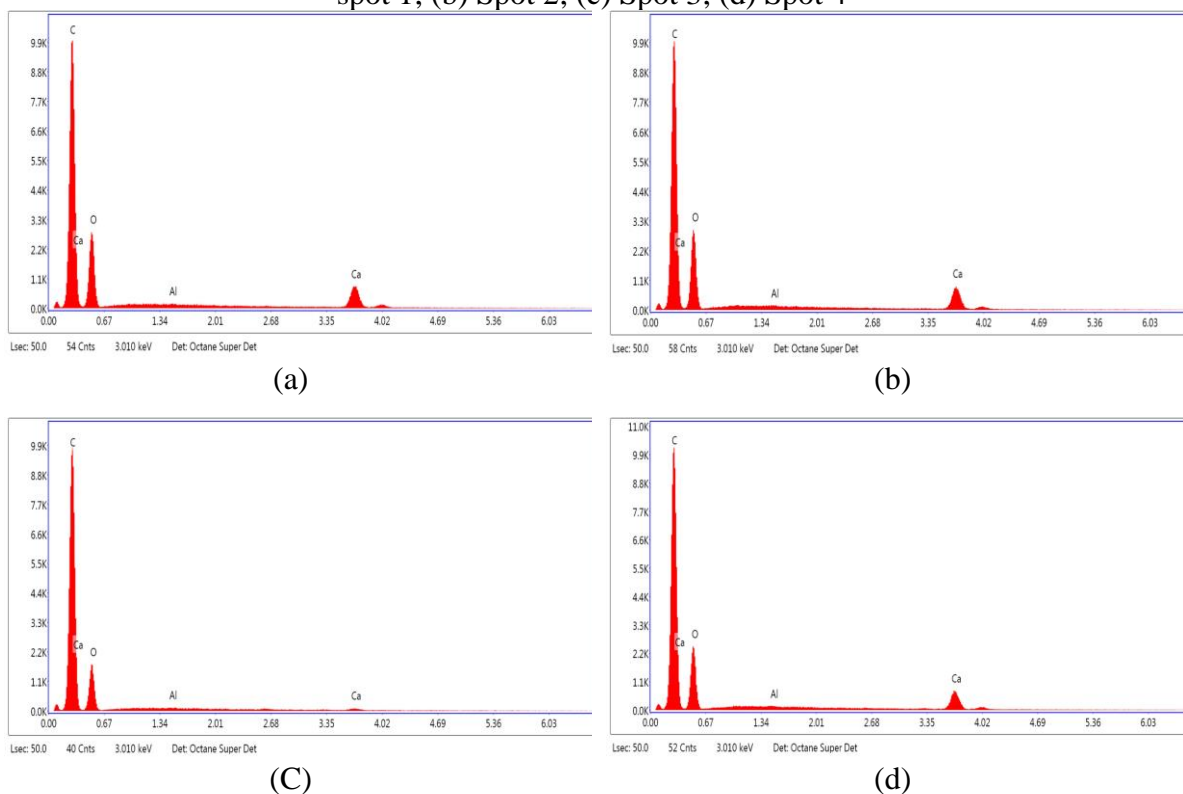


(b)



(c)

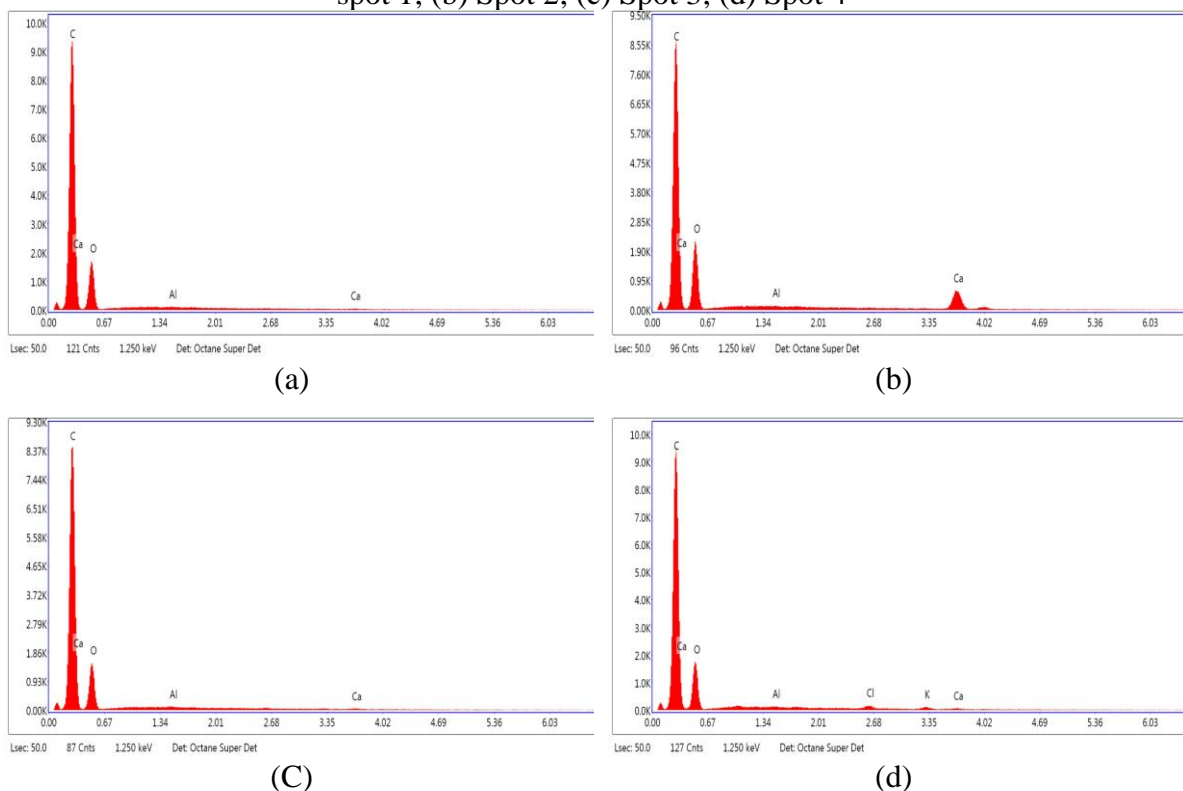
Appendix A 31: eZAF smart quant curve of M stage (mechanically extracted fine fibre) of (a) spot 1; (b) Spot 2; (c) Spot 3; (d) Spot 4



Appendix A 32: Chemical composition of M stage (mechanically extracted fine fibre)

Spot 1					Spot 2				
Element	Weight %	Atomic %	Net Int.	Error %	Element	Weight %	Atomic %	Net Int.	Error %
C K	56.21	68.73	1408.99	4.28	C K	55.55	68.1	1401.57	4.3
O K	27.57	25.3	398.08	9.47	O K	28.13	25.88	411.54	9.44
AlK	0.13	0.07	5.3	60.09	AlK	0.1	0.05	4.01	61.62
CaK	16.09	5.89	191.67	4.64	CaK	16.22	5.96	194.99	4.53
Spot 3					Spot 4				
Element	Weight %	Atomic %	Net Int.	Error %	Element	Weight %	Atomic %	Net Int.	Error %
C K	76.03	81.7	1455.67	3.42	C K	60.02	72.01	1459.77	4.12
O K	21.8	17.58	229.37	9.73	O K	25.12	22.63	340.5	9.58
AlK	0.1	0.05	2.78	62.06	AlK	0.1	0.05	3.79	61.47
CaK	2.07	0.67	17.46	15.91	CaK	14.76	5.31	167.51	4.91

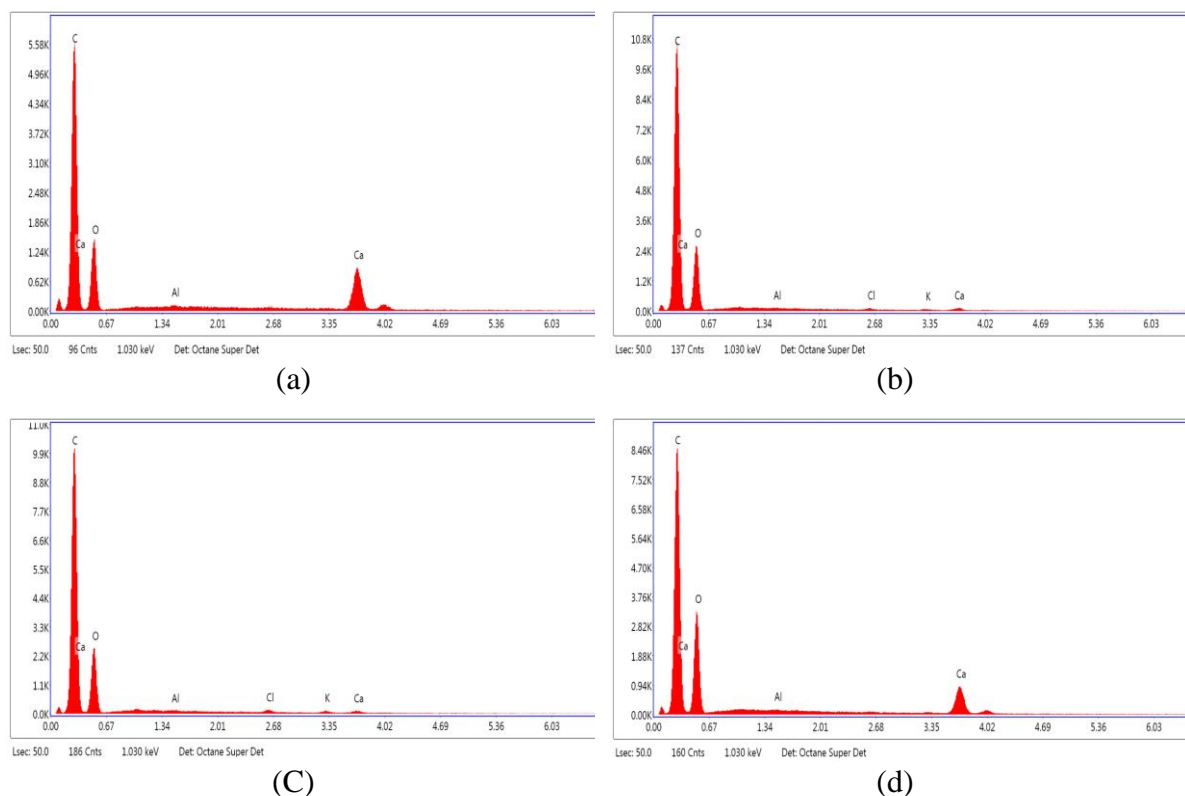
Appendix A 33: eZAF smart quant curve of M stage (chemically extracted fine fibre) of (a) spot 1; (b) Spot 2; (c) Spot 3; (d) Spot 4



Appendix A 34: Chemical composition of M stage (chemically extracted fine fibre)

Spot 1					Spot 2				
Element	Weight %	Atomic %	Net Int.	Error %	Element	Weight %	Atomic %	Net Int.	Error %
C K	76.82	81.78	1397.34	3.42	C K	59.43	71.36	1232.79	4.19
O K	22.49	17.98	228.15	9.68	O K	25.9	23.35	301.29	9.63
AlK	0.17	0.08	4.7	55.43	AlK	0.07	0.04	2.26	62.28
CaK	0.51	0.16	4.16	49.26	CaK	14.6	5.25	142.4	5.09
Spot 3					Spot 4				
Element	Weight %	Atomic %	Net Int.	Error %	Element	Weight %	Atomic %	Net Int.	Error %
C K	77.09	82.04	1281.1	3.42	C K	74.2	80.91	1360.77	4.52
O K	22.15	17.7	203.48	9.76	O K	21.38	17.5	242.5	9.74
AlK	0.11	0.05	2.65	63.61	AlK	0.42	0.2	12.91	12.49
CaK	0.66	0.21	4.87	38.35	ClK	1.63	0.6	28.49	10.03
					K K	1.5	0.5	18.04	15.05
					CaK	0.87	0.28	7.96	29.6

Appendix A 35: eZAF smart quant curve of M stage (chemically extracted coarse fibre) of (a) spot 1; (b) Spot 2; (c) Spot 3; (d) Spot 4



Appendix A 36: Chemical composition of M stage (chemically extracted coarse fibre)

Spot 1					Spot 2				
Element	Weight %	Atomic %	Net Int.	Error %	Element	Weight %	Atomic %	Net Int.	Error %
C K	48.37	64.63	747.63	4.72	C K	69.75	76.63	1516.02	4.01
O K	24.36	24.44	200.43	10.34	O K	26.97	22.24	360.85	9.18
AlK	0.07	0.04	1.76	66.5	AlK	0.09	0.04	3.1	61.91
CaK	27.2	10.89	207.53	4.4	ClK	0.53	0.2	10.23	22.17
					K K	0.7	0.24	9.56	20.89
					CaK	1.96	0.64	19.97	16
Spot 3					Spot 4				
Element	Weight %	Atomic %	Net Int.	Error %	Element	Weight %	Atomic %	Net Int.	Error %
C K	69	76.47	1454.07	4.49	C K	50.45	63.32	1187.16	4.54
O K	26.2	21.8	357.07	9.22	O K	31.85	30.01	455.85	9.34
AlK	0.44	0.22	15.51	11.97	AlK	0.07	0.04	2.77	61.35
ClK	1.22	0.46	24.32	12.18	CaK	17.63	6.63	203.1	4.5
K K	1.21	0.41	16.83	15.63					
CaK	1.93	0.64	20.19	15.1					

Appendix A 37: Raw data of dorsal fibres

ID	Diameter	Tensile stress at Break (Standard)	Tensile strain at Break (Standard)	Modulus (Automatic Young's)
D-1	75.56	260.75024	0.02139	19.28884
D-2	133.33	94.28094	0.0233	7.00097
D-3	44.44	435.63934	0.02429	23.41829
D-4	22.22	670.81683	0.01925	53.00431
D-6	33.33	465.7178	0.0126	54.74183
D-8	53.33	578.74915	0.02854	35.6554
D-9	31.11	452.71112	0.01441	38.42615
D-10	44.44	1,474.73	0.03928	58.78338
D-11	47.78	307.71896	0.01957	20.51109
D-13	55.56	312.46063	0.01669	24.63755
D-14	33.33	647.6037	0.01962	48.92353
D-15	57.78	225.96011	0.01459	20.6776
D-16	44.44	994.39203	0.05008	24.62098
D-17	22.22	1,192.50	0.02021	79.03651
D-18	44.44	499.83008	0.02405	34.63779
D-19	33.33	455.52173	0.01893	34.15163
D-20	66.67	416.14423	0.03492	17.73222
D-21	66.67	362.83566	0.0226	29.10731
D-22	13.33	1,013.57	0.01169	156.78557
D-23	44.44	1,170.44	0.03361	59.34548
D-24	55.56	329.66879	0.01813	25.00408
D-26	44.44	369.03009	0.01655	38.66212
D-27	53.33	386.66522	0.0163	36.61102
D-28	66.67	189.98006	0.01722	15.40671
D-30	50	344.20596	0.01662	27.8591
D-31	33.33	416.2659	0.01528	42.83768
D-32	44.44	210.97418	0.01364	24.9512
D-33	42.22	427.87589	0.01633	42.45588
D-34	55.56	165.63321	0.015	16.07634
D-35	38.89	947.96417	0.01687	73.83451
D-36	38.89	746.82208	0.01229	89.70158
D-40	44.44	543.20874	0.02605	32.61263
D-41	44.44	140.84399	0.01521	24.97831
D-42	54.44	94.28195	0.01267	14.80649
D-45	43.33	442.10364	0.03555	20.34153
D-46	40	273.48032	0.01804	26.89008

Appendix A 38: Raw data of ventral fibre

ID	Diameter	Tensile stress at Break (Standard)	Tensile strain at Break (Standard)	Modulus (Automatic Young's)
V-1	55.56	440.24753	0.04686	13.16565
V-3	55.56	584.75513	0.03736	21.76183
V-4	31.11	983.77679	0.02984	51.81234
V-5	46.67	301.01730	0.02242	21.71093
V-6	31.11	787.05963	0.03081	34.80502
V-7	64.44	362.60617	0.02444	22.59083
V-8	42.22	301.51288	0.01478	29.89095
V-9	64.44	111.29919	0.01593	11.53711
V-10	48.89	548.98499	0.04038	16.81966
V-11	56.67	192.17470	0.01895	15.11139
V-12	32.22	554.32794	0.02092	32.87086
V-13	32.78	584.31805	0.0263	30.51567
V-14	46.67	350.32657	0.03209	14.62963
V-15	60	402.43405	0.02983	23.80417
V-16	46.33	583.44037	0.03174	24.77436
V-17	45.56	173.12965	0.02268	11.30682
V-18	43.33	348.72800	0.02117	21.81886
V-19	54.44	568.93658	0.04115	17.77681
V-20	40	910.25610	0.03441	42.04323
V-22	55	597.88458	0.03439	25.74559
V-23	46.67	450.73245	0.04162	12.57856
V-24	44.44	292.29279	0.04853	7.535
V-25	46.67	557.70190	0.02078	36.0414
V-28	43.33	367.82275	0.04862	9.38653
V-29	23.33	925.10809	0.03465	34.36603
V-30	50	246.77095	0.03242	9.28033
V-32	50	448.55844	0.0162	36.08063
V-33	42.22	453.56985	0.0369	18.77346
V-34	33.33	542.75214	0.02122	33.7195
V-36	42.22	620.37036	0.03768	22.35617
V-37	46.67	546.56464	0.01954	38.0697
V-38	28.89	649.04462	0.01339	74.93745
V-39	35.56	579.20087	0.0198	39.36245
V-41	53.33	356.84863	0.04549	10.04197
V-42	20	786.33441	0.02316	55.78891
V-44	53.33	322.93732	0.02685	21.80216
V-45	46.67	662.64166	0.02745	35.12456
V-46	32.22	761.60315	0.02924	33.66308
V-47	21.11	672.38293	0.01915	54.9903
V-48	34.44	558.60974	0.03685	63.05017
V-49	44.44	526.62244	0.02943	27.50456

Appendix A 39: Raw data of central fibre

ID	Diameter	Tensile stress at Break (Standard)	Tensile strain at Break (Standard)	Modulus (Automatic Young's)
C-2	22.22	86.91378	0.02695	4.18385
C-4	23.33	106.17566	0.05299	7.55858
C-5	20.00	169.87439	0.03958	5.9313
C-6	21.11	140.04251	0.04563	10.37569
C-7	16.67	251.56998	0.03613	8.88036
C-8	22.22	230.86	0.04182	7.38379
C-9	18.89	82.85581	0.02819	7.23484
C-10	22.22	344.96674	0.03922	12.88278
C-11	16.67	347.392	0.05623	17.96914
C-12	13.33	664.03003	0.04478	21.08577
C-13	16.67	102.34087	0.03224	18.97518
C-14	20.00	309.78	0.03933	13.21145
C-15	12.22	406.35886	0.04541	12.92053
C-16	16.67	186.10011	0.04312	10.12589
C-17	20.00	206.88834	0.04497	7.34998
C-18	20.00	142.61246	0.04591	10.80073
C-19	22.22	238.51	0.04325	7.93553
C-20	15.56	379.71	0.05007	14.93147
C-22	13.33	226.09412	0.03453	14.49435
C-23	20.00	263.41385	0.0219	17.99329
C-24	10.00	436.83615	0.02707	18.7302
C-25	13.33	258.48114	0.01918	18.95665
C-26	20.00	145.12254	0.0156	35.21773
C-27	20.00	197.81935	0.04016	8.89835
C-29	21.11	86.63313	0.02547	50.93318
C-35	12.22	446.51297	0.0202	23.14939
C-45	16.67	288.8356	0.05944	35.25414

Appendix A 40: Source Python Code of Weibull Distribution

```

1 import pandas as pd
2 import numpy as np
3 import Weibull
4
5 df = pd.read_excel('D:/UoM Study/Project/Py/M-L1.xlsx')
6 batch = df.to_numpy()
7
8 no_of_sample = len(batch[:])
9 data = []
10
11 for i in range (no_of_sample):
12     data.append(batch[i,1])
13
14 analysis = weibull.Analysis(data, unit='Tensile stress')
15 analysis.fit(method='lr')
16 #for LR method; line 15 would be unchanged
17 #for MLE method; line 15 would be "analysis.fit(method='mle')"
```

Appendix A 41: Pseudocode for Weibull distribution

- Import pandas, numpy and Weibull libraries
- Import the raw data file from the path relative to its current location
- Calculate the number of samples
- Extract data from the raw data file and assign them to a list
- Analyze the data from the list and fit the curve
- Select the method as 'lr' or 'mle'
- Print the result of shape and scale parameter
- Print the plotted graph

Appendix A 42: Source Python Code of Suitability Analysis of M-L1 (HLV-S/R/Y)

```
1 import pandas as pd
2 import numpy as np
3
4 df = pd.read_excel('D:/UoM Study/Project/Py/M-L1.xlsx')
5
6 data = df.to_numpy()
7 no_of_sample = len(data[:])
8
9 strength = 2000
10 strain = 3.3
11 modulus = 103
12
13 count = 0
14 for i in range(no_of_sample):
15     if data[i,1] >= strength and data[i,2] <= strain and data[i,3]>=
        modulus:
16 # for 3 parameters (S/R/Y); line 15 would be unchanged
17 # for 2 parameters (S/R); line 15 would be "if data[i,1] >= strength and
        data[i,2] <= strain:"
18 # for 2 parameters (Y/R); line 15 would be "if data[i,3]>= modulus and
        data[i,2] <= strain:"
19 # for 2 parameters (S/Y); line 15 would be "if data[i,1] >= strength and
        data[i,3]>= modulus:"
20 # for 1 parameter (S); line 15 would be "if data[i,1] >= strength:"
21 # for 1 parameter (R); line 15 would be "if data[i,2] <= strain:"
22 # for 1 parameter (Y); line 15 would be "if data[i,3]>= modulus:"
23         count = count+1
24
25 percentage = (count * 100)/no_of_sample
26 print(str(percentage) + '% Fibre is suitable for composite')
```

Appendix A 43: Pseudocode of Suitability Analysis of M-L1

- Import pandas and NumPy libraries
- Import raw data file from the path relative to its current location
- Convert the imported excel file to NumPy object
- Calculate the number of samples
- Set a threshold value of 3 parameters
- Assign zero to a counter
- Using a loop, check every sample, whether it fulfills the threshold value. If yes, add 1 to the counter.
- Calculate the percentage that fulfills the threshold value using the counter's value.
- Print the value

Appendix A 44: Source code of Ranking (Combination of Growth Stage and Length) of HLV-S/R/Y

```
1 import pandas as pd
2 import numpy as np
3
4 df = pd.read_excel('D:/UoM Study/Project/Py/Ranking/HLV-SRM.xlsx')
5
6 data = df.to_numpy()
7 no_of_row = len(data)
8 no_of_column = len(data[0])
9 list1 = []
10 for i in range (no_of_row-1):
11     for j in range (no_of_column-1):
12         list1.append(data[i+1,j+1])
13         j=j+1
14     i=i+1
15
16 list1.sort()
17
18 for i in range (len(list1)):
19     result = np.where(data == list1[i])
20
21     if i != 0 and list1[i] == list1[i-1]:
22         continue
23
24     elif len(result) >= 2 and (len(list1)-i) != (len(result[0])):
25         for j in range (len(result[0])):
26             print(data[result[0][j],0] + '-' + data[0,result[1][j]] + '
growth stages rank is: ' + str(i+1))
27             j=j+1
28
29     elif len(result) >= 2 and (len(list1)-i) == (len(result[0])):
```

```

30     for j in range (len(result[0])):
31         print(data[result[0][j],0] + '-' + data[0,result[1][j]] + '
growth stages rank is: ' + str(len(list1)))
32         j=j+1
33
34     else:
35         print(data[result[0],0] + '-' + data[0,result[1]] + ' growth stages
rank is ' + str(i+1))
36         i=i+1

```

Appendix A 45: Pseudocode of Ranking of HLV-S/R/Y

- Import pandas and NumPy libraries
- Import raw data file from the path relative to its current location
- Convert the imported excel file to NumPy object
- Calculate the number of rows and columns
- Declare an empty list and append all the data from the NumPy object to the list using a nested loop
- Sort the list in ascending order
- Using a loop, check the index number of NumPy array for each element of the list, and find the heading index of row and column
- Declare the growth stage using the index number of headings and their ranking using the index number of the list
- Print the growth stage and ranking values

Appendix A 46: Weibull Parameters of tensile stress after removing outliers

ID	\bar{x}_{stress} (MPa)	LR Method															MLE method	
		σ_{avg} (GPa)			α				β (MPa)				R^2_{σ}				α	β (MPa)
		DR	HE	MR	DR	HE	MR	*DR	DR	HE	DR	*DR	DR	HE	MR	*DR		
NF-L1	1065 [504]	1026	1028	1023	2.33	2.41	2.22	2.39	1201	1197	1207	1179	0.98	0.98	0.99	0.98	2.28	1190
NF-L2	1006 [330]	1004	1005	1002	3.25	3.37	3.11	3.1	1123	1121	1127	1107	0.98	0.97	0.98	0.98	3.37	1105
NF-L3	757.0 [166]	766	767	765	5.25	5.44	5.02	4.01	821.4	820	823	819.9	0.98	0.97	0.98	0.89	4.71	810.9
F-L1	1242 [578]	1202	1206	1199	2.39	2.47	2.3	2.54	1401	1398	1406	1366	0.95	0.94	0.96	0.94	2.34	1390
F-L2	979.1 [351]	977	979	975	3.34	3.45	3.21	3.35	1090	1088	1093	1067	0.92	0.91	0.93	0.96	2.92	1082
F-L3	939.1 [342]	935	937	933	3.11	3.22	2.99	3.21	1052	1050	1055	1024	0.9	0.89	0.92	0.94	2.97	1039
LF-L1	690.2 [252]	684	685	682	2.89	2.99	2.76	2.9	776.5	775	779	759.3	0.96	0.95	0.96	0.96	3.02	762.4
LF-L2	621.9 [267]	612	614	611	2.74	2.83	2.64	3.04	699.9	699	702	675.2	0.88	0.86	0.89	0.9	2.5	694.2
LF-L3	478.0 [218]	459	460	458	2.25	2.33	2.16	2.37	540.3	538	542	527.0 3	0.96	0.95	0.97	0.96	2.39	531.7
FM-L1	556.7 [214]	551	552	550	2.98	3.08	2.85	2.99	623	622	625	610.8	0.96	0.95	0.97	0.98	2.78	617.5
FM-L2	538.9 [207]	536	537	535	3.07	3.16	2.95	3.33	604.3	603	606	584.4 2	0.86	0.84	0.87	0.91	2.76	598.4
FM-L3	460.4 [148]	461	462	460	3.5	3.62	3.35	3.35	512.1	511	513	503.1	0.93	0.92	0.94	0.97	3.35	505.7
M-L1	993.5 [489]	935	938	932	1.86	1.93	1.78	1.95	1139	1134	1146	1113	0.97	0.96	0.97	0.97	2.18	1108
M-L2	1419 [646]	1385	1387	1381	2.63	2.72	2.52	2.75	1592	1587	1598	1555	0.96	0.95	0.96	0.95	2.35	1585
M-L3	809.9 [213]	817	818	816	4.48	4.64	4.29	3.81	886.9	886	889	879.8	0.95	0.94	0.96	0.95	3.85	877.9

Standard deviation is shown in square bracket; \bar{x}_{stress} : Experimental tensile stress; σ_{avg} : Weibull average; α : shape parameter; β : scale parameter; DR: median rank estimator; HE: Hazen estimator; MR: mean rank estimator; LR: linear regression; MLE: maximum likelihood estimation

Appendix A 47: Weibull Parameters of modulus after removing outliers

ID	\bar{x}_{modulus} (GPa)	LR Method														MLE method		
		E_{avg} (GPa)			α				β (GPa)				R^2_E			α	β (GPa)	
		DR	HE	MR	DR	HE	MR	*DR	DR	HE	MR	*DR	DR	HE	MR	*DR		
NF-L1	40.1 [18.5]	38.79	48.92	38.67	2.35	2.80	2.25	2.54	45.34	55.77	45.50	43.96	0.93	0.93	0.95	0.93	2.37	44.81
NF-L2	55.3 [19.2]	55.25	56.11	55.14	3.46	2.26	3.31	3.41	61.44	66.01	61.59	60.20	0.92	0.93	0.93	0.96	3.00	60.97
NF-L3	46.7 [12.4]	47.11	38.81	47.04	4.31	2.44	4.13	3.69	51.29	45.10	51.41	50.86	0.96	0.89	0.97	0.96	3.95	50.67
F-L1	58.8 [31.2]	55.97	46.52	55.80	2.18	3.01	2.09	2.35	66.22	52.55	66.50	64.43	0.94	0.90	0.95	0.94	2.06	65.98
F-L2	28.0 [10.5]	27.84	27.89	27.78	3.06	3.16	2.94	3.12	31.38	31.33	31.47	30.65	0.93	0.91	0.94	0.95	2.88	31.06
F-L3	63.5 [20.0]	63.89	55.34	63.76	3.71	3.57	3.57	3.66	70.53	61.32	70.66	68.88	0.87	0.91	0.88	0.93	3.29	69.69
LF-L1	34.5 [13.6]	34.05	59.68	33.98	2.90	4.04	2.77	2.92	38.64	65.35	38.79	37.85	0.97	0.91	0.97	0.97	2.71	38.26
LF-L2	39.1 [17.1]	38.36	63.99	38.26	2.72	3.82	2.61	2.95	43.90	70.43	44.03	42.55	0.91	0.85	0.92	0.91	2.47	43.64
LF-L3	39.3 [18.2]	38.41	47.17	38.32	2.65	4.47	2.54	2.80	44.10	51.21	44.28	43.02	0.94	0.95	0.95	0.95	2.30	43.94
FM-L1	29.6 [11.4]	29.28	34.12	29.21	2.92	3.01	2.80	2.95	33.20	38.54	33.30	32.51	0.96	0.96	0.97	0.96	2.81	32.86
FM-L2	37.4 [11.3]	37.64	38.45	37.58	4.02	2.80	3.85	3.78	41.24	43.82	41.33	40.51	0.90	0.90	0.91	0.94	3.34	40.90
FM-L3	29.0 [7.6]	29.28	38.48	29.23	4.36	2.75	4.18	3.77	31.84	43.97	31.91	31.50	0.93	0.94	0.94	0.94	3.95	31.44
M-L1	49.7 [21.1]	48.82	29.34	48.67	2.70	3.02	2.58	2.84	55.92	33.13	56.10	54.39	0.94	0.95	0.95	0.94	2.55	55.38
M-L2	46.9 [19.1]	46.42	37.69	46.29	2.91	4.15	2.80	3.13	52.64	41.17	52.77	51.03	0.89	0.89	0.91	0.92	2.63	52.22
M-L3	59.3 [17.9]	59.59	1.31	59.49	3.91	4.50	3.76	3.64	65.44	1.42	65.59	64.43	0.92	0.92	0.93	0.96	3.40	64.82

Standard deviation is shown in square bracket; \bar{x}_{modulus} : Experimental modulus; E_{avg} : Weibull average; α : shape parameter; β : scale parameter; DR: median rank estimator; HE: Hazen estimator; MR: mean rank estimator; LR: linear regression; MLE: maximum likelihood estimation